

AD-A070 367

NAVAL POSTGRADUATE SCHOOL MONTEREY CA

F/6 20/13

EXPERIMENTAL DETERMINATION OF MELTING RATES OF ICE MOVING IN SE--ETC(U)

MAR 79 W F CLIFFORD, R J ERMAN

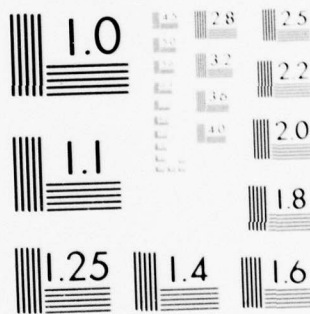
UNCLASSIFIED

NL

1 OF 3

AD
A070 367





MICROCOPY RESOLUTION TEST CHART
NATIONAL BUREAU OF STANDARDS-1963-A

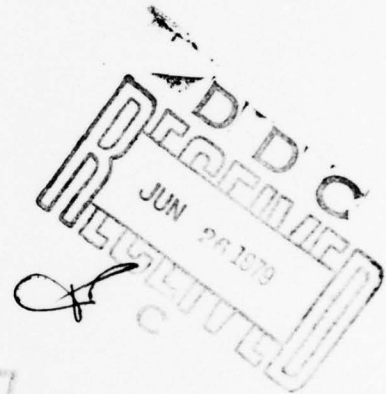
LEVEL

2

AD A 070367

NAVAL POSTGRADUATE SCHOOL
Monterey, California

12 22 pp.



9 Master's THESIS

6 EXPERIMENTAL DETERMINATION OF MELTING
RATES OF ICE MOVING IN SEAWATER

by

10 William Francis/Clifford

Reginald Joseph/Erman

11 March 1979

Thesis Advisor: A. E. Fuhs

Approved for public release; distribution unlimited.

DDC FILE COPY

251 450
New

UNCLASSIFIED

SECURITY CLASSIFICATION OF THIS PAGE (When Data Entered)

REPORT DOCUMENTATION PAGE		READ INSTRUCTIONS BEFORE COMPLETING FORM
1. REPORT NUMBER	2. GOVT ACCESSION NO.	3. RECIPIENT'S CATALOG NUMBER
4. TITLE (and Subtitle) Experimental Determination of Melting Rates of Ice Moving in Seawater		5. TYPE OF REPORT & PERIOD COVERED Master's Thesis; March 1979
		6. PERFORMING ORG. REPORT NUMBER
7. AUTHOR(s) William Francis Clifford Reginald Joseph Erman		8. CONTRACT OR GRANT NUMBER(s) NPS Research Foundation
9. PERFORMING ORGANIZATION NAME AND ADDRESS Naval Postgraduate School Monterey, California 93940		10. PROGRAM ELEMENT, PROJECT, TASK AREA & WORK UNIT NUMBERS
11. CONTROLLING OFFICE NAME AND ADDRESS Naval Postgraduate School Monterey, California 93940		12. REPORT DATE March 1979
		13. NUMBER OF PAGES 219
14. MONITORING AGENCY NAME & ADDRESS (if different from Controlling Office)		15. SECURITY CLASS. (of this report) Unclassified
		15a. DECLASSIFICATION/DOWNGRADING SCHEDULE
16. DISTRIBUTION STATEMENT (of this Report) Approved for public release; distribution unlimited.		
17. DISTRIBUTION STATEMENT (of the abstract entered in Block 20, if different from Report)		
18. SUPPLEMENTARY NOTES		
19. KEY WORDS (Continue on reverse side if necessary and identify by block number) Ice Melting Rates Flow-Separation Theory Ice Ablation Model <i>lower case x</i>		
20. ABSTRACT (Continue on reverse side if necessary and identify by block number) Large, fresh-water ice blocks (0.5m X 1.25m X 5m) were towed in Monterey Bay at speeds in range from 0.7 to 1.2 knots. The Experimental objectives of the experiments included measurement of gross regression rates of ice surfaces, wake temperature, turbulent thermal boundary layer, ice interior temperature profile, and observation of shape changes over the melting period. The research was conducted over a period from October 1977 to <i>measuring</i>		

UNCLASSIFIED

SECURITY CLASSIFICATION OF THIS PAGE/When Data Entered:

(20. ABSTRACT (Continued) → Jan. 1979. Measured

January 1979. The measured regression rates at several points on the ice blocks were compared to theoretical predictions using a turbulent flow ice ablation model developed by Dr. Owen Griffin of the Naval Research Laboratory. Griffin's model predicted a regression rate of 280mm/hr compared with the measured value of 260mm/hr at a selected point. Temperature profiles in the ice interior and ice-water boundary layer were used in a one-dimensional energy balance across the melting interface. Ice ripples were observed on all ice block tests. The ripples are important for both heat transfer and drag considerations. The wavelengths of the ripples were measured and the average wavelength determined. The measured average wavelength was 6.1 inches compared to the theoretical average predicted by Tatinclaux and Kennedy of 5.8 inches for a selected experiment.

A

in.

Accession For	
NRIC Grant	<input checked="checked" type="checkbox"/>
DOC TAB	<input type="checkbox"/>
Unannounced	<input type="checkbox"/>
Justification	<input type="checkbox"/>
By	
Distribution/	
Availability Codes	
Dist	Available/or special

UNCLASSIFIED

SECURITY CLASSIFICATION OF THIS PAGE/When Data Entered:

Approved for public release; distribution unlimited

EXPERIMENTAL DETERMINATION OF MELTING
RATES OF ICE MOVING IN SEAWATER

by

William Francis Clifford
Lieutenant Commander, United States Navy
B.S., United States Naval Academy, 1969

and

Reginald Joseph Erman
Lieutenant, United States Navy
B.S., North Carolina State, 1973

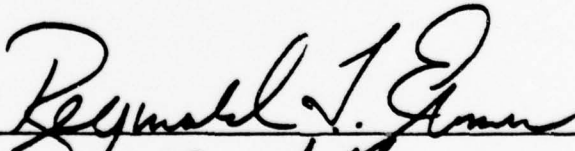
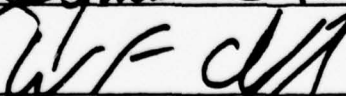
Submitted in partial fulfillment of the
requirements for the degree of

MASTER OF SCIENCE IN MECHANICAL ENGINEERING


from the

NAVAL POSTGRADUATE SCHOOL
March 1979

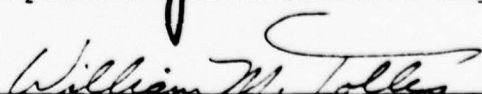
Authors

Approved by:


Thesis Advisor


Chairman, Department of Mechanical Engineering


Dean of Science and Engineering

ABSTRACT

Large, fresh-water ice blocks (0.5m X 1.25m X 5m) were towed in Monterey Bay at speeds in range from 0.7 to 1.2 knots. The objectives of the experiments included measurement of gross regression rates of ice surfaces, wake temperature, turbulent thermal boundary layer, ice interior temperature profile, and observation of shape changes over the melting period. The research was conducted over a period from October 1977 to January 1979. The measured regression rates at several points on the ice blocks were compared to theoretical predictions using a turbulent flow ice ablation model developed by Dr. Owen Griffin of the Naval Research Laboratory. Griffin's model predicted a regression rate of 280mm/hr compared with the measured value of 260mm/hr at a selected point. Temperature profiles in the ice interior and ice-water boundary layer were used in a one-dimensional energy balance across the melting interface. Ice ripples were observed on all ice block tests. The ripples are important for both heat transfer and drag considerations. The wavelengths of the ripples were measured and the average wavelength determined. The measured average wavelength was 6.1 inches compared to the theoretical average predicted by Tatinclaux and Kennedy of 5.8 inches for a selected experiment.

TABLE OF CONTENTS

I.	INTRODUCTION -----	17
	A. JUSTIFICATION FOR STUDY -----	17
II.	BACKGROUND OF STUDY -----	19
III.	ICE MODEL SCALING AND INITIAL LABORATORY TESTS -	21
	A. GENERAL -----	21
	B. HYDRODYNAMIC REQUIREMENTS -----	21
	C. HEAT TRANSFER ANALYSIS REQUIREMENTS -----	23
	D. WATER CHANNEL FACILITIES AT THE NAVAL POSTGRADUATE SCHOOL -----	25
	E. INITIAL LABORATORY EXPERIMENTS -----	26
	F. WATER CHANNEL TEST RESULTS -----	29
	G. CONCLUSIONS -----	32
IV.	LARGE-SCALE ICE MODEL EXPERIMENTS IN MONTEREY BAY -----	34
	A. SIZE AND SHAPE DETERMINATION OF MODEL -----	34
	B. CONSTRUCTION OF THE ICE MODEL FREEZING CONTAINER -----	35
	C. ICE MODEL CONSTRUCTION -----	36
	D. GENERAL TEST PROCEDURE -----	39
	E. SUMMARY OF TESTS IN MONTEREY BAY -----	42
	1. Test No. 1, September 23, 1977 -----	42
	2. Test No. 2, September 26, 1977 -----	43
	3. Test No. 3, October 3, 1977 -----	44
	4. Test No. 4, November 6, 1977 -----	46
	5. Test No. 5, December 10, 1977 -----	48
	6. Test No. 6, April 27, 1978 -----	52
	F. COMMENTS -----	56

V.	TANDEM ICE MODEL EXPERIMENTS -----	57
A.	BACKGROUND -----	57
B.	LABORATORY TESTS -----	58
C.	RESULTS OF LABORATORY TESTS -----	61
D.	MONTEREY BAY TANDEM TEST, DECEMBER 10, 1978 ----	62
E.	RESULTS OF TANDEM BAY TEST -----	63
VI.	EXPERIMENTAL RESULTS WITH THEORETICAL CORRELATIONS -	65
A.	GENERAL -----	65
B.	COMPARISON OF EXPERIMENTALLY MEASURED ABLATION RATES WITH THEORETICAL PREDICTIONS -----	65
C.	MEASUREMENT AND VERIFICATION OF THERMAL BOUNDARY LAYER PROFILE -----	68
D.	RIPPLE EFFECTS AND MEASUREMENTS -----	71
1.	General -----	71
2.	Ripple Effects on Drag -----	71
3.	Ripple Effects on Heat Transfer -----	72
4.	Measurement of Ripple on NPS Tests -----	72
E.	THEORETICAL PREDICTIONS AND MEASUREMENTS OF ICE INTERIOR TEMPERATURE PROFILES -----	73
F.	MEASUREMENTS OF ICE MODEL WAKE TEMPERATURE ----	76
G.	FLOW SEPARATION ON THE ICE MODELS -----	77
VII.	RECOMMENDATIONS FOR FUTURE WORK -----	80
A.	GENERAL -----	80
B.	TOPICS FOR FUTURE RESEARCH -----	80
1.	Measurement of Drag -----	80
2.	Tandem Towing -----	81
3.	Influence of Buoyancy on Heat Transfer -----	81
4.	Instabilities of Insulating Material, e.g., Flagwaving Instability -----	82

5. Solid Mechanics of Icebergs -----	82
6. Development of Instrumentation -----	83
7. Laboratory Tests -----	83
8. Field Tests -----	84
9. Insulation -----	85
10. Potential Flow Computer Code -----	85
APPENDIX A: AREAS OF CONCERN WITH ICEBERG DETERIORATION -----	87
APPENDIX B: SOLUTION OF TRANSIENT THERMAL CONDUCTION EQUATION -----	98
LIST OF REFERENCES -----	215
BIBLIOGRAPHY -----	217
INITIAL DISTRIBUTION LIST -----	218

LIST OF FIGURES

1. Regimes of flow and wave producing conditions as functions of Reynolds and Froude Numbers -----	107
2. NPS water tunnel -----	108
3. NPS mobile water table -----	109
4. NPS water channel -----	110
5. NPS water channel -----	111
6. Progressive regression of second laboratory model -----	112
7. Progressive regression of streamlined laboratory model -----	113
8. Effectiveness of heat transfer -----	114
9. Flow reattachment with accompanying large heat flux -----	115
10. Trapped vortex filament -----	116
11. Ice model freezing container -----	117
12. Top view of ice model freezing container -----	118
13. Towing bollard -----	119
14. Premature disintegration of ice model -----	120
15. Archimedes box (core box) -----	121
16. Core box installation -----	122
17. Ice model underway with core box installed -----	123
18. Ice model with towing bollard integral with core box -----	124
19. Scale used to weigh ice and container -----	125
20. Positioning of ice container near water and towing vessel -----	126
21. Ice container being lowered into the water -----	127

22.	Seawater flooding into ice container -----	128
23.	Ice model separation from container -----	129
24.	Ice model underway -----	130
25.	Coast Guard vessel with model in tow -----	131
26.	Boston whaler with model in tow -----	132
27.	Tow rope and instrumentation wire arrangement ----	133
28.	Current meter and readout assembly -----	134
29.	Ice model positioned for recovery -----	135
30.	Recovered ice model clear of water -----	136
31.	Ice model on pier; Test 5 -----	137
32.	Ice model underway; Test 1 -----	138
33.	Premature disintegration of ice model; Test 2 ----	139
34.	Ice model underway; Test 3 -----	140
35.	Ice model recovery; Test 3 -----	141
36.	Ice model recovered; Test 3 -----	142
37.	Ice model on pier; Test 3 -----	143
38.	Ice model bow erosion; Test 3 -----	144
39.	Ripples along the complete post side of the ice model; Test 3 -----	145
40.	Detailed view of port side, rear of ice model; Test 3 -----	146
41a.	Thermocouple arrangement; Test 4 -----	147
41b.	Thermocouple with digital readout -----	148
42.	Thermcouple arrangement; Test 4 -----	149
43.	Ice model underway; Test 4 -----	150
44.	Forward section of ice model underway; Test 4 ----	151
45.	Bow undercutting of ice model; Test 4 -----	152
46.	Ice model recovery; Test 4 -----	153

47.	Recovered ice model with exposed thermocouple array; Test 4 -----	154
48.	Ice model on pier; Test 4 -----	155
49.	Detailed view of ice model layering and ripples; Test 4 -----	156
50.	Ripple measurement technique; Test 4 -----	157
51.	Ice model prior to launch; Test 5 -----	158
52.	Thermocouple arrangement; Test 5 -----	159
53.	Cross section view of pontoon bridge -----	160
54.	Thermocouple installation on pontoon bridge; Test 5 -	161
55.	Ice model and pontoon bridge underway; Test 5 -----	162
56.	Ice model and pontoon bridge towing arrangement; Test 5 -----	163
57.	Ice model on pier; Test 5 -----	164
58.	Rear view of ice model ripples; Test 5 -----	165
59.	Rear view of ice model layering; Test 5 -----	166
60.	Thermocouple arrangement; Test 6 -----	167
61.	Ice model prior to launch; Test 6 -----	168
62.	Forward section separation; Test 6 -----	169
63.	Forward section separation; Test 6 -----	170
64.	Rear view pushing arrangement; Test 6 -----	171
65.	Frontal view pushing arrangement; Test 6 -----	172
66.	Forward section of ice model; Test 6 -----	173
67.	Ice model positioning for recovery; Test 6 -----	174
68.	Frontal view of recovered ice model; Test 6 -----	175
69.	Reference grid on ice model for ripple measurement; Test 6 -----	176
70.	Linear motion position transducer used for ripple measurement; Test 6 -----	177
71.	Strip-chart recording of ripples; Test 6 -----	178

72.	Ice model immediately after insertion in water channel -----	179
73.	Ice model after two minutes in water channel showing dye injection -----	180
74.	Tandem models in water channel immediately after insertion - separation Distance = $W/3$ -----	181
75.	Tandem models after one minute in channel at $W/3$ separation distance -----	182
76.	Tandem models after two minutes in channel at $W/3$ separation distance -----	183
77.	Forward ice model bottom view -----	184
78.	Rear ice model bottom view -----	185
79.	Dye accentuated flow visualization around tandem models at $W/3$ separation distance after two minutes in channels -----	186
80.	Hookup of tandem ice models in Monterey Bay -----	187
81.	Side view of tandem ice models underway -----	188
82.	End view of tandem models underway -----	189
83.	End view of tandem models underway oscillation left -----	190
84.	End view of tandem models underway oscillation right (Note drag rope from rear model) -----	191
85.	Bow view of forward tandem ice model on pier -----	192
86.	Bow view of rear tandem ice model on pier -----	193
87.	General results second tabular ice flow experiment, 2 October 1977 -----	194
88.	General results fourth tabular ice flow experiment, 6 November 1977 -----	195
89.	General results fifth tabular ice flow experiment, 10 December 1977 -----	196
90.	Local ice ablation rate: 2 October 1977 -----	197
91.	Turbulent flow Stanton number vs. Reynolds number -----	198

92.	Turbulent flow Stanton number vs. Prandtl number ---	199
93.	Boundary layer profile, 6 November 1977 -----	200
94.	Forward boundary layer profile, 10 December 1977 ---	201
95.	After boundary layer profile, 10 December 1977 -----	202
96.	Ice interior temperature profile, 6 November 1977 --	203
97.	Histogram of ripples along ice, 3 October 1977 -----	204
98.	Histogram of ripples along ice, 10 December 1977 ---	205
99.	Histogram of ripples along ice, 27 April 1978 -----	206
100.	Time interval 1; solid line represents theoretical calculations and data points * experimental -----	207
101.	Time interval 2 -----	208
102.	Time interval 3 -----	209
103.	Time interval 4 -----	210
104.	Time interval 5 -----	211
105.	Time interval 6 -----	212
106.	Wake temperature profile, 10 December 1977 -----	213
107.	Ice-water interface -----	214
B-I.	Ice interior temperature program -----	105
B-2.	Program for minimum 'S' value -----	106

LIST OF TABLES

I.	Naval Postgraduate School Water Channel Characteristics -----	27
II.	Melt of Second Rectangular Ice Model -----	30
III.	Regression Rates of Second Rectangular Ice Model -----	30
IV.	Specifications of Ice Model Container -----	37
V.	Summary of Results -----	67
VI.	Comparison of Ripple Data Measurement -----	74
B-1.	Nomenclature -----	99

ACKNOWLEDGMENTS

Reflecting back over this two year Glacial Ice Project, we have come to the realization that we should have kept a record of all those that contributed their time and effort to make this an enjoyable and rewarding endeavor. Since each test required the coordination of at least six departments or agencies, the record would be lengthy indeed.

We have been fortunate and privileged to have Distinguished Professor Allen Fuhs as our Thesis Advisor, who was also a major force behind the Glacial Ice Project. The debt of gratitude owed to him for his professional counseling and personal friendship is immeasurable.

Several other professors at NPS were an integral part of the Glacial Ice Project Interdisciplinary Team, and their areas of expertise certainly broadened our learning experience through our association with them. They are: Robert Bourke and Warren Denner of Oceanography, Russel Stolfi of National Security Affairs, and Peter Wang of Mathematics.

The complex Glacial Ice tests in Monterey Bay would have been impossible without the knowledgeable support of The NPS Public Works Department. A special note of appreciation goes to Mr. Woodrow "Woody" Rienhart, who developed the ice model launch and recovery rigging and kept us all out of trouble with his rigging experience.

We are most appreciative of the constantly superior technical support rendered by the Mechanical Engineering Laboratory personnel. Whatever we envisioned, their ingenuity made it a reality. A special thanks goes to Mr. Thomas Christian who developed the entire electronics package for the test series.

Throughout the test series we received the closest possible cooperation and support from Captain Woodrow "Woody" Reynolds and his crew aboard the R.V. Acania. If they didn't have what we needed on hand, they always devised a way to get it.

The launch and recovery site for the tests was the U.S. Coast Guard Pier in Monterey. The Coast Guard came forth with equipment and personnel and a high degree of cooperation without which the tests could not have been safely accomplished.

We sincerely appreciate the professional and personal interest and work applied unselfishly to the Project by Mrs. Vicky Culley and her staff in the Mechanical Engineering Administrative Office. They cheerfully handled countless memos, letters, schedule changes, and meetings that continually revolved around the Project. They always knew where and when to make those "quick phone calls" that made a difference.

Finally, we would like to express our sincerest appreciation to our wives, Joyce and Jackie, for their unrelenting

support, understanding and encouragement throughout our studies at NPS.

This research was funded in FY77 and FY78 by the Naval Postgraduate School Research Foundation.

I. INTRODUCTION

A. JUSTIFICATION FOR STUDY

There has been significant interest in recent years concerning the movement and deterioration of the large ice bodies that drift from the regions of the Arctic and Antarctic to the warmer waters of the Northern and Southern Hemisphere. The United States Navy in particular has been concerned about the impact these icebergs have on the temperature, density, and salinity of surrounding waters. Changes in these characteristics result in significant modification of the speed of sound through the water, which in turn complicates the problem of submarine detection, submarine navigation, and bottom navigation. The Navy and Coast Guard want the capability to predict with some degree of certainty the "life" of an iceberg and thus how it will affect surface ship operations over a period of time. In addition, as the need for additional sources of crude oil expands, offshore drilling in near-arctic regions surely will necessitate the movement of an iceberg by artificial means to avoid drifting into a drilling rig. How far to push or pull the iceberg, the power required, and the effect on the iceberg as a result of this movement are questions that must be dealt with before such an undertaking. A most important interest in iceberg deterioration, is the possibility of supplying water from icebergs to the

extremely arid regions of the world. A discussion of this area is given in Appendix A of this thesis.

II. BACKGROUND OF STUDY

This thesis concerns a study conducted by the Naval Postgraduate School (NPS) in conjunction with the Naval Research Laboratory (NRL) on the ablation of ice bodies moving thorough seawater. Relatively large (16' x 4' x 1.5') ice models were manufactured and moved through a body of salt water (Monterey Bay, California). In addition, smaller models were placed in a laboratory flow channel for experiments and analysis. The ultimate goal was the ability to predict the overall ablation rate of an ice body moving through seawater. The prediction should be verified by comparing the experimental results for this thesis with ablation theory previously published by Owen Griffin [1,2] of NRL.

A first important step in the study was to analyze the scaling problem relating a large iceberg (15,000' x 2500' x 700') to a much smaller model. For the tests in Monterey Bay, the size of the model was constrained by manufacturing, crane, and transportation facilities available. In addition, for the experiments in the flow channel, the model size was limited by the flow channel equipment at NPS. The scaling is important because the experimental results are more valuable if the information can be extrapolated to a full-scale iceberg. The physical effects of the ice moving relative to the seawater (i.e.: shape change, ripple

effect, and wake temperatures) were examined. The thermal boundary layer between the ice and water was measured and compared with that theoretically predicted. Finally the heat transfer through the ice was analyzed by comparing temperature profiles in the ice over a period of time with those predicted from a solution of the equations governing transient heat transfer.

III. ICE MODEL SCALING AND INITIAL LABORATORY TESTS

A. GENERAL

The problems encountered in modeling a large ship for laboratory water channel experiments are also inherent, but to a greater magnitude, in modeling a large ice body. This is due to several factors, the most predominant being the immense size of the ice bodies to be modeled coupled with the low speed of transport (1.0 kt). Also resolving the hydrodynamic requirements with those of the heat transfer analysis to realize an acceptable model from which melt rates can be extrapolated to the full size ice body is also an important consideration. Water channel and towing tank modeling in general are discussed thoroughly in Chapter 7 of ref [3], and modeling particular to ice bodies is discussed by Murphy [4] and Griffin [1,2]. Murphy discussed the methods used to determine towing forces and mass loss during transit, and Griffin treated the heat transfer problem specifically to predict ablation rates of large ice bodies.

B. HYDRODYNAMIC REQUIREMENTS

Two well-understood dimensionless groups of variables are commonly used to relate the forces on a body moving through a fluid. These are:

$$\text{Reynolds number (Re)} = \frac{VL}{\nu} = \frac{\text{inertial effects}}{\text{viscous effects}} \quad (1)$$

$$\text{Froude number (Fn)} = \frac{V}{\sqrt{gL}} = \frac{\text{inertial effects}}{\text{gravity effects}} \quad (2)$$

The Reynolds number is important in defining whether a fluid over a body is laminar or turbulent, a fact that has implications in both towing force and heat transfer analyses. Since the kinematic viscosity (ν) is a property of the fluid, the only variables for Reynolds number which can be easily controlled by the experimenter in ice model testing are the velocity of the fluid (v) and the characteristic length of the model (L). For ideal modeling, the Reynolds numbers of the model and prototype should be identical to assure the same laminar or turbulent flow conditions. This means that a much smaller model must move through the fluid at a very high velocity. The high speed of the test fluid, however, is in direct conflict with the Froude number which is used in determining residuary resistance of a prototype. In addition, the Froude numbers of the model and prototype should be identical for ideal modeling. Note that the Froude number also has only fluid velocity and model length as independent parameters.

The solution commonly used in ship modeling for the conflicting Reynolds number - Froude number requirements is to scale the velocity and model size to satisfy Froude number similitude. Reynolds number scaling is unavoidably violated. However, models are tested at either moderately high Reynolds numbers (10^6) to assure natural transition to

turbulent flow over forward regions of the model or with the use of artificial boundary layer trip mechanisms placed so as to stimulate transition at the predicted natural transition point on the model.

C. HEAT TRANSFER ANALYSIS REQUIREMENTS

Griffin [1,2] at NRL proposed a heat transfer model for a large glacial ice body moving through seawater with turbulent flow. In Griffin's model the local turbulent melting rate is given by:

$$\xi_{\text{TURB}} = D St_{h,\text{TURB}} \quad (3)$$

where:

$$\xi_{\text{TURB}} = \text{Local turbulent melting rate (m/s)}$$

$$D = \text{Stefan number parameter determined by:}$$

$$D = \frac{A}{1 + B} \quad (4)$$

and:

$$A = \text{Seawater Stefan number} = C_{PF}(T - T_F)M^{-1}$$

$$B = \text{Ice Stefan number} - C_{PS}(T_F - T_O)M^{-1}$$

$$St_{h,\text{TURB}} = \text{Local turbulent Stanton number} \quad (5)$$

where R is the ratio of interfacial heat transfer with and without melting; R is assumed to have the same value in laminar as well as turbulent flow.

The local turbulent Stanton number on a flat plate is:

$$St_{h,REF} = \frac{Nu_x}{Re_x Pr} = \frac{.0297 Re_x^{-1/5}}{1 + 1.48 Re_x^{-1/10} Pr^{-1/6} (Pr-1)} \quad (6)$$

By substituting eq. (6) into eq. (5), and then into eq. (3), the variables affecting the local turbulent heat transfer rate can be seen as:

$$\xi_{TURB} = DR \left[\frac{.0297 Re_x^{-1/5}}{1 + 1.48 Re_x^{-1/10} Pr^{-1/6} (Pr-1)} \right] \quad (7)$$

Since Prandtl number (Pr) and Stefan number (D) are properties of the seawater and ice, both numbers are the same for model and prototype. Likewise R, which is dependent on the properties of ice and the solid-liquid phase transformation, is also invariant between model and prototype.

For ideal modeling:

$$\frac{\xi_{model}}{\xi_{prototype}} = 1 \quad (8)$$

From eq. (7) it is obvious that agreement between Reynolds numbers of the model and prototype is paramount for ideal modeling as stated by eq. (8).

From the above consideration, model testing of ice bodies is limited to a regime of Reynolds numbers and Froude numbers as shown in Figure 1. The points indicated on the figure are for experiments that will be discussed later in this chapter and in succeeding chapters.

D. WATER CHANNEL FACILITIES AT THE NAVAL POSTGRADUATE SCHOOL

The Naval Postgraduate School has several water channels which are pictured in Figures 2-5. The characteristics of each channel are summarized in Table I. Since buoyancy was considered an important factor in the heat transfer modeling analysis, the water tunnel shown in Figure 2 was eliminated as a testing facility. The water channel in Figure 3 was also eliminated because of the extensive modifications required to obtain a uniform velocity profile over the width of the channel. The remaining two water channels were utilized; however, their relatively small size prohibited the achievement of Reynolds numbers and accompanying turbulent flow conditions equivalent to those on a large ice body. The inability to achieve these conditions was a direct result of the conflicting requirements of high water channel velocities (2-4 ft per sec) and long model lengths (3-6 ft) necessary for moderately high Reynolds numbers and the low velocities needed for satisfactory Froude number scaling.

Large water channels, similar to the new Environmental Protection Agency water channel in North Carolina, with

dimensions of $L = 80$ ft, $W = 8$ ft, and $D = 4$ ft, would allow the testing of models large enough to achieve a more satisfactory scaling of Reynolds number, geometric size, and velocity. This scaling would be achieved by virtue of the relatively long models (8-16 ft) that could be tested at the relatively low velocities (0.1 - 0.5 ft per sec) required. However, the time, expense, and coordination involved in conducting experiments remote from NPS were deemed prohibitive; therefore the decision was made to conduct a series of large scale model tests in Monterey Bay adjacent to NPS. The details of the experiments in the bay are discussed in Chapters IV-VI.

A review of literature dealing with large ice bodies revealed no experimental data on melt rate, shape change, or regression rates of fresh water ice moving through seawater. Therefore, in order to gain at least a qualitative understanding of what these characteristics were, a series of model tests were conducted in the NPS water channels.

E. INITIAL LABORATORY EXPERIMENTS

The water channel selected for the initial tests is pictured in Figure 4 with characteristics listed in Table I. The size of the ice models was selected to avoid both blockage and side and bottom wall flow interference in the channel.

Four rectangular pieces of ice were constructed with overall dimensions of $L = 8.0$ in, $W = 1.5$ in, and $D = 1.3$ in,

TABLE I

Naval Postgraduate School Water
Channel Characteristics

Figure No.	Test Section Dimensions L, W, H (in)	Velocity Range ft/sec	Re
2	16/4/8	0 - 30	10^7
3	96/48/5	0 - 0.5	10^5
4	36/12/16	0.2 - 3.0	10^6
5	36/24/8	0 - 1.0	10^5

thus achieving a satisfactory ratio of channel width to model width of 10:1. The models were frozen in a standard freezing compartment at a temperature of 10°F. A wire restraining device was frozen into the body of the model for handling during testing. To test the effect of a streamlined shape during identical flow channel conditions, one model was constructed with all sides sloping at 30 degrees from the vertical. Overall dimensions at the top surface were $L = 9.7$ in, $W = 3.7$ in, and $D = 1.2$ in. The ratio of channel width to model width for this model was a less satisfactory 4:1; however, the low channel water flow velocity virtually precluded any significant wall interference.

Each model test was similar and consisted of transferring the model from the freezing compartment to a scale immediately above the flow channel where the model was weighed and photographed simultaneously in the side view. The model was lowered into the flowing water and allowed to float naturally. Directional control of the model was accomplished by attaching the model restraining device to a cross-beam over the channel. At regular intervals (1 min), the model was removed, weighed, and photographed until the restraining device separated from the model. Dyes were frozen into the models, or, alternatively, were injected in front of the model for visualization of the flow patterns. In four out of five tests conducted, the data on weights of the receding

models, air and water temperature, flow velocity, and regression rates at several areas of the models were noted. The total time in water for each model was as follows:

- (1) 2 min/50 sec, (2) 2 min/30 sec, (3) 3 min/30 sec,
- (4) invalid (due to hookup difficulties), and (5) 2 min/30 sec.

F. WATER CHANNEL TEST RESULTS

The first four models melted through a series of shapes similar to those illustrated in Figure 6. The second model tested is shown in Figure 6; results of the melting are given in Table II. The rates of regression at three selected surfaces for the model in Figure 6 are given in Table III.

The frames of Figure 6 are side views with the front of the ice oriented to the right of the photograph. The streamlined ice model was the fifth to be tested. The sequenced melting shape configuration for this model is shown in Figure 7 with similar orientation. It was noted that despite the significant geometric differences between the streamlined model and the four previous models, the melting configuration is practically identical. The regression on the front, bottom, and rear of the models can be seen in Figures 6 and 7 which clearly illustrate the area of highest regression as that on the bottom, approximately three-tenths of the model length from the front. The laboratory conditions included relatively small Reynolds numbers (approx. 10^4) compared with the large numbers

TABLE II

Melt of Second Rectangular Ice Model

(See Figure 6)

<u>Photo Frame</u>	<u>Weight (g)</u>	<u>Time (sec)</u>
Upper	152	0
Upper Middle	92	60
Lower Middle	49	120
Lower	15	150

Air Temperature - 23°C Water Temperature 21.3°C

Flow Velocity - 0.55 ft/sec

TABLE III

Regression Rates of Second Rectangular Ice Model

(See Figure 6)

Average Rates for 120 Seconds

Rear	Bottom (neck)	Front
0.10 $\frac{\text{mm}}{\text{sec}}$	0.16 $\frac{\text{mm}}{\text{sec}}$	0.13 $\frac{\text{mm}}{\text{sec}}$

(approx. 10^9) associated with large Atlantic ice bodies. Given these small Reynolds numbers achieved in the laboratory, it was concluded that the flow conditions in the laboratory were largely laminar and that the decisive necking effect observed was associated with the reattachment of the laminar boundary layer initially separated from the model by the sharp corners of the blunt bow.

For the melting observable in Figures 6 and 7 along the profile surfaces of the models, the Nusselt numbers, which measure the effectiveness of heat transfer, can be calculated to show this effectiveness at any distance along the profile surface. Figure 8 shows a plot of Nusselt number as a function of length along the ice model. The plot shows a well-defined region of intense heat transfer at a distance of approximately $2D$ (D = Depth) from the front of the model and an accompanying decay of melting at approximately $3.5D$ from the same point. A representative theory for laminar flow on a flat plate with constant surface temperature is also shown on the plot in contrast to highlight the empirical results observed in the laboratory.

To explain the high melting rate in the forward third region on the models, the following hypothesis is proposed: Due to the initially sharp corner on the model, the flow separates from the model as it passes the corner point. In the region $0 - 2D$, there occurs a recirculating flow with reattachment near $X = 2D$. As is well known, the area where

reattachment occurs is a region of high heat flux as analyzed by Meyer [5] and Köseman [6]. Figure 9 illustrates this hypothesis.

An alternate hypothesis involves a trapped vortex filament as shown in Figure 10. The sense of the vorticity is shown by the arrows and follows the customary right-hand rule. The vorticity originates because of the flow separation from the blunt bow. Initially the vorticity is shed; but as the ice ablates, the vortex filament becomes trapped. Due to the vorticity, the warm channel water is circulated close to the ice resulting in large temperature gradients and accompanying high heat flux. The observations made during the model experiments were consistent with either the reattachment or trapped vortex filament hypothesis.

G. CONCLUSIONS

The normal problem of resolving the conflicting requirements of Reynolds number and Froude number scaling in modeling ships is magnified when applying standard modeling techniques to large ice bodies. This difficulty in modeling is primarily due to the extremely large size and low transport speed of these full-size bodies. The high Reynolds number required for the model is necessary to assure turbulent flow and to minimize the difference in theoretical melt rate between the small-scale ice model and full-size ice body. The only practical controlling variables available in developing the model are the size of the model and the

velocity of the water. The flow separation around the frontal corners of small models results in an extremely high heat flux and accelerated melting rate at the point of reattachment. This severe melting tends to mask all other characteristics that could be determined from such a small model. The test results indicated that large scale model testing in Monterey Bay, despite the lesser controllability of environmental conditons, was needed in order to determine more accurately the melt-rates, shape changes, and other characteristics of a full-scale ice body underway in seawater.

IV. LARGE-SCALE ICE MODEL EXPERIMENTS IN MONTEREY BAY

The following is a discussion of the ice model size and shape determination, freezing container design, freezing technique, and general test procedure and a summary of each test conducted in the Bay. Specific data results and theoretical correlations from the various tests are presented in Chapter VI.

A. SIZE AND SHAPE DETERMINATION OF MODEL

Several major considerations of both scientific and practical nature were important in determining the minimum and maximum size of the ice body model to be tested in Monterey Bay. The controlling minimum dimension was the model length, which must be sufficient to achieve natural transition to turbulent flow at speeds of 1-2 ft/sec ($Re \ 10^6$). The model required sufficient volume to withstand the following test conditions: a one-hour loading and transit time (20 mi) from the vendor to the launch site on an open truck with minimal insulation, a second hour period at the launch site for testing preparations and launch, a 30-minute underway period in the Bay, and recovery from the water intact for examination of resulting changes in physical characteristics. The maximum size of the model was limited primarily by the size of the freezing compartment which was the only large compartment available in the immediate

geographical area. However, other factors such as the load capacity of a flatbed semi-truck, pier side space restrictions, the available crane lifting capability, and the maneuverability of a boat with ice in tow within the restricted harbor were also important in determining the maximum size. The utmost consideration throughout the development of this previously untried test series was the complete safety of all personnel during the tests.

The model shape was desired to simulate a tabular Antarctic iceberg similar to those that continually break off from the ice shelves and drift Northward. These icebergs have considerable length as compared to width and depth and thus have good longitudinal hydrodynamic stability for towing. The ends of these icebergs are blunt and have a flat table-top appearance above the waterline. The tabular icebergs are readily duplicated in shape using an easily manufactured rectangular container.

The result of the foregoing size and shape considerations was an ice model with dimension of $L = 16$ ft, $W = 4$ ft and $D = 1.5$ ft. This particular size and shape satisfied all of the requirements and was used unchanged throughout the entire series of experiments conducted in Monterey Bay.

B. CONSTRUCTION OF THE ICE MODEL FREEZING CONTAINER

The container was manufactured by a local vendor from galvanized steel sheeting with welded seams. The

specifications for the container are listed in Table IV, and the container is pictured in Figures 11 and 12. Sufficient integral bottom support structure was included to facilitate the lifting of the 6000 lb. ice model and test accessories. Removable plugs were installed to allow flooding of seawater into the container during launching and draining of this water after launch of the model. This simple design proved successful requiring no modifications throughout the test series.

C. ICE MODEL CONSTRUCTION

For the first two experiments conducted in Monterey Bay, the container was placed in the vendor's freezing compartment, filled to the 18-inch level with demineralized water (18 ppm dissolved solids), and frozen as a single layer. Prior to filling with water, the towing bollard, seen in Figure 13, was suspended over the container centerline, 48 inches behind the front wall, with the bollard base 9 inches above the bottom for freezing into the ice. The bollard position was determined to afford maximum lateral towing stability, while remaining intact in the ice during the course of the test with rapid melting of the front and bottom surfaces of the ice. This position also precluded any hydrodynamic interference with the water flowing past the ice and the subsequent masking of natural physical characteristics by this flow interference.

TABLE IV

Specifications of Ice Model Container

1. Dimensions (bottom)

Length - 16 ft

Width - 4 ft

Height - 1.66 ft

2. Slope of Sides

Seven degrees out on all sides from bottom.

3. Material

Sides - 12 GA galvanized mild steel.

Bottom support structure - mild steel of
sufficient strength to support 6500 lbs.

4. Drain Plugs

Install two 2" dia drain plugs on center line
bottom of front and rear sides.

The size of the bollard vertical post and the horizontal base plate were designed to minimize the towing stress concentrations on the ice. This was accomplished by distributing the towing forces over a wide area in both horizontal and vertical planes, without significantly weakening the ice at the critical vertical lateral lane passing through the bollard installation point. The bollard protruded above the ice, as pictured in Figure 12, and also served as an anchoring point for instrumentation during the tests.

Two problems developed from freezing the ice as a single 18-inch layer. First, the expansion of the ice during freezing resulted in a large upheaval of the top surface as the core solidified. The upheaval of the ice was accompanied by large vertical fissures up to one inch in width on the surface and extending several inches into the ice at some points as shown in Figure 12. Second, as a result of the upheaval, the effective freeboard (distance from top surface to waterline) was significantly lowered allowing seawater to flow over the top surface of the ice. The result was rapid erosion of the upper surface of the bow and fissured areas with premature disintegration of the model as shown in Figure 14.

To eliminate the model's top surface upheaval and low freeboard, two modifications were made to the model construction technique. First, the ice was frozen in a series of layers 1-2 inches in depth to minimize the extreme expansion

and subsequent fissures. Second, a hollow wooden box (Archimedes box) was frozen into the ice immediately behind the bollard and at the same nine-inch depth. The Archimedes box, which is identified here as the core box, reduced the weight-to-volume ratio of the model and increased its freeboard 1.5 inches. The core box and the installation are shown in Figures 15 and 16. The combination of layered-freezing and flotation box installation resulted in a hydrodynamically stable, non-fissured, model with sufficient freeboard for testing as shown in Figure 17.

The addition of a small bollard on the rear of the core box improved the waterborne handling of the model. Furthermore the box served as a reference centerline and anchoring point for test instrumentation. The only further modification made to the model throughout the remainder of the test program was to include the towing bollard as an integral part of the core box as shown in Figure 18. The revised method of holding the bollard resulted in a weight savings of approximately 25 lbs, while reducing the quantity of foreign material frozen into that area of the model. From all considerations ranging from transportability to hydrodynamic similitude, the model was satisfactory for the test series.

D. GENERAL TEST PROCEDURE

The test procedure described below is typical of the series of experiments. Specific deviations from this

general procedure are described in the summary of each experiment later in this chapter.

Approximately two weeks prior to each experiment, the ice container was delivered by the Naval Postgraduate School Public Works Department to Growers Ice, Salinas, California. The container was placed in a freezing tunnel and filled with a 1 - 2 inch layer of demineralized water and allowed to freeze. Once the layer was frozen, the tunnel was opened and allowed to warm to outside ambient temperature, and an additional layer of water was added over the frozen ice for freezing. This process was continued to the 9-inch level at which time the core box, bollard, and thermocouples were installed. The process was then continued to the 18-inch level with the model components firmly frozen in position. The average temperature of the tunnel during freezing was 0°F, and the total time to complete the freezing process was 10 - 12 days. The model was further cooled to minus 18 - 20 °F twenty-four hours prior to pickup in order to inhibit melting during the transit and testing preparation period as previously discussed.

In order to exploit the early morning quiescent wind and sea conditions, to avoid marine traffic interference, and to minimize the melting by direct sunlight, the tests were conducted between 0700 and 1100. The ice was brought to the launching site at the U.S. Coast Guard Pier, and launch preparations were made. Launch preparations included

inspection of ice for fissures, dimensional measurements, hookup of instrumentation, and attachment of towing cables and lifting rigging as shown in Figures 11, 12, 16, and 18. At launch time the entire assembly was weighed and lowered into the water as pictured in Figures 19-22. As seawater flowed into the container, the assembly was lowered slowly by the crane until the buoyant ice model floated freely as seen in Figure 23. Connections were made to the towing boat, the model pulled clear of the rigging, and the underway portion of the experiment commenced as pictured in Figure 24.

Primarily for safety purposes, considering that the tests were to be conducted in a restricted harbor, the towing vessel for the first experiment was a Coast Guard patrol vessel as shown in Figure 25. All subsequent tows were conducted utilizing a Boston Whaler with a small outboard motor pictured in Figure 26. A wire bridle connected both arms of the towing bollard to a tow rope, and the thermocouple wire bundle was streamed parallel to the tow rope as illustrated in Figure 27. The ice was towed at an average speed of 1 knot (1.78 ft/sec); the speed was determined using a Marine Advisor Ducted Current Meter and Readout, shown in Figure 28, which was suspended on a rigid arm from the towing boat. The model was towed for approximately thirty minutes in a "race track" shaped pattern approximately 600 yards (.34 mi) in length on a side. The

actual time of each tow varied, with the object being to have the model underway for a sufficient period to allow the full development of surface ablation characteristics, while maintaining adequate structural strength for recovery at the pier. During the tow, temperatures of the ice interior, ice-seawater boundary layer, and model wake were recorded.

Recovery was accomplished by positioning the ice model in a web cargo net with a tubular-steel bottom frame and raising the entire assembly onto the pier as sequenced in Figures 29-31. The assembly was weighed as before to determine the total mass lost during the test. Once on the pier, the model was photographed thoroughly, surface ablation characteristics noted, and overall dimensions recorded. Subsequently the ice was broken for disposal and recovery of the core box and thermocouples.

E. SUMMARIES OF TESTS IN MONTEREY BAY

The following sections are brief discussions of each test conducted in the Bay. The discussion includes details of deviations from the general test procedure and evolution of the test procedure as experience was gained on each experiment.

1. Test No. 1, September 23, 1977

The ice was transported from the vendor to the launch site after a four-day freezing period as a single large block. The characteristic "hump" and fissures previously

described were present as a result of the freezing technique. A large wooden reference grid was attached prior to launch as seen in Figure 12; the grid provided a reference for measuring regression of the ice surface. The container was placed in the water, and the ice floated free and was taken under tow as pictured in Figure 32. The large towing vessel had difficulty maintaining the desired speed of 1 knot. The low freeboard and numerous fissures allowed water to flow over the top surface resulting in premature breakup of the ice and detachment of the towing bollard while underway.

The bollard and reference grid were recovered; however, the ice was not recovered. Therefore, significant data were not obtained. Though this test was largely inconclusive from a scientific view, the photographs obtained and the experience gained in the launching and towing procedure were useful for future experiments.

2. Test No. 2, September 26, 1977

The ice was removed from the freezing compartment after a three-day freezing period as a single layer as before. However, three days were apparently insufficient to solidify the model completely. Ice formed on the outside with water on the inside. The water was covered by a thin layer of ice. The thin layer ruptured prior to arrival at the launch site as illustrated in Figure 33. The overriding point which is apparent from Figure 33 is that the center of the ice did not have sufficient time to solidify. The second experiment was scheduled only a few days after the first experiment in

order to obtain additional information for presentation at the First International Iceberg Utilization Conference on October 3, 1977.

The container with the partially melted ice was returned immediately to the vendor to resume freezing.

3. Test No. 3, October 3, 1977

The ice model for Test No. 3 was frozen during a five-day period as a single layer. Note that the ice for Test No. 3 was in part the same as for Test No. 2. The "hump" and fissures were again present on the top surface. The reference grid was attached, and the model was launched. The model freeboard was slightly higher as pictured in Figure 34 but was still insufficient to prevent water flow over the top surface. The towing vessel used was a 16-foot Boston Whaler with an outboard motor which had little difficulty maintaining the desired speed. Underway photographs were obtained; however, the reference grid could not be used to determine regression rates over the length of the model because of the relatively small differential in these rates and the inability to obtain photographs directly over the ice.

The ice model was recovered successfully for the first time as illustrated in Figures 35 and 36. The recovery net shown in Figures 35 and 36 did not have the bottom tubular steel frame pictured in Figure 30. The tubular frame, which was included for later tests, spread the net over the width of the model. Also, the frame submerged

the net in the water to ease the positioning of the model in the net for recovery. In addition, the frame distributed the lifting forces over the bottom of the model, thus minimizing loads applied to the delicate sides and corners.

The model was placed on the pier where the weight, dimensions, and surface ablation characteristics were recorded. Numerous photographs were taken similar to Figure 37 which illustrate the erosion caused by the seawater flowing through the fissures on the model. Two significant surface features were noted: First, a heavily eroded cavern-shaped area on the bow as shown in Figure 38 and, second, as illustrated in Figures 39 and 40, a series of well-defined, vertical, periodic ripples extending the length of either side of the model. These two surface characteristics also were observed in subsequent experiments and are discussed with other test results in Chapter VI.

One surface characteristic that was not present on this and subsequent tests was the decisive "necking" observed on the laboratory models. However, if this process did occur, it was only present in the first few inches and then was so insignificant that its effect was masked by the ripple system on the model. An amplifying discussion of this surface characteristic is presented in Chapter VI. This test was judged successful in that a complete cycle from launch to recovery was accomplished along with observations of the ice model dimensions and weight which were

measured as a result of the cycle. However, modifications to the freezing technique, increased freeboard, and improvement of the useless reference grid were necessary for the next model test. In addition, temperature sensing devices and ripple measuring techniques were required to increase the amount of experimental information obtained.

4. Test No. 4, November 6, 1977

Test No. 4 marked the first attempt to obtain comprehensive data on the ice interior temperatures, ice-seawater boundary layer temperatures, and ripple wavelength. The model was frozen using the layered technique previously described, with the bollard, core box, and thermocouples frozen at the nine-inch level. Figure 41a is a top view of the model illustrating the placement of these devices with an amplifying pictorial view in Figure 42. The numerals in Figure 41a denote the amplifier channel for that particular thermocouple.

The thermocouples were 1/16 inch diameter Omega fast responses Copper-Constantan Type T with beaded sensory tips. Five of these thermocouples were bonded together near the tips to form an array of five thermocouples spaced at 1/16 inch intervals (channels 11-15). The array was mounted on the bollard (Figure 41b) and placed in the ice with the outermost thermocouple 1.5 inches from the side surface. The purpose of the array was to indicate both the interior ice temperature profile as the side receded towards the array and the ice-seawater boundary layer profile as the array became exposed to seawater.

Interior ice temperatures were recorded on channels 16-20 (Figure 41a). The output of a particular thermocouple was selected by a channel selection and amplified with accompanying electronic reference junction (zero degrees Centigrade) as shown in Figure 41b. The output of the digital voltmeter was recorded by voice using a tape recorder. The data were later transcribed and converted to °C using the thermocouple conversion tables.

The model was launched without incident and, as pictured in Figures 43 and 44, had a completely flat top surface and sufficient freeboard. At regular intervals all thermocouples were read and recorded. The model was towed until all five thermocouples in the array indicated ambient seawater temperature and significant undercutting was observed as in Figure 45. At that point the model was recovered without difficulty. Once clear of the water, the extent of the differential in melt rates between submerged and above-water surfaces readily became apparent as shown in Figures 46 and 47. Close examination of Figure 47 shows the exposed array protruding down from the top surface.

Once on the pier, the various layers comprising the model were very well defined as shown in Figures 48 and 49, as were the ripples and heavily eroded bow section noted in the previous experiment. The ripples were measured by pushing a multi-fingered contour gage against the surface until the fingers conformed to the surface shape. The contour was traced onto a strip-chart paper in succession

with the end result being a profile of the ice surface drawn on the paper. Relative depths were measured using a metal reference frame prepositioned on the centerline of the core box as illustrated in Figure 50.

Test No. 4 was considered successful, although the ripple measurement method was cumbersome and needed improvement. The effect of the ice layering on the regression rates and ripple formation was a question. In the next test the freezing layer thickness was increased to three inches to evaluate any dependence on ice layer thickness. In addition, the rapid regression at the ice-seawater boundary layer with the subsequent exposure of the array resulted in difficulty of monitoring these channels with the current recording equipment. For future tests a single thermocouple with direct output to a portable strip-chart recorder was utilized to collect boundary layer temperature profile data.

5. Test No. 5, December 10, 1977

The alternative 3-inch layer freezing technique was applied to this model with adverse results. The increased net expansion of the ice buckled the bottom and the sides of the core box breaking water tight seals. Broken seals allowed water to flow into the box with subsequent freezing. As a result the buoyancy of the box was reduced. The top of the core box was opened at the launch site, and the ice within the box was chipped out as shown in Figure 51. The box was resealed, and the model was launched. Although the

bottom surface of the box was buckled upward reducing volume, sufficient buoyancy remained to provide an adequate free-board during the test.

The thermocouple arrangement for the ice model is shown in Figure 52. The arrangement was designed to measure boundary layer profiles near the bow stagnation point (Channel 13) and at the indicated side points (Channels 11 and 12). Since only one portable strip-chart recorder was available, the thermocouples were placed accurately at carefully selected distances from their respective receding edges so that they would be sequentially exposed and recorded. The sequence of channels was 13, 11 and 12. The sequence was determined using previous regression rate data. The thermocouples were monitored initially on a digital readout and then transferred to the strip chart recorder when the output approached 0°C. Each channel was switched back to a digital readout when the strip chart indicated ambient seawater temperature.

In addition to the boundary layer, an effort was made to measure the temperature profile across the wake of the model. The purpose of this effort was to determine the extent of cooling experienced by the water flowing past the ice. If cooling proved to be significant, a second ice body towed in the wake of a first would be "insulated" effectively by cooler water; and the melting rate of the second body could be reduced considerably. The temperature measurement was accomplished with an array of seven thermocouples positioned across a bridge between two pontoons as

shown in Figures 53 and 54. The pontoon bridge was pulled behind the ice by a rope attached to the rear bollard on the model. Figures 55 and 56 illustrate the towing arrangement which had the thermocouples positioned one model width (4 ft) behind the ice. A distance of 4 feet was a compromise based on being sufficiently close to the model to detect cooling while remaining clear of the immediate eddies behind the model which could distort overall temperature gradients in the wake. The array measured the wake temperature at a depth of 6 inches, and over a lateral distance 30 inches on either side of the centerline. Thermocouple output was voice recorded from the digital indicator at periodic intervals during the test.

During the underway portion of the test, the added drag of both the pontoon bridge and fouling by floating kelp proved beyond the capacity of the electric outboard motor to maintain desired speed. Thus only 80 percent of desired speed was attained during the test. The lower speed had the effect of decreasing the ablation rate and increasing the time required for the boundary layer thermocouples to become exposed. Although the boundary layer thermocouples eventually became exposed and their outputs recorded, recovery of the model was necessary due to a large crack forward of the core box precluding exposure of the stagnation point thermocouple.

The recovered ice is pictured in Figure 57 where close examination shows the stagnation point thermocouple

tip visible through the ice surface, while the forward side thermocouple tip clearly protrudes through the side of the ice. The crack forward of the core box also can be seen clearly in Figure 57. The bow erosion, ripples, and undercutting were again observed in this test and are pictured in Figures 57-59. These features were less pronounced, however, due to the reduced towing speed. Ripple data were obtained using the same contour gage method. An improved method was under development but not available for Test No. 5. The thicker freezing layers also were well defined, but their effect on the ripple system and undercutting was inconclusive due to the lower speed of Test No. 5.

A matter of practical importance became apparent during this test in that the complexity limitations of the ice model testing were being rapidly reached. The towing vessel which required an operator, line handler, and data recorder/instrumentation operator, plus all the equipment, was running out of room! Also, trying to monitor and record simultaneously, with minimal acceptable accuracy, multiple-point thermocouple outputs on two different instruments was difficult.

The test was viewed as a success despite the problems with the core box, towing speed, and crack development. A larger electric motor was used in future experiments to increase the power available to overcome excess drag. The freezing technique reverted to the original 1-2 inch layer thicknesses. If additional wake temperature data were to

be obtained, the pontoon bridge would require modification so that it would remain exactly behind the ice model and not drift to either side. The pontoon vehicle did not follow in the wake of the ice model. In addition, a second portable strip chart recorder was obtained to reduce the switching complexity when recording multiple-point boundary layer temperature profiles.

6. Test No. 6, April 27, 1978

In addition to the overall test objectives of previous experiments, two additional areas of investigation were considered during this test. The first area was the determination of the effect, if any, of the turbulence created by the towing cable and thermcouple wire bundle on the regression rate of the bow of the model. The second area was the examination of the difference in melt rates at two points on a side ripple.

The ice was frozen using the 1-2 inch layer thickness technique with the core box and thermcouples placed as shown in Figure 60. The box had been repaired from the damage incurred in Test No. 5, and the towing bollard was added as an integral part of the structure of the box. The model appeared in excellent condition at the launch site as illustrated in Figure 61, which also shows the thermcouple positions for this test. The channels were assigned as follows: stagnation point boundary layer (11), bottom surface boundary layer (12), ice center forward (13), forward ripple boundary layer (14 and 15), rear ripple boundary layer (16 and 17), and rear ice center (18).

Previous ripple data measurements indicated the average peak-to-peak wavelength of the ripples was approximately 6 inches. The melting rate varies at different points between the crest and trough of a ripple. The arrangement of thermocouples was an attempt to measure the different melt rates due to a ripple. Two stations were selected where boundary layer profiles previously had been recorded. A pair of thermocouples was positioned at each station with a 4-inch separation. Initially the sensory tips were at identical distances from the receding edge and at equal depths in the ice. Both thermocouples were monitored simultaneously on a real-time basis by a two-channel strip chart recorder. Since the separation was less than one ripple wave length, the position of each tip relative to the ripple was indicated by the sequence of exposure and shape of the temperature profile.

The thermocouples were placed in the ice to achieve the following exposure sequence: stagnation point, forward side station, rear side station, and bottom station. Test No. 6 was the most ambitious attempt at multipoint boundary layer recording throughout the series of tests. However, launching difficulties during the test diminished the thermocouple data. The difficulties began when the ice container was placed in the water and prematurely lowered before the ice could free itself. This resulted in two adverse consequences; first, the thermocouple electrical connections were

flooded effectively nullifying their output, and, second, the ice separated from the container unevenly stern-first putting excessive stress on the forward section; as a result, the forward section of ice broke at a location behind the forward ice center thermocouple as pictured in Figures 62 and 63. The decision was made immediately to disconnect the thermocouple wires from the forward section and continue the test as planned with the remaining section of the model.

The ice model was pushed from the rear rather than towed during this test, as pictured in Figures 64-66, to determine the effect of the towing cable and thermocouple wire bundle on the development of the bow erosion pattern. The wood pushing bar was hinged on either end to allow vertical movement of the model and boat. The bar was bolted with a facing plate to the rear bollard while clamped to the bow of the boat. Two torque lines, running from both arms of the main bollard back to the line handler on the boat, aided in directional control of the model and minimized the torque applied on the rear bollard and bow of the boat. The underway portion of the test was continued until significant undercutting was observed on the model, at which time the ice was recovered as shown in Figures 67 and 68.

Observations of the model on the pier showed that the same bow surface erosion characteristics developed to the same extent on this test as when the model was towed. Although the bow erosion did not have exactly the identical

shape because of its slanted front as a result of the break, close examination showed clearly that the same process of erosion had taken place. The well-defined periodic ripples were present as in previous tests. An improved method of measuring these ripples was utilized as shown in Figures 69-71. A wooden reference frame was prefabricated and positioned in slots on the core box. A Longfellow Linear Motion Position Transducer Model LF-6-101, pictured in Figure 70, was mounted on either rail of the frame and moved the entire length of the frame is illustrated in Figure 71. As the transducer moved along the rail, the position arm moved over the ice surface, and the resulting changes in transducer output voltage were recorded by a strip chart recorder. The end of the chart paper was attached to the transducer chassis so that the transducer moved along the rail at the same speed as the chart paper moved through the recorder. Thus the recorder printed an exact geometrical profile of the ripples over the length of the model.

This test was the last in the series to study a single ice model. The knowledge and experience gained from the series were applied to another test in which two similar models were towed in tandem to determine the effect of the first model on the melting rate and surface regression characteristics of the second. This test and the work leading to it are discussed in Chapter V.

F. COMMENTS

An invaluable store of knowledge and experience on testing large scale ice models underway in seawater was gained as a result of the series of experiments in Monterey Bay. While not every test objective was met on every test, those that were accomplished added to the experience that was nonexistent prior to this series.

One important point was highlighted by the test series. That was the necessity of controlled laboratory conditions for experiments with the wide scope of the tests. The arrangements alone for the ice model, transportation, launch site, boats, equipment, and assistance required the coordination of six different agencies. Add to this the unpredictability of weather, and one soon grasps the extensiveness in preparing for a single test. The complexity involved during the tests in monitoring instrumentation while controlling the boat and model has been previously discussed.

V. TANDEM ICE MODEL EXPERIMENTS

A. BACKGROUND

The ice model test series described in Chapter IV showed that the most intensive melting and subsequent regression occurs at the bow of the model. This rapid melting is a function of pressure gradients due to variation in the local velocity and the higher local temperature gradient profile on the bow of the model. The "cavern"-shaped eroded area on the lower frontal surface of the model is that area at which the higher local velocity and acute pressure gradients are most pronounced, which results in the high melting and regression rate in this portion of the bow. Griffin's [1,2] model showed the strong dependence of melting rate on the differential between the ice surface temperature and the local ambient seawater temperature.

One possible solution to minimizing the pressure and velocity gradients and the ice surface-seawater temperature differential is to tow the iceberg in the wake of a "sacrificial" iceberg. The sacrificial iceberg could shield the rear iceberg by lowering the velocity of the seawater impinging on the bow and also provide a plume of seawater cooled to a lower temperature than the ambient seawater temperature. The former would reduce the pressure gradients on the bow while the latter would reduce the ice surface-seawater temperature differential, possibly resulting in a

substantial reduction of the high regression rate of the rear iceberg.

While the general theoretical heat transfer principles were well-known and understood, previous research in this area with ice bodies underway in seawater was nonexistent. As a concluding experiment for this thesis and an introduction into possible future work, a test was conducted in Monterey Bay consisting of towing two large-scale ice models in tandem on December 10, 1978. The models were an identical pair and similar in size and construction to those in the previous single-model series.

B. LABORATORY TESTS

Due to limitations on time and resources, only one large-scale experiment on tandem-towed models could be conducted for this thesis. In order to obtain decisive results from the large-scale test, a series of laboratory experiments were conducted first on small-scale models utilizing the water-channel pictured in Figure 5. The characteristics of this water channel are listed in Table I. The primary issue to be addressed in these experiments was the distance the second model should be towed behind the first to illustrate most dramatically the "protection" the bow of the second would derive from the presence of the first. Of practical concern was the realization that full-size ice bodies could not be towed so close in tandem that longitudinal variations in their individual velocities could cause

an "accordion" effect which would result in catastrophic collisions between the icebergs.

Froude number scaling was utilized to model the Monterey Bay ice model for the laboratory experiments. In Chapter III it was stated that for Froudenumber scaling:

$$Fn_{\text{model}} = Fn_{\text{prototype}} \quad (9)$$

while eq. (2) showed that

$$Fn = \frac{V}{\sqrt{gL}}$$

with velocity (V) and model length (L) as the controlling parameters. Substituting:

$$\left(\frac{V}{\sqrt{gL}}\right)_{\text{model}} = \left(\frac{V}{\sqrt{gL}}\right)_{\text{prototype}} \quad (10)$$

rearranging;

$$V_{\text{model}} = V_{\text{prototype}} \left(\frac{L_{\text{model}}}{L_{\text{prototype}}}\right)^{1/2} \quad (11)$$

The length and velocity of the prototype (16 ft., 1.78 ft/sec) are known. A freezing container was available with dimensions of L = 13.5 inches, W = 4.5 inches, and D = 2.5 inches for forming the laboratory model. From eq. (11) the model velocity was 0.472 ft/sec. The model Froude number from

eq. (2) was 0.023, thus precluding attached bow waves. The low channel velocity eliminated any possibility of significant blockage or wall interference. Although the width and depth of the model was not scaled exactly relative to the length, their sizes were satisfactory for the laboratory tests since drag of the model was not at issue.

The laboratory models were frozen in a standard freezing compartment for a two day period at a temperature of 0°F. The model was frozen as a single 2.5-inch layer with two wooden handling devices. Two devices were frozen in each model to assure lateral directional stability during the tests.

The laboratory tests were conducted by placing the ice models in the flow channel and allowing them to float using their own natural buoyancy as pictured in Figure 72. Directional control was attained by forcing the wooden handling devices to ride in a slot formed by two guide rails that ran longitudinally the length of the channel centerline. Each test was conducted for a continuous period of two minutes. This two-minute period was determined by placing a single model in the channel for a sufficient period to allow decisive erosion of the bow as pictured in Figure 73. The rear model was placed initially at a separation distance corresponding to one model width ($W = 1.5$ inches), the characteristic model dimension chosen for the tests. On each successive test the rear model was moved incrementally

closer reducing the separation distance. During each test the flow immediately adjacent to the front and rear models was studied by injecting a colored dye in the water in close proximity to the area of interest as shown in Figure 73.

C. RESULTS OF LABORATORY TESTS

The decisive "necking" observed in the initial laboratory experiments was also noted during this series of experiments. This "necking" effect served a very useful purpose during the tandem laboratory experiments by providing a well-defined bow erosion signature for comparing erosion on the two models. Chapter I and Chapter VI describe the "necking" on the laboratory models and the flow characteristics which cause this rapid erosion to occur. The flow recirculation was seen easily with the aid of the injected dye as pictured in Figure 73.

When placed at the initial separation distance of one model-width (W), the rear model bow eroded to exactly the same shape as the forward model bow. The rear model appeared to have derived no substantial benefit from the presence of the forward model. At separation distances of $2W/3$ and $W/2$ the rear model bow eroded in the identical shape of the forward model, but at a slower rate. At a separation distance of $W/3$, the rear model bow eroded in a decisively different manner from that of the forward model as shown in the sequence of Figures 74 - 76. The decisiveness of this change in erosion pattern can be observed further by examining

Figures 77 and 78, which show the bottom surfaces of the forward and rear model respectively. The complex flow pattern between the two models at the W/3 separation distance is shown in Figure 79.

As a result of this experiment in the laboratory, the large-scale tandem-towed model test in Monterey Bay was conducted utilizing the W/3 separation distance between models. Shorter separation distances were not examined due to the practical uncertainties of longitudinal oscillations with resulting collisions mentioned earlier in this chapter.

D. MONTEREY BAY TANDEM TEST, DECEMBER 10, 1978

The models used in the tandem experiment were frozen in identical fashion, utilizing the 1-2 inch layer freezing technique with similar core boxes installed. Thermocouples were not installed in the ice due to the complexity of the experiments in handling two large ice models simultaneously. Since only one crane was available, the models were launched separately (forward model first) and then linked together in the Bay as pictured in Figure 80. The linking was accomplished by two rigid metal rods connected to either arm of the towing bollards that were sized to provide a constant W/3 (16 inch) separation distance between the models.

The models were towed over the same course as in previous experiments utilizing the same Boston Whaler towing vessel as pictured in Figure 81. While the rear model remained behind the lead model for some brief periods (Figure 82), lateral instabilities in the models resulted in lateral

motions and misalignment of the models during the major portion of the experiment as shown in Figures 83 and 84. Attempts at restoring the misalignment by providing a drag force from a following Boston Whaler on the model train (Figure 84) were unsuccessful.

Recovery was initiated after 21 minutes underway when significant undercutting was observed on the lead ice model. The rear model was recovered first, followed by the lead model. Both models were again weighed to determine total net weight lost during the test.

E. RESULTS OF TANDEM BAY TEST

While decisive indications were obtained from the experiment, the results were in a large measure inconclusive due to the nature of the experiment. Weight indications showed that the lead model lost 2750 lbs. and the rear model 2000 lbs. While this large weight loss differential would appear to prove decisively the "sacrificial" iceberg theory, one must remember that the lead model was in the water an additional 36 minutes due to the limited single launch and recovery capability available.

The recovered lead and rear models are shown in their bow view in Figures 85 and 86 respectively. The bow erosion of the rear model is approximately the same as the lead model which would negate the shielding theory provided by the lead; however, the rear model was underway eight additional minutes over the lead in order to link up with the

naturally drifting lead model in the Bay. Additionally, the misalignment resulted in the rear model's bow being exposed to the full flow of the oncoming seawater during the major portion of the test.

The Tandem Bay test procedure can be improved by utilizing two lifting cranes to effect a simultaneous launch of both models and by connecting the tandem models through a lightweight rigid frame to prevent lateral motion between the models. The former would be more expensive and require additional pier space, but the result would be a more accurate reflection of the actual underway mass loss differential between the models. The latter would assist in better defining the bow erosion differential between the models.

VI. EXPERIMENTAL RESULTS WITH THEORETICAL CORRELATIONS

A. GENERAL

The following are discussions of the experimental results determined from the ice model test series described in Chapters III-VI. Comparisons with appropriate theoretical predictions or other experimental results are made including descriptions of the theoretical models and experimental techniques.

B. COMPARISON OF EXPERIMENTALLY MEASURED ABLATION RATES WITH THEORETICAL PREDICTIONS

Griffin developed a model for predicting the ablation rates of icebergs moving through seawater in laminar flow [1]. He modified his model [2] to account for turbulent flow in conjunction with the large-scale ice model experiments conducted at NPS.

The analysis model considers turbulent flow over a flat plate with zero pressure gradient and solves the boundary layer equations for simultaneous heat, mass, and momentum transfer. The two-dimensional problem is reduced to one dimension by integrating across the boundary layer. The phase transformation from solid to liquid occurs under steady-state conditions enabling a coordinate system to be affixed to the melt interface. A constant density is assumed, and the ice is a pure solid phase. Gravity is neglected, thus neglecting the buoyancy effects on the heat

transfer. The model requires inputs for the physical properties of seawater and ice, including the applicable dimensions and free-stream velocity. The properties of ice and seawater are assumed to be constant for the solution.

The graphical results for overall surface regression for three of the large-scale experiments in Monterey Bay are shown in Figures 87 - 89 and summarized in Table V. A comparison of the actual regression rates at three points on the model tested on October 2, 1977, with the prediction from Griffin's Computer Code is shown in Figure 90. The agreement between experimental values and theoretical predictions is good. A plot of turbulent flow Stanton numbers versus Reynolds numbers is shown in Figure 91 for the range of Prandtl numbers typical for seawater. Data points from Table V of NPS experiments are shown again to be in good agreement with the theoretical curves. A similar plot of Stanton numbers versus Prandtl numbers is shown in Figure 92 for a range of Reynolds numbers from laminar to turbulent flow conditions.

The conclusion drawn from the above comparisons was that the Griffin turbulent-flow iceberg ablation model was satisfactory for predicting the ablation rate at various points on the sides an iceberg given the appropriate physical conditions such as ice and water properties, velocity, and water temperature. However, the bow area of the iceberg requires further treatment.

TABLE V

SUMMARY OF RESULTS

ICEBERG TOWING EXPERIMENTS
NPGS, FALL 1977.

TEST NO.	DISTANCE ALONG THE ICE (m)	WATER TEMPERATURE (°C)	TOW SPEED, U (kt)	MELT RATE, V _S (mm/hr)	V _S /U	PRANDTL ^a NUMBER	REYNOLDS ^b NUMBER	STANTON ^c NUMBER
1	3 (9/77)	17	0.9	150	9.0×10^{-5}	7.6	21.0×10^5	4.1×10^{-4}
5	2.4 (12/77)	12	0.78	150	10.5×10^{-5}	9.0	7.8×10^5	6.4×10^{-4}
	4.8			119	8.4×10^{-5}		16.0×10^5	5.1×10^{-4}
	0.15			221	15.5×10^{-5}		4.9×10^4	9.4×10^{-4}
3	2.4 (10/77)	16	0.9	206	12.5×10^{-5}	7.9	10.1×10^5	6.1×10^{-4}
	4.6			206	12.5×10^{-5}		19.4×10^5	5.1×10^{-4}
	0.15			381	23.1×10^{-5}		6.5×10^4	11.3×10^{-4}
4	2.4 (11/77)	13.3	1.42	211	8.0×10^{-5}	8.6	14.9×10^5	4.6×10^{-4}
	4.6			211	8.0×10^{-5}		28.6×10^5	4.6×10^{-4}
	0.15			495	8.0×10^{-5}		9.5×10^4	10.8×10^{-4}

^aPRANDTL NUMBER = KINEMATIC VISCOSITY/THERMAL DIFFUSIVITY *^bREYNOLDS NUMBER = TOW SPEED x DISTANCE/KINEMATIC VISCOSITY *^cSTANTON NUMBER = HEAT TRANSFER COEFFICIENT/(DENSITY x SPECIFIC HEAT* x TOW SPEED)

* Values for Seawater

C. MEASUREMENT AND VERIFICATION OF THERMAL BOUNDARY LAYER PROFILE

The profiles of the water temperature versus distance from the ablating surface for experiment Nos. 4 and 5 in Monterey Bay are shown in Figures 93 - 95. The data on Experiment No. 4 were obtained by recording a digital readout from the thermocouple array described in Chapter IV while the data for Experiment No. 5 were recorded by a single thermocouple output to a continuous strip chart recorder.

Due to the integral solution technique applied across the mass diffusion, thermal, and momentum boundary layers, Griffin's model does not provide predictions for the thermal boundary layer profile. However, an approximate determination of the accuracy of the initial profile slope could be calculated by applying a one-dimensional energy balance across the ice-water interface as shown in Figure 107.

From Figure 107:

$$q_w = \text{heat transfer from water } \left(\frac{\text{cal}}{\text{Sec cm}^2} \right)$$

$$q_i = \text{heat transfer into solid ice } \left(\frac{\text{cal}}{\text{Sec cm}^2} \right)$$

$$M = \text{latent heat of fusion } \left(\frac{\text{cal}}{\text{g}} \right)$$

The energy balance is:

$$q_w = \rho_i V_s M + q_i \quad (12)$$

where

$$\rho_i = \text{ice density } \left(\frac{\text{g}}{\text{cm}^3}\right)$$

$$V_s = \text{regression rate } \left(\frac{\text{in}}{\text{hr}}\right)$$

Also:

$$q_w = K_w \left(\frac{\partial T}{\partial y}\right)_w \quad (13)$$

and

$$q_i = K_i \left(\frac{\partial T}{\partial y}\right)_i \quad (14)$$

where K is the respective thermal conductivity and $\frac{\partial T}{\partial y}$ is the respective initial slope of the temperature profile.

From Ref. [7] at 0°C :

$$K_i = 5.35 \times 10^{-3} \quad \frac{\text{cal}}{^\circ\text{C cm-sec}}$$

$$K_w = 5.33 \times 10^{-3} \quad \frac{\text{cal}}{^\circ\text{C cm-sec}}$$

$$M = 79.77 \quad \frac{\text{cal}}{\text{g}}$$

$$\rho = .9168 \quad \text{g/cm}^3$$

The ice interior temperature Profile - Test No. 4:

From Figure 96;

$$\left(\frac{\partial T}{\partial Y}\right)_i = \frac{1.1 \text{ }^{\circ}\text{C}}{(.0625 \text{ in})(2.54 \frac{\text{cm}}{\text{in}})}$$

From Figure 94;

$$\left(\frac{\partial T}{\partial Y}\right)_w = \frac{6 \text{ }^{\circ}\text{C}}{(.04 \text{ in})(2.54 \frac{\text{cm}}{\text{in}})}$$

From Table V;

$$V_s = 5.9 \text{ in/hr (at } L = 2.4 \text{ m)}$$

Solving eq. (14) and substituting into eq. (12) gives

$$q_w = 0.34 \frac{\text{cal}}{\text{sec-cm}^2}.$$

Solving eq. (13) gives a value of

$$q_w = 0.3 \frac{\text{cal}}{\text{sec-cm}^2}.$$

Reasonable agreement occurs between theoretical and observed results indicating that the measured profile is a reasonably accurate representation in at least the critical initial slope.

D. RIPPLE EFFECTS AND MEASUREMENT

1. General

Throughout the test series, ripples were observed to have formed on the sides of the ice models tested in Monterey Bay. The ripple formation is not unusual as turbulent flows in nature are observed to produce several different types of regular waves, including wind-generated water waves. Carey [8,9], Larsen [10], Ashton and Kennedy [11,12], and Hsu [13] have described and analyzed the occurrence and behavior of regular waves on the underside of river ice covers. These waves are known as ice ripples and can be expected to form at any ice surface exposed to a turbulent water flow, at least when the boundary is receding due to melting. Tatinclaux and Kennedy [14] developed an analytical model for formation of ripples on icebergs.

2. Ripple Effects on Drag

Both heat and momentum are transferred between the ice-water boundary layer and the surrounding flow by means of turbulent exchange processes. In addition, the ripples eventually will become sufficiently high so that the flow will separate near the crest of each ripple. The normal relatively low pressure at the crest will then continue across the rear face of the ripple until the flow reattaches at the frontal face of the next ripple. The large pressure differential across the ripple results in a significant drag force exerted on each ripple. Also there will be

gravity waves generated in the water by the ripples, thus adding to the iceberg drag.

Several methods have been proposed for calculating the composite friction coefficient by Carey [8], Larsen [10], and Uzuner , et. al. [15]. Larsen showed that drag increases almost linearly with ripple steepness (peak-to-peak ripple height divided by ripple length) up to a value of about 0.1 and much more rapidly thereafter. For fully developed ice ripples, values of steepness in a range of 0. - 0.15 are not uncommon. Further, such ripples could increase frictional resistance by 50 - 100 percent.

3. Ripple Effect on Heat Transfer

The formation of ripples at the ice boundary has the effect of increasing the rate of heat transfer at the boundary. The increase in heat transfer is due, first, to the increased hydraulic roughness which affords a larger net area available for heat transfer and, second, to the increased turbulent intensity and flow separation caused by the ripples.

4. Measurement of Ripples on NPS Tests

Chapter IV described the various techniques used to measure the ripples on the sides of the ice models tested in Monterey Bay. From the data gathered, histograms of ice ripple wavelength were constructed and are shown in Figures 97 - 99. From the histograms the average wavelength was determined for each experiment.

Experimental programs conducted at the Iowa Institute of Hydraulic Research on the formation of ice ripples have been reported by Ashton and Kennedy [12] and Hsu [13]. The experiments were conducted on an ice slab of dimensions $L = 40$ ft. and $W = 2$ ft. over a velocity range of 0.30 ft/sec to 2.7 ft/sec. Hsu reported that the average wavelength (λ) is inversely proportional to the mean flow velocity (U) and that the Reynolds number based on wavelength is constant and given by:

$$R = \frac{U\lambda}{\nu} = 6.2 \times 10^4 \quad (15)$$

The standard deviation of the experimental results from this average is 1.1×10^4 .

The average wavelength for each NPS experiment was determined from eq. (15) and compared to the corresponding average wavelength determined from the histograms. The results are listed in Table VI and show good agreement.

E. THEORETICAL PREDICTIONS AND MEASUREMENT OF ICE INTERIOR TEMPERATURE PROFILES

The temperature profile within the ice model was measured during the underway portion of Test No. 4 in Monterey Bay. The thermocouple array discussed in Chapter IV and shown in Figures 41 and 42, was read at specific time intervals for a period in excess of 37 minutes; readings were voice recorded.

TABLE VI
COMPARISON OF RIPPLE DATA MEASUREMENT

DATE:	10/3/77	12/10/77	4/27/78
Velocity (U) (ft/sec)	1.5	1.4	1.9
Wavelength (λ_1) (in)	5.4	6.1	4.4
Wavelength (λ_2) (in)	5.4	5.8	4.7

Note:

λ_1 Wavelength from eq. (15)

λ_2 Wavelength from histograms.

The transient thermal conduction equation for one spatial dimension was solved, and the results were used to correlate the experimental measurements. The equation and development of the solution is given in Appendix B. Included in Appendix B is a Hewlett-Packard-9831-A computer program to generate the theoretical temperature profiles, thermal diffusivity of ice (α), and ice regression rate (V_s).

The comparison of the theoretical and experimental temperature profiles is shown in Figures 100 - 105 for each respective time interval. The theoretical curves represent a best parametric fit with the experimental values by independently varying such parameters as thermal diffusivity and regression rate as described in Appendix B. The resulting theoretical thermal diffusivity and ice regression rate from the best fit condition were $3.0 \times 10^{-7} \text{ m}^2/\text{sec}$ and $2.2 \times 10^{-5} \text{ m/sec}$ respectively. The actual thermal diffusivity of ice determined from Ref. [7] was $5.3 \times 10^{-7} \text{ m}^2/\text{sec}$ for pure solid ice. The actual regression rate, determined by initial and final ice model dimensions for the 37 minutes of underway time, was $3.53 \times 10^{-5} \text{ m/sec}$.

Figures 100 - 105 show comparability between the theoretical and experimental data for temperature profiles within the ice. The theoretical curves and experimental values do diverge to some extent at time intervals 5 and 6. One hypothesis for the divergence is the significant change in thermal diffusivity in the relatively steep temperature gradient.

The variance between theoretical and actual ice thermal diffusivity is explained by Mellor [16] as the result of air bubble entrapped in the ice which lowers the thermal diffusivity from that of pure bubble-free ice. There was a significant bubble population throughout each model tested in the bay.

Since the time over which the regression rate was calculated did not include the 7 minutes the ice was motionless in the water, it was not surprising that the measured regression rate was higher than the theoretical prediction.

F. MEASUREMENT OF ICE MODEL WAKE TEMPERATURE

The method used to measure the wake plume on Test No. 5 in Monterey Bay is described in Chapter IV. The method proved largely unsuccessful for the following reasons. First, the pontoon bridge did not remain aligned continuously with the centerline of the model throughout the test which limited the opportunities to obtain data. Second, the thermocouples had to be read individually in stepwise fashion due to recording equipment limitations thus adding variance to the recorded temperature profile at any given time. Third, variations in surface water temperatures, large scale eddies in the wake, wave motion and similar effects added to scatter in the measured values. The recorded temperature profiles are shown in Figure 106 for five different time intervals. A search of the literature showed no data for similar measurements for comparison with the

NPS experimental results. Further, efforts at measuring the wake plume were not attempted due to limited time and resources.

The conclusion is that measurement of wake temperatures is not as straightforward as one might expect. While the equipment recording problem could be solved by continuous monitoring and recording techniques, the large scale eddies, which were observed in the wake with dye injection, significantly complicate the interpretation of temperature profiles obtained.

One obvious reason for measuring the ice model wake temperatures is to aid in the determination of the effective cold-water "insulation" provided by the model for a similar model being towed in the wake.

One alternative method for measuring the wake temperature would be to measure it with the second model in tow. The close proximity of the bow of the trailing model to the stern of the lead model would have a stabilizing effect on the flow leaving the lead model. An attempt at this method was planned for the tandem test in Monterey Bay but could not be executed because of the lateral oscillations of the models.

G. FLOW SEPARATION ON THE ICE MODELS

The decisive "necking" observed on the small-scale laboratory ice models was due to the recirculating flow in the forward one-third region on the models. The recirculation

was a result of the initial flow separation around the sharp frontal corners and subsequent reattachment as described in Chapter III. The separation region, where the necking occurred, was observed visually with use of dyes as described in Chapter V. However, the "necking" was never observed on the large-scale ice models tested in Monterey Bay, despite the fact that flow separation around the initial 90-degree corners certainly occurred. A discussion of the flow separation conditions for the two modeling situations follows.

Consider first the frontal corners on the small- and large-scale models. The corners are initially areas of intense heat transfer and erode rapidly once the model starts moving in the fluid medium. As the corners erode, their radius of curvature increases thus decreasing the tendency for flow separation. The actual rate of decrease in the flow separation tendency will vary depending on the laminar or turbulent condition of the flow. In the laboratory tests, the flow was laminar due to the low Reynolds numbers involved. The small frontal area of the laboratory model did not offer sufficient opportunity for the flow to reach turbulent conditions prior to rounding the corners. Laminar flow is more sensitive to flow separation even on relatively streamlined bodies. Therefore, although the corners became rounded on the small-scale model, the flow, which remained laminar, continued to separate with the subsequent "necking"

as previously seen in Figures 6 and 7 of Chapter III and Figure 73 of Chapter V.

On the large-scale model, the flow was turbulent as evidenced by the full-length ripple system on the sides and "cavern"-shaped area on the bow of the model. Due to the significantly larger frontal area on the large-scale model as compared to the small-scale model, the flow has an enhanced opportunity to reach a turbulent condition prior to rounding the corners. A well-known fact is that turbulent flow has a lower tendency than laminar flow for separation. Therefore, one hypothesis is that once the corners on the large-scale model become rounded, the flow separation ceased and no observable "necking" occurred. Such a hypothesis could be tested using both potential flow theory and actual continuous observation of the large-scale model as was done in the laboratory experiments.

The significant difference in the melting shapes of the small- and large-scale models emphasizes the importance of careful treatment of the scaling factors such as Reynolds number when modeling a large iceberg. The melting shapes were obviously strongly dependent on Reynolds number, which was on the order of 10^4 in the laboratory tests and 10^6 in the Bay tests.

VII. RECOMMENDATIONS FOR FUTURE WORK

A. GENERAL

There are many areas of research concerning glacial ice moving through seawater which strongly merit future examination. Included are improvements in testing techniques and instrumentation used to obtain such basic data as drag force, velocity, temperatures, and salinity. The following are brief discussions concerning these research areas.

B. TOPICS FOR FUTURE RESEARCH

1. Measurement of Drag

For a square bow, such as shown in Figures 27, 29, and 31, the drag is dominated by form drag. At the low Froude numbers, the wave drag is negligible. Skin friction is relatively insignificant.

As the iceberg melts, the shape tends to a geometry yielding lower form drag. Also the bow may be shaped to give lower form drag. In that case, skin friction becomes more significant. There is an obvious interaction between convective heat transfer and skin friction. One expression of the relation is Reynold's analogy.

As a result of the past towing experience, the NPS team should develop techniques to measure drag accurately. Drag information is useful in the interpretation of shape changes and for correlation with melting rates.

2. Tandem Towing

Only one test was conducted at NPS in this interesting and complex method of moving icebergs. One potential advantage of tandem towing is the fluid mechanical insulation (cold water) provided by the lead iceberg. The lead iceberg can be considered to be a "sacrificial" iceberg providing the cold water for insulation. Evaluation should include boundary layer temperature profile measurement and flow field surveys at the rear of the lead iceberg.

3. Influence of Buoyancy on Heat Transfer

The paper by Josperger [17] clearly demonstrates the importance of buoyancy forces on natural convective heat transfer. The critical Grashof number for transition to turbulent flow is a factor of 10 lower for fresh water ice melting in seawater than for a vertical hot plate in air.

An analytical model should be developed to determine the influence of buoyancy. A buoyancy term should be introduced in the equations of motion developed by Griffin. The impact of this term on heat transfer should be examined.

The Naval Postgraduate School is about 60 miles from San Antonio Reservoir which is near King City, California. In order to test the theory concerning buoyancy and heat transfer under forced convection (i.e., moving iceberg), several icebergs could be towed in San Antonio Reservoir. A comparison could be made between melting rates in fresh water and seawater. Furthermore, the inverse melting problem, i.e., an iceberg of frozen seawater melting in

fresh water, can be studied to gain insight on buoyancy effects in forced convection.

4. Instabilities of Insulating Material, e.g.,
Flagwaving Instability

Consider an insulation scheme using thin plastic sheets. A protective layer of cold water develops between the iceberg and the plastic sheet.

There are several excellent books, e.g., Lin [18], Chandrasekhar [19], and Shen [20], which discuss stability of flows. In rotating coordinates, the book by Greenspan [21] is especially relevant. One well-known instability is that which occurs in parallel flows of fluids with unequal densities.

A survey is needed of the instabilities that may arise in the context of icebergs with insulation. Such a survey is proposed here.

5. Solid Mechanics of Icebergs

The Naval Postgraduate School has a Chair in Arctic Research. The incumbent starting in July, 1978, is Dr. Wilford F. Weeks, who is a Research Glaciologist with the U.S. Army Cold Region Research and Engineering Laboratory. Dr. Weeks has agreed to devote some of his time to the question of solid mechanics of icebergs.

It is apparent from the technical papers at the Iceberg Utilization Conference that many of the existing engineering techniques relative to cracks, fractures, stress distribution, multiaxial stresses, etc., are applicable to iceberg structures.

6. Development of Instrumentation

To verify the computer code of Griffin, measurement of temperature, salinity, and velocity profiles would be especially helpful.

Velocity of the iceberg is measured using standard oceanographic equipment. Drag is measured also using standard equipment.

Measurement of salinity and velocity profiles requires special consideration. The surface of the ice is receding. The iceberg is a remote vehicle.

As a research task, techniques should be developed, or improved, for measuring:

1. velocity of iceberg
2. drag
3. salinity profile
4. velocity profile
5. temperature profile

As a further aid to the experiment, underwater photographs and underwater movies of an iceberg in motion should be made.

7. Laboratory Tests

Towing tests in Monterey Bay are time consuming and expensive. Hence, each test must be planned carefully and overall test objectives must be defined clearly. To supplement the towing tests in Monterey Bay, tests can be conducted using the water tunnel and water channel located in the Department of Mechanical Engineering.

By using a larger test facility, larger test specimens, and higher flow velocity, turbulent flow may be achieved in the laboratory. Special emphasis should be placed on defining the usefulness of boundary layer trips.

Due to the relative simplicity of laboratory testing, many tests can be conducted in the laboratory compared to larger scale towing tests in the ocean.

8. Field Tests

There have been three options for large scale tests discussed and evaluated by the Naval Postgraduate School research team. Option 1, which is towing in Monterey Bay, has been exercised six times. Option 2 involves use of tidal currents at Moss Landing. Elkhorn Slough has a narrow opening; the bridge for State Highway 1 crosses the Slough at this point. Due to tides, a velocity of 1.0 knot occurs and persists for about 30 minutes. Using the bridge as a point to tie the two ropes, tests could be conducted with the 16-foot iceberg. The bridge and the nearby navigational pilings could be used as observation points.

Option 3 is to tow the large scale iceberg in San Antonio Reservoir. The goal of these tests would be to determine influence of buoyancy on heat transfer. Also at San Antonio Reservoir water temperature would allow use of swimmers near the iceberg; the swimmers could observe the flow at close hand.

Experience has shown that the field tests would be facilitated greatly if an observer could ride the iceberg.

Hence a double wall box is proposed. For the size of manned iceberg, the weight of the ice is 7735 lbs. With a payload of 1500 lbs, which includes the weight of the inner box, the freeboard is almost 12 inches. The design uses a broad beam to avoid stability problems if ice were to break away.

Advantages of a manned iceberg include the following:

1. ability to observe the flow.
2. ability to conduct experiments, start recorders, and vary profile instruments.

9. Insulation

Many different forms of insulation have been proposed including plastic sheets, frozen wood chips, plastic foam, etc. An alternate scheme might be the use of air bubbles at locations with high heat transfer rates.

To examine the concept, an experimental program is proposed. First, the bubble insulation would be investigated in the water channel. Second, one or more of the large scale icebergs would be dedicated to an evaluation of bubbles for insulation. Third, depending on the outcome of the experiments, a study would be made of pumping requirements. Also, the study would examine installation of bubble source on the iceberg.

10. Potential Flow Computer Code

Pressure gradients have a pronounced effect on boundary layers. A potential flow computer code would be used to calculate pressure coefficients and pressure gradients.

The shape of the body will be that shape observed during experiments conducted in Monterey Bay.

A computer code has been developed by Professor C.J. Garrison under a NSF grant. Professor Garrison is a faculty member in the Mechanical Engineering Department at NPS.

APPENDIX A

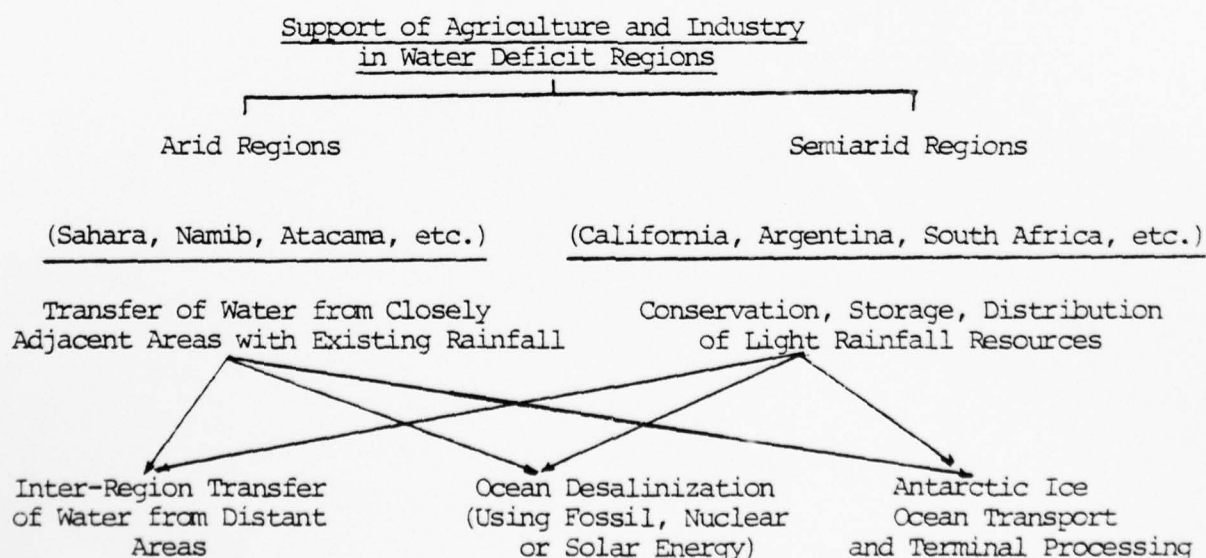
AREAS OF CONCERN WITH ICEBERG DETERIORATION

The following is a discussion by Stolfi, et al [22] of the motivation and scope of interest in iceberg deterioration.

A large percentage of the land surface of the globe consists of arid and semiarid regions which support less agriculture and smaller populations than other areas. In certain semiarid regions where agriculture is successful, that activity is dependent upon well-developed irrigation technology and the light variable rainfall of the region. The arid regions, and especially the areas in them lying far from the world's oceans, present extraordinarily challenging problems for development in some future time frame. Certain arid regions and many semiarid regions which lie close to the world's oceans contain significant populations and present special opportunities for expanded development and insurance against the periodical, economically damaging droughts associated with rainfall scarce areas in which productive agricultural activity is being conducted.

Several approaches can be envisaged for the support of agriculture and associated populations and industry in arid and semiarid regions. The light, existing rainfall can be gathered, stored, managed, and metered out to the surrounding countryside and cities in water storage and irrigation works which conserve and distribute the existing rainfall. Similar

water storage and distribution works can transport water from heavier rainfall regions located economically close of the drier areas, to make the water available for agriculture and maintain the water tables and other underground water resources. In cases of deep and extensive drought, however, as in Western North America, 1975-1977, the lack of rainfall will empty reservoirs, lower permanent rivers, and drive down water tables over large regions threatening immense damage to grazing, agriculture, and ultimately industry. In both arid and semiarid regions in which productive agriculture has been developed through water conservation, storage, and distribution technology, the water supplies can be supplemented by (1) inter-region transfer of water from distant heavier rainfall areas, (2) fossil-fuel, nuclear, or solar desalinization of ocean water, and (3) transfer and terminal processing of Antarctic ice. The approaches can be summarized as follows:



The expansion of economic activity into arid regions and the intensification and assurance of uninterrupted activity in semiarid regions demand advances in technology related with Inter-Region Transfer, Ocean Desalinization, and Antarctic Ice Transport and eventual assignment of financial and economic resources to such projects. Inter-region transfer involving the movement of water from assured, excess supplies, for example, in the Northwest Territories in Canada to the California-Nevada-Arizona area in the United States, would involve immense cost, formidable engineering difficulties and long time periods. Ocean desalinization, especially with the use of nuclear or solar technology, offers substantial opportunities for support of economic activity although at immense expense, with potential physical dangers and extended time of development. The transport of Antarctic ice and the melting of it in arid and semiarid coastal regions, although a relatively new idea and largely untried, offers possibilities for the support of economic activity. The transport of Antarctic ice presently appears to be comparatively inexpensive, involves the use of existing technology, and is capable of implementation in the near future for areas south and possibly even north of the equator.

In arid regions, e.g., Sahara, Saudi, Atacama, Peruvian, Kalahari, and Australian Deserts, most parts of which lie far from adequate rainfall areas and desert rivers, the expansion of civilization will be dependent ultimately on

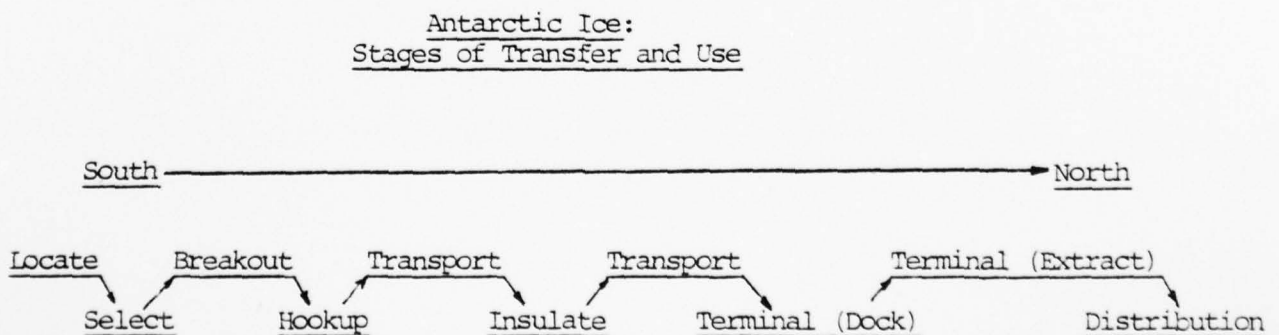
ocean desalinization and the transfer of Antarctic ice. In semiarid regions, e.g., South Africa, Angola, Argentina, Iran, Pakistan, California, Mexico, Australia, etc., economic expansion and the support of larger populations will depend on exploitation of the local rainfall in combination with ocean desalinization, the transfer of Antarctic ice, and the expanded use of adjacent but distant stored rainfall. The western half of the United States, except for the relatively small, rain-rich Pacific Northwest stands as a monument to agricultural opportunity which is dependent upon the availability of water. The imposing total of 15 western states is predominately semiarid or arid and dependent upon irrigation works and scanty rainfall for the sometimes intense but mostly modest or nonexistent development of agriculture.¹ Additional immense regions of the globe in similar favorable latitudes lie agriculturally dormant because of the water deficit and high evaporation and transpiration characteristics of the areas.

In arid and semiarid areas lying south of the equator and within reasonable proximity to the oceans, e.g., parts of the Republic of South Africa, scientific theory and experiment support a view that the transfer of Antarctic ice is limited more by the problems of potential resettlement and

¹Arizona, California, Colorado, Idaho, Montana, Nevada, New Mexico, North Dakota, Oklahoma, Oregon, South Dakota, Texas, Utah, Washington, Wyoming.

the cost of irrigation works than by limits on the ice transfer technology. Given the relatively short distances from the tabular icebergs, and the comparatively cool intervening water and air temperatures for movement, the NPS scientists feel that scientific feasibility is close to being established for movement from Antarctica to South Africa, Argentina, Atacama, and Australia. Opportunities exist for the United States Government to increase its influence peacefully through the use of superior technology in Southern Africa, South America, and Australia. Engineering, economic, and political studies will be required to guide U.S. government policy makers in the exploitation of the scientific opportunities for the settlement of populations and the expansion of agriculture and industry in previously excluded arid regions.

The stages of transfer and use of Antarctic ice run in the following generalized pattern:



The stages through which an Antarctic ice transfer project must necessarily proceed are common for ice delivered to any location on the globe. The individual conditions of

ocean routing, terminal docking, etc., may vary enormously, for example, between ice delivered to Southern California and South Africa, but the general process, or stages, of transfer will be virtually identical. With two noteworthy exceptions, the technology for each of the stages is largely in hand. Space photographic technologies are available to locate and select tabular bergs which have the sizes and shapes to meet other delivery criteria. The breakout of large glacial tabular bergs may not be necessary depending upon the time of the year, e.g., Antarctic summer, and the location of the glaciers relative to open water. The hookup and towing of the tabular bergs can be forecast to be engineering challenges of the first magnitude but surmountable with present technology. Ocean routing and terminal environmental impact should be able to be mastered with existing technology.

The most imposing scientific challenge is the one of the melting of ice moving in seawater, and little theoretical or experimental knowledge is available on the subject. If rates of melt can be described adequately and predicted, the scientists can present the ultimate reality of ice transfer projects in terms of (1) the amount of melting and (2) the associated necessity of lack thereof for insulation. The most imposing potential problem in the transfer of Antarctic ice can be forecast to be the one of placing insulation on the ice and maintaining it there during the transportation to the terminal area. If the experimentally supported

theory shows that insulation is not necessary for the movement of tabular bergs to areas like Southern Australia, Argentina, and Southwestern Africa, the potential costs of movement would fall steeply, and the economics of transfer would be more attractive. The absence of insulation reduces costs and engineering difficulties to a point where the NPS scientists tentatively conclude that the transfer of ice to Australia, Argentina, and South Africa is technically and economically within the grasp of governments and the larger private businesses associated with those areas. The perception of the necessity for agricultural expansion on the parts of the governments and the economic attractiveness on the part of private business remain to complete a picture of Antarctic ice capable of being transferred to southern regions in the immediate (one to three years) future.

The transfer of Antarctic ice to regions north of the equator present greater cost and engineering problems largely because of the problems of melting and the prima facie necessity for insulation. No realistic schemes presently exist for the insulation of the large tabular bergs in terms of physical or chemical barriers between ice and seawater. The NPS scientists, based on recognition of the fact that increased water temperature exponentially increases the rate of melt of ice, are gathering experimental data both in Monterey Bay and in the NPS mechanical engineering laboratories on the cooling effects of ice moving through water. A

"plume" of cool water is assumed to exist behind ice in water which could reduce water temperatures to the degree that other ice bathed in the plume would experience significantly reduced melting. The potential insulation scheme, in effect, would involve either (1) towing several bergs in column with a small "sacrificial" berg in front or (2) towing several bergs in column while removing the lightly compacted snow and ice from the top of the leading berg and depositing it in front of the leading berg as a coolant for the most exposed ice.

Several challenging but surmountable problems exist at the terminal area for the tabular bergs. The ice upon arrival will have imposing drafts of approximately 200 - 500 feet depending upon the distance and velocity of the tow and the water temperatures encountered. The immense drafts of the bergs will demand carefully selected terminal areas in order to place the ice conveniently close to the receiving water system and reduce the impact of adverse sea conditions on the floating reservoirs of fresh water. Ice, for example, delivered to Southern California could be "docked" immediately south of Santa Cruz Island, 20 miles from the California coast protected from the prevailing northwesterly winds and representing a reduced impact on the local environment. The most difficult engineering problem at the terminal location would be the one of establishing a barrier between the tabular bergs and the seawater in order to extract the most fresh water possible from the ice. Given the static situation of

the bergs at the terminal location, one can envision engineering solutions ranging from the production and transfer ashore of ice water slurries through the static wrapping of the ice in a waterproof plastic barrier and the extraction of the fresh water melt.

If the technology can be developed to transfer Antarctic ice at reasonable cost to the coasts of arid and semiarid regions, immense opportunities would accrue to governments with the resources to exploit the technology. A government like that of the United States could work in a cooperative, positive way with the government of the Republic of South Africa to open up approximately 50,000 square miles of territory to agriculture and grazing in the more arid sections of the Cape of Good Hope and Orange Free State Provinces. The projects would be based ultimately on the technology necessary (1) to extract the maximum water from the existing rainfall and (2) to transfer and distribute additional water from Antarctic tabular bergs. The financial support for the water supply and agricultural project would involve investment in a water distribution system and encouragement for settlement in the new territories. Such financing might be accomplished through a combination of U.S., Western European, South African government, World Bank, and private capital. The governments involved in cooperating in such a venture would be presented with opportunities to effect change in the hypothetical case of South Africa, without recourse to the hackneyed, aging and brutal techniques of insurgent and

AD-A070 367

NAVAL POSTGRADUATE SCHOOL MONTEREY CA

F/6 20/13

EXPERIMENTAL DETERMINATION OF MELTING RATES OF ICE MOVING IN SE--ETC(U)

MAR 79 W F CLIFFORD, R J ERMAN

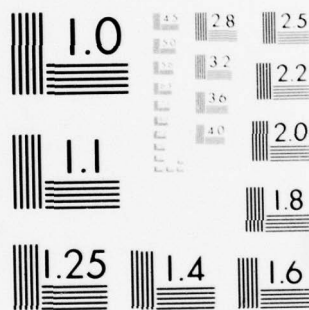
UNCLASSIFIED

NL

2 OF 3

AD
A070367





counter-insurgent warfare, without the advantages accruing in insurgency situations to the weaker and less developed Eurasian communist countries, and with the strong possibility of effective change and political accommodation based on rising standards of living within the Republic of South Africa. The United States, in particular, with its advanced technology, large financial resources, powerful and advanced allies, and traditional predominance at sea is faced with the opportunity to use its natural strengths to support successful political accommodation and settlement in Southern Africa.

In other parts of the world, in situations less traumatic than in South Africa, the U.S. has the opportunity through the exploitation of its technology to intensify agricultural activity in some areas and open up agricultural and associated economic activity in others. On the west coast of North America, the California and U.S. Governments are faced with a three-year drought crisis (1975, 1976, 1977). The crisis may require the positive supply of water in addition to the present negative provision of relief funds in order to master the situation and continue to support the existing overpopulation of California relative to scarce and ultimately limited water supplies. In the absence of the timely availability of water from inter-region transfer and nuclear desalinization, Antarctic ice transfer probably will emerge as an imaginative, relatively low-cost alternative for the provision of fresh water to areas south of the equator.

With knowledge of the processes of melting, scientists, engineers, and governments could provide water to arid and semiarid regions north of the equator.

APPENDIX B

SOLUTION OF TRANSIENT THERMAL CONDUCTION EQUATION

The comparison between the theoretical curves and experimental data points contained in Chapter VI, Figures 100 - 105 were obtained utilizing the computer program, "Reduce Data on Temperatures Internal to Ice", Figure B-1. The terminology used for the text and computer programs is listed in Table B-I.

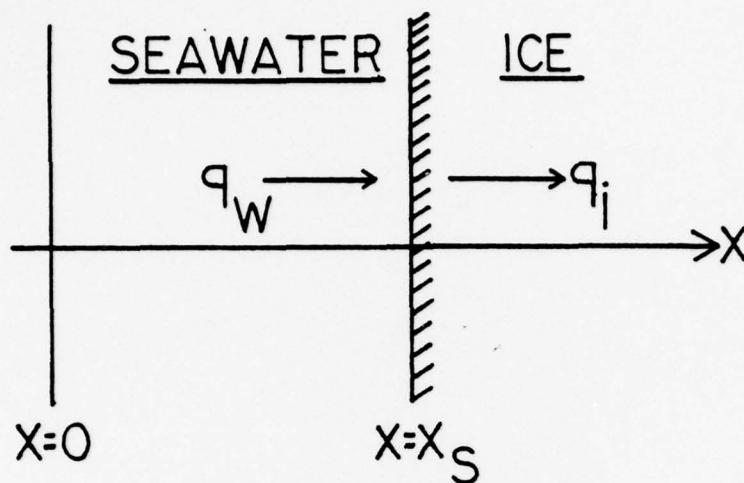
The computer program, "Select a best S", Figure B-2, was utilized to assist in obtaining values for thermal diffusivity, ice regression rate, and X_0 for program Figure B-1. The value "S" is found by subtracting the experimentally determined values from the calculated values, squaring the difference and summing over the set of experimental data points. The theoretical function, which provides calculated values, was varied by changing the parameters α , X_0 , and V_s . A minimum value of "S" represented the best set of above values.

After experimenting with the aforementioned parameters, a minimum value of "S" of 1329 was attained using $V_s = 2.2 \times 10^{-5}$ and $\alpha = 3.0 \times 10^{-7}$; these values of V_s and α are utilized in the program shown in Figure B-1.

The theory used to generate computer program 1 was the solution of the heat conduction equation as follows:

TABLE B-I
NOMENCLATURE

Symbol in Computer Program HP 9831	Symbol in Text	Definition	Units
H	H	heat of fusion for ice	joule/kg
Q	q	heat flux to melt ice	joule/m ² sec
A/A1	α	thermal diffusivity of ice	m ² /sec
K	K	thermal conductivity of ice	joule/msec °K
V	V _s	ice regression rate	m/sec
XO	X _O	distance from edge of ice to first thermocouple	meters
T1	T _s	surface temperature of ice	°C
TØ	T _i	interior temperature of ice	°C
X9	ΔX	thermocouple spacing	meters
I	I	time intervals (1 - 6)	minutes
ρ	ρ	density of ice	kg/m ³
W	W	V _s / α	1/meters



An energy balance at the water-ice interface from above is:

$$q_w = Q + q_i = H\rho V_s - \left(k \frac{\partial T}{\partial X}\right)_{X=X_s} \quad (B-1)$$

Of the heat transferred from the water the amount of heat which causes melting is:

$$Q = H\rho \frac{dX_s}{dt} = H\rho V_s \quad (B-2)$$

For the purpose of analysis, the temperatures within the ice are modeled using the one-dimensional unsteady heat transfer equation as follows:

$$\frac{\partial^2 T}{\partial X^2} - \frac{1}{\alpha} \frac{\partial T}{\partial t} = 0 \quad (B-3)$$

The following assumptions were made:

- 1) $q_w = \text{constant}$
- 2) Steady state melting occurs
- 3) $V_s = \text{constant} = \text{velocity of surface of ice}$

The boundary conditions at the water-ice interface are as follows:

$$\left(K \frac{\partial T}{\partial X}\right)_{X=X_s} = H\rho V_s - q_w \quad (\text{B-4})$$

$$T[X_s, t] = T_s \quad (\text{B-5})$$

The boundary condition for the ice interior is:

$$T[\infty, t] = T_i \quad (\text{B-6})$$

which mathematically is as $X \rightarrow \infty$.

Define a variable which involves both space and time

$$\xi = X - V_s t \quad (\text{B-7})$$

Note that the solution of eq. (B-3) will use ξ as an independent variable. Consequently the temperature profile propagates with the same shape into the ice as the ice melts. Combining equations, one can derive the following:

$$-(T_s - T_i)f'' - \frac{1}{\alpha}[(T_s - T_i)V_s f'] = 0 \quad (\text{B-8})$$

where the function "f" is given by:

$$T(X,t) = T_s - [T_s - T_i] f(\xi) \quad (B-9)$$

We now define:

$$\psi = f' \quad (B-10)$$

$$f'' + \frac{V_s}{\alpha} f' = \psi' + \frac{V_s}{\alpha} \psi = 0$$

$$\frac{d\psi}{d\xi} + \frac{V_s}{\alpha} \psi = 0$$

$$\frac{d\psi}{\psi} = - \frac{V_s}{\alpha} d\xi$$

$$\psi = ae^{-V_s \xi / \alpha} + b$$

Taking the derivative of f with respect to ξ and then integrating to solve for f as follows:

$$\frac{df}{d\xi} = ae^{-V_s \xi / \alpha}$$

$$f = \int ae^{-V_s \xi / \alpha} d\xi = -a \frac{V_s}{\alpha} e^{-V_s \xi / \alpha} + b$$

$$c = -a V_s / \alpha$$

$$f = ce^{-V_s \xi / \alpha} + b \quad (B-11)$$

Utilizing boundary condition (6) and combining eq. (B-9) and (B-11) we obtain the following:

$$T[\infty, t] = T_s - [T_s - T_i][ce^{-\infty} + b] = T_i \quad (B-12)$$

$$b = 1.0$$

Utilizing boundary condition (5) when $X = X_s$ we obtain the following:

$$\xi = \xi_s = X_s - V_s t = 0 \quad (B-13)$$

$$T[X_{s_1}, t] = T_s = T_s - [T_s - T_i][ce^{-0} + 1]$$

$$c = -1$$

It therefore follows that:

$$T[X_1, t] = T_s - [T_s - T_i][1 - e^{-V_s \xi / \alpha}] \quad (B-14)$$

$$\xi = X - V_s t \geq 0$$

Utilizing boundary condition (4) we obtain the following:

$$\frac{\partial T}{\partial X} \Big|_{X=X_s} = [T_s - T_i] [-V_s / \alpha] e^{-V_s \xi / \alpha} - V_s \xi / \alpha \frac{\partial \xi}{\partial X} = -\frac{V_s}{\alpha} [T_s - T_i] \quad (B-15)$$

We note that when $X - X_s$, $\xi = 0$, therefore:

$$\frac{-k V_s}{\alpha} [T_s - T_i] = H\rho V_s - q_w$$

$$q_w = H\rho V_s + k/\alpha V_s [T_s - T_i]$$

The final result is as follows:

$$q_w = V_s [H\rho + k \frac{[T_s - T_i]}{\alpha}] \quad (B-16)$$


```

10 PRINT "REDUCE DATA ON TEMPS INTERNAL TO ICE"
20 PRINT "TRACK 0, FILE 1"
30 REM v sub s is v; alpha is a.
40 REM t sub s is t1; t sub ice is t0.
50 DISP "PLOT ?YES=1,NO=0":
60 INPUT 00
70 DISP "INPUT V":
80 INPUT V
90 DISP "INPUT A1":
100 INPUT A1
110 M0=720
120 DISP "INPUT X0":
130 INPUT X0
140 DISP "INPUT I":
150 INPUT I
160 W=V/A1
170 M9=300
180 T1=0
190 T0=-21.7
200 PRINT "SURF TEMP IS "T1" DEG C, ICE INTERIOR TEMP IS "T0" DEG"
210 PRINT " C."
220 PRINT "V="V" THERMAL DIFFUSIVITY"R1" MTS SEC."
230 PRINT "X0="X0
240 REM Greek K1 is Z.
250 REM s2 in meters.
260 S2=X9=0.00158
270 DISP "DATA TABLE ? YES=1 , NO=0":
280 INPUT Z5
290 PRINT
300 FORMAT 4F16.4
310 IF I=1 THEN 360
320 A=X0
330 T8=0
340 PRINT "TIME T8="T8
350 GOTO 390
360 A=X0-V*(M0+(I-1)*M9)
370 T8=M0*(I-1)+M9
380 PRINT "TIME T8="T8/60
390 B=A+4*X9
400 IF 00=0 THEN 490
410 DISP "INPUT Y AXIS SCALE C":
420 INPUT C
430 DISP "INPUT Y AXIS SCALE D":
440 INPUT D
450 R=B-A
460 PRINT "R="R
470 N=(B-A)/93
480 PRINT "N="N
490 PRINT "      TEMP C      TEMP F      W1-METER"
500 IF 00=0 THEN 540
510 SCALE A,B,C,D
520 XAXIS D*(B-A)/4
530 YAXIS A*(D-C)/5
540 N=(B-A)/93
550 R=B-A
560 FOR Z=A TO A+R STEP R/N
570 T=T1-(T1-T0)*(1-EXP(-W*Z))
580 T3=1.8+T*33
590 IF Z5=0 THEN 620
600 WRITE (2,300)T,T3,Z
610 IF 00=0 THEN 630
620 PLOT C,T
630 NEXT Z
640 IF 00=0 THEN 740
650 FOR J=1 TO 5
660 Q8=D+J*(D-C)/5
670 XAXIS Q8
680 NEXT J
690 FOR K=1 TO 4
700 Q7=A+K*(B-A)/4
710 YAXIS Q7
720 NEXT K
730 PEN
740 STOP
750 END

```

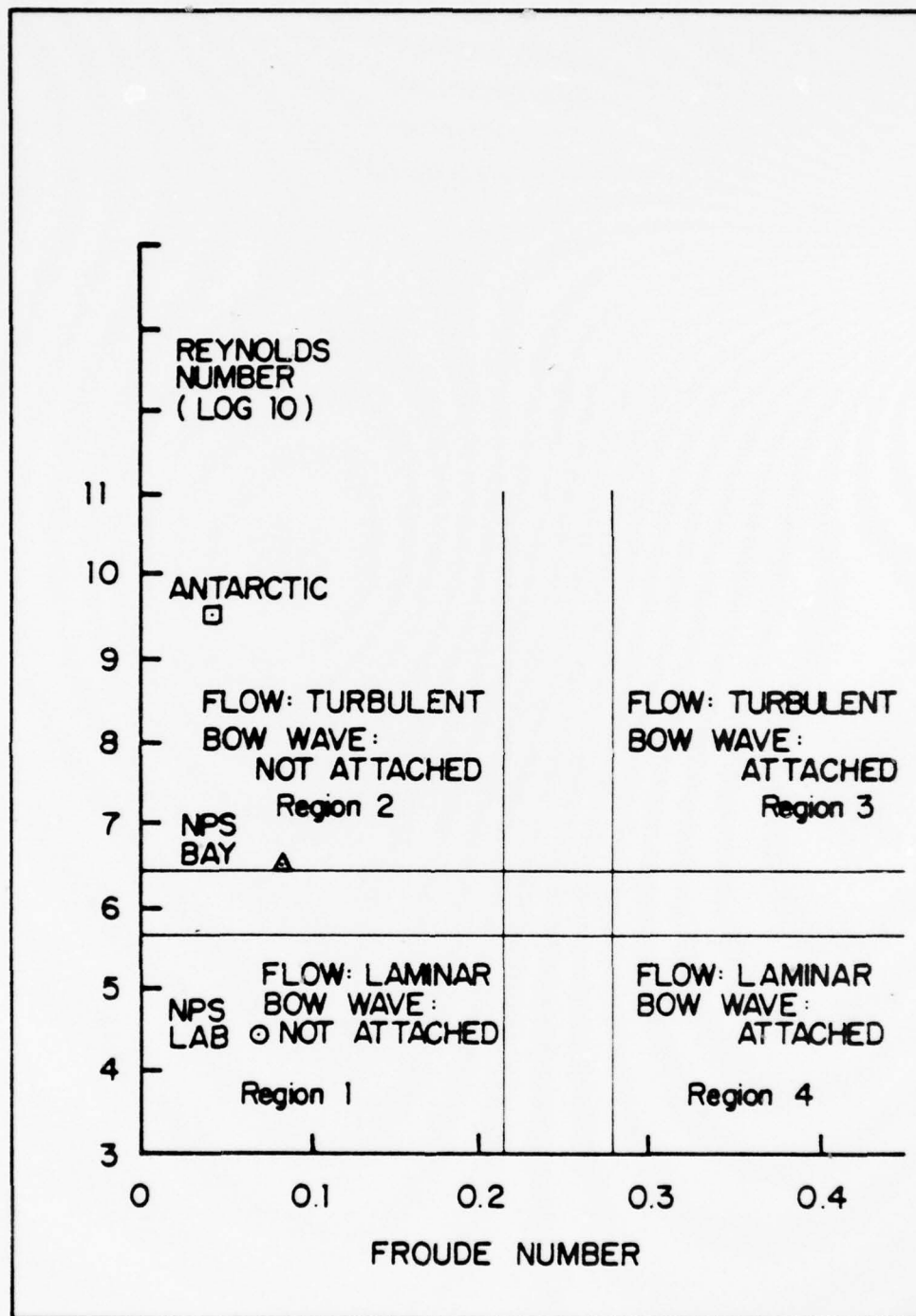
B-1. Ice interior temperature program

```

10 PRINT " This program will select a best S for program 1."
20 PRINT "Program stored in track 0, file 3."
30 DIM YES(5),MC(5)
40 DIM YES(5),TC(5,5),Z(5,5)
50 GOTO 530
60 M9=300
70 X9=1/(39.37+16)
80 DISP "INPUT A":
90 INPUT A
100 DISP "INPUT X0":
110 INPUT X0
120 DISP "INPUT V":
130 INPUT V
140 DISP "TABLE WANTED YES=1 NO=0":
150 INPUT OS
160 FORMAT 2F4.0,F7.3,F9.0,3F9.1,F7.3,F3.0
170 IF OS=0 THEN 190
180 PRINT "I,J,K(U),M(I),T(I,J),V(I,J),S"
190 DISP "INPUT M0":
200 INPUT M0
210 T1=0
220 T0=-10
230 W=V/A
240 S=0
250 FOR J=1 TO 5
260 X(J)=X0+(J-1)*X9
270 FOR I=1 TO 5
280 M(I)=M0+I*M9
290 Z(I,J)=X(J)-V*MC(I)
300 TC(I,J)=T1-(T1-T0)*(1-EXP(-W*Z(I,J)))
310 S1=(TC(I,J)-V(I,J))/13
320 S=S+S1
330 IF OS=0 THEN 350
340 WRITE (2,160) I,J,X(J),M(I),TC(I,J),V(I,J),Z(I,J),S
350 NEXT I
360 NEXT J
370 PRINT "SUM S IS"
380 PRINT
390 PRINT "A="A      "X0="X0      "V="V      "M0="M0
400 PRINT
410 S=0
420 GOTO 80
430 PRINT "      I      J      V(I,J)"
440 FOR I=1 TO 5
450 FOR J=1 TO 5
460 WRITE (2,500) I,J,V(I,J)
470 NEXT J
480 PRINT
490 NEXT I
500 FORMAT 2F12.0,F12.3
510 STOP
520 END
530 VC(1,1)=(-2.5-30)/1.3
540 VC(1,2)=(-3-30)/1.3
550 VC(1,3)=(-3.5-30)/1.3
560 VC(1,4)=(-3.5-30)/1.3
570 VC(1,5)=(-3.5-30)/1.3
580 VC(2,1)=(-3-30)/1.3
590 VC(2,2)=(-1-30)/1.3
600 VC(2,3)=(-1.4-30)/1.3
610 VC(2,4)=(-1.5-30)/1.3
620 VC(2,5)=(-1.5-30)/1.3
630 VC(3,1)=(-2.5-30)/1.3
640 VC(3,2)=(-1.5-30)/1.3
650 VC(3,3)=(-1.5-30)/1.3
660 VC(3,4)=(-1.3-30)/1.3
670 VC(3,5)=(-1.1-30)/1.3
680 VC(4,1)=(-3.4-30)/1.3
690 VC(4,2)=(-2.7-30)/1.3
700 VC(4,3)=(-2.3-30)/1.3
710 VC(4,4)=(-2.5-30)/1.3
720 VC(4,5)=(-2-30)/1.3
730 VC(5,1)=(-22.5-30)/1.3
740 VC(5,2)=(-21-30)/1.3
750 VC(5,3)=(-19.5-30)/1.3
760 VC(5,4)=(-18.7-30)/1.3
770 VC(5,5)=(-17.5-30)/1.3
780 GOTO 60

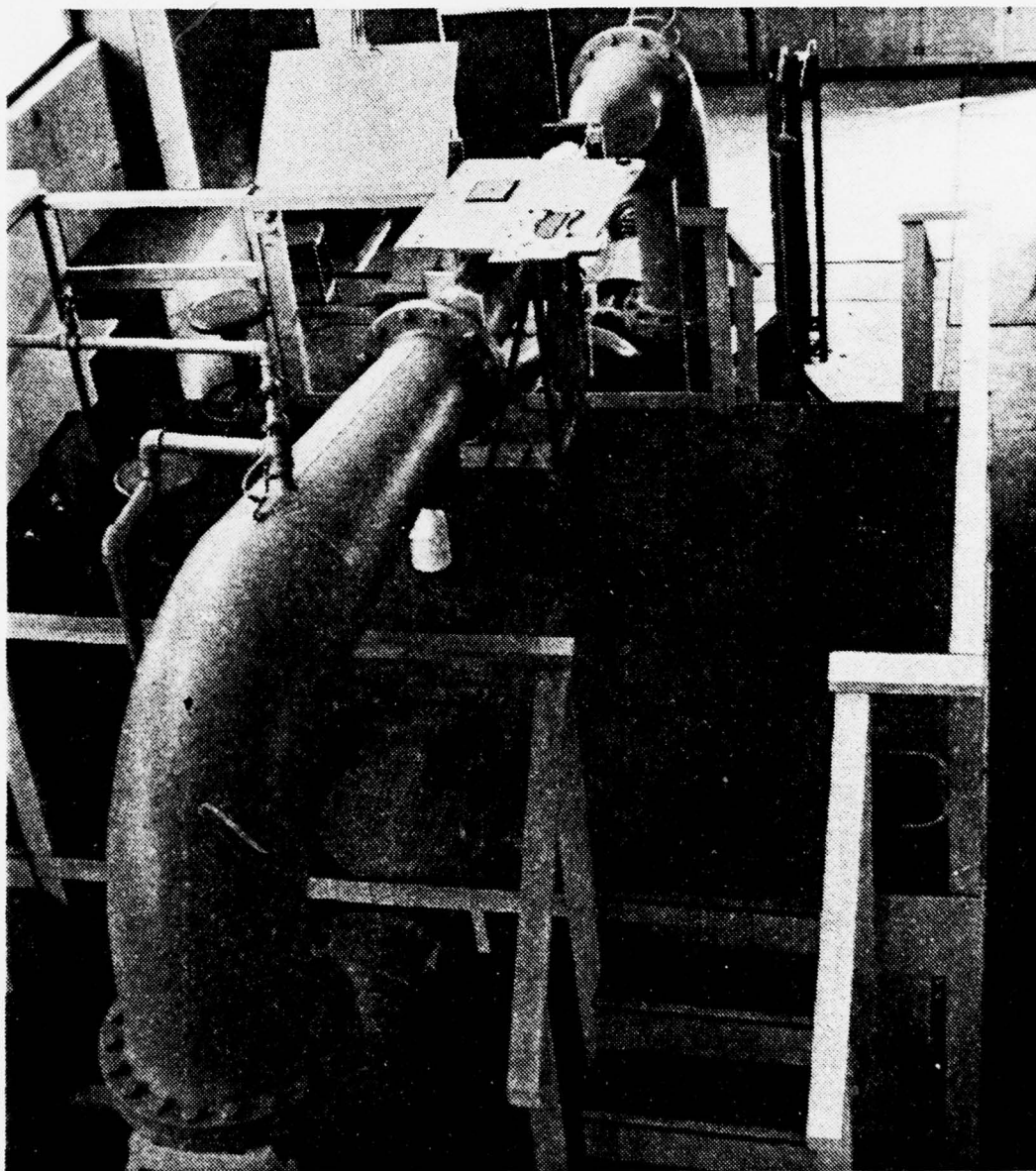
```

B-2. Program for minimum 'S' value.

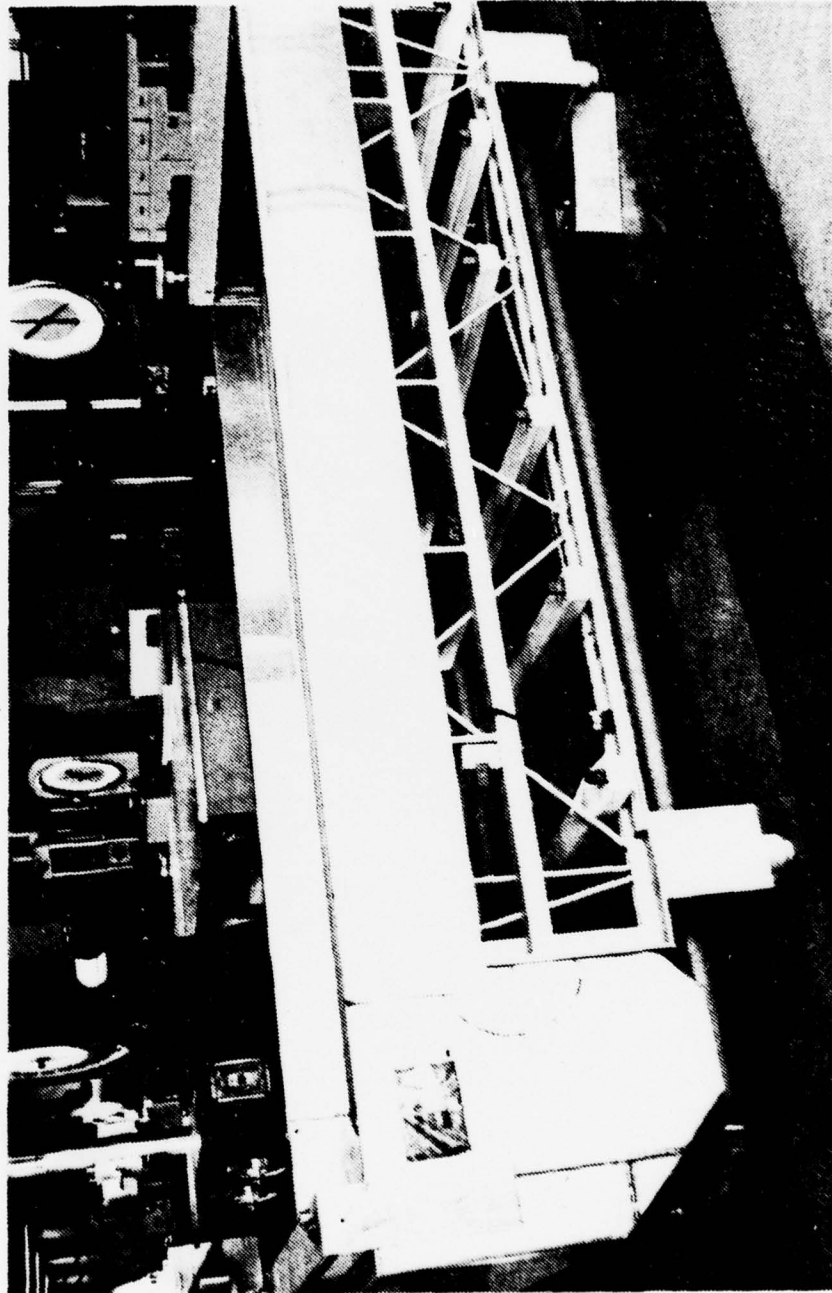


Regimes of flow and wave producing conditions as functions of Reynolds and Froude numbers.

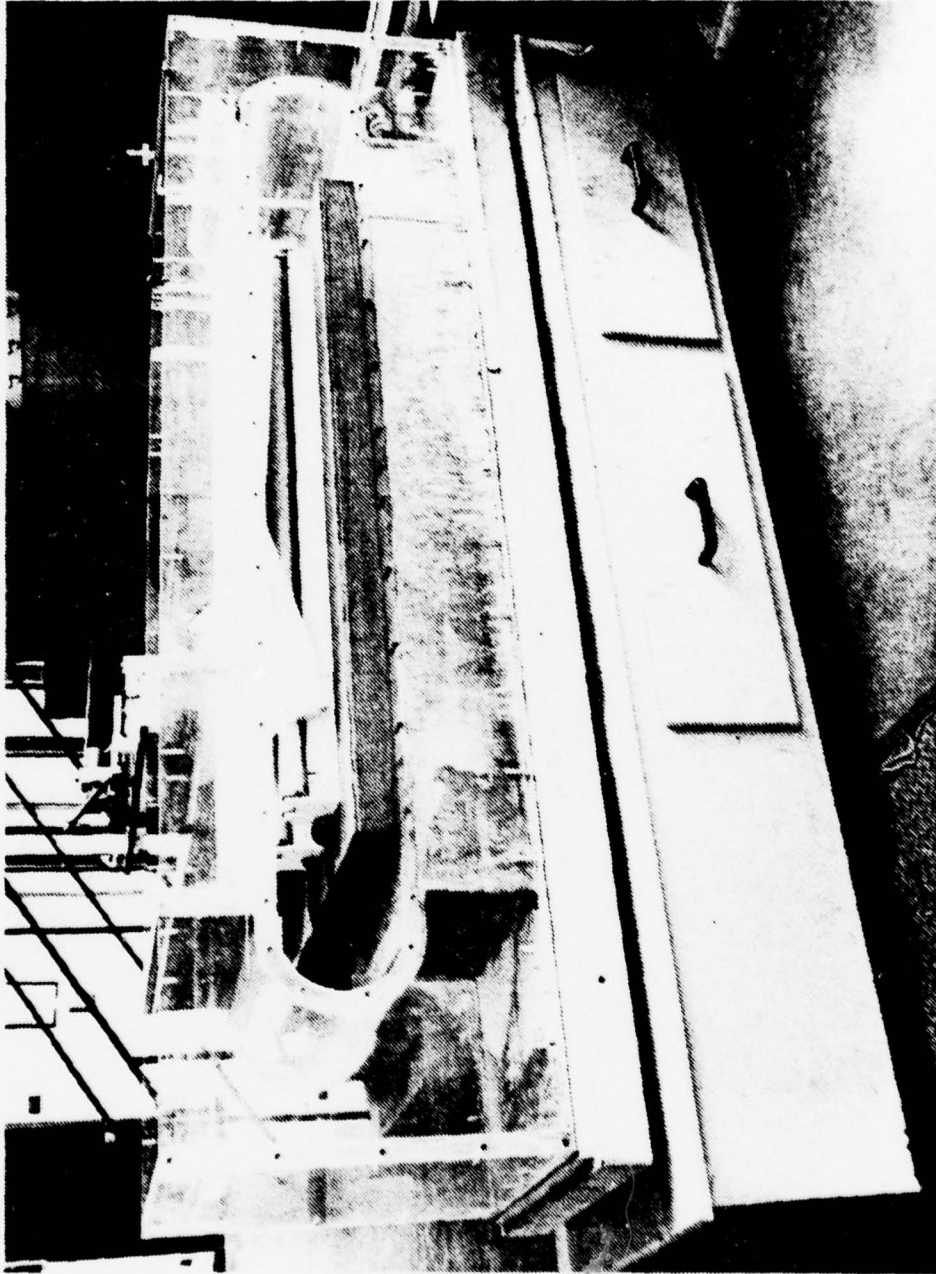
1. Regimes of flow and wave producing conditions as functions of Reynolds and Froude Numbers.



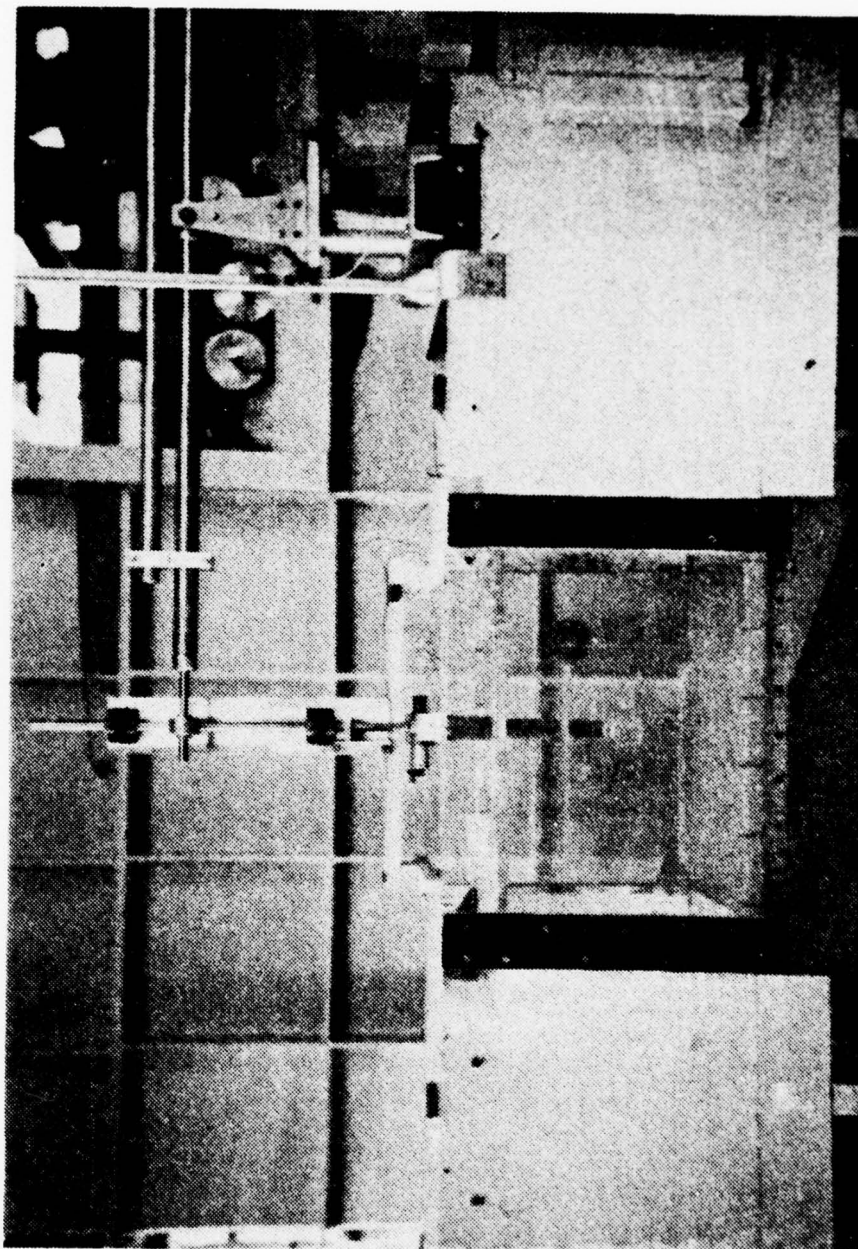
2. NPS water tunnel.



3. NPS mobile water table.



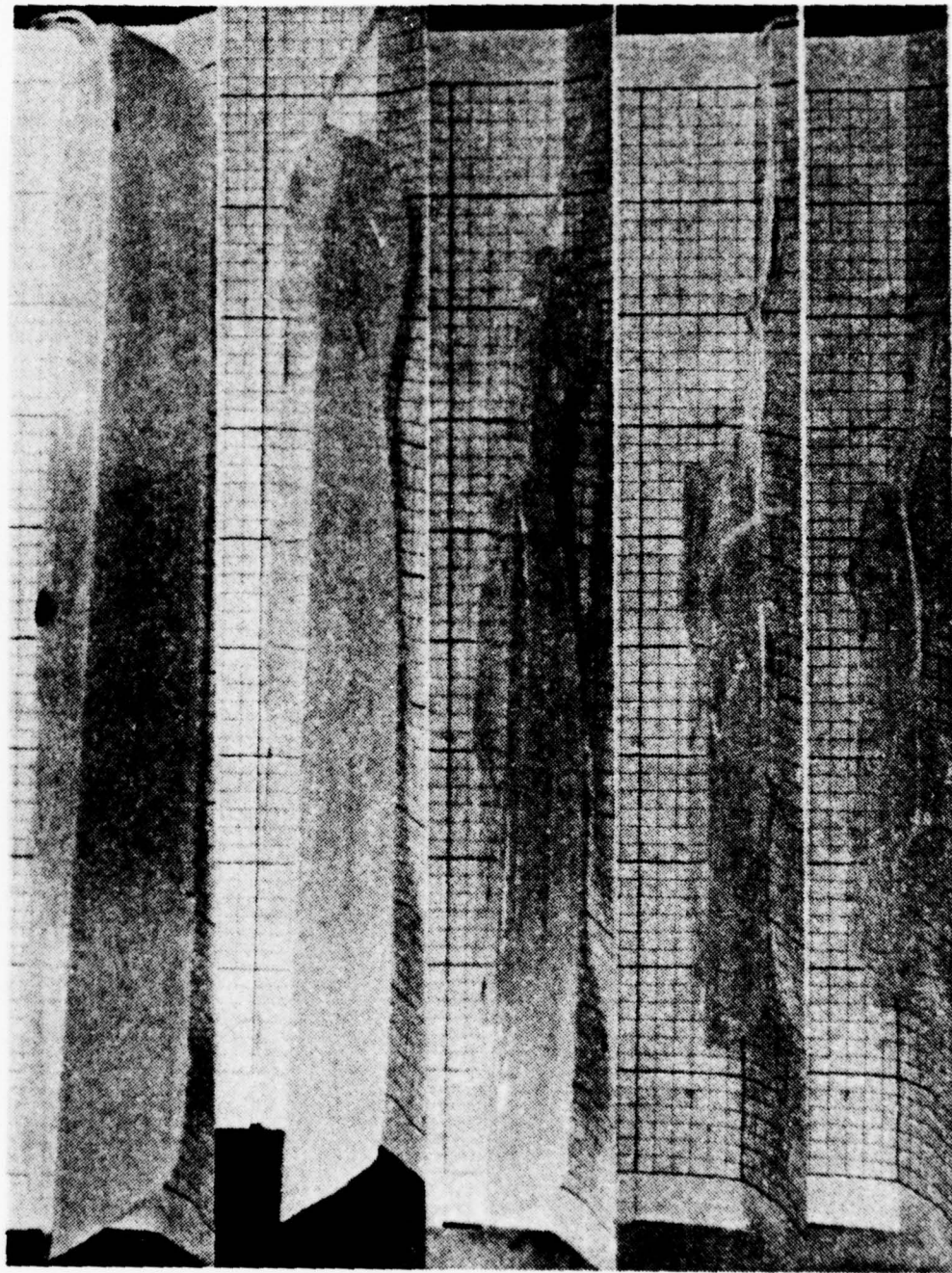
4. NPS water channel.



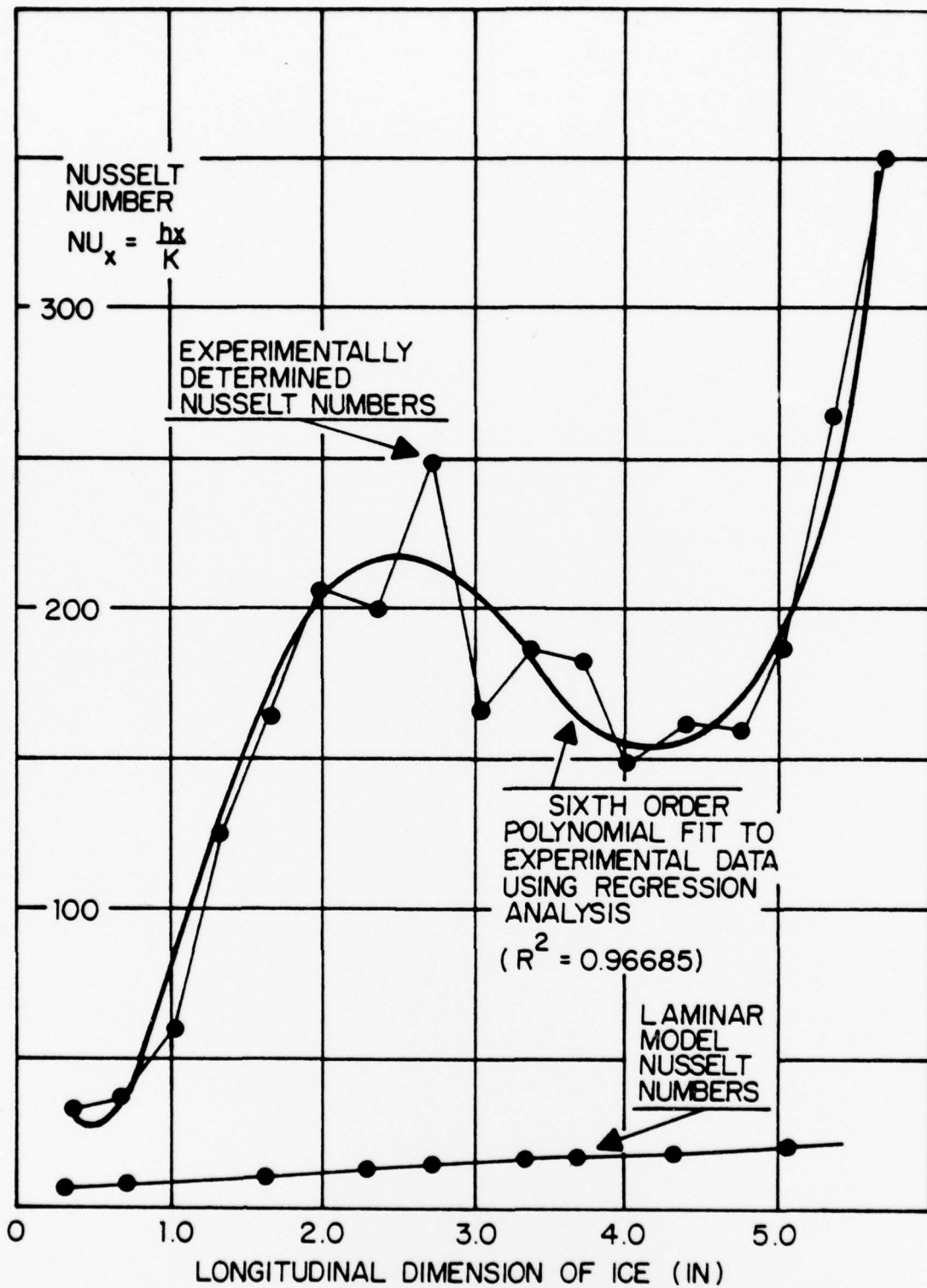
5. NPS water channel.



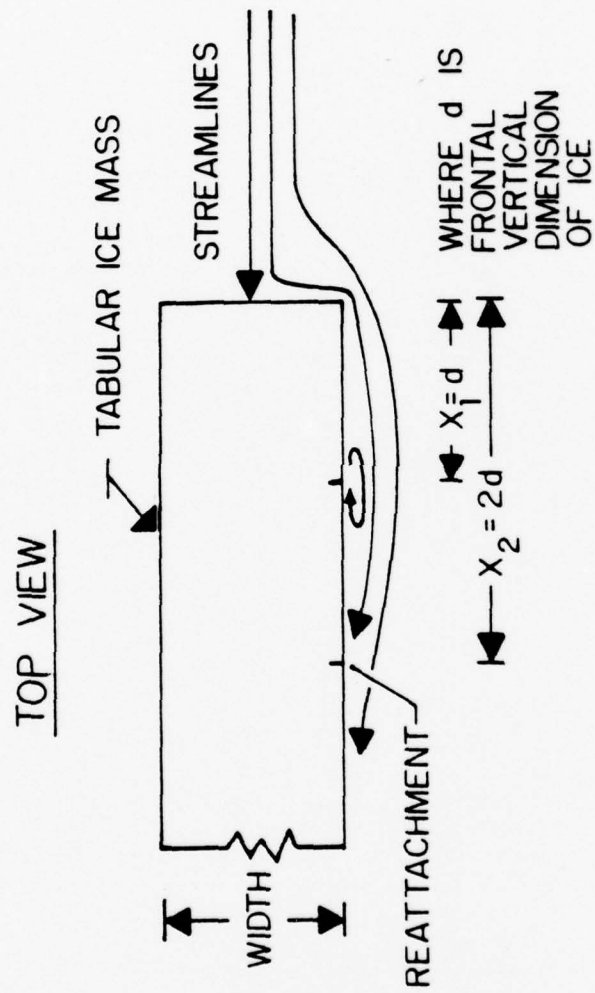
6. Progressive regression of second laboratory model.



7. Progressive regression of streamlined laboratory model.



8. Effectiveness of heat transfer.



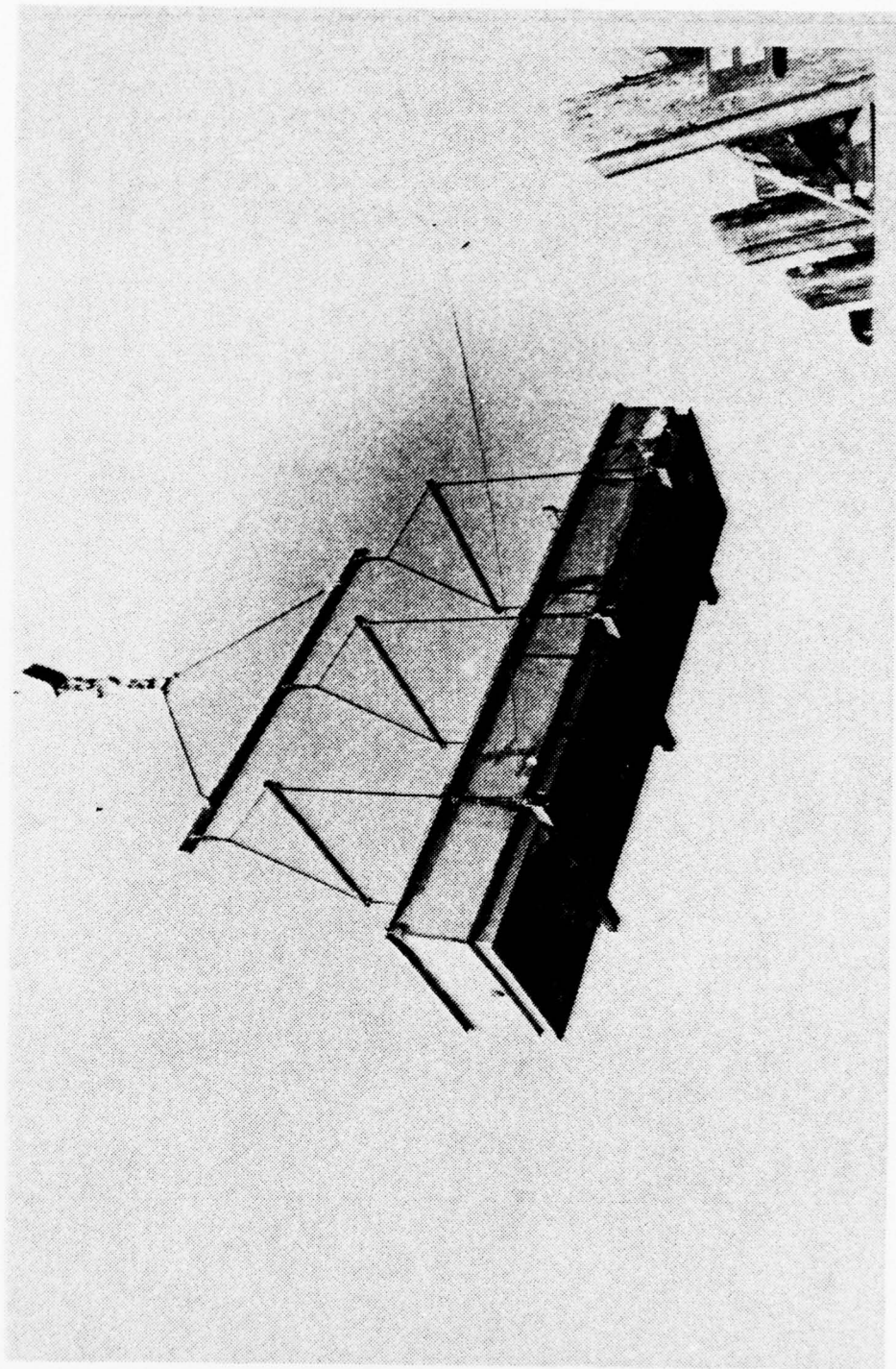
FLOW REATTACHMENT WITH ACCOMPANYING LARGE
HEAT FLUX.

9. Flow reattachment with accompanying large heat flux.

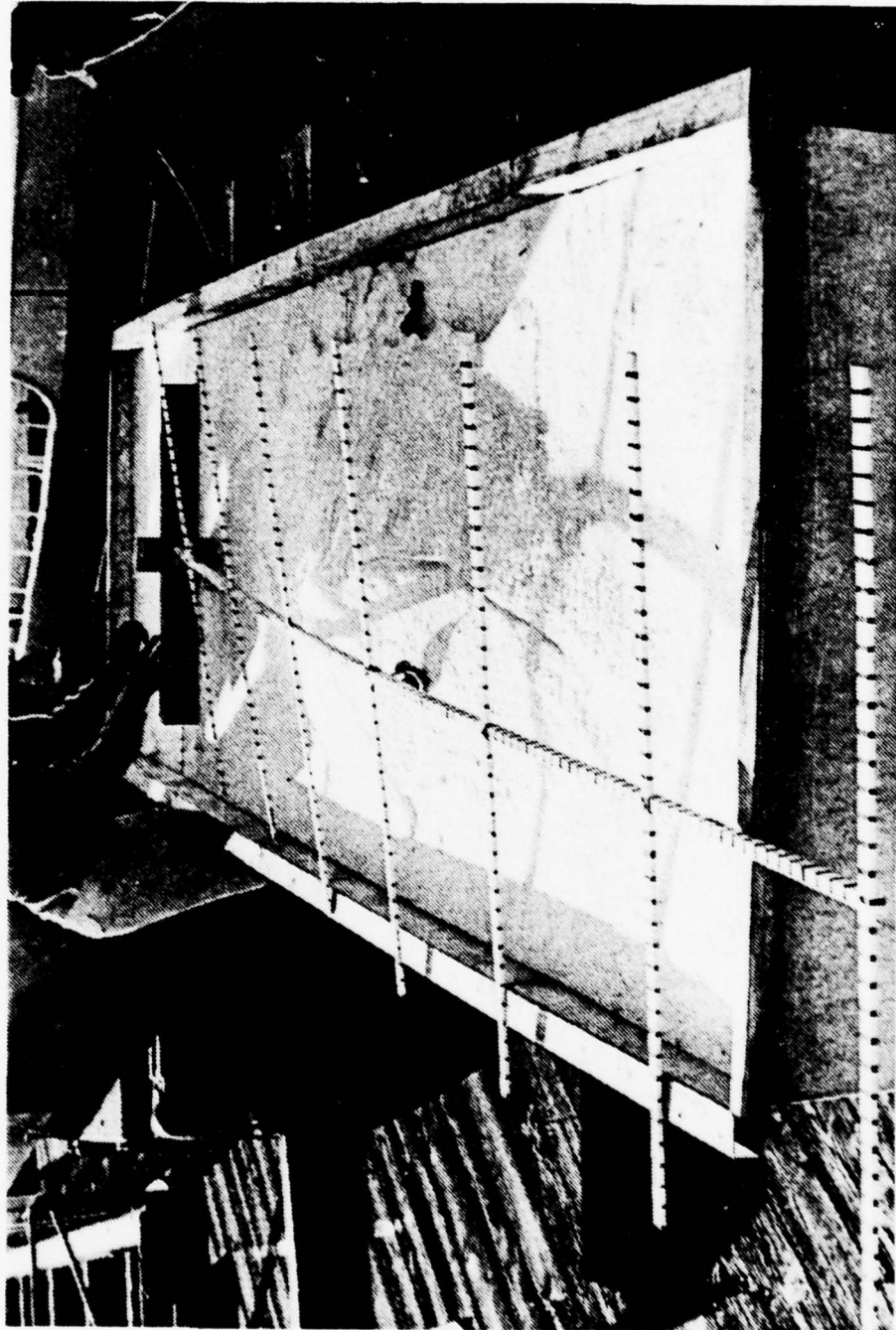


TRAPPED VORTEX FILAMENT

10. Trapped vortex filament.

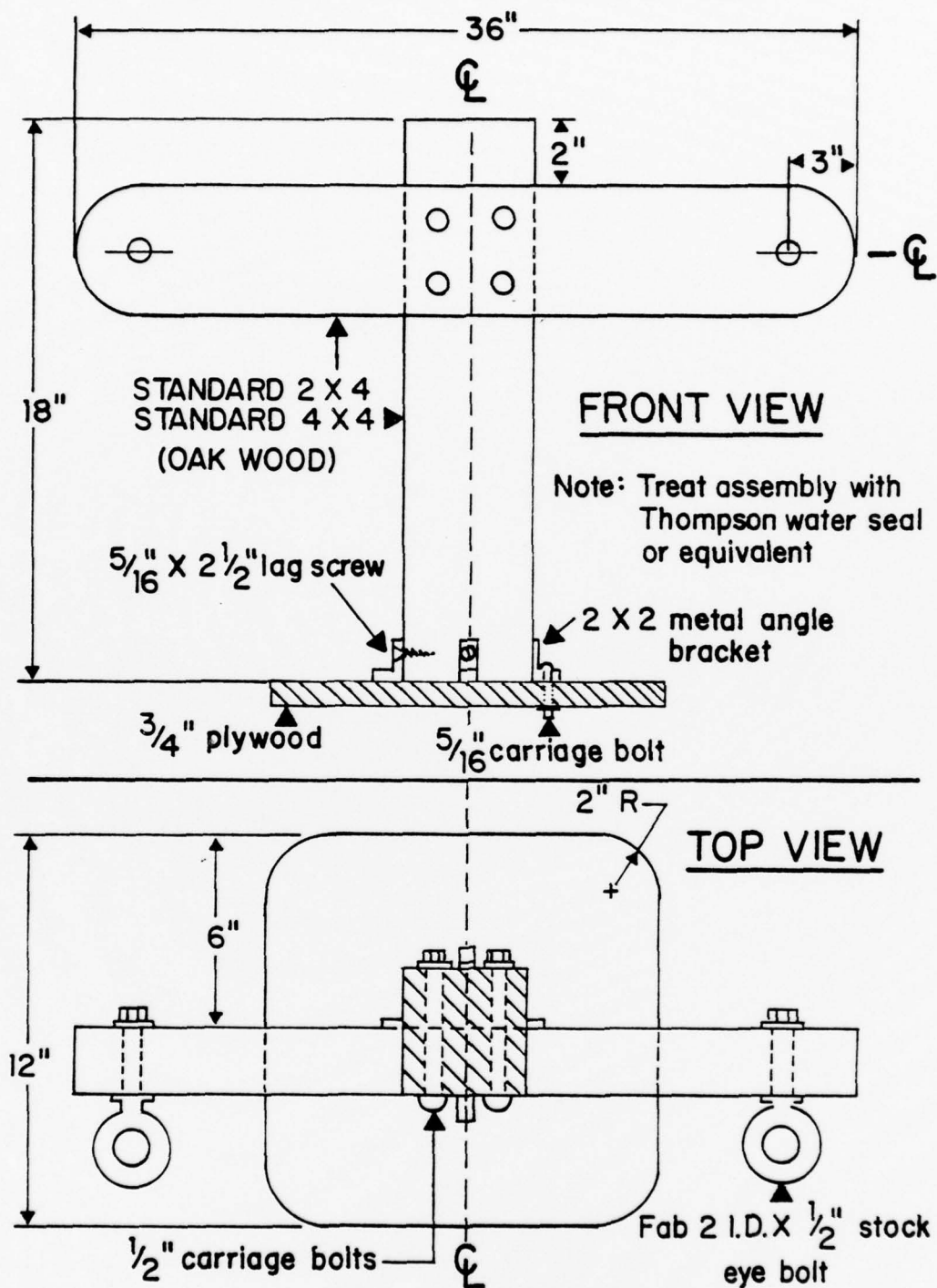


11. Ice model freezing container.

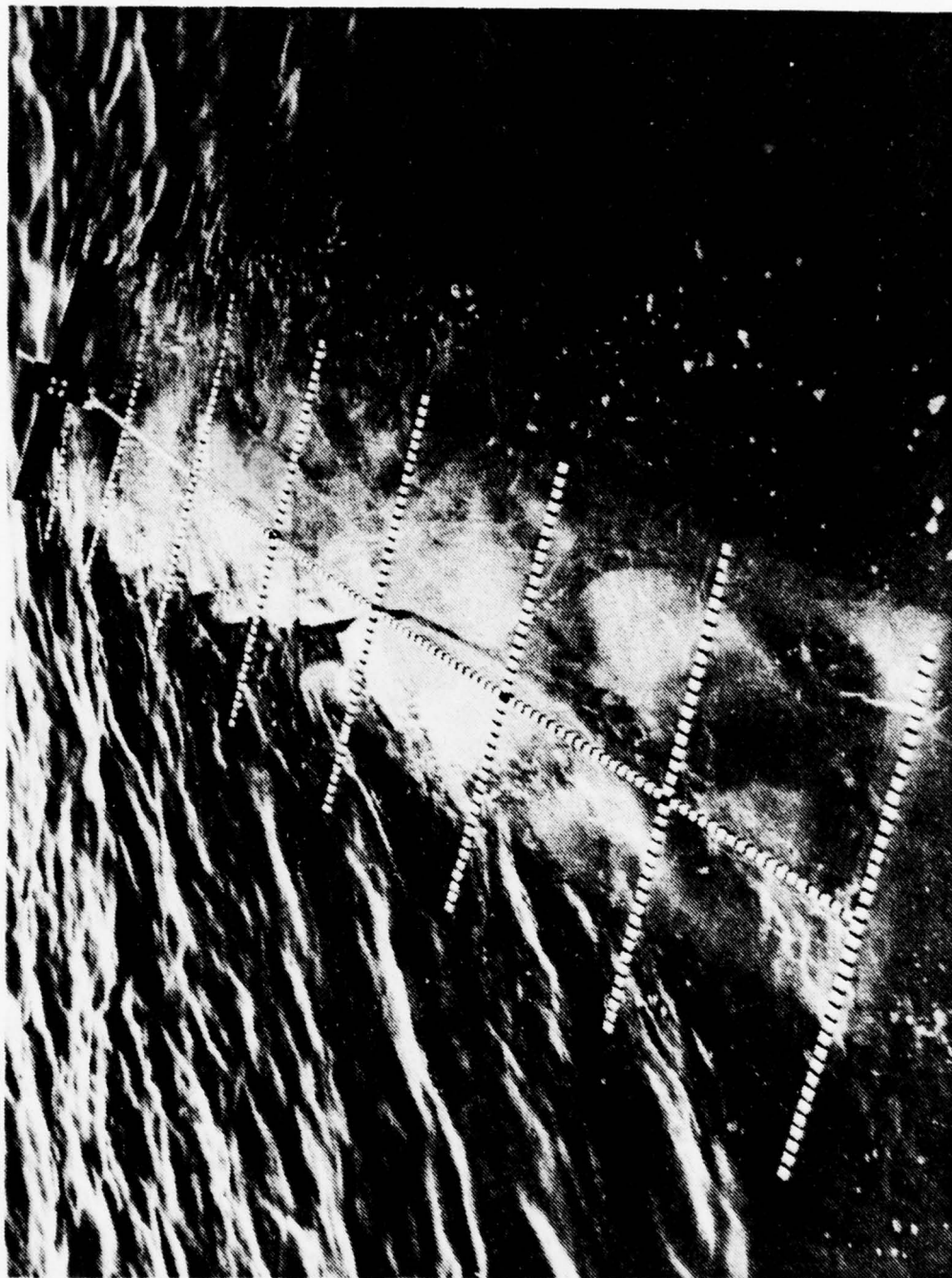


12. Top view of ice model freezing container.

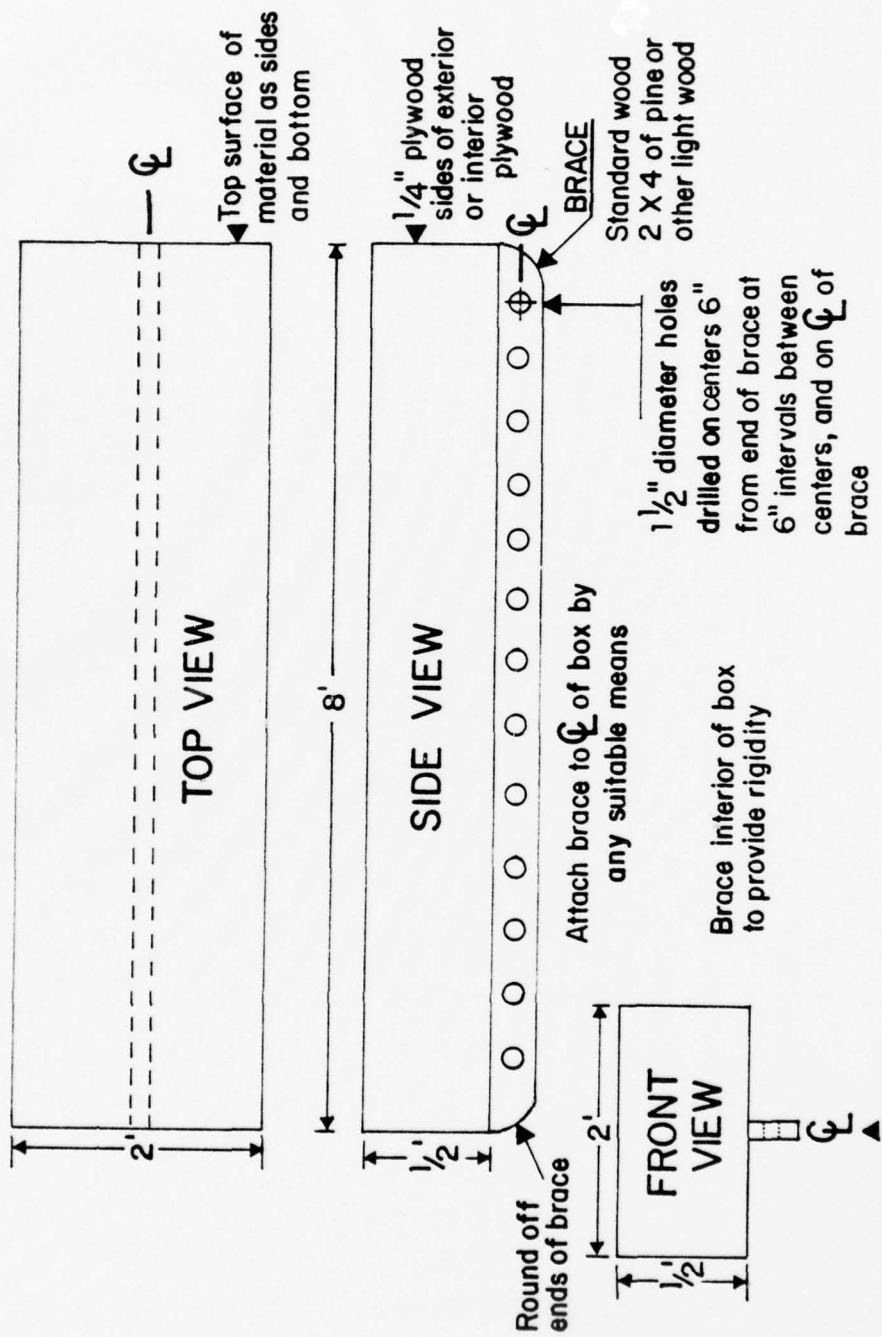
GLACIAL ICE TOWING BOLLARD



13. Towing bollard.

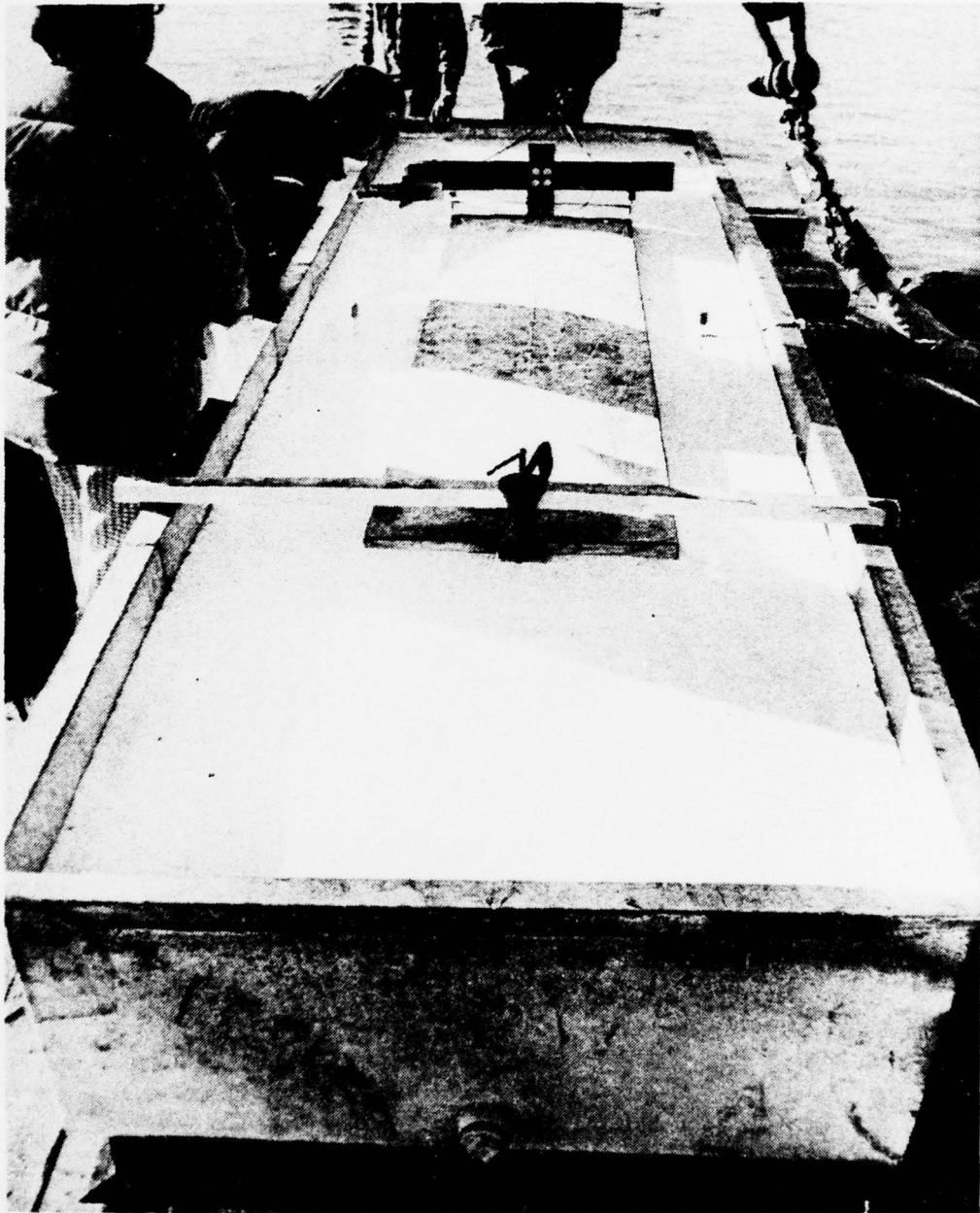


14. Premature disintegration of ice model.

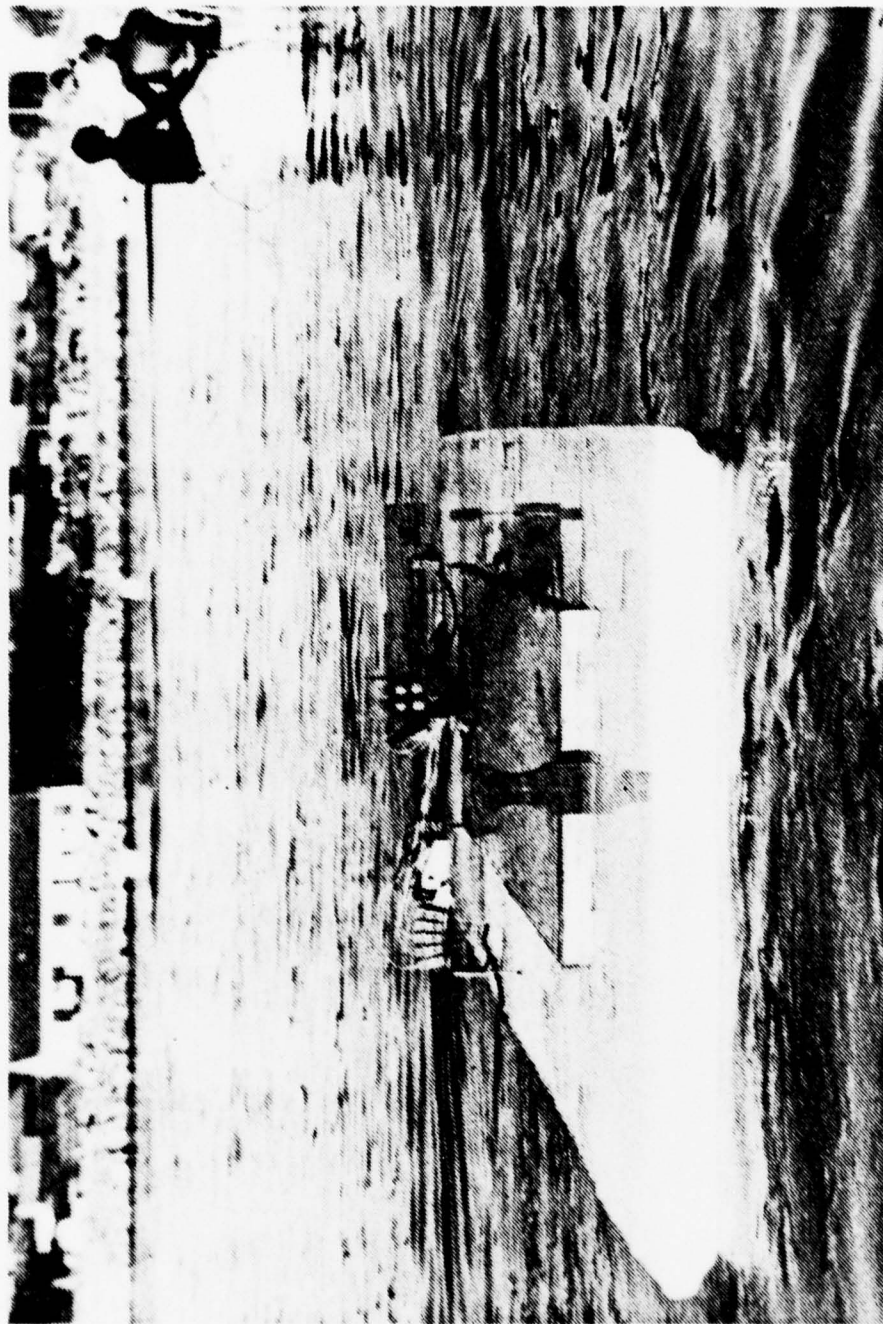


GLACIAL ICE CORE BOX

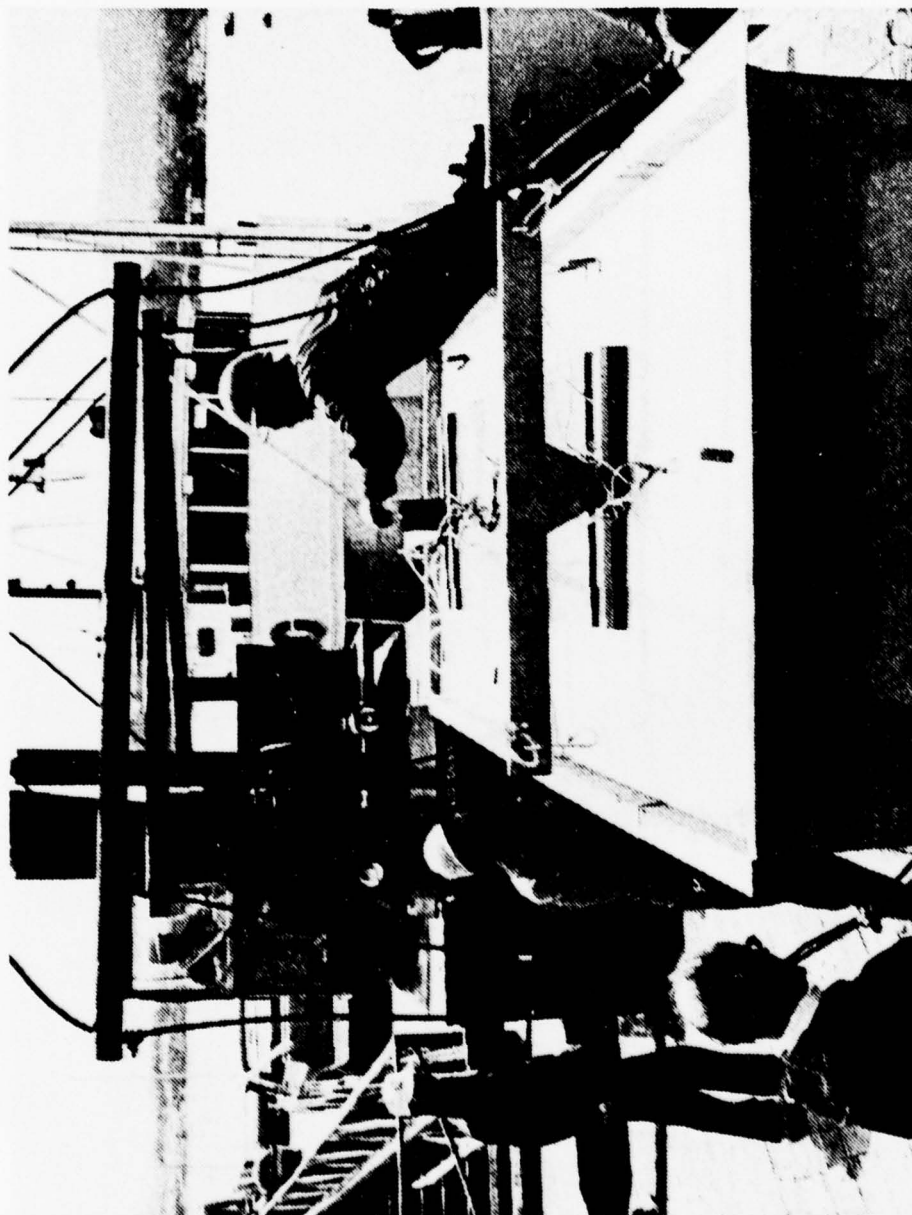
15. Archimedes box (core box).



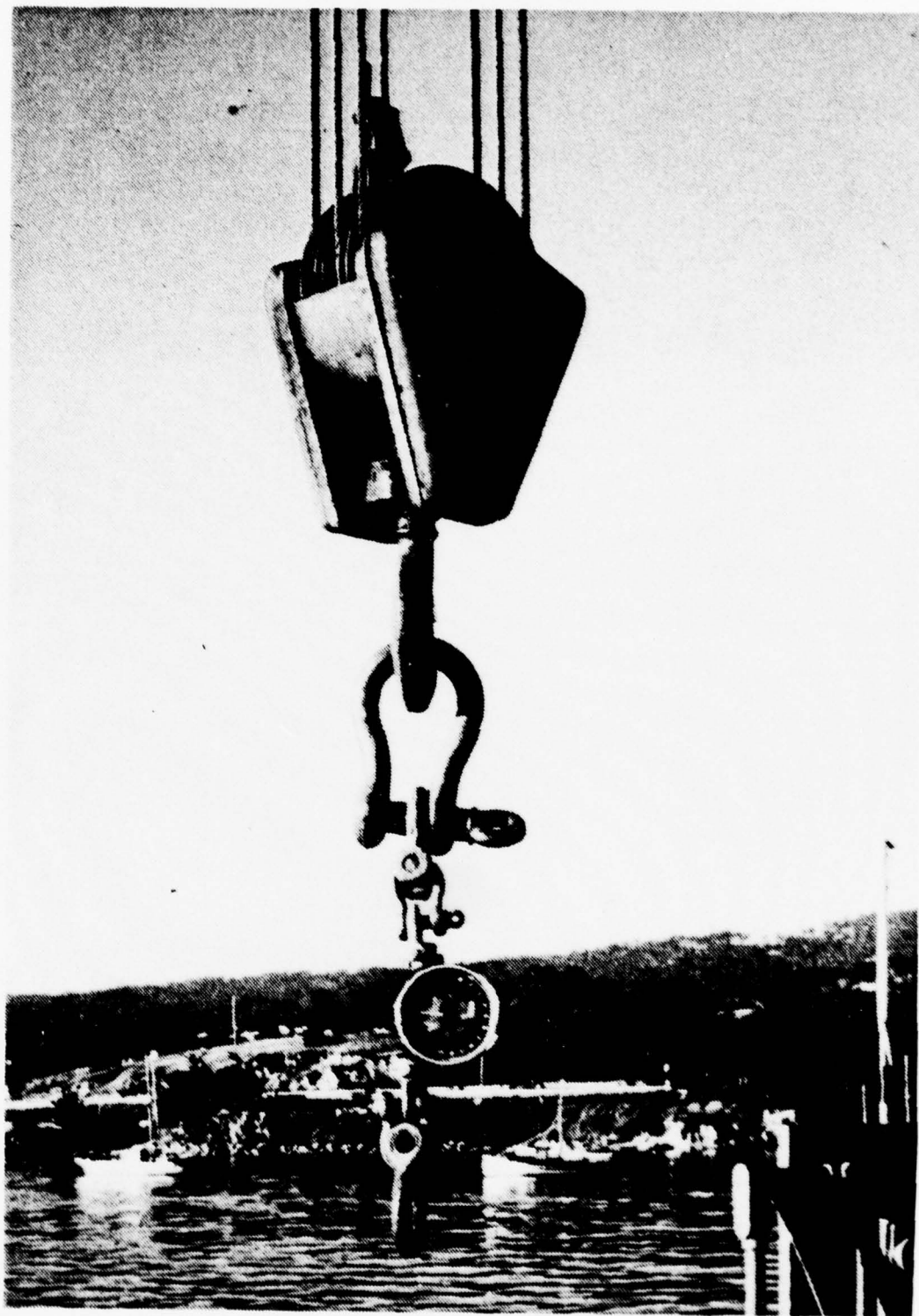
16. Core box installation.



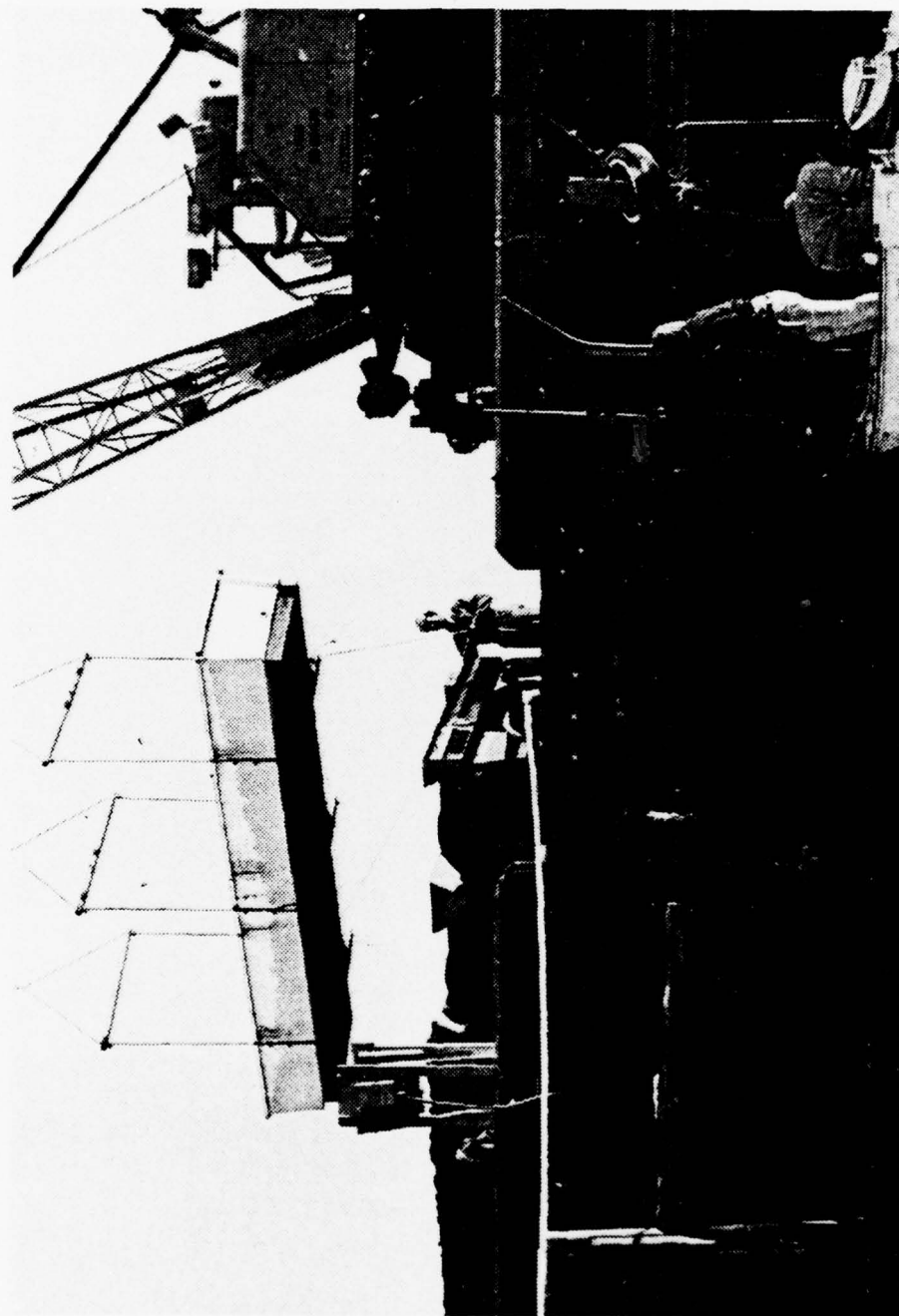
17. Ice model underway with core box installed.



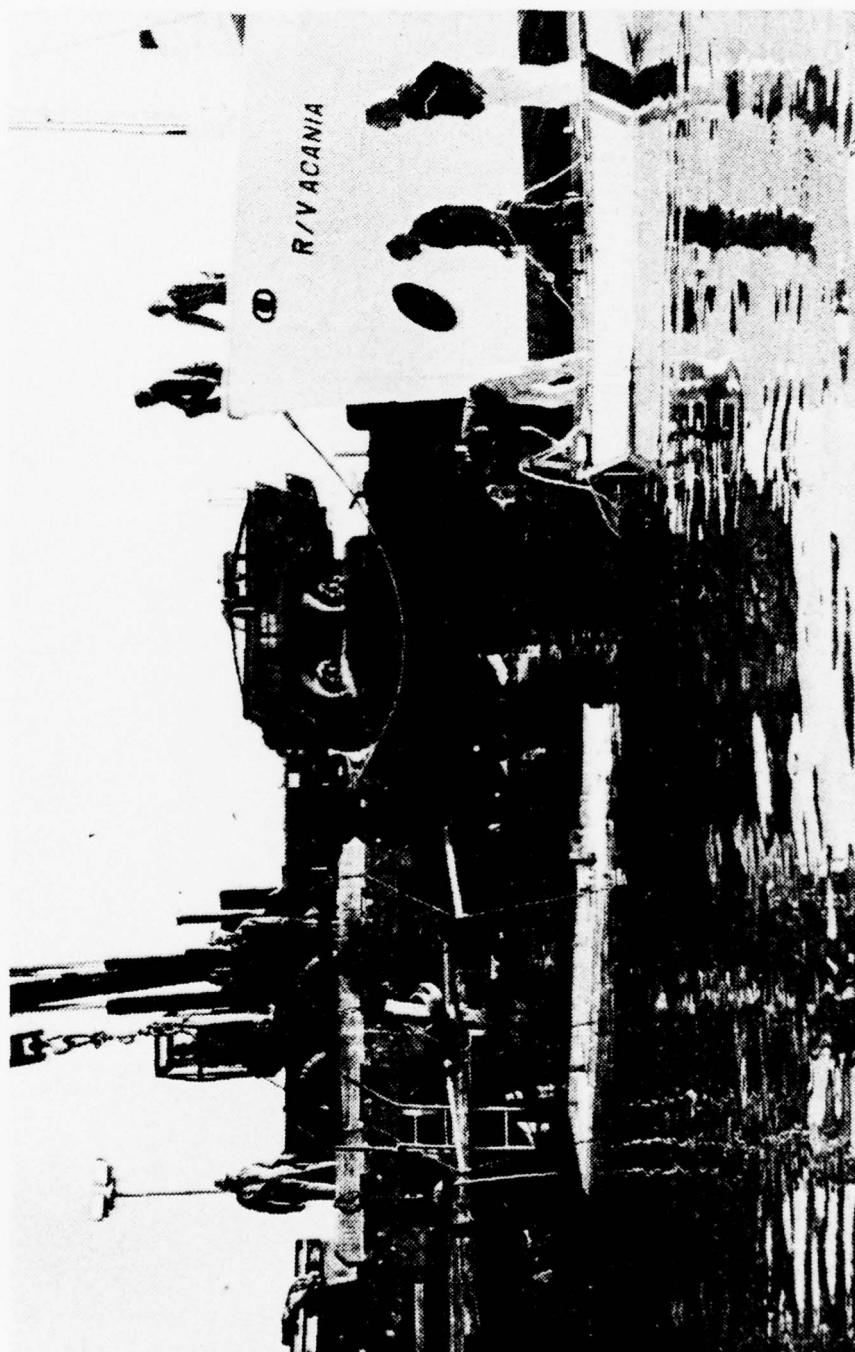
18. Ice model with towing bollard integral with core box.



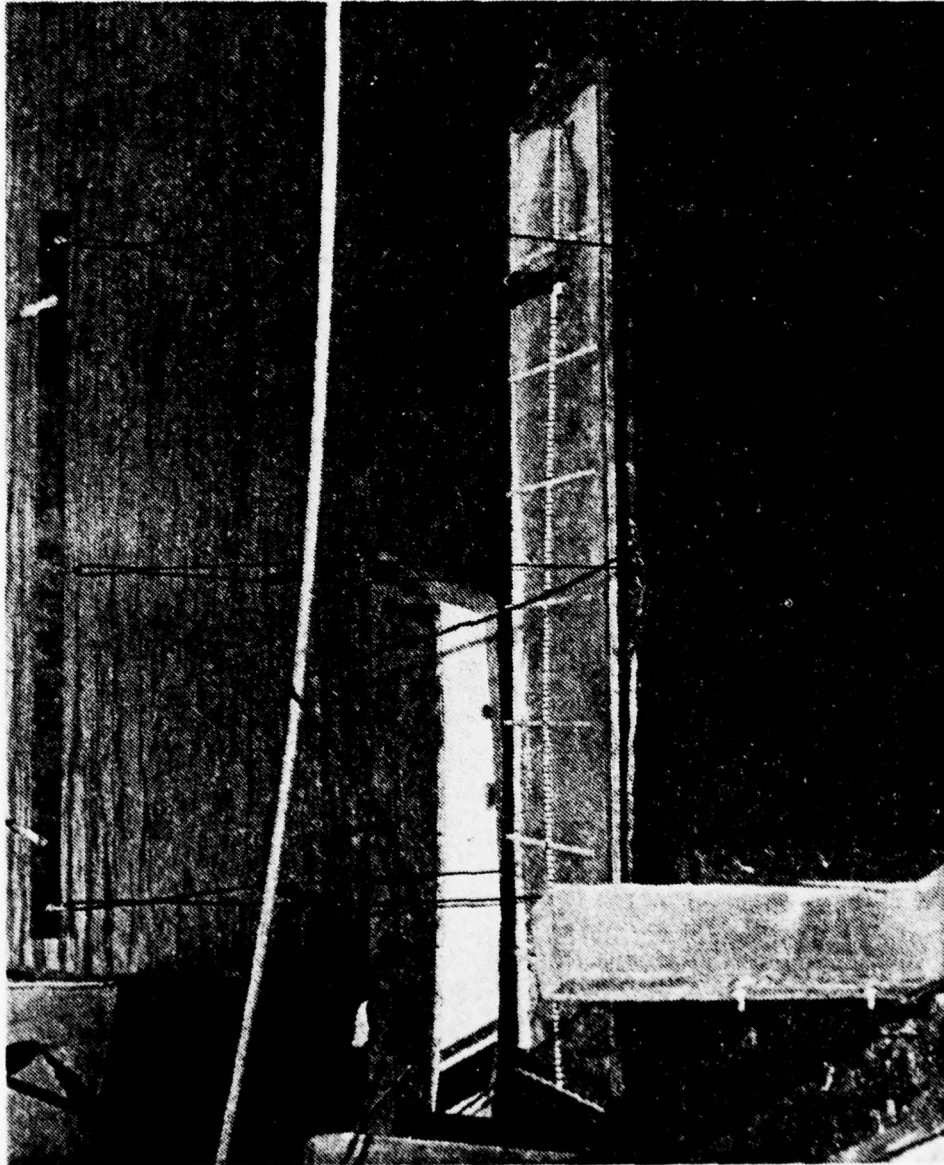
19. Scale used to weigh ice and container.



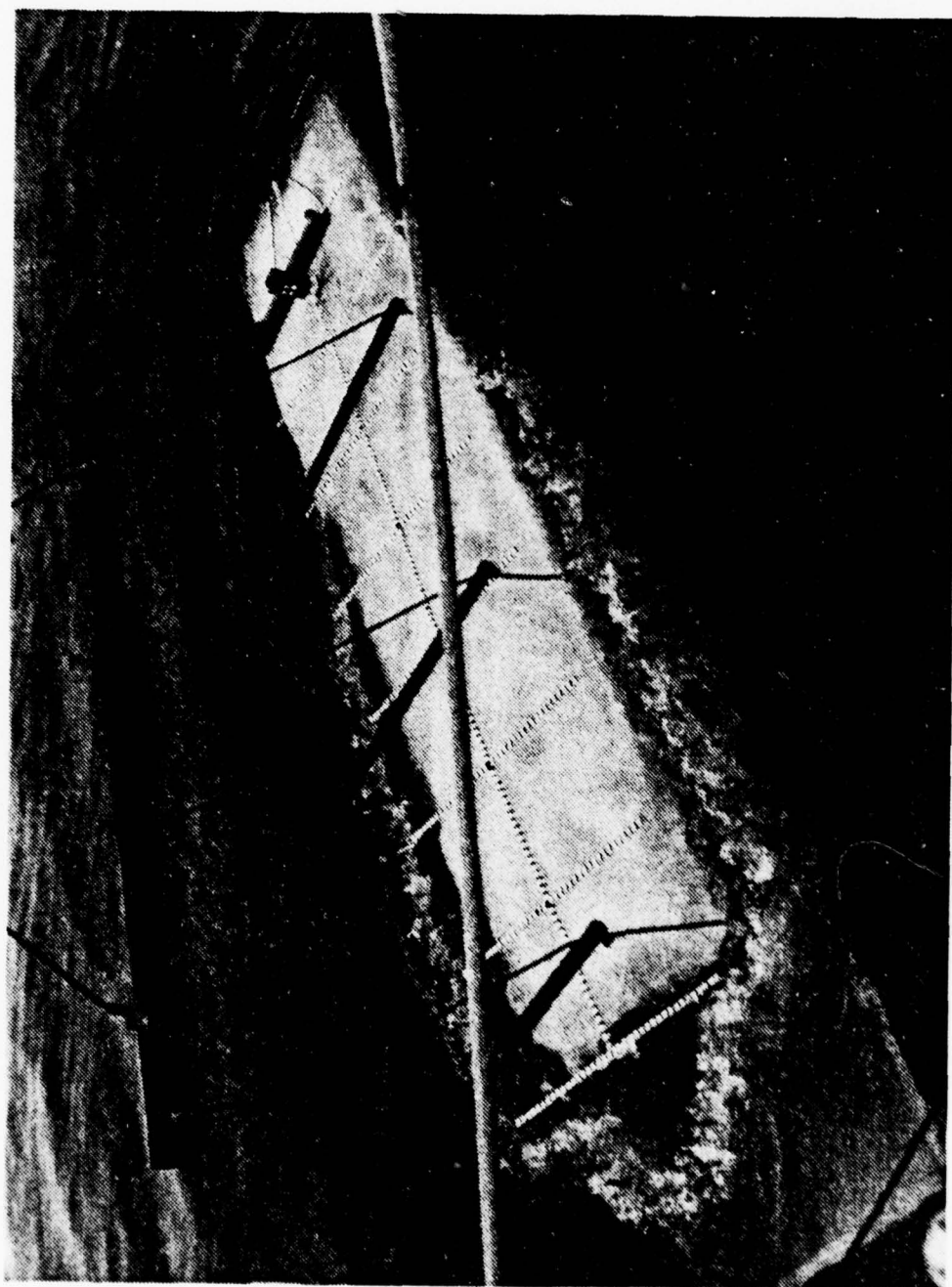
20. Positioning of ice container near water and towing vessel.



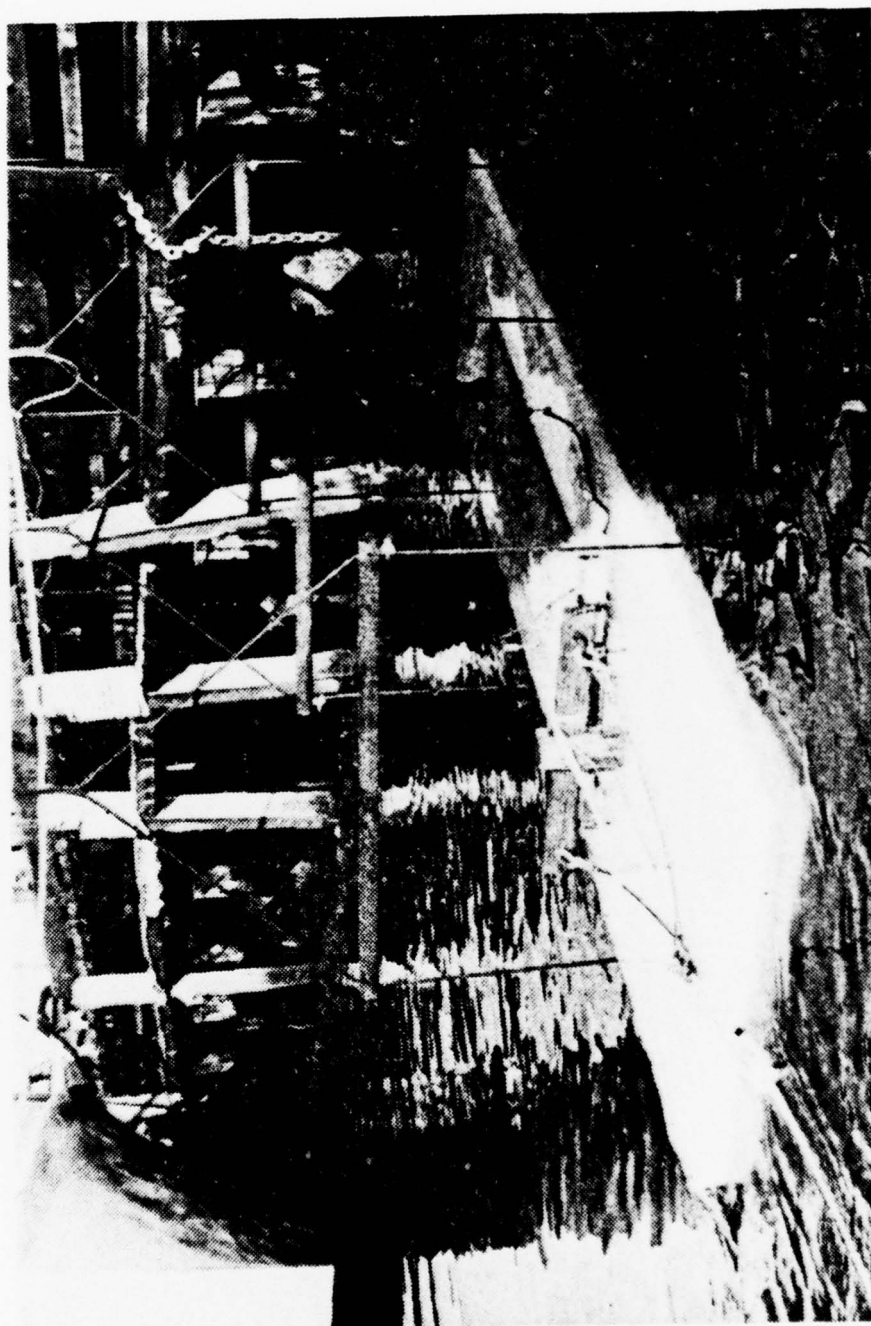
21. Ice container being lowered into the water.



22. Seawater flooding into ice container.



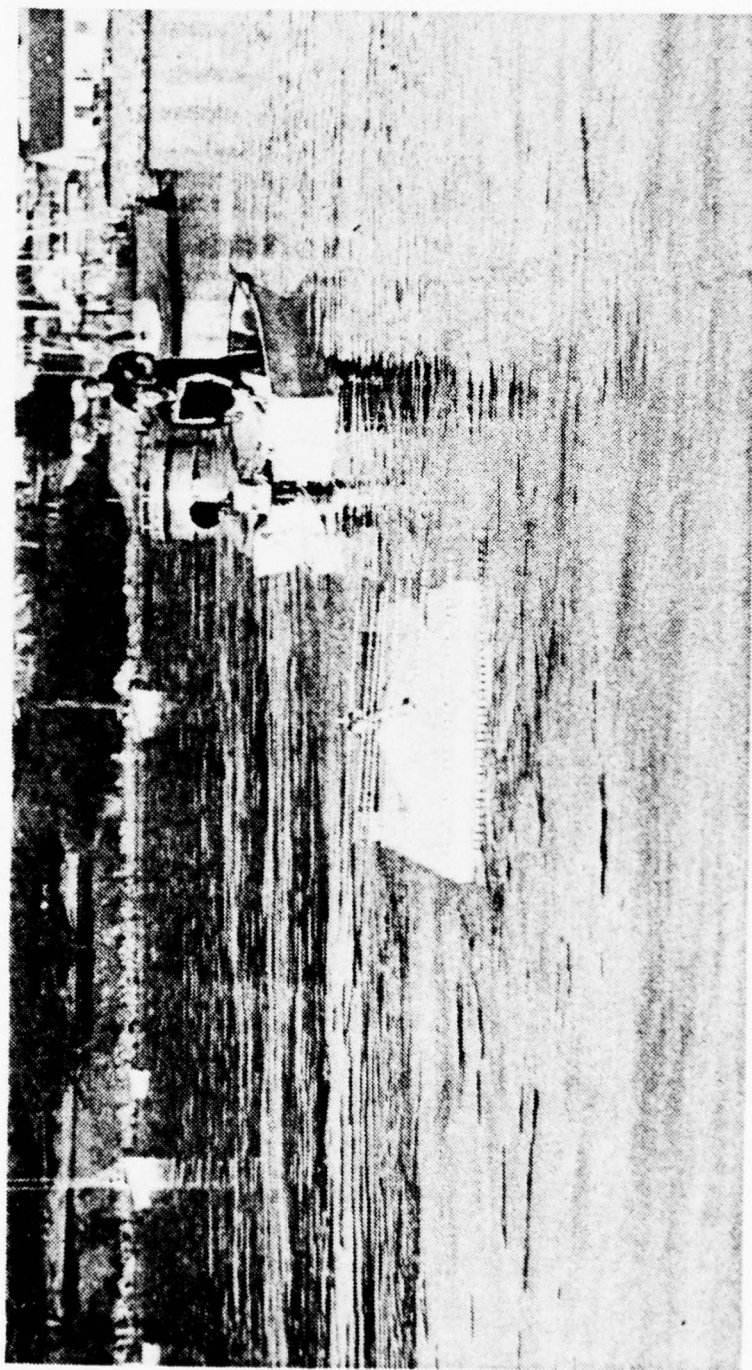
23. Ice model separation from container.



24. Ice model underway.



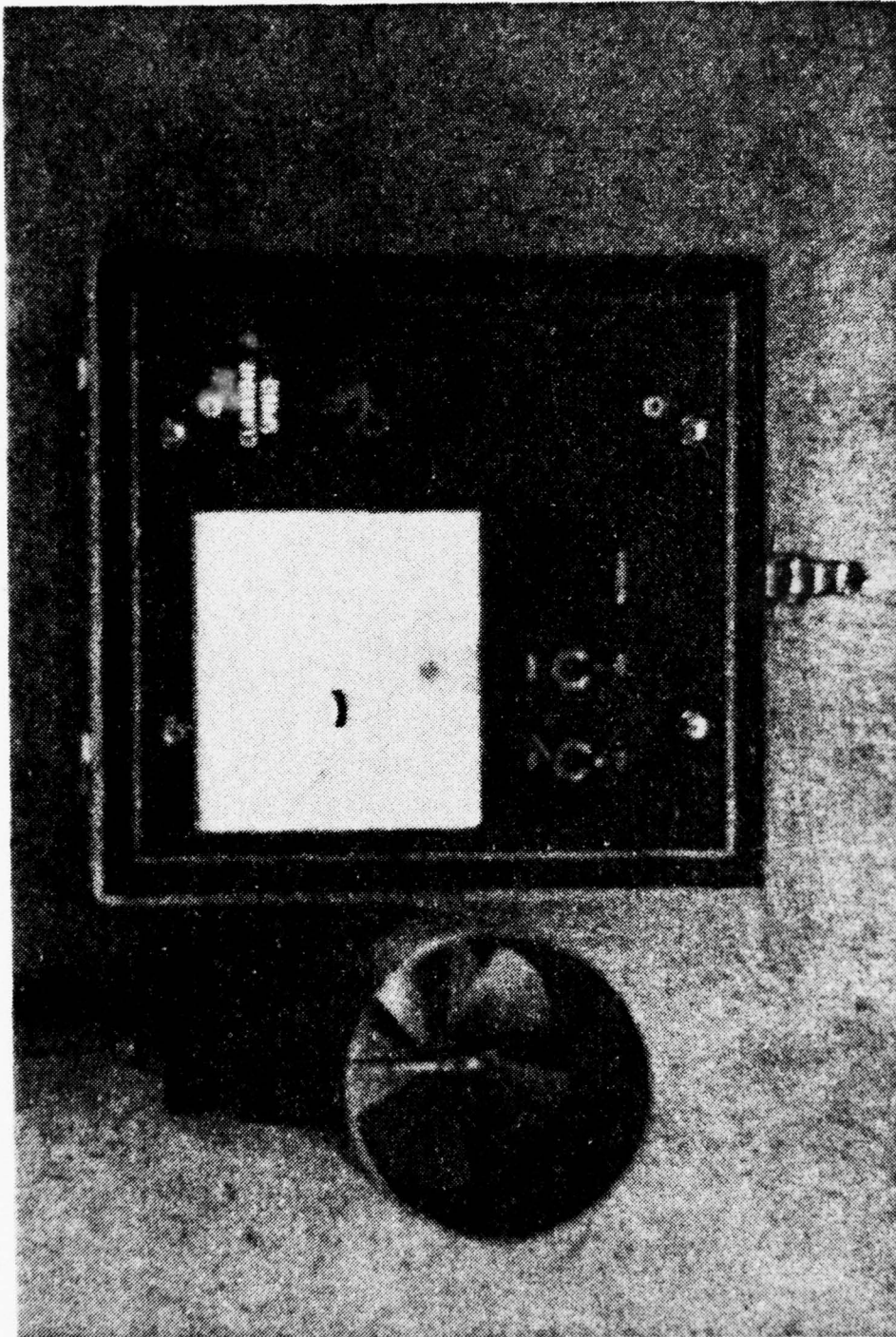
25. Coast Guard vessel with model in tow.



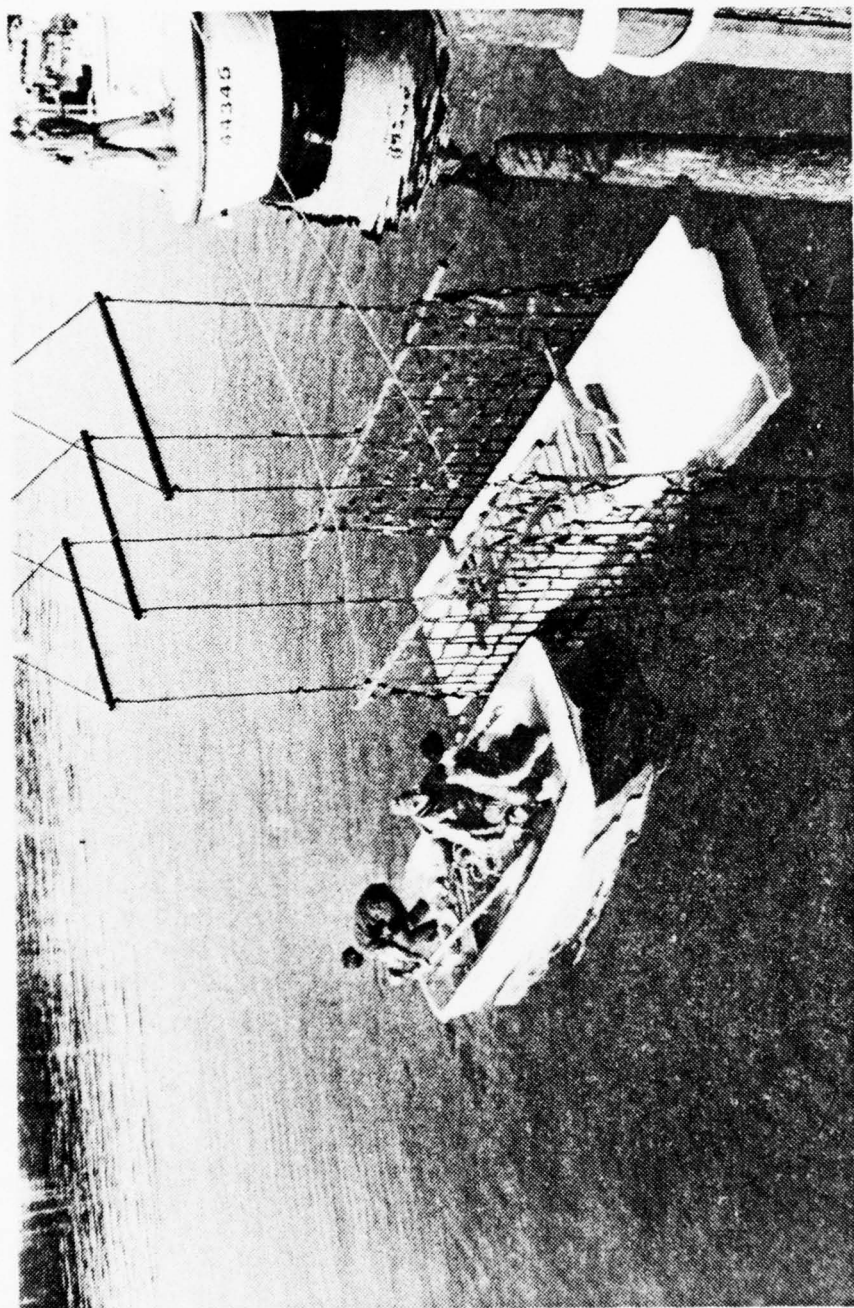
26. Boston whaler with model in tow.



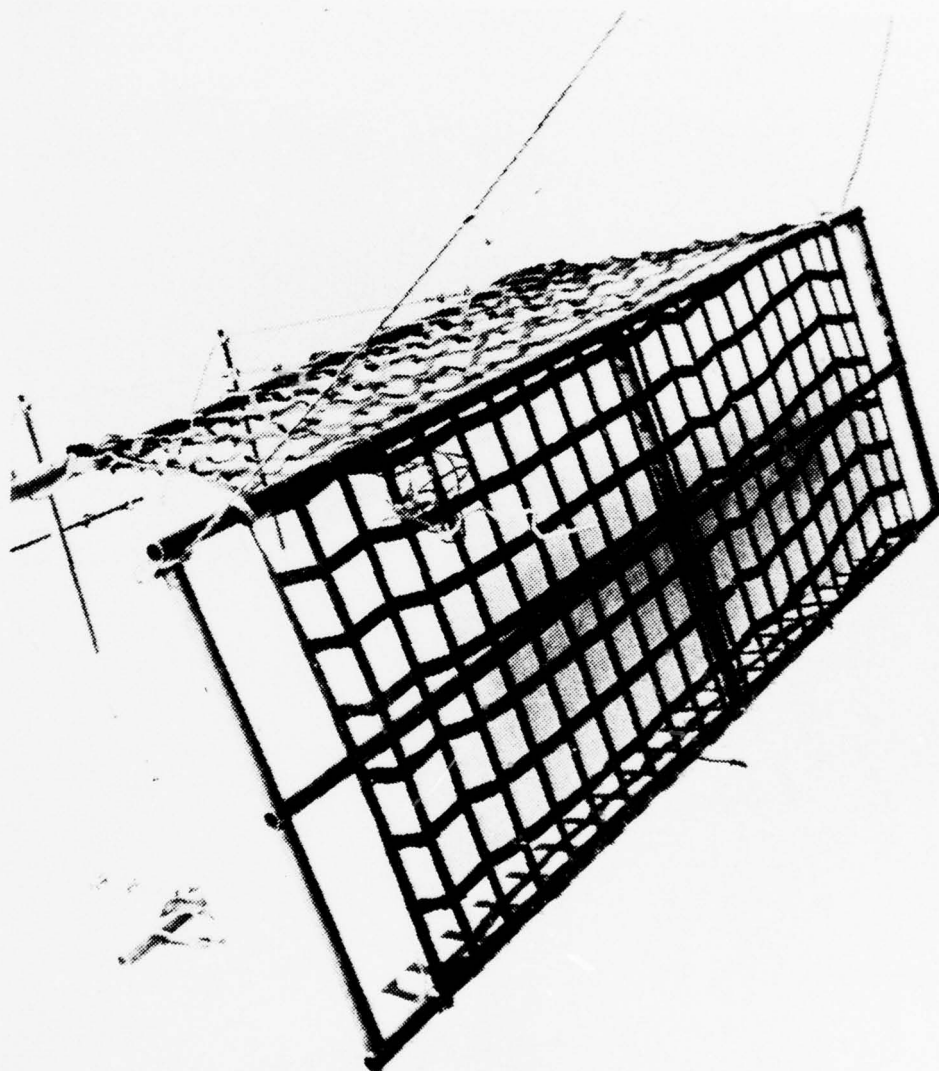
27. Tow rope and instrumentation wire arrangement.



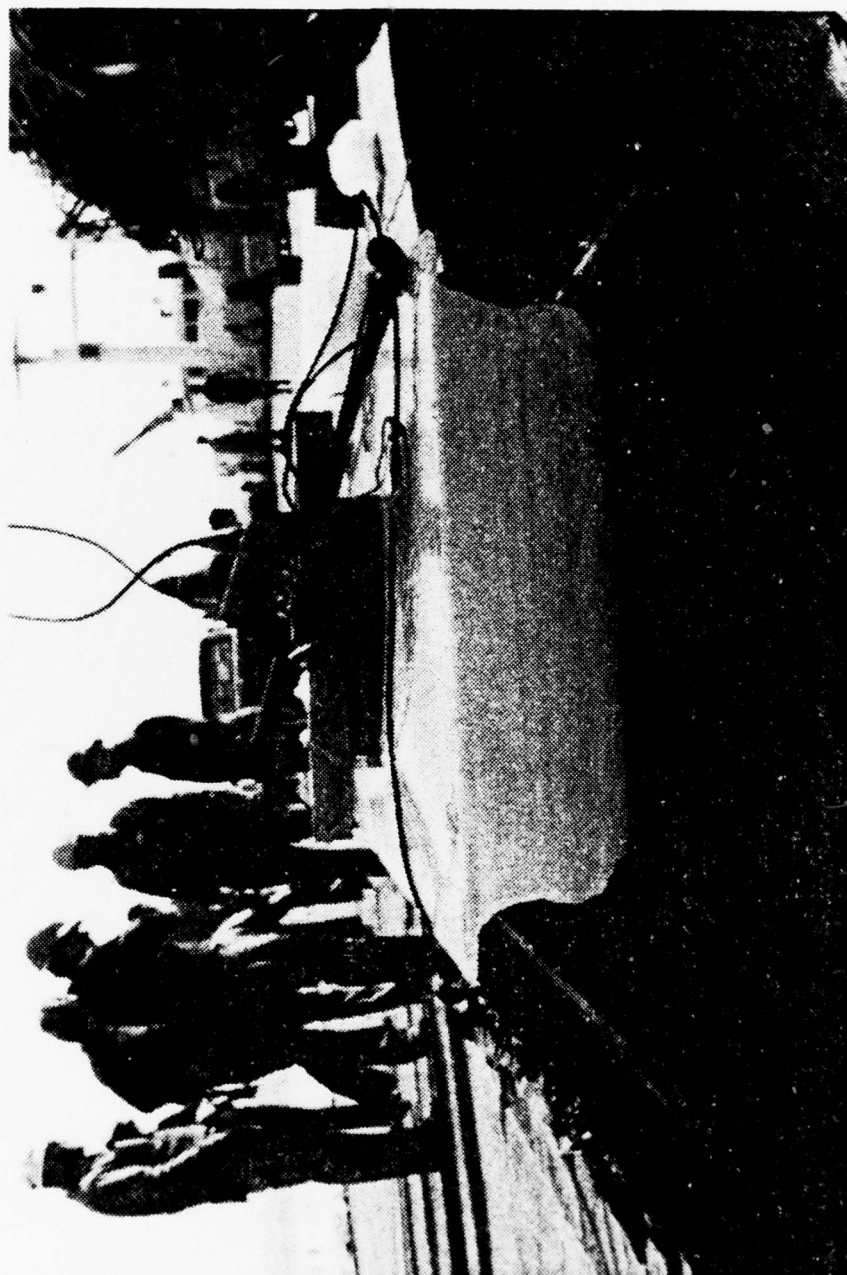
28. Current meter and readout assembly.



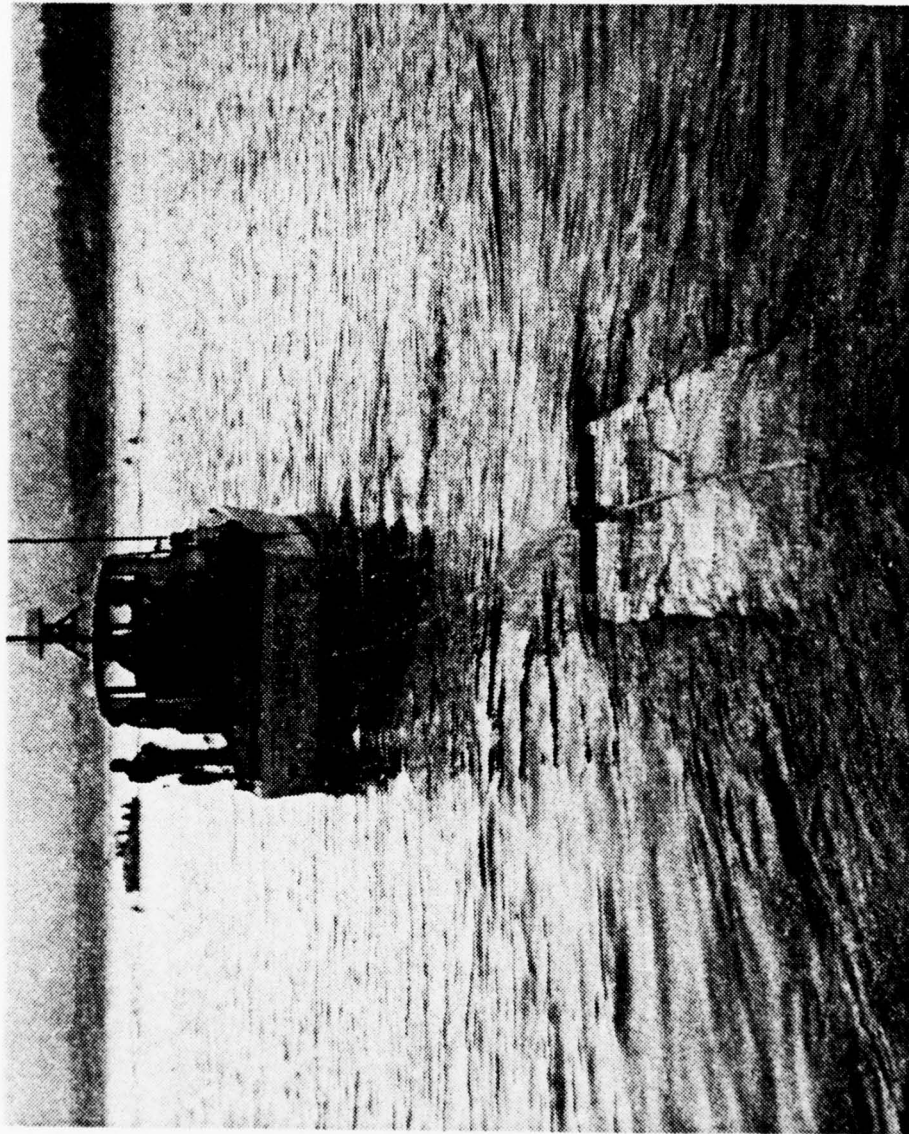
29. Ice model positioned for recovery.



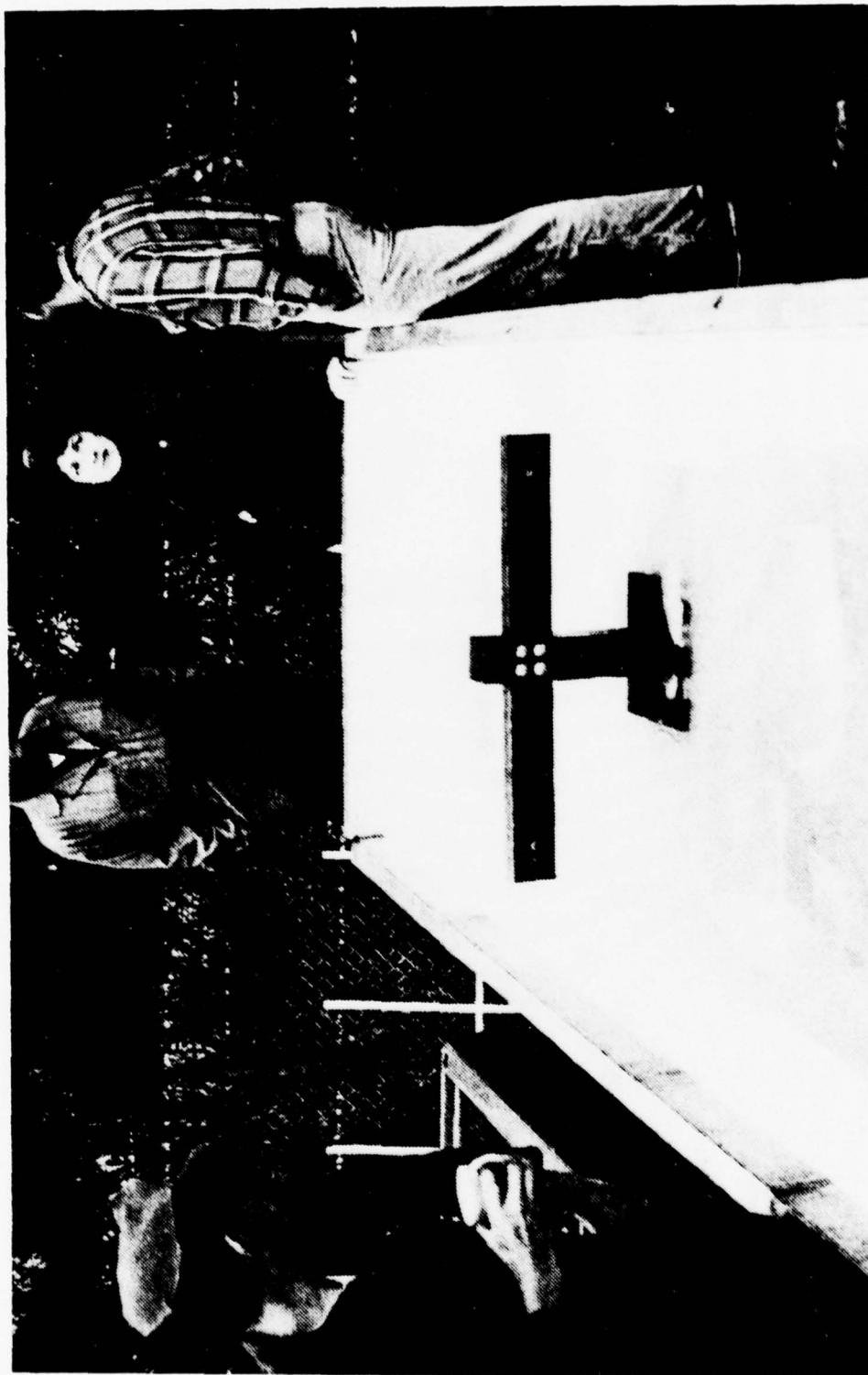
30. Recovered ice model clear of water.



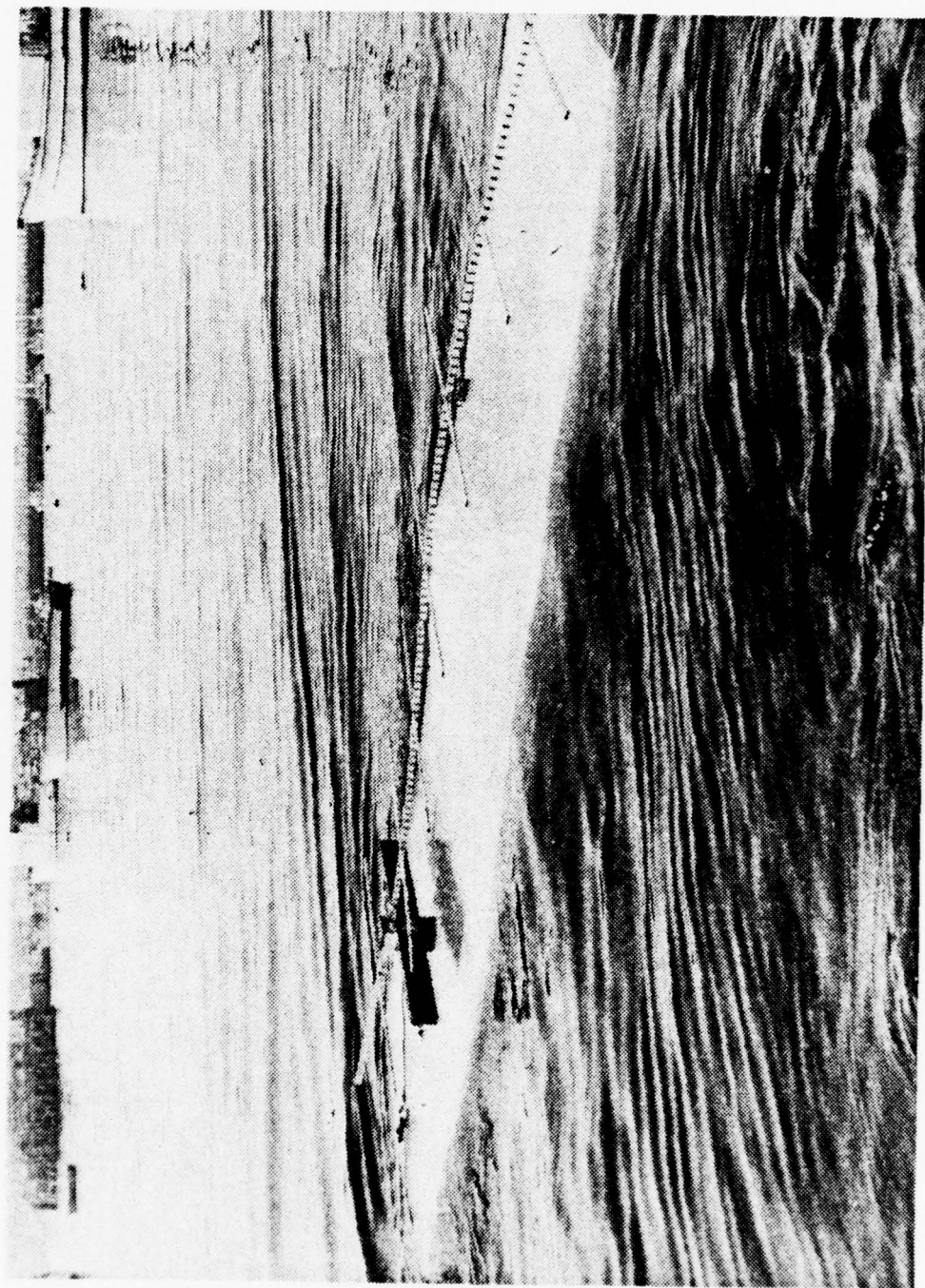
31. Ice model in pier; Test 5.



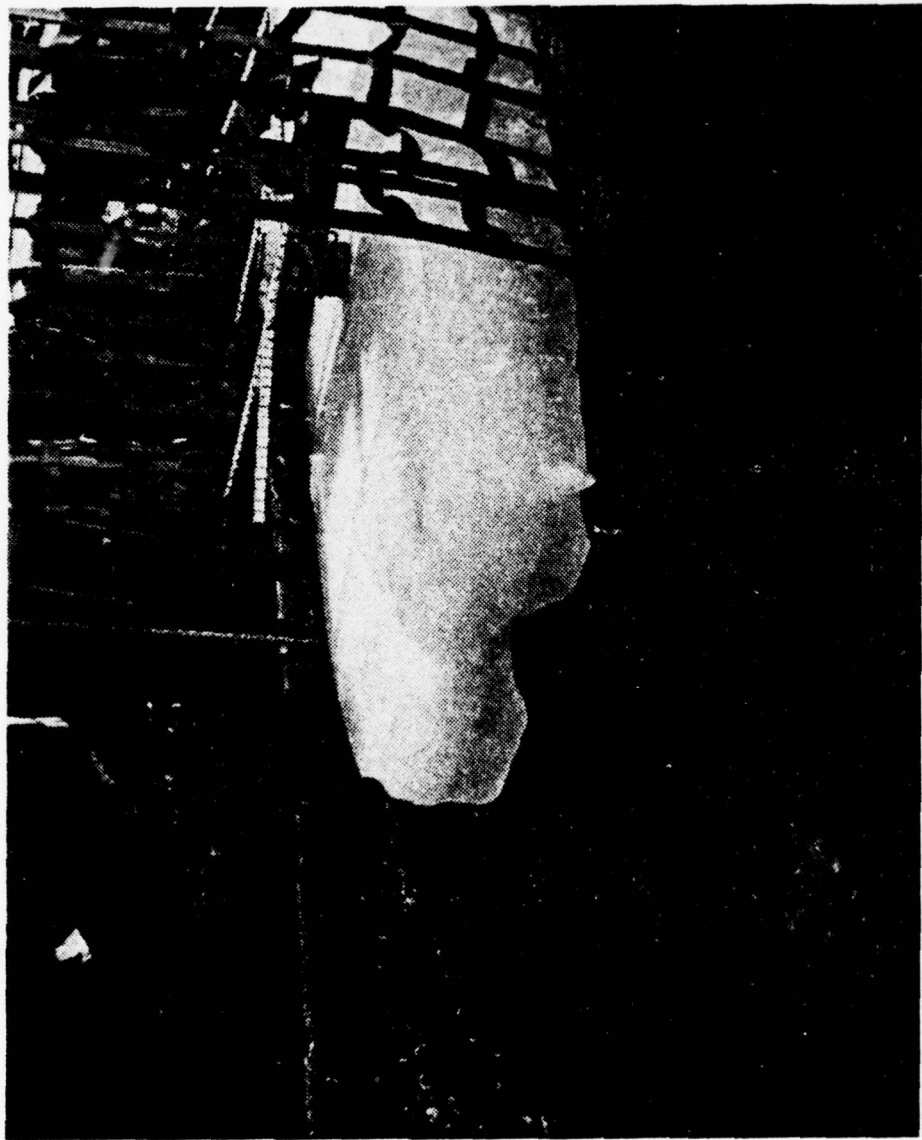
32. Ice model underway; Test 1.



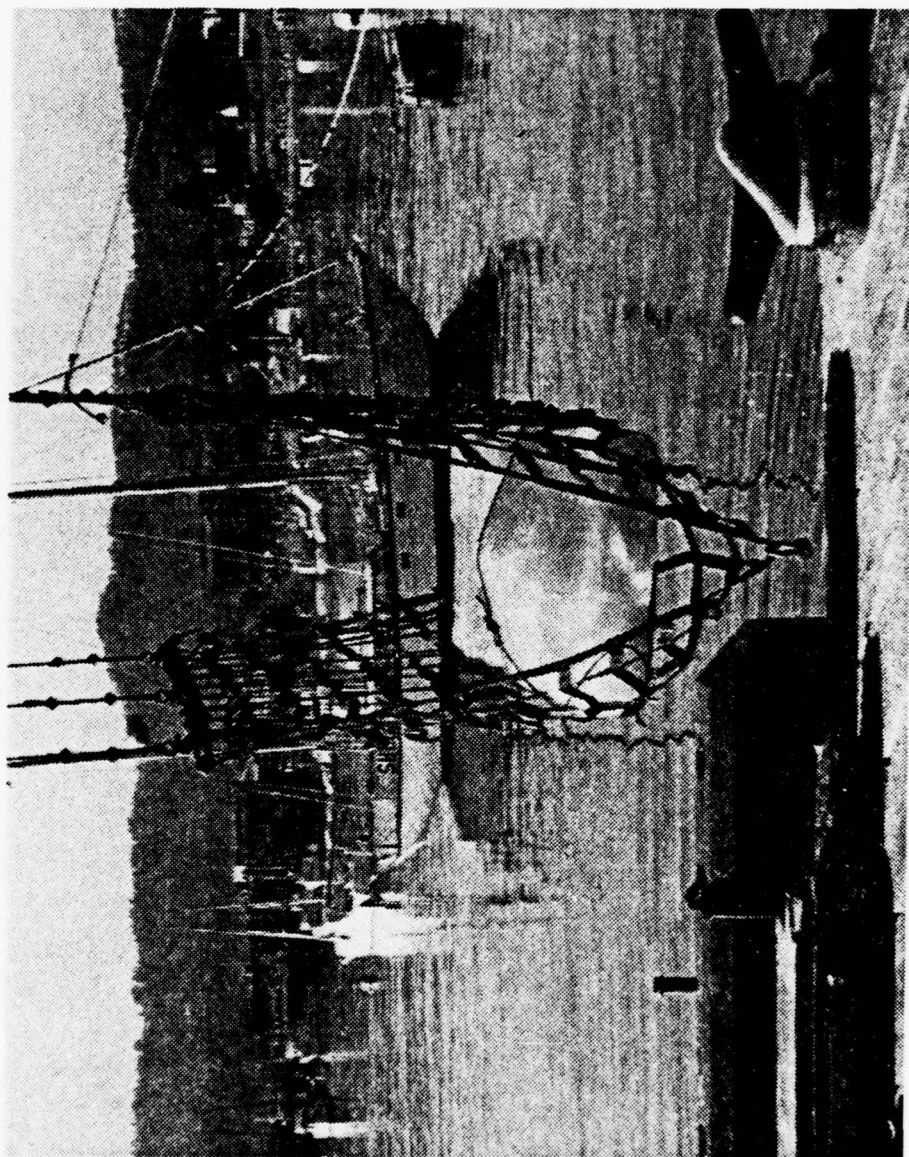
33. Premature disintegration of ice model; Test 2.



34. Ice model underway; Test 3.



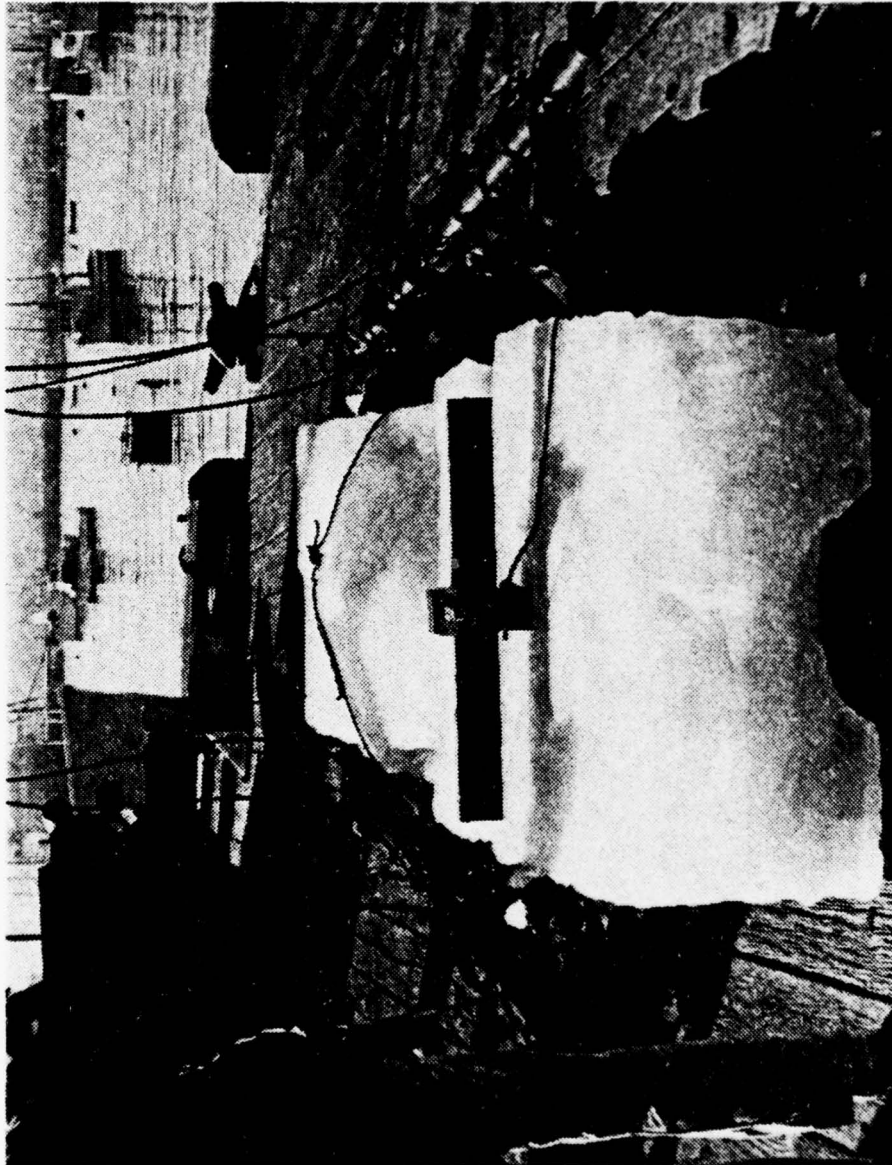
35. Ice model recovery; Test 3.



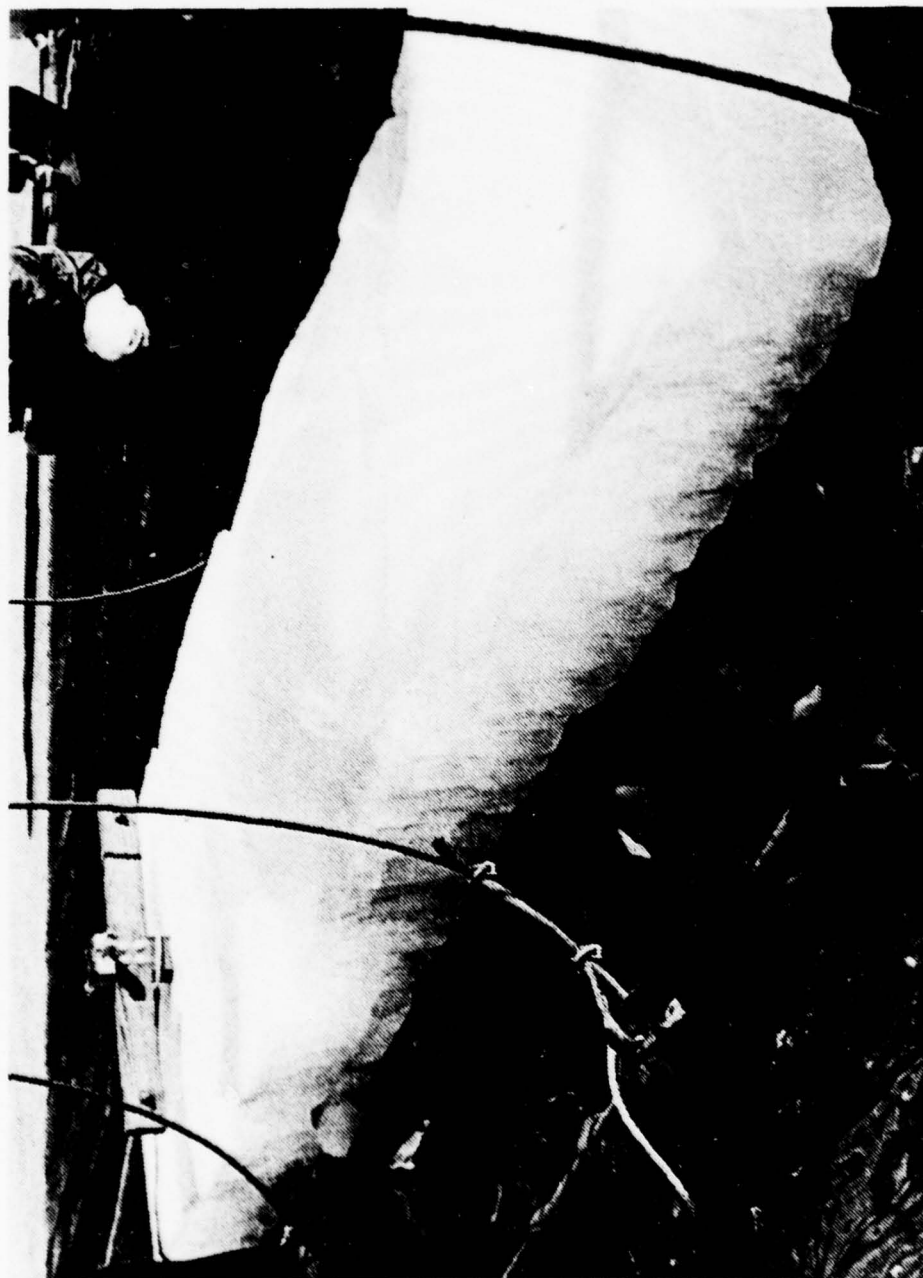
36. Ice model recovered; Test 3.



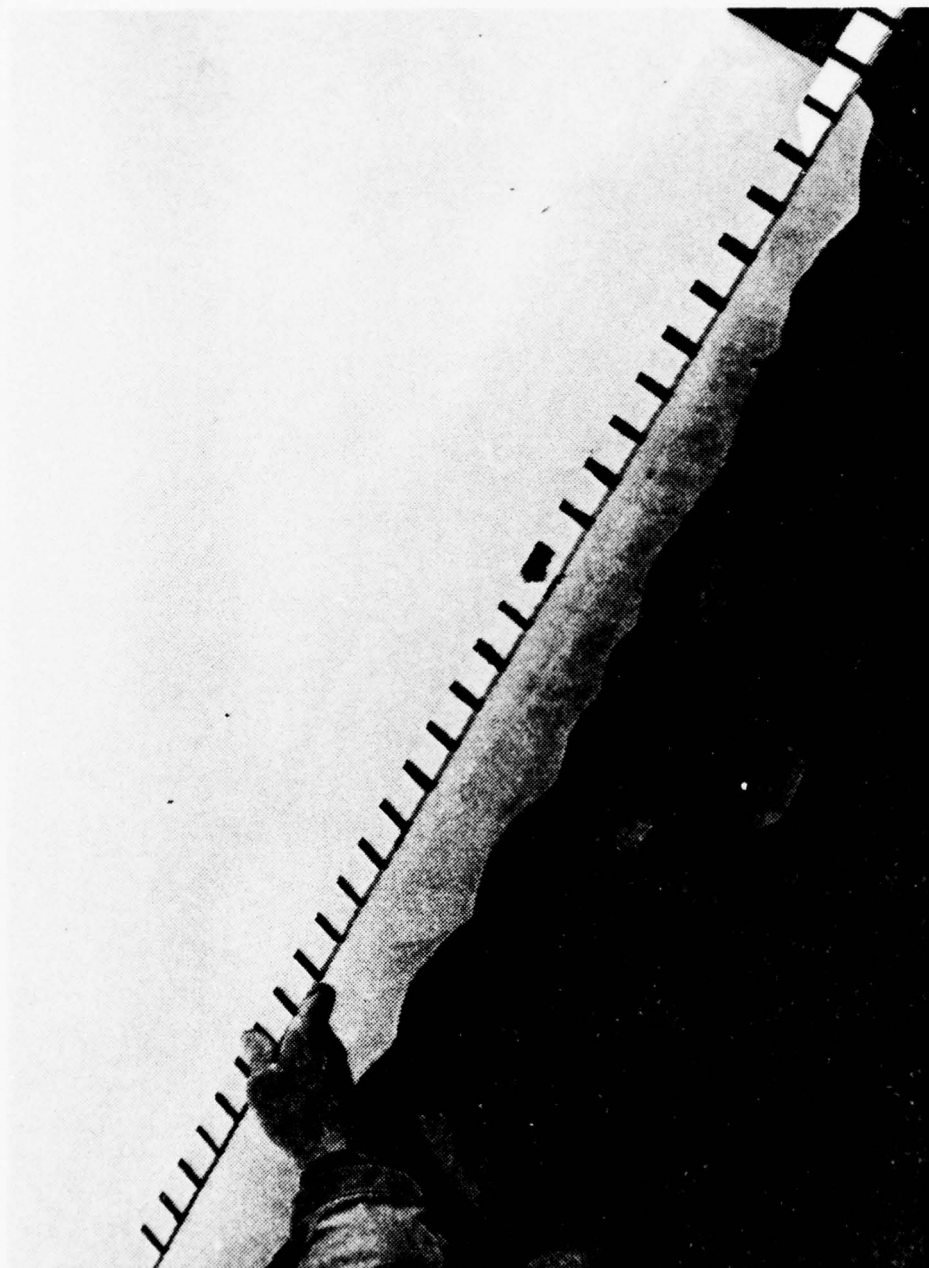
37. Ice model on pier; Test 3.



38. Ice model bow erosion; Test 3.

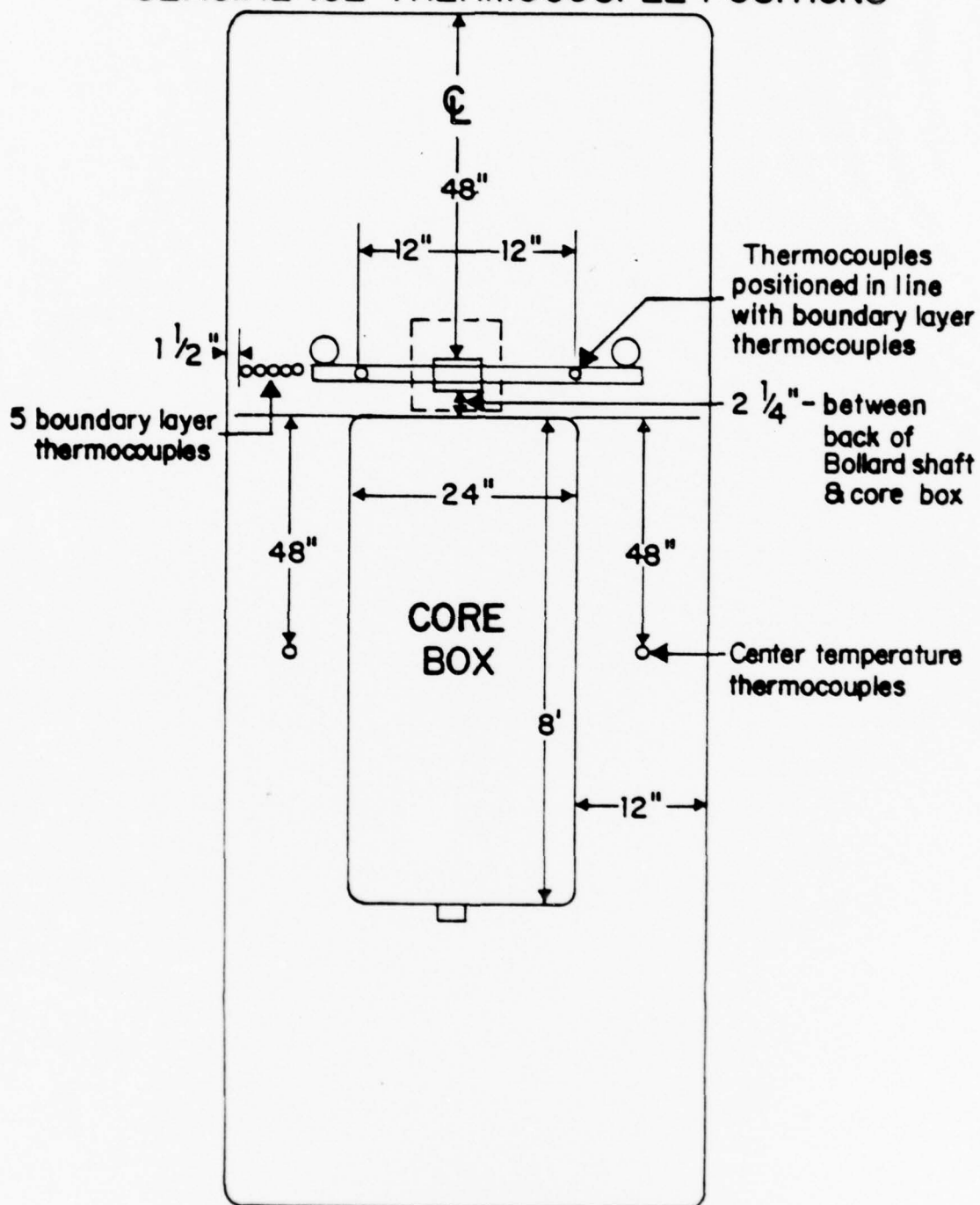


39. Ripples along the complete port side of the ice model; Test 3.

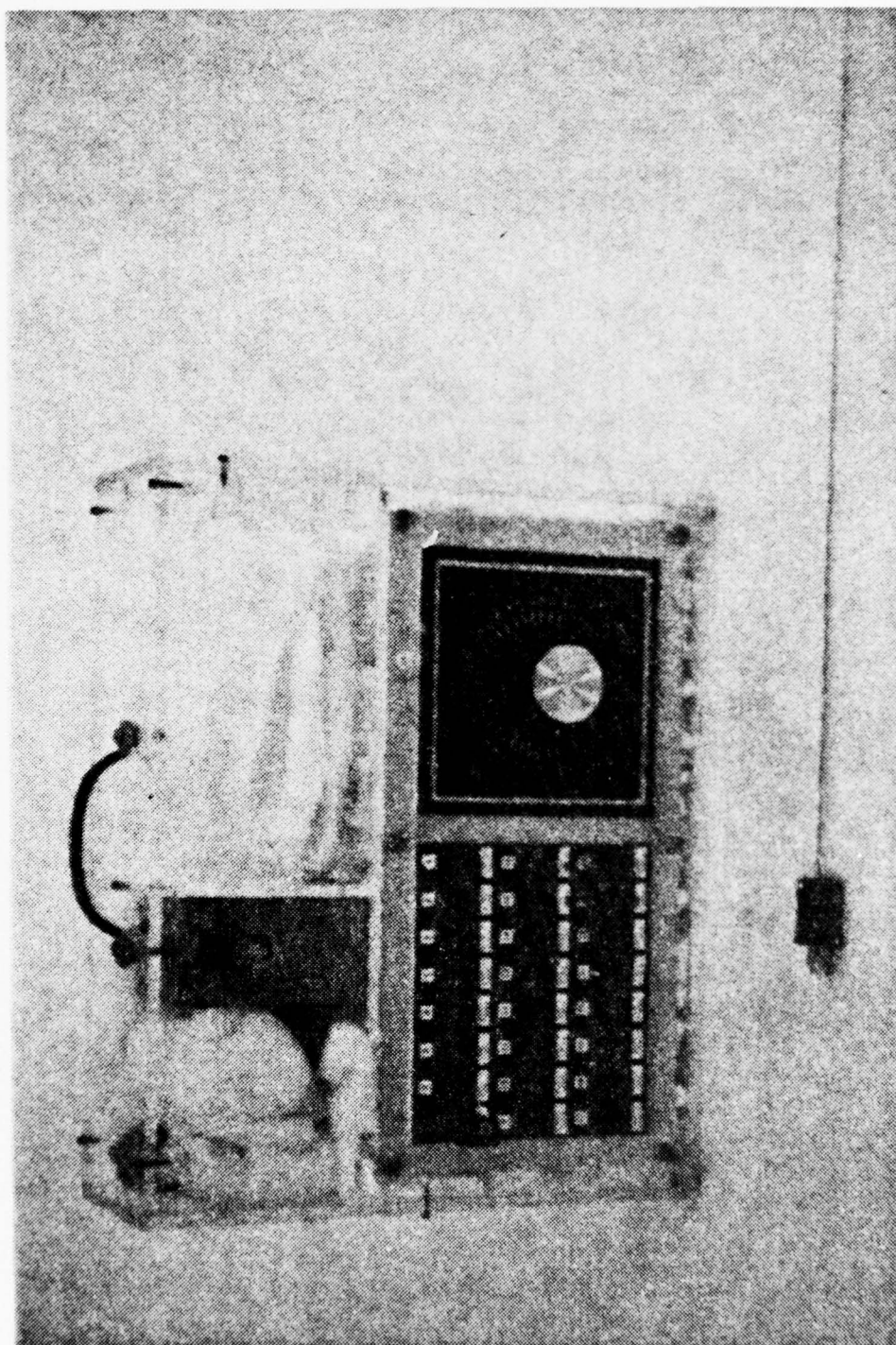


40. Detailed view of port side, rear of ice model; Test 3.

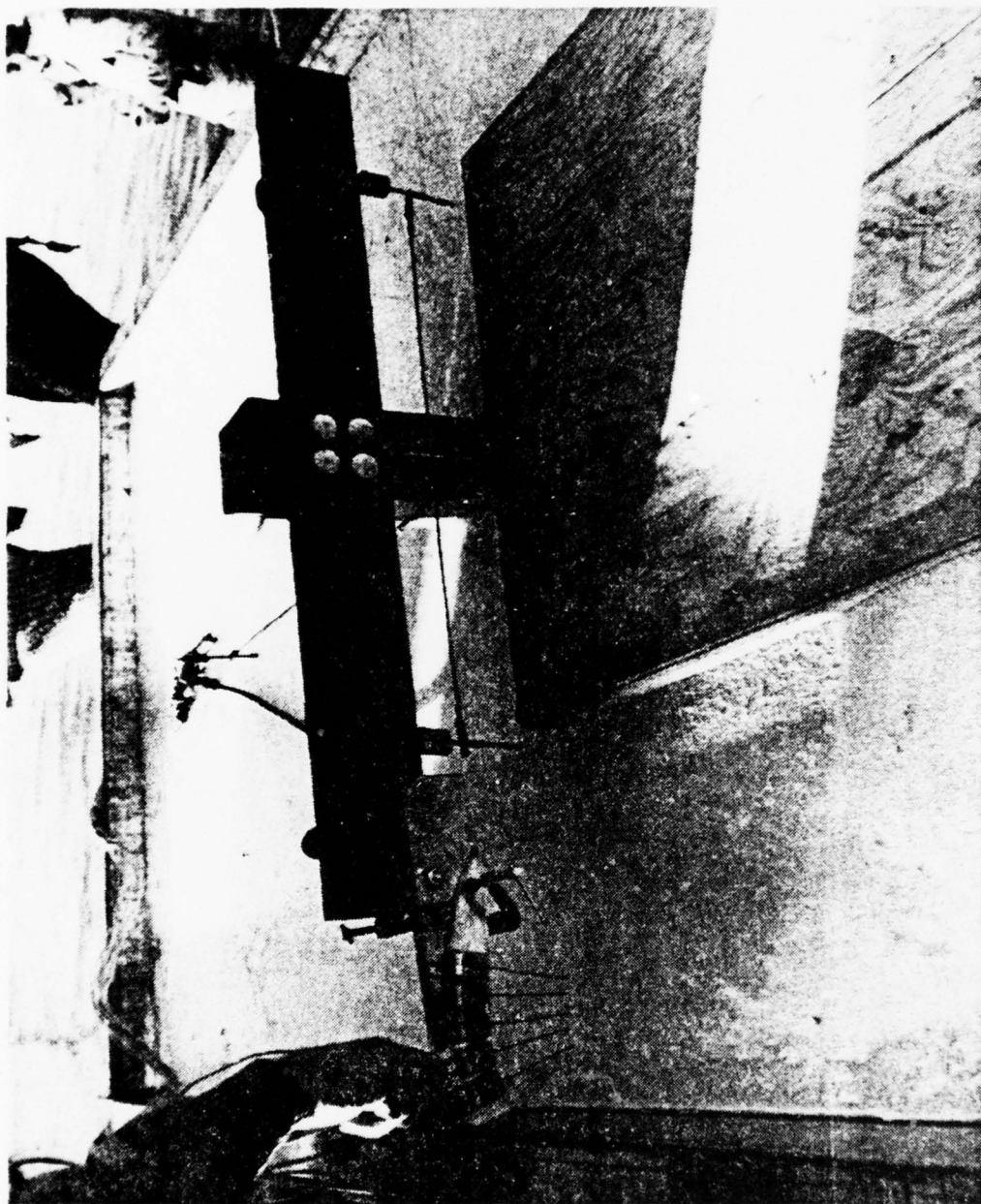
GLACIAL ICE THERMOCOUPLE POSITIONS



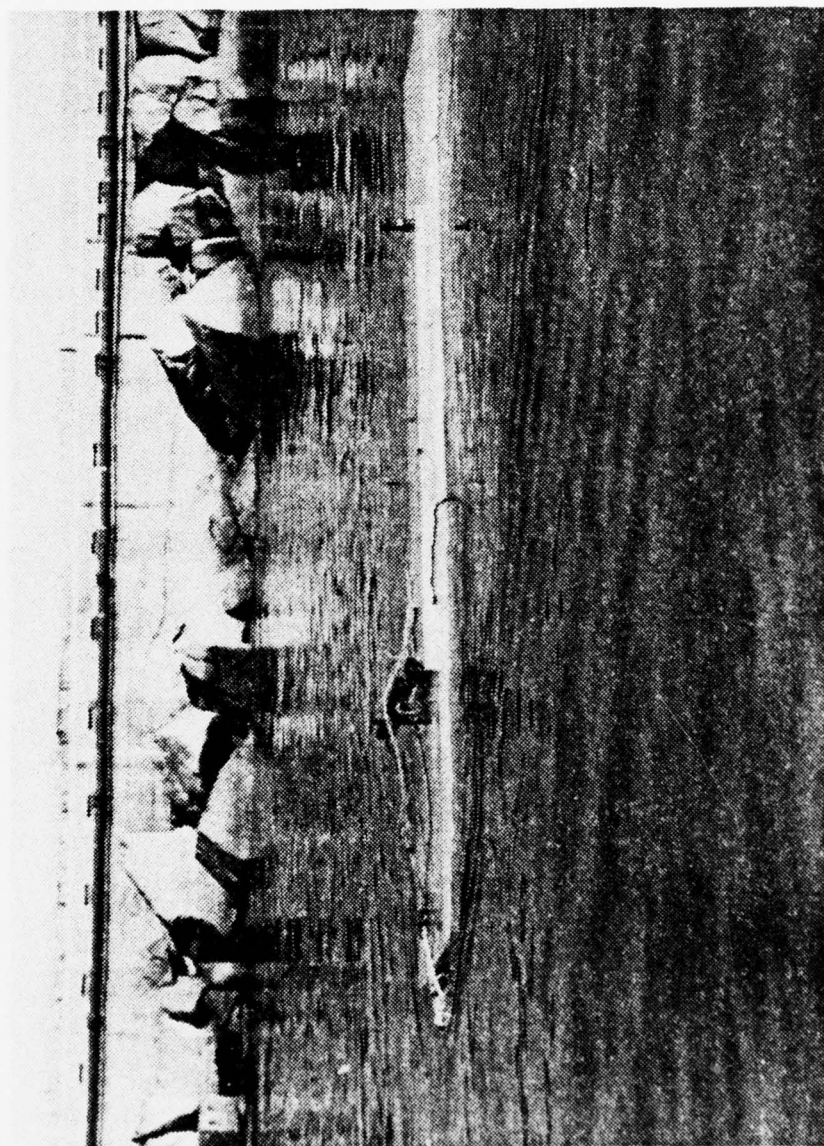
41a. Thermocouple arrangement; Test 4.



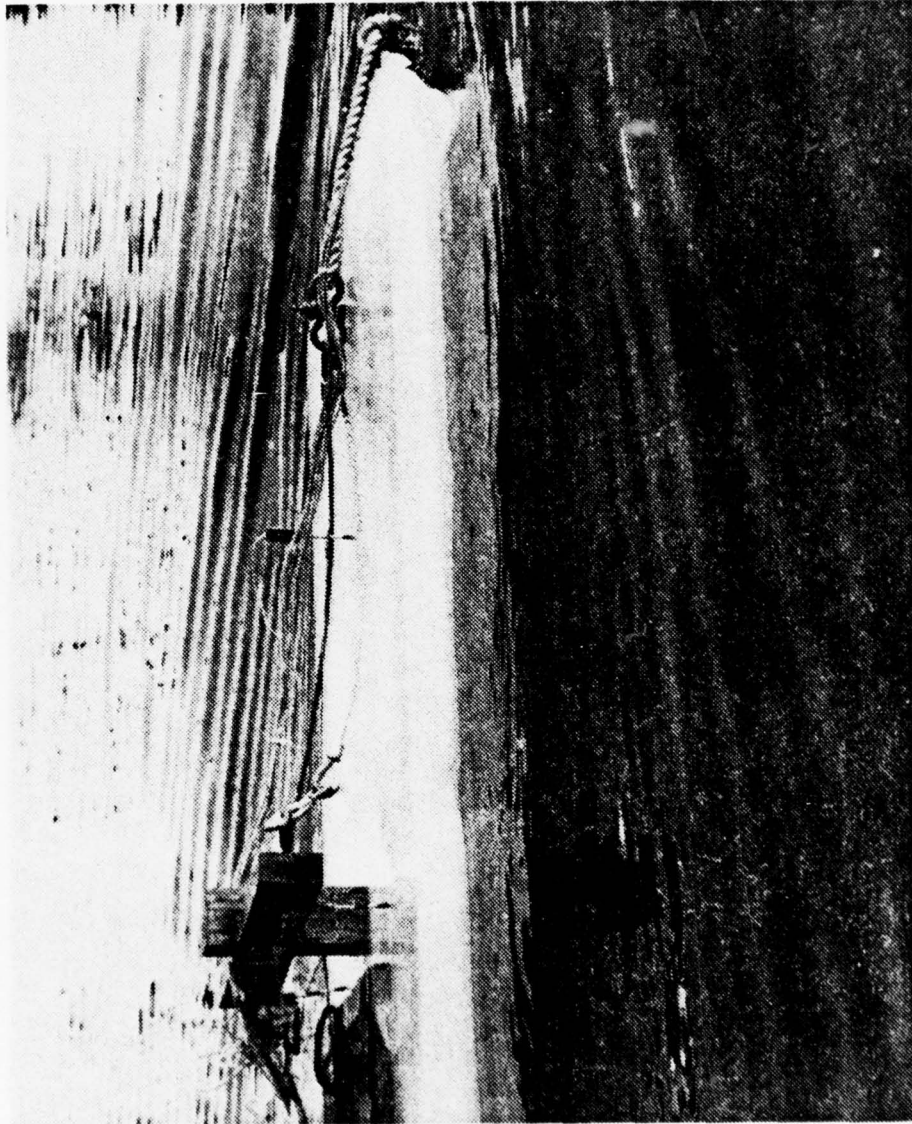
4lb. Thermocouple with digital readout.



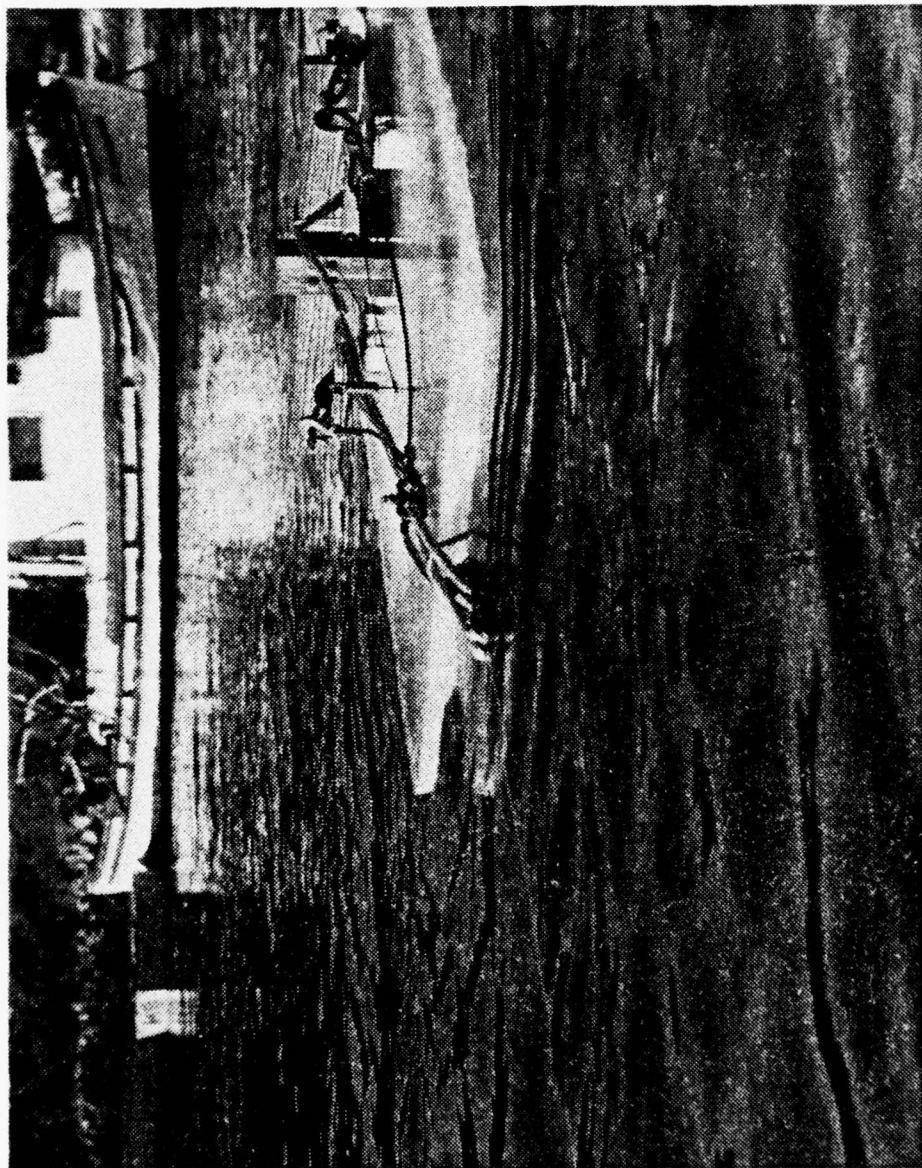
42. Thermocouple arrangement; Test 4.



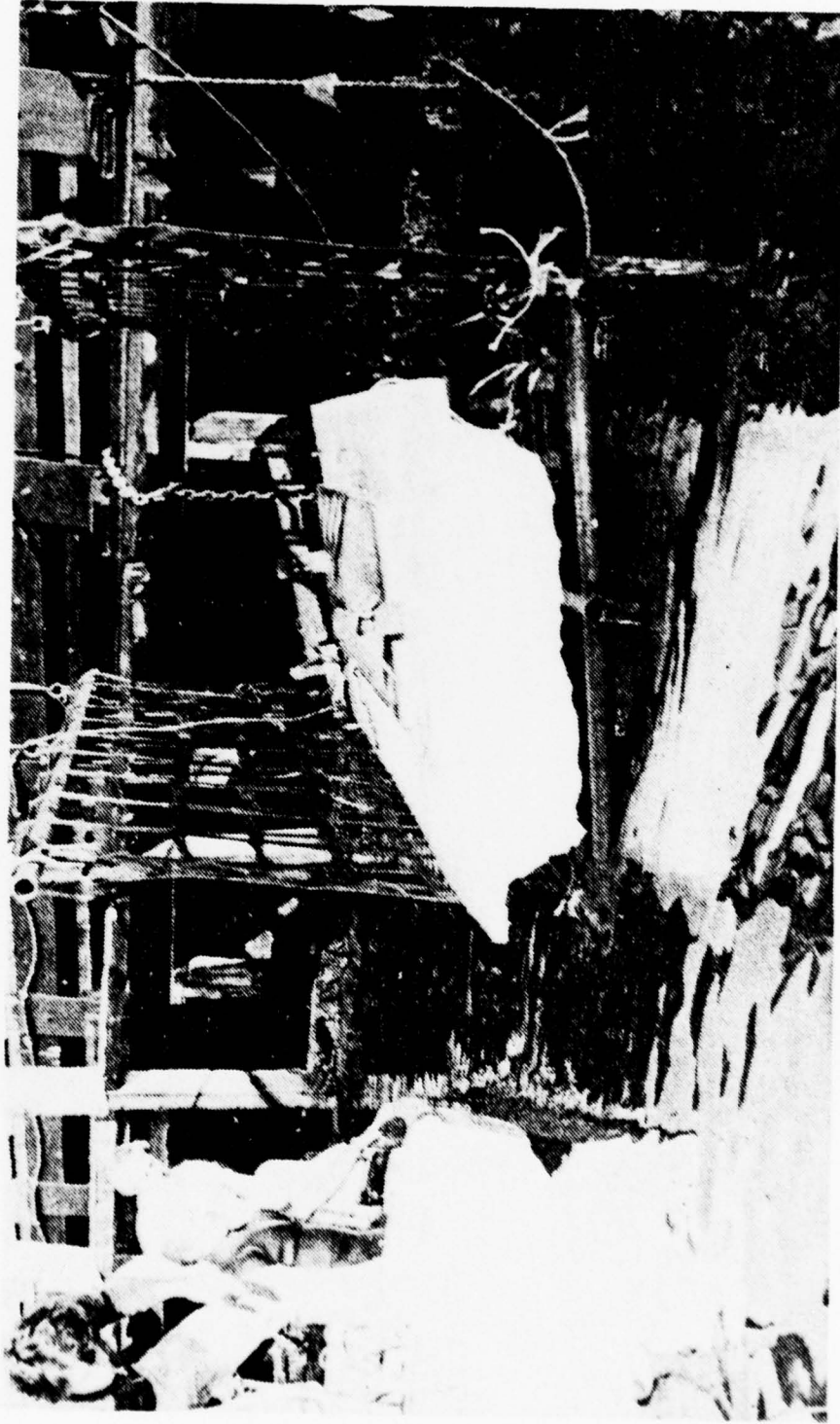
43. Ice model underway; Test 4.



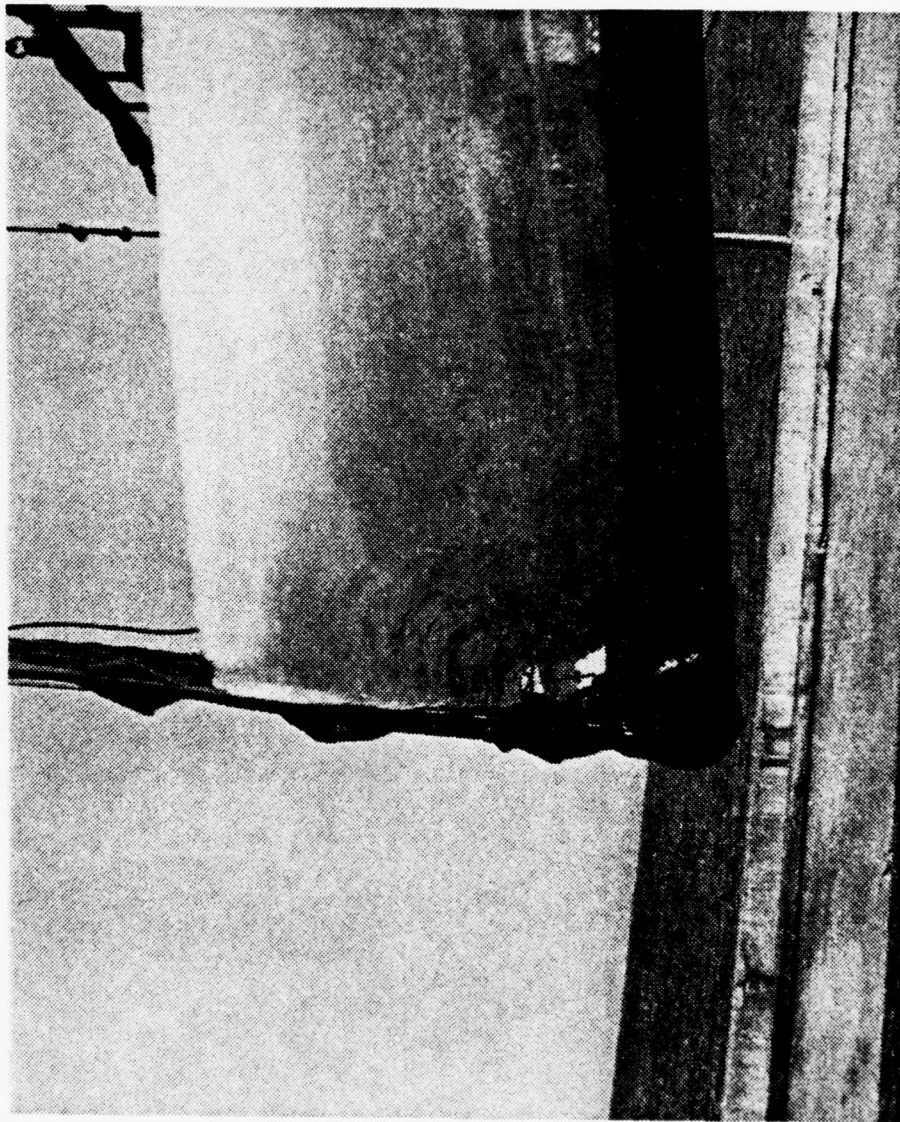
44. Forward section of ice model underway; Test 4.



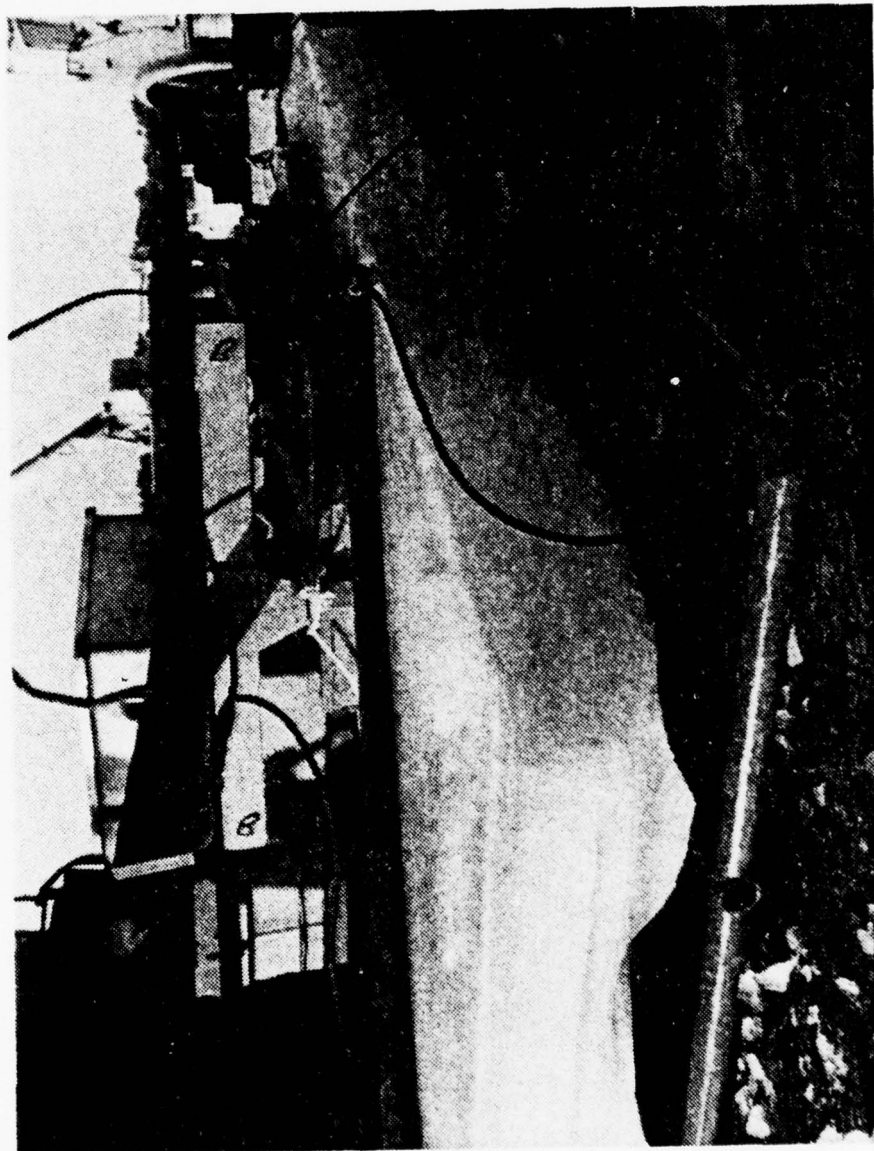
45. Bow undercutting of ice model; Test 4.



46. Ice model recovery; Test 4.



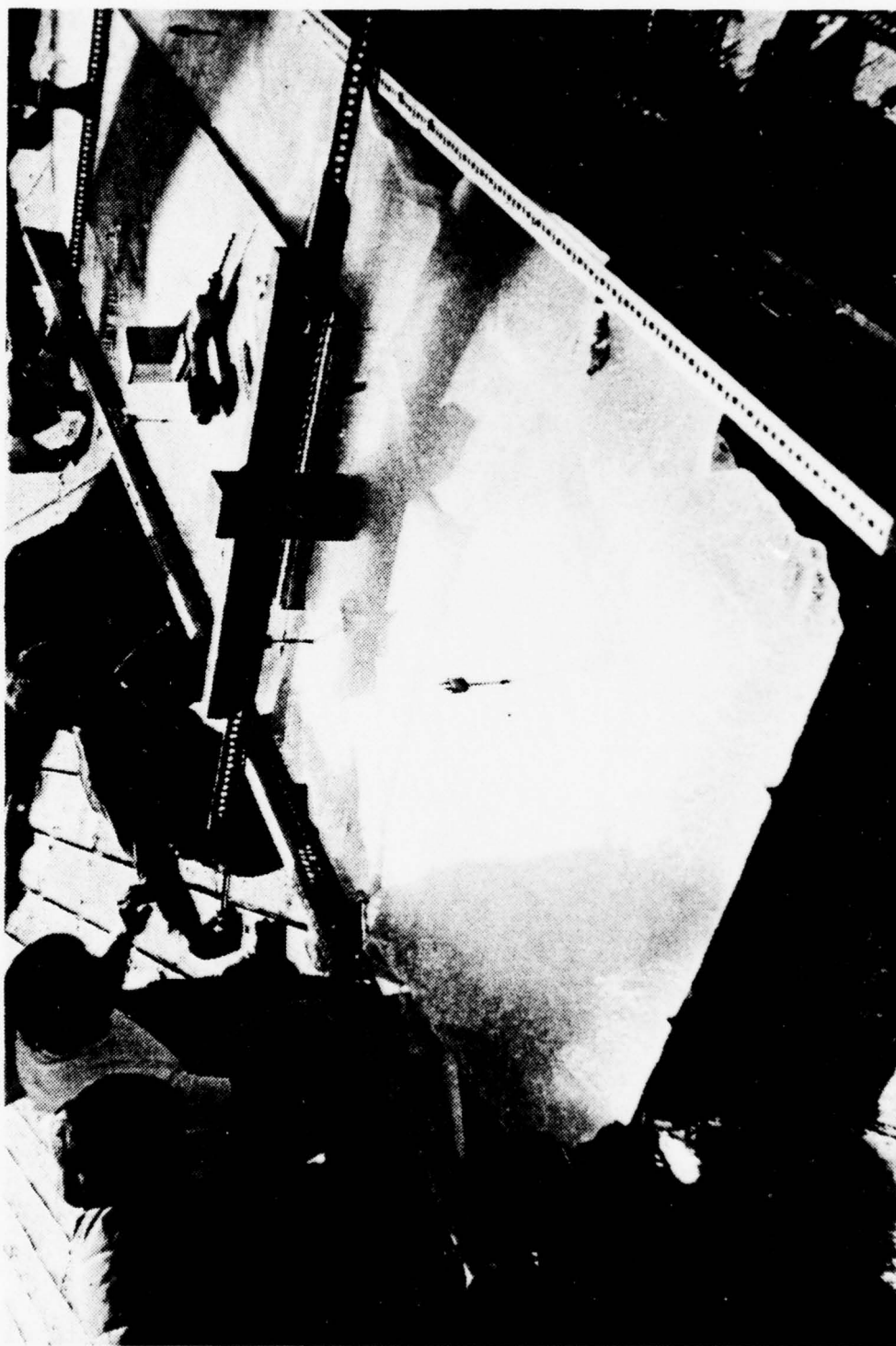
47. Recovered ice model with exposed thermocouple array; Test 4.



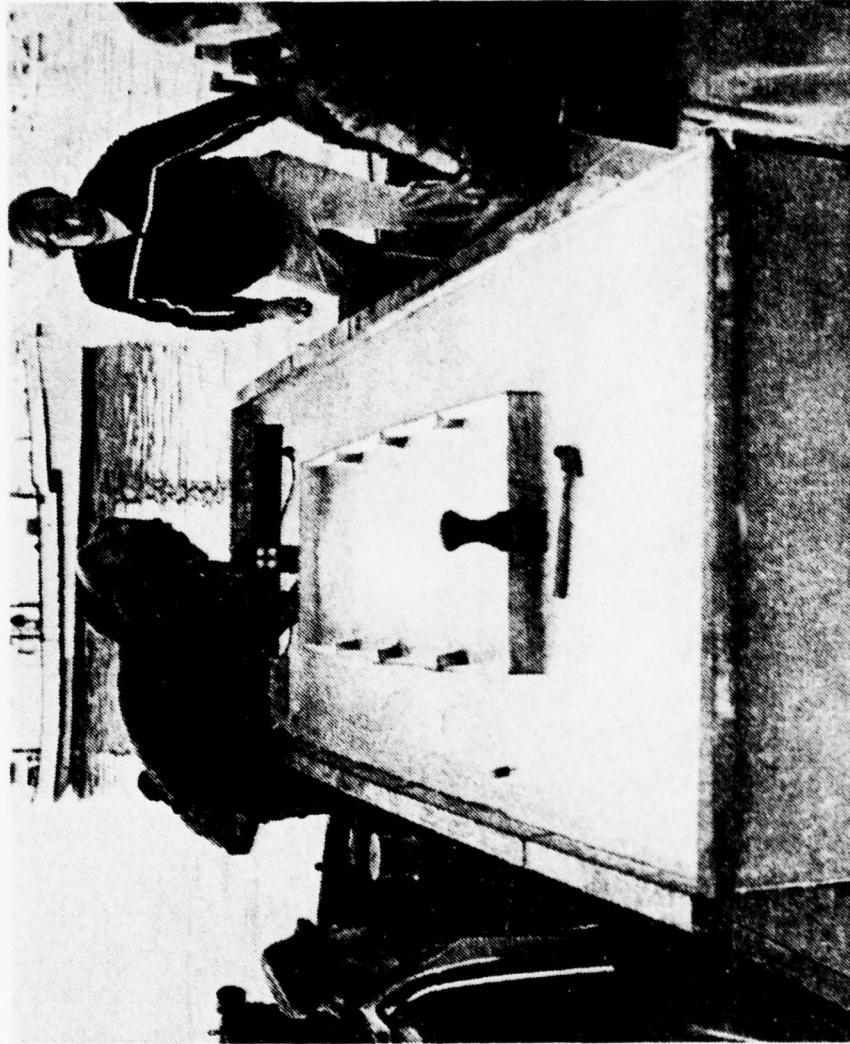
48. Ice model on pier; Test 4.



49. Detailed view of ice model layering and ripples; Test 4.

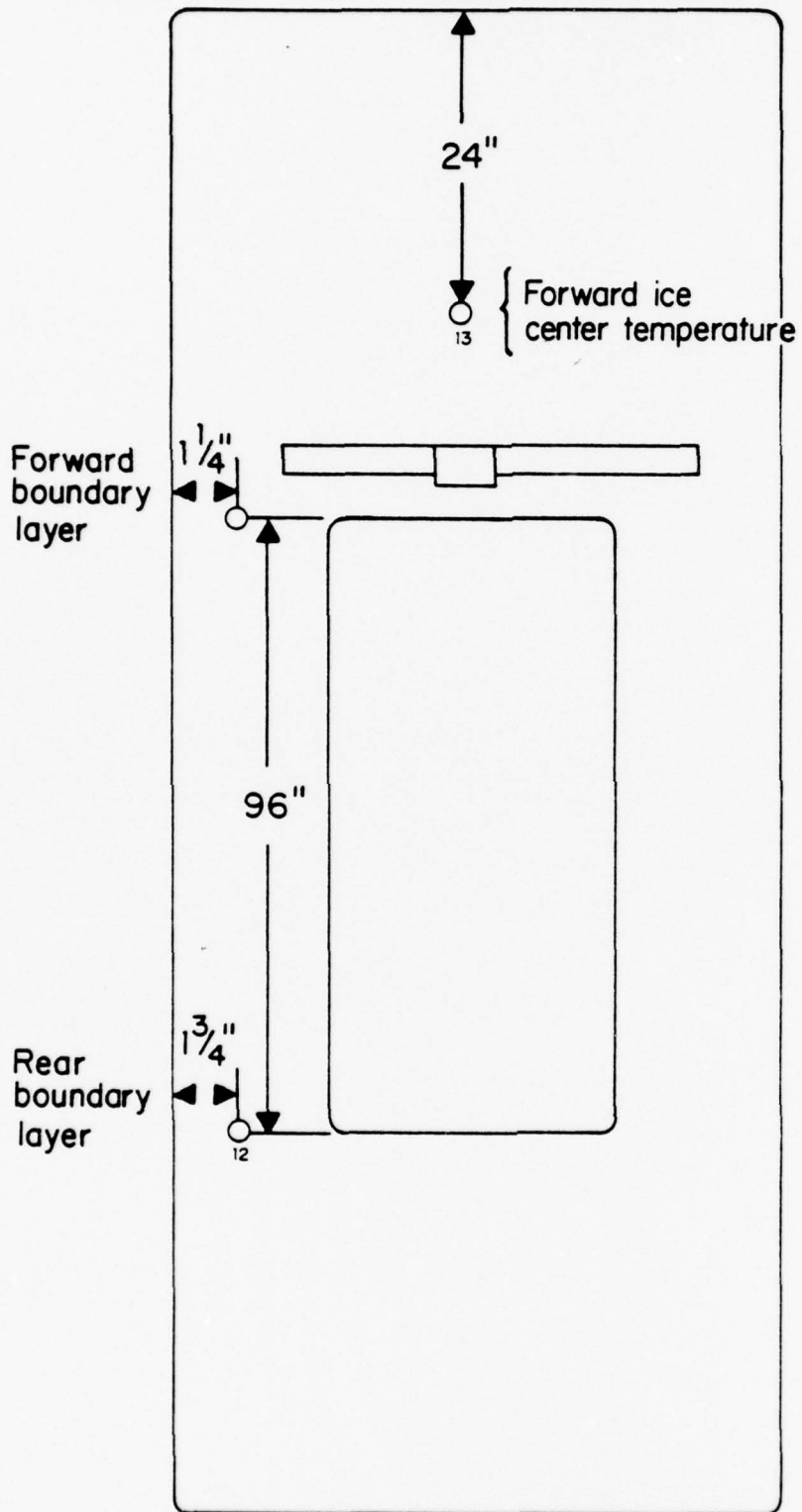


50. Ripple measurement technique; Test 4.

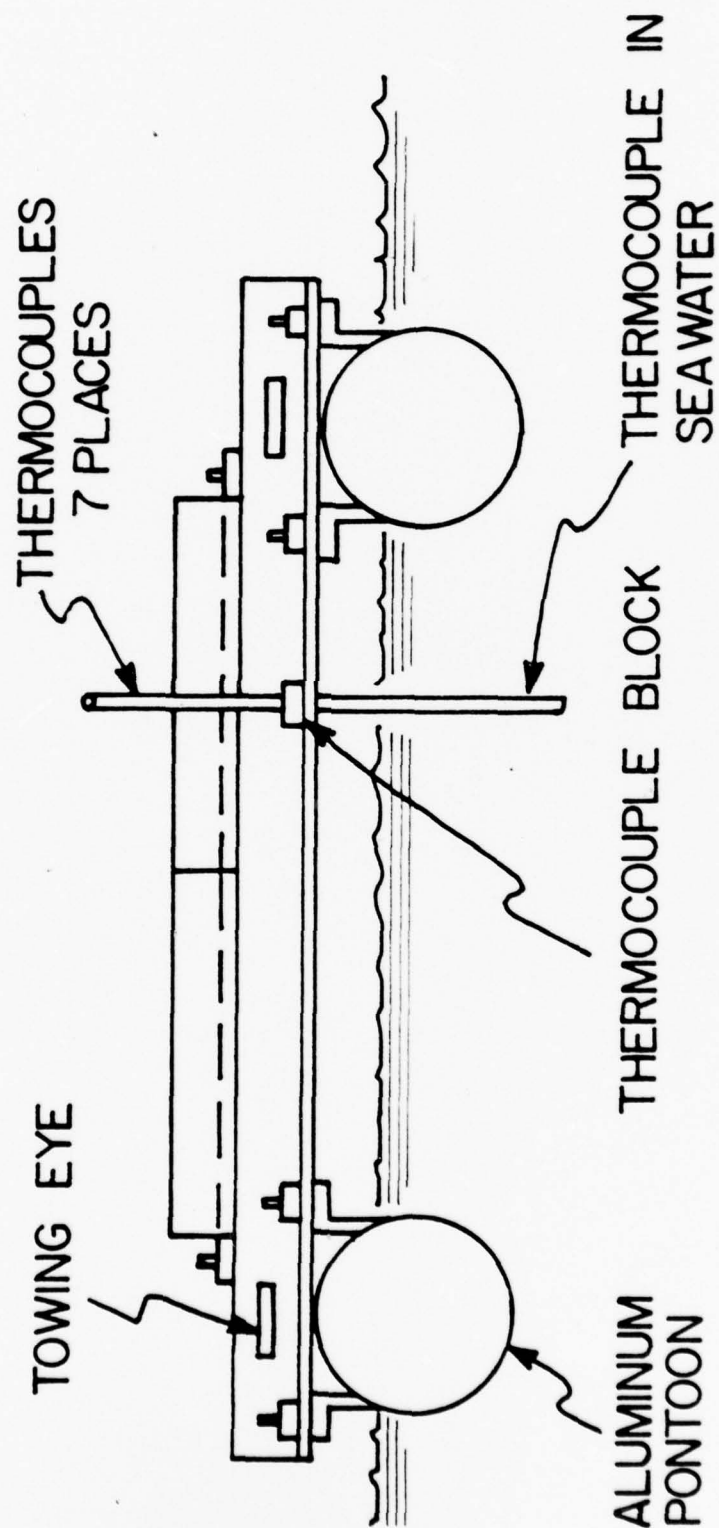


51. Ice model prior to launch; Test 5.

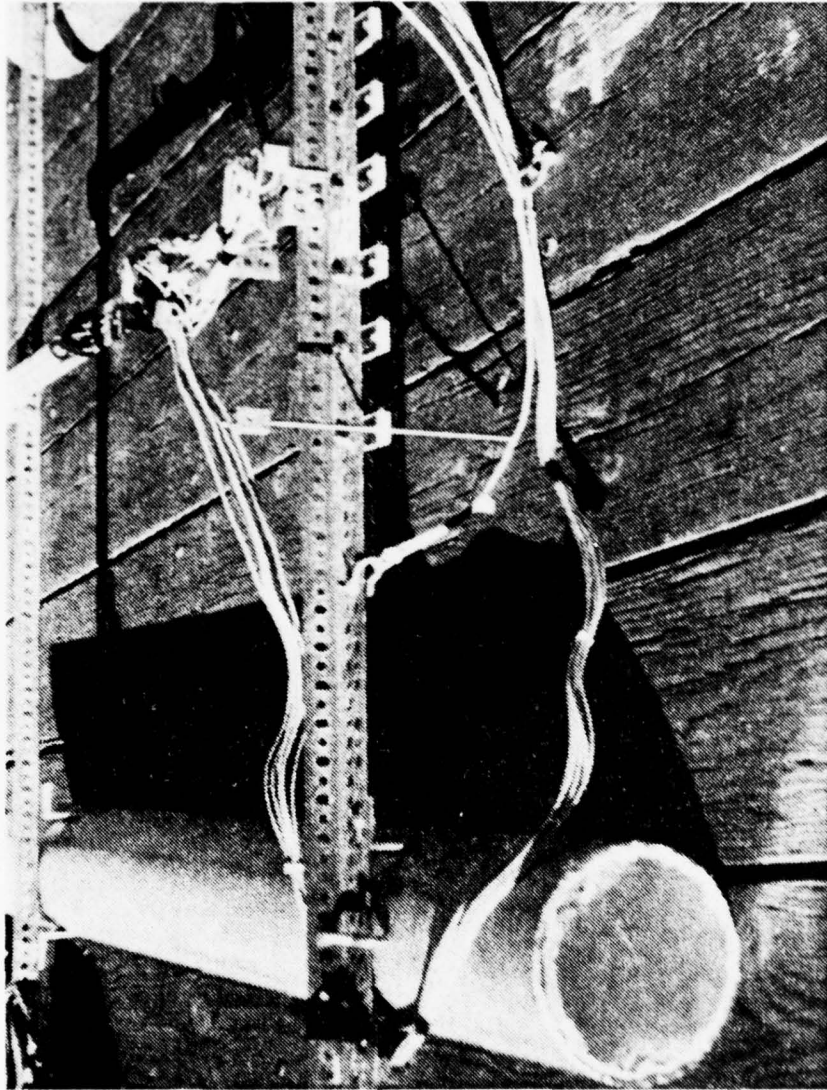
GLACIAL ICE THERMOCOUPLE POSITIONS



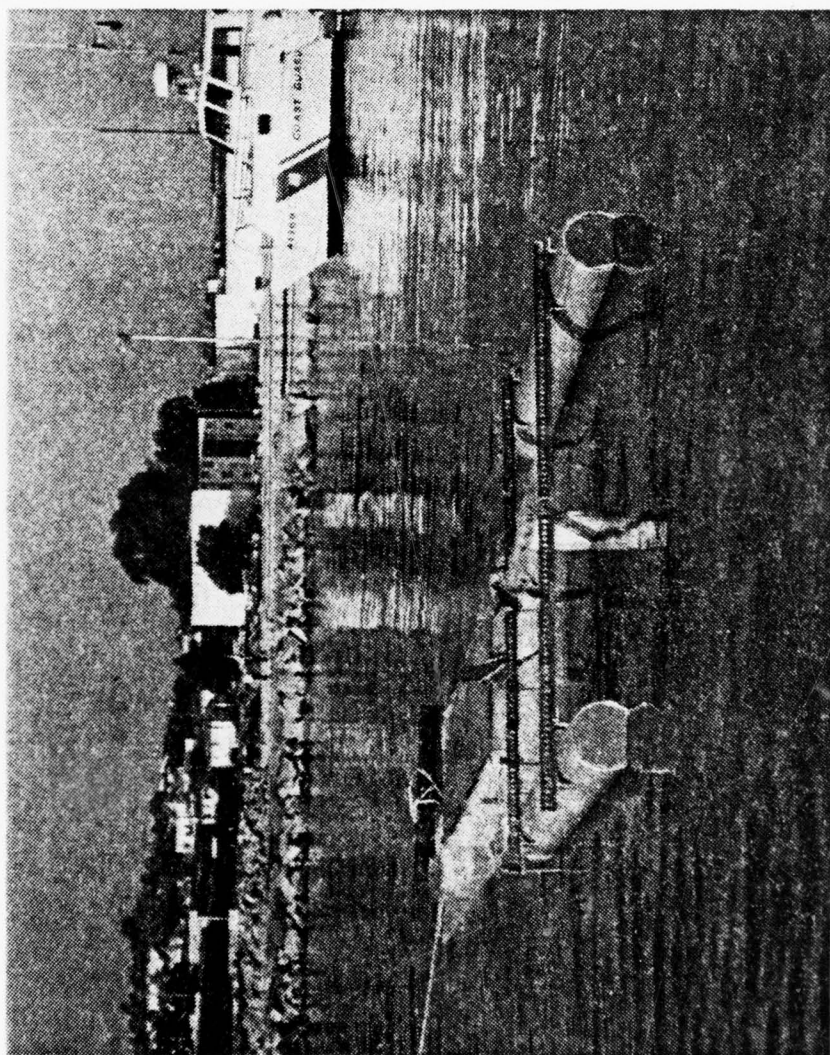
52. Thermocouple arrangement; Test 5.



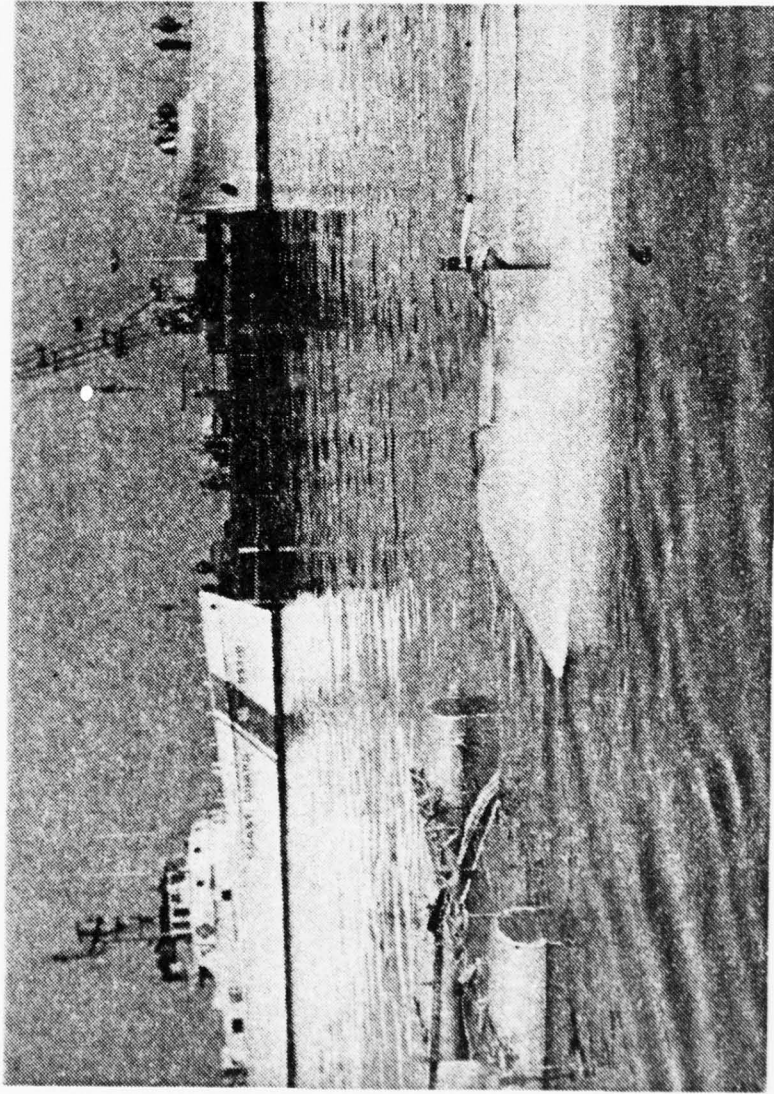
53. Cross section view of pontoon bridge.



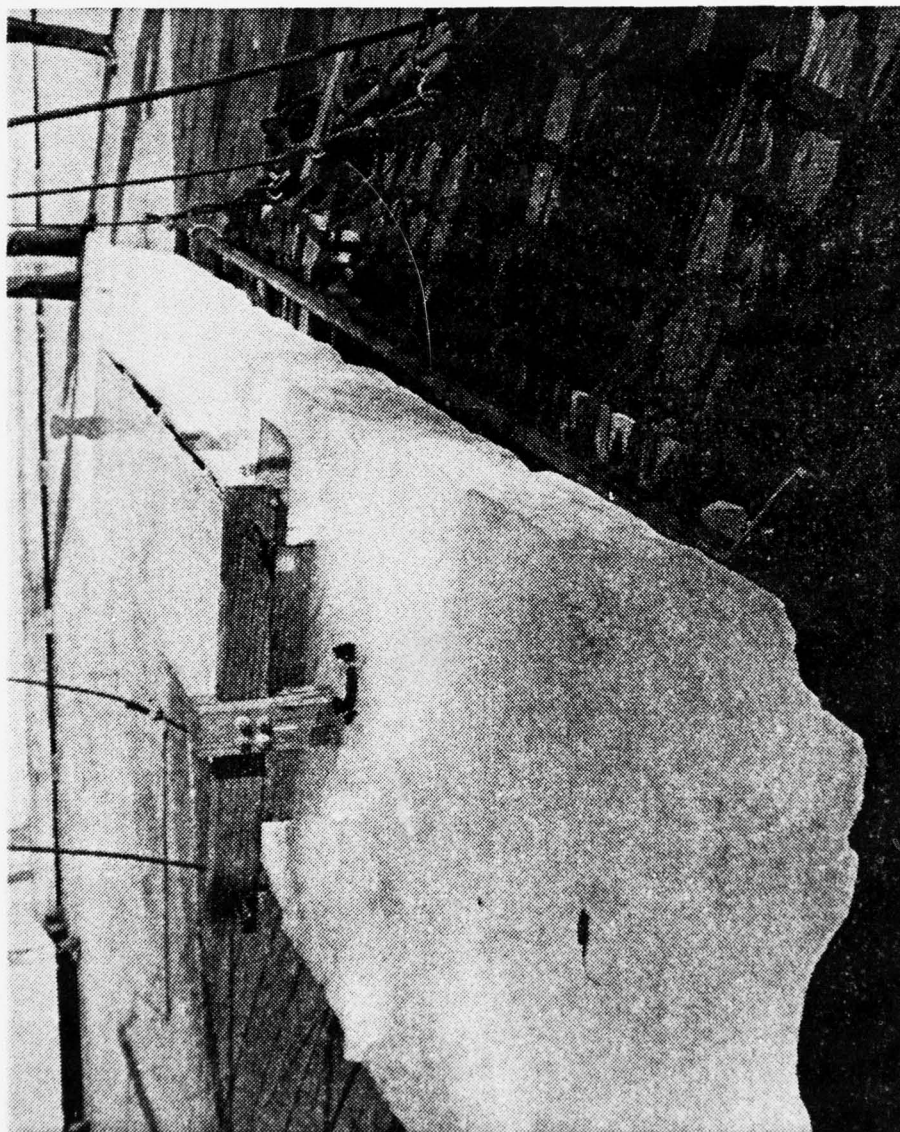
54. Thermocouple installation on pontoon bridge; Test 5.



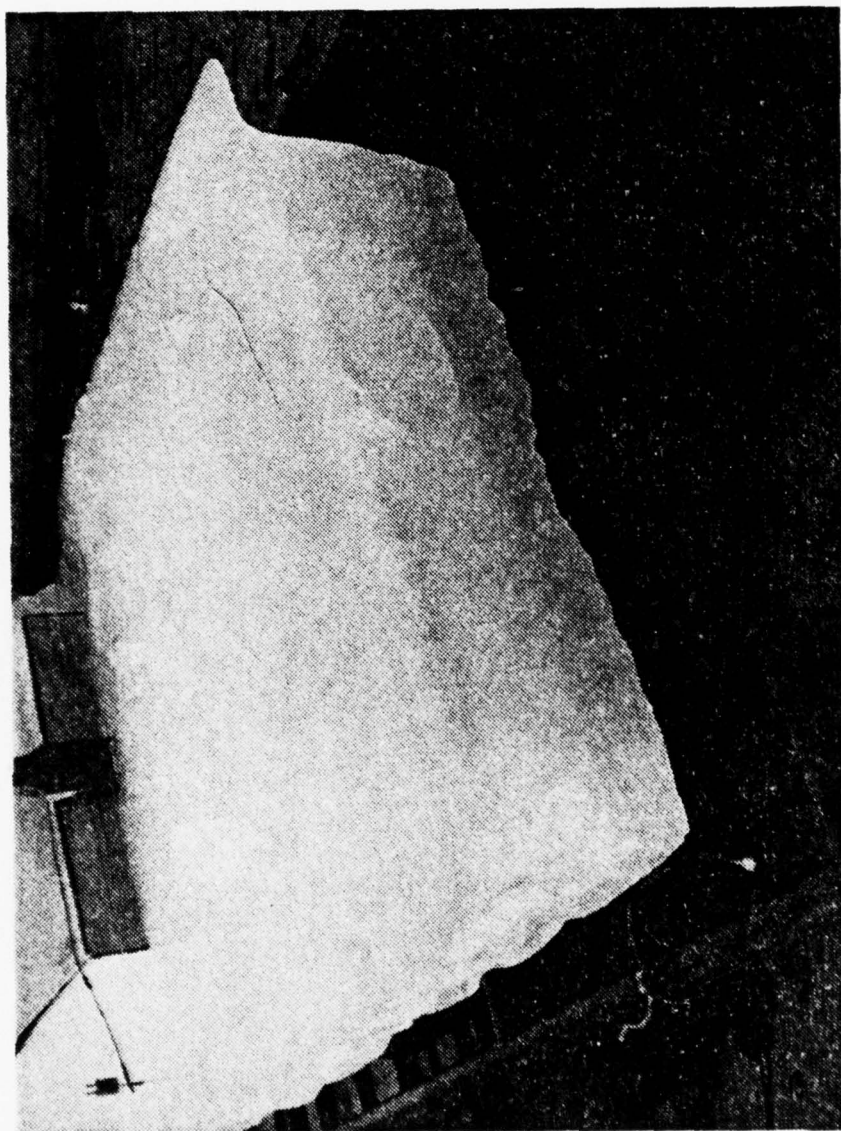
55. Ice model and pontoon bridge underway; Test 5.



56. Ice model and pontoon bridge towing arrangement; Test 5.



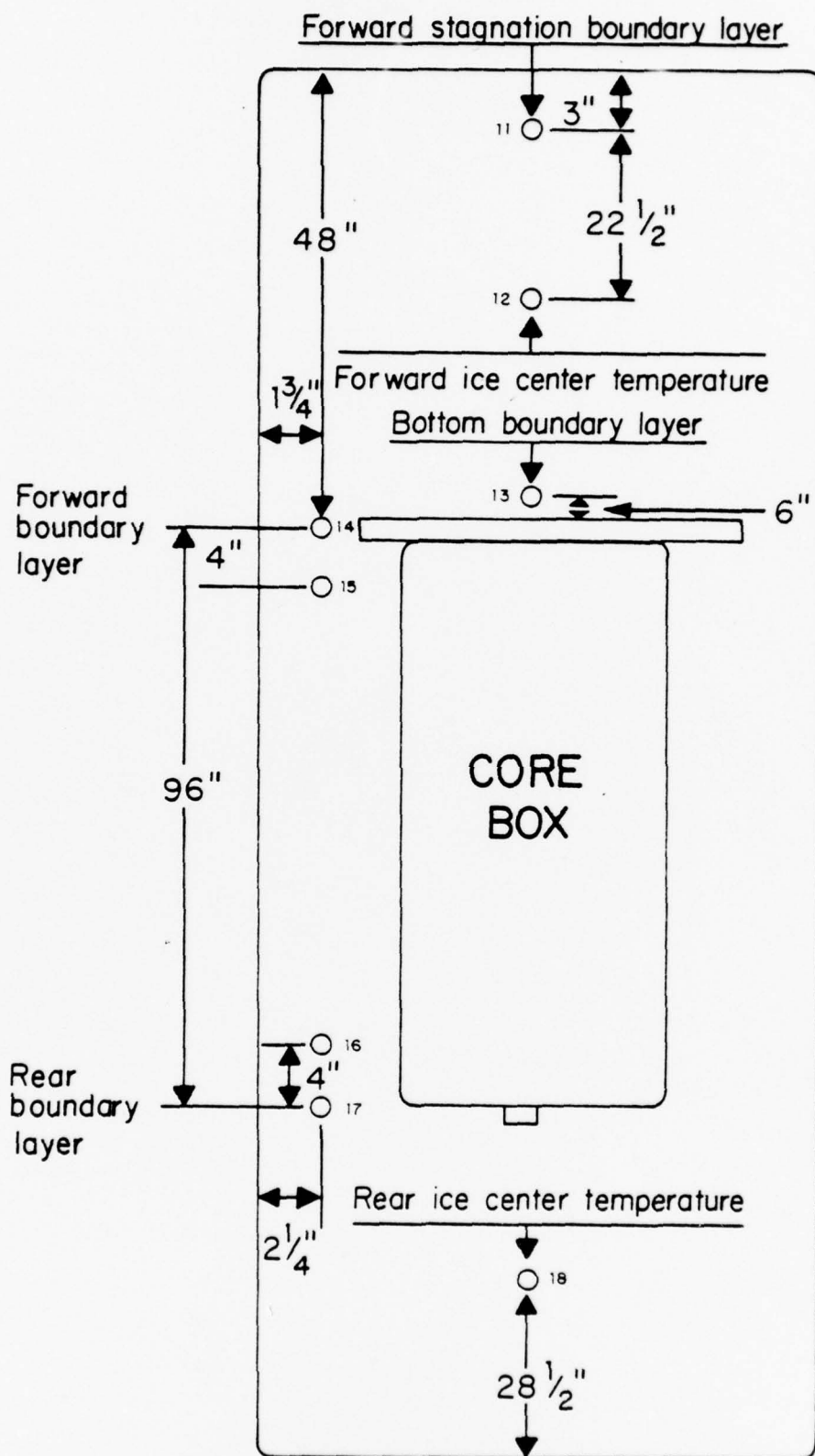
57. Ice model on pier; Test 5.



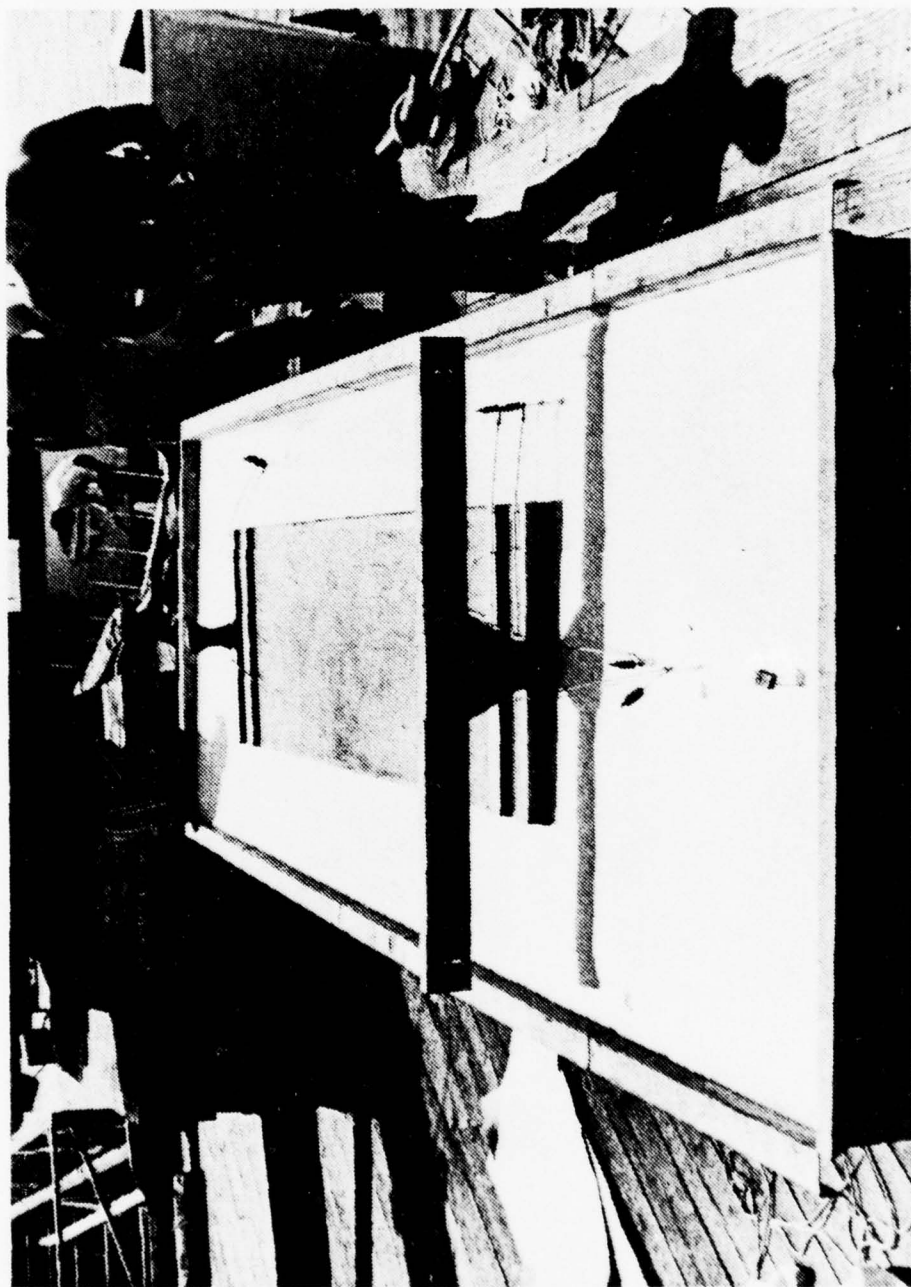
58. Rear view of ice model ripples; Test 5.



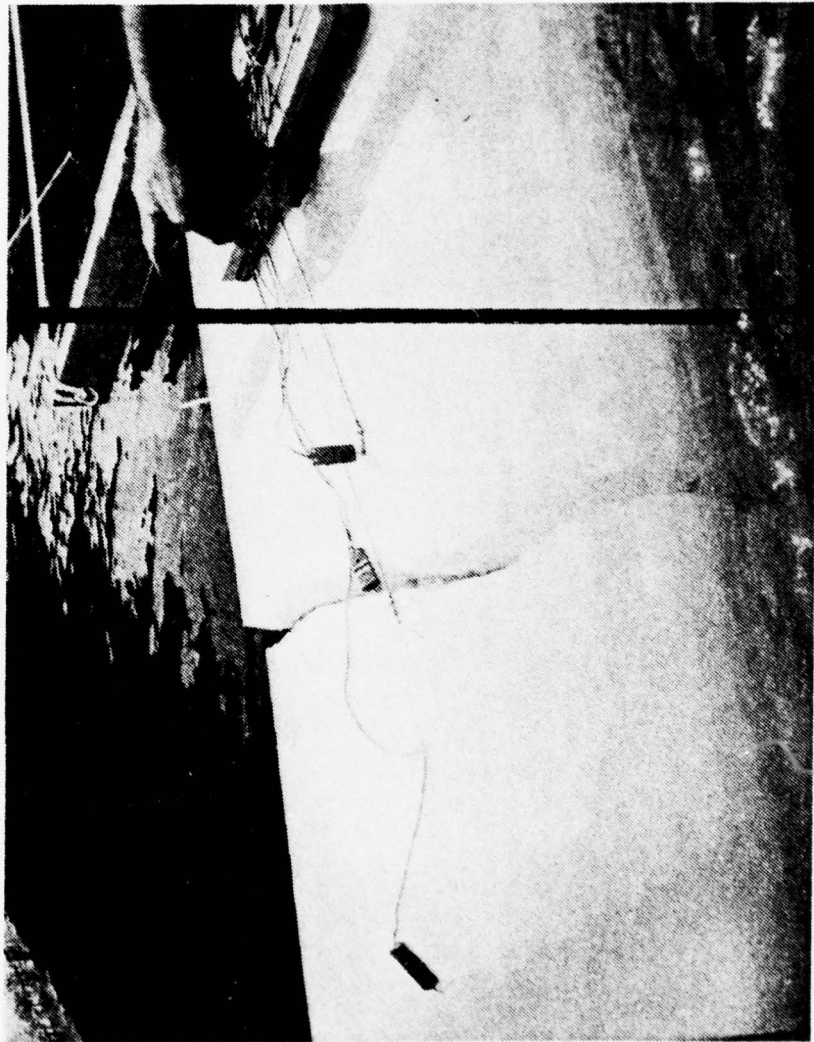
59. Rear view of ice model layering; Test 5.



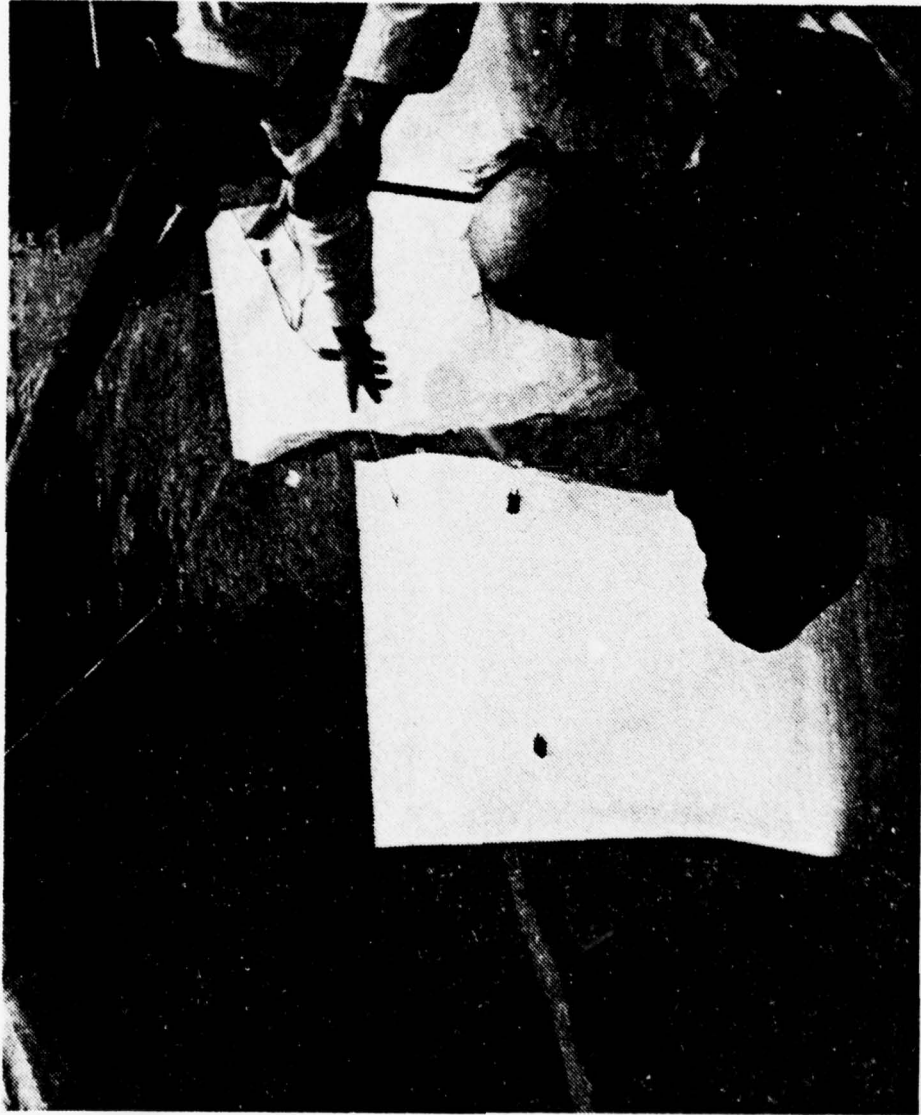
60. Thermocouple arrangement; Test 6.



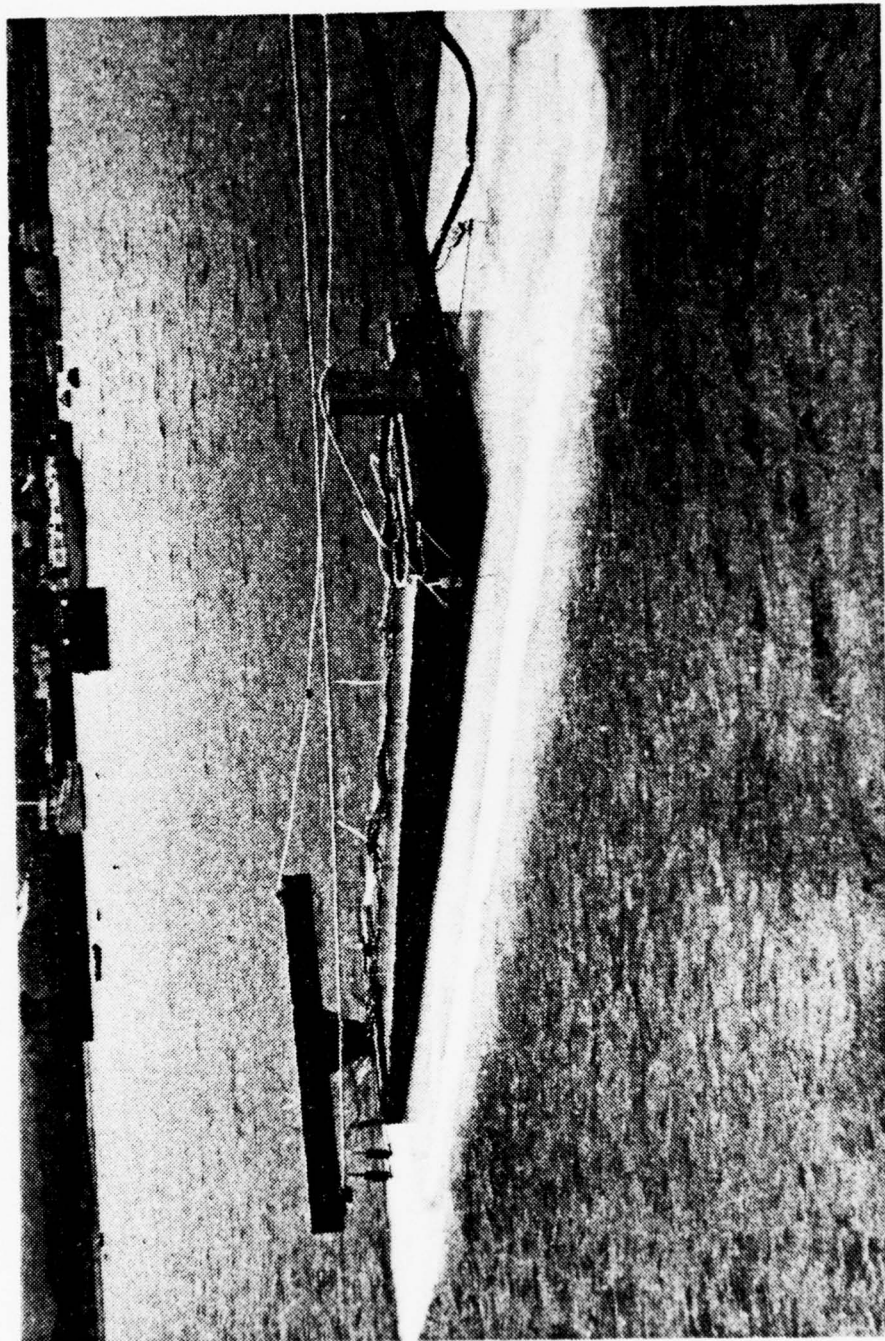
61. Ice model prior to launch; Test 6.



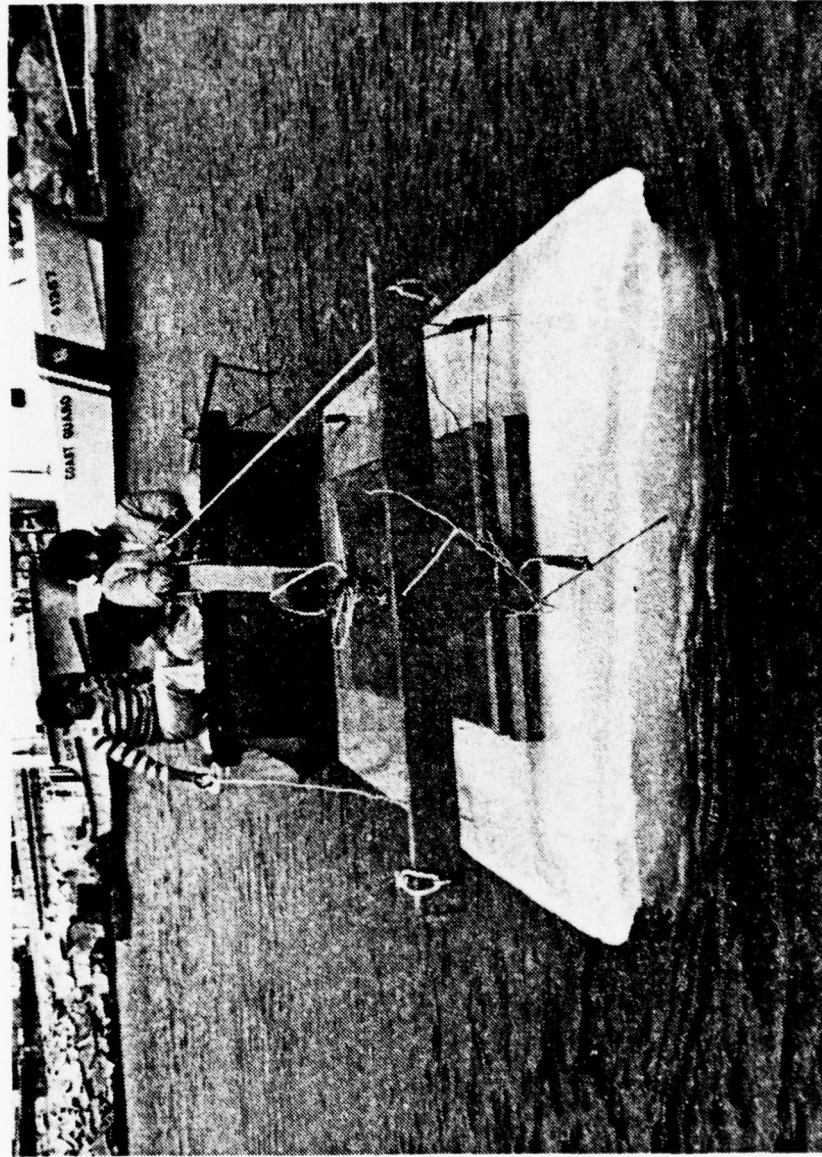
62. Forward section separation; Test 6.



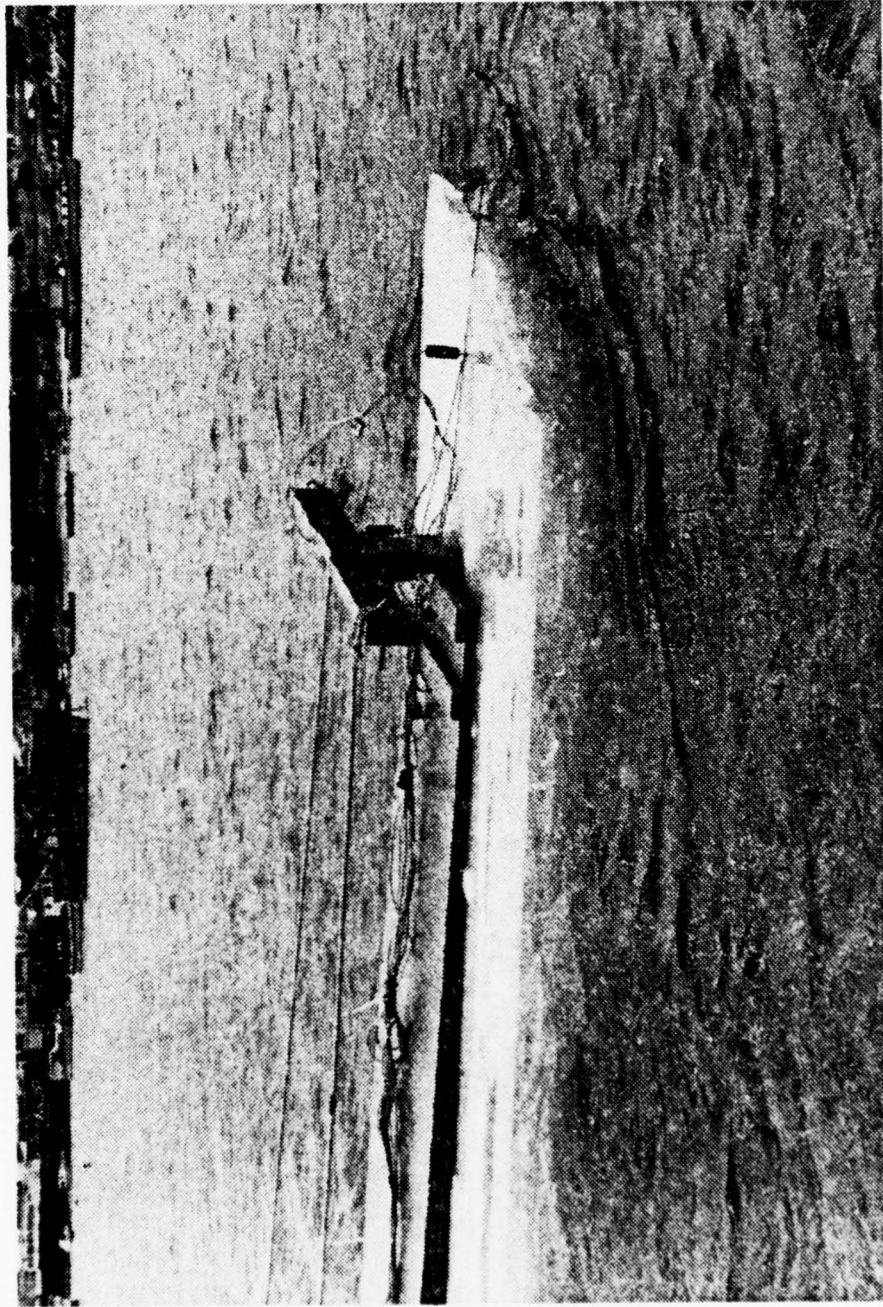
63. Forward section separation; Test 6.



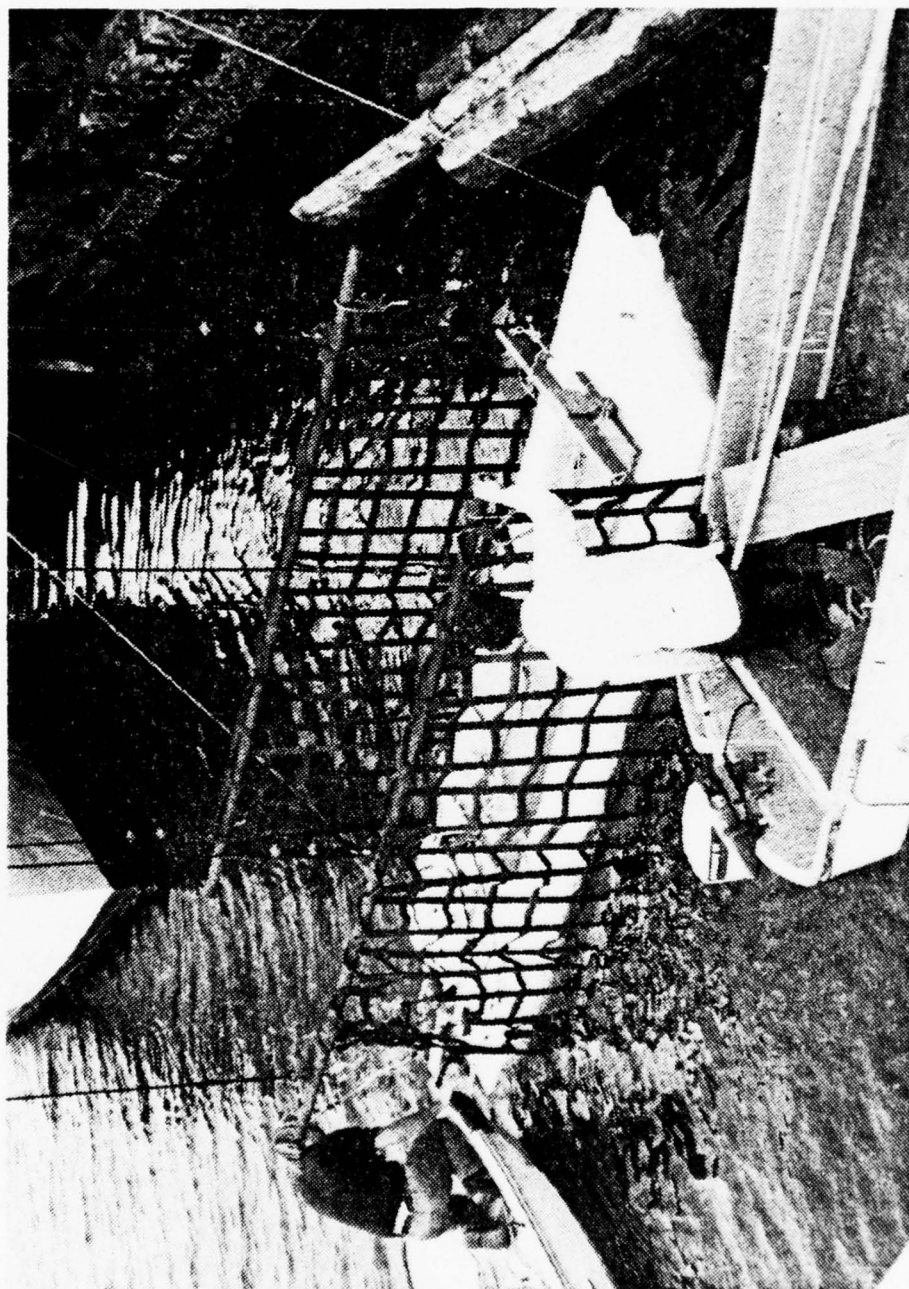
64. Rear view pushing arrangement; Test 6.



65. Frontal view pushing arrangement; Test 6.



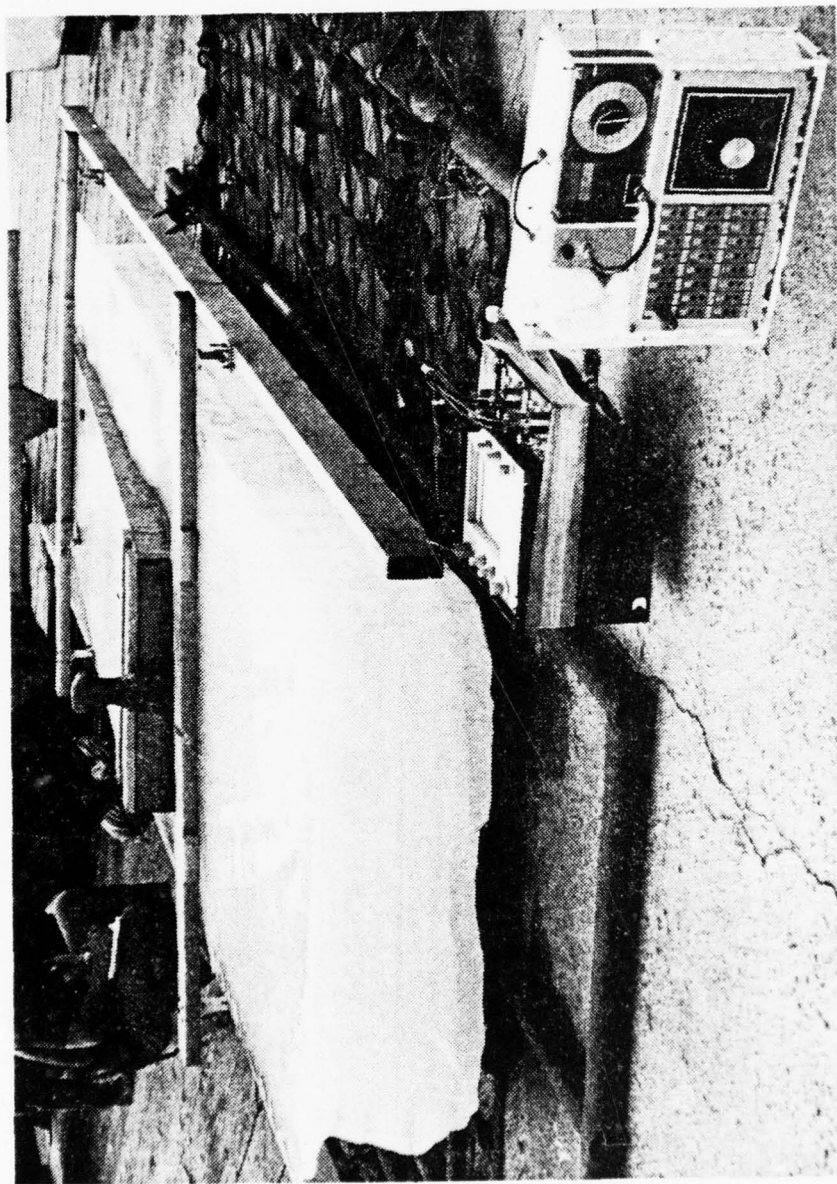
66. Forward section of ice model; Test 6.



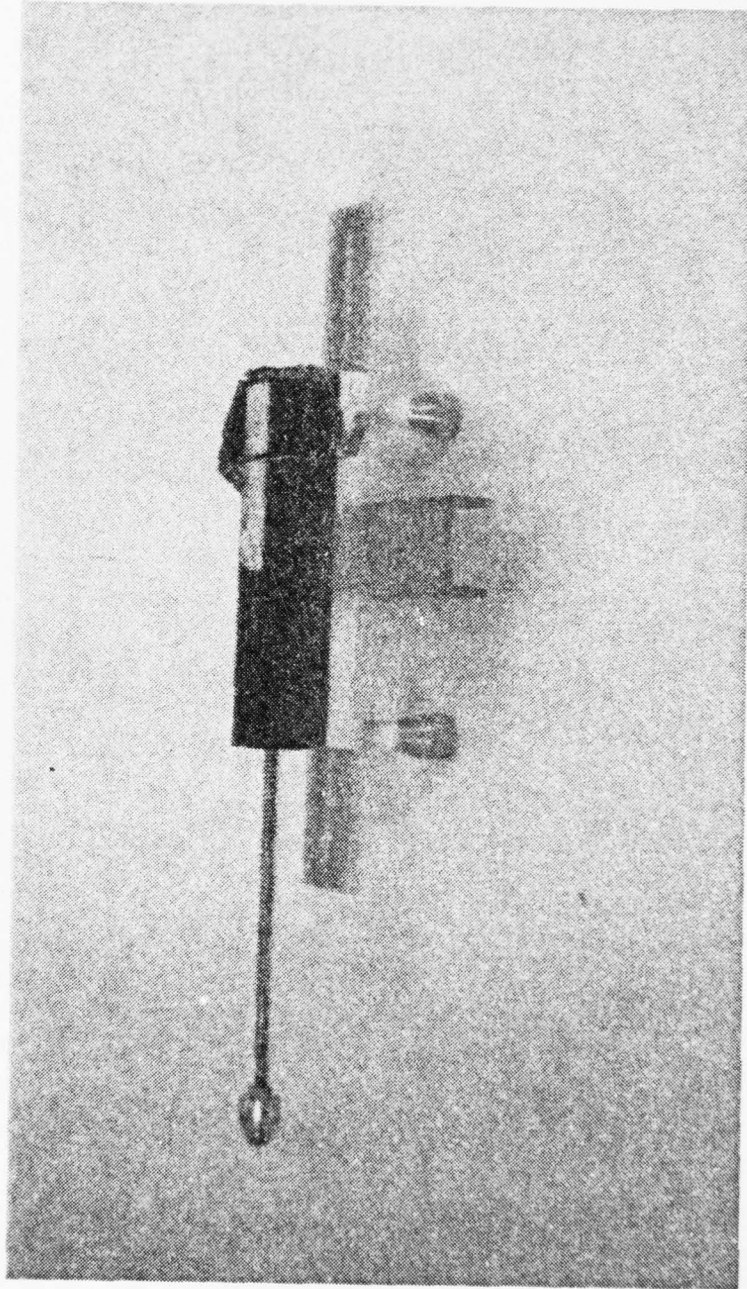
67. Ice model positioning for recovery; Test 6.



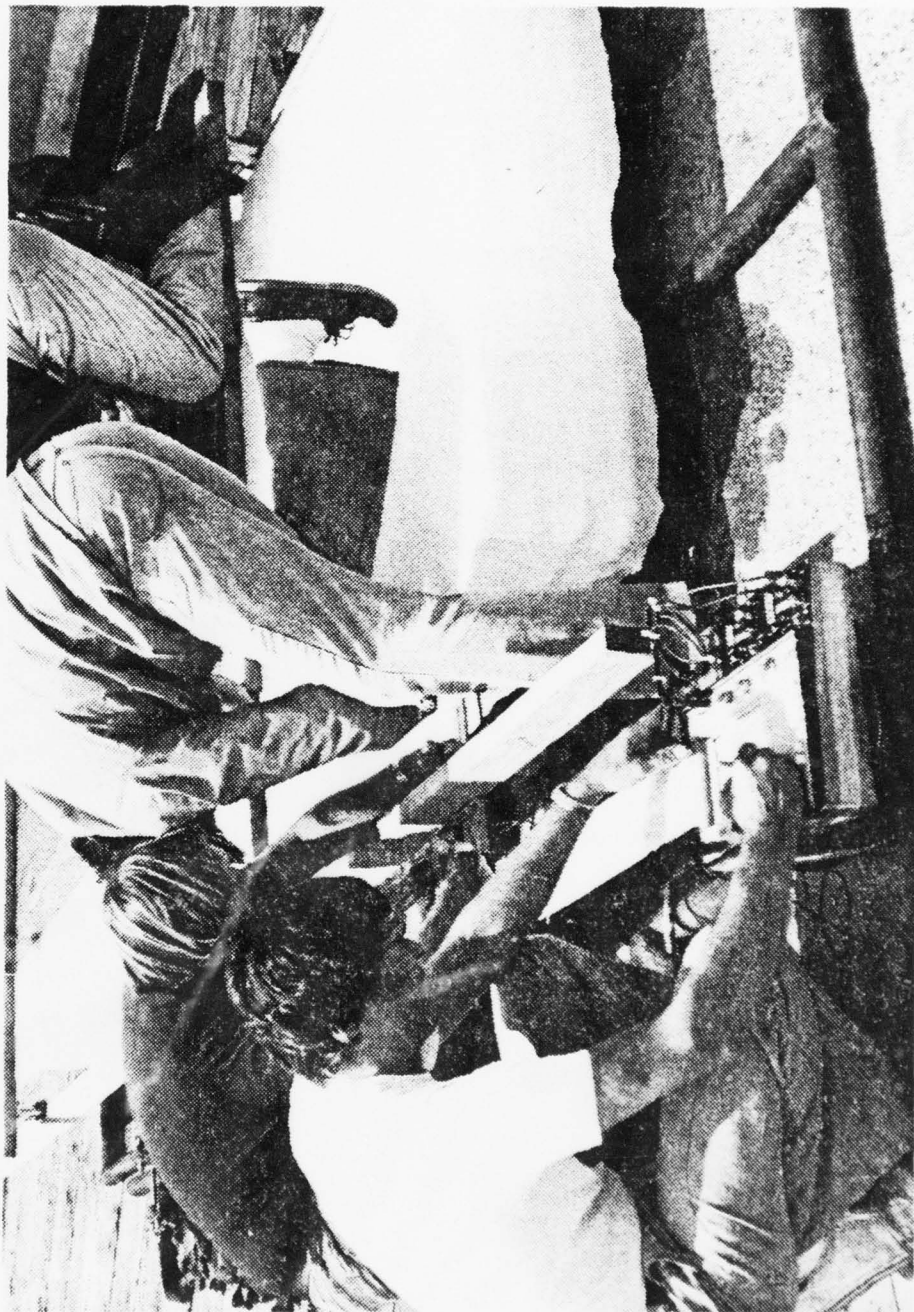
68. Frontal view of recovered ice model; Test 6.



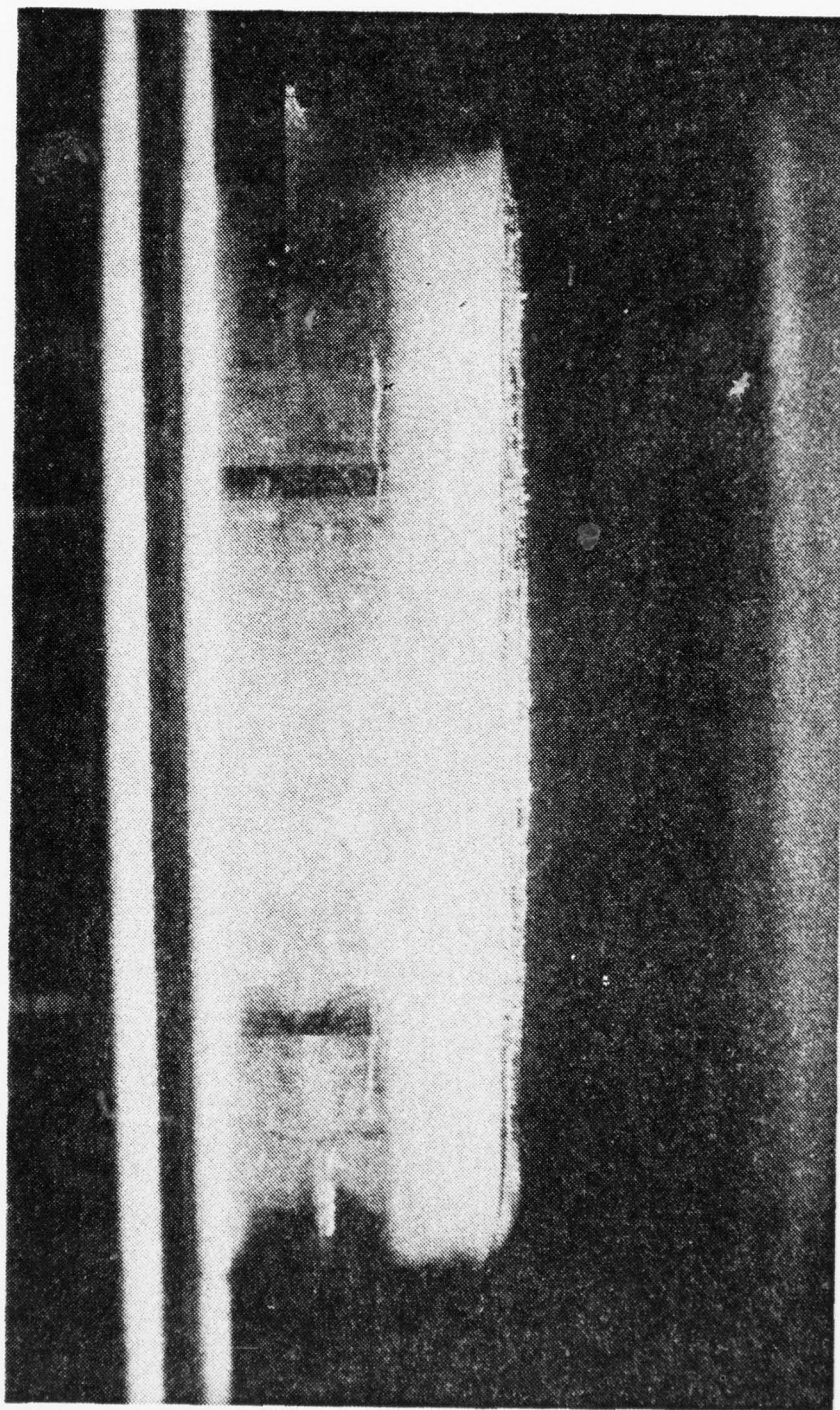
69. Reference grid on ice model for ripple measurement; Test 6.



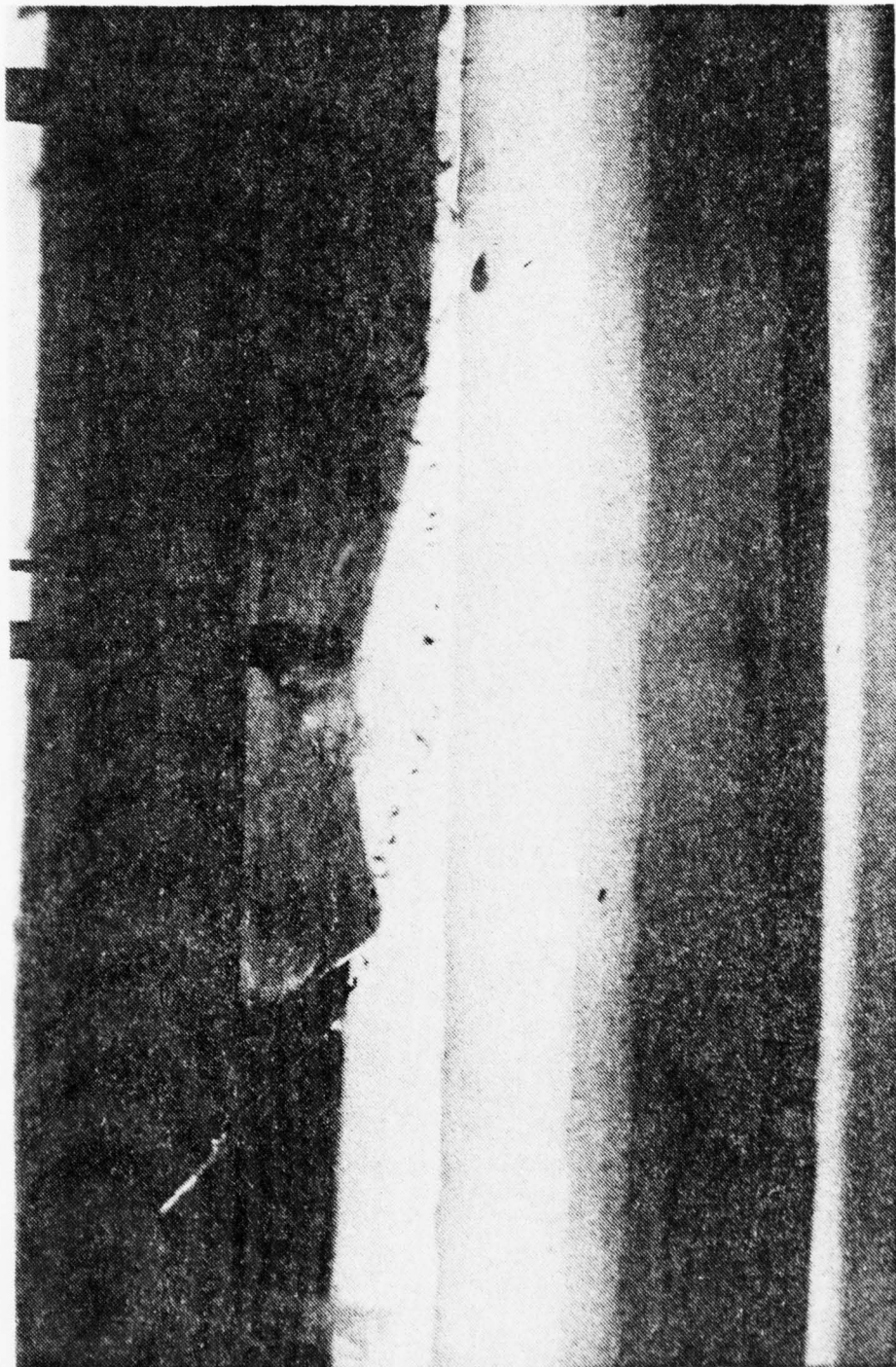
70. Linear motion position transducer used for ripple measurement; Test 6.



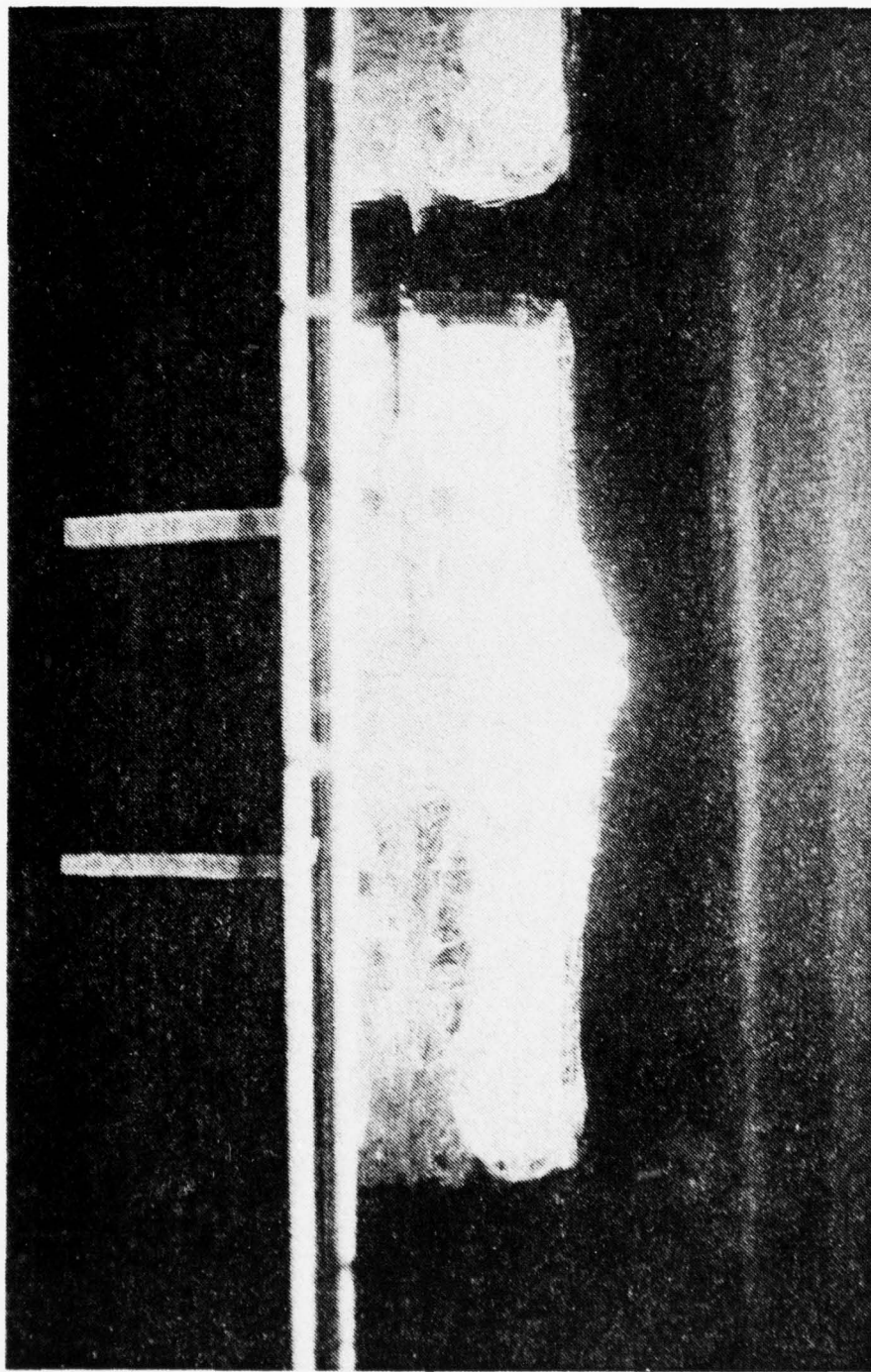
71. Strip chart recording of ripples; Test 6.



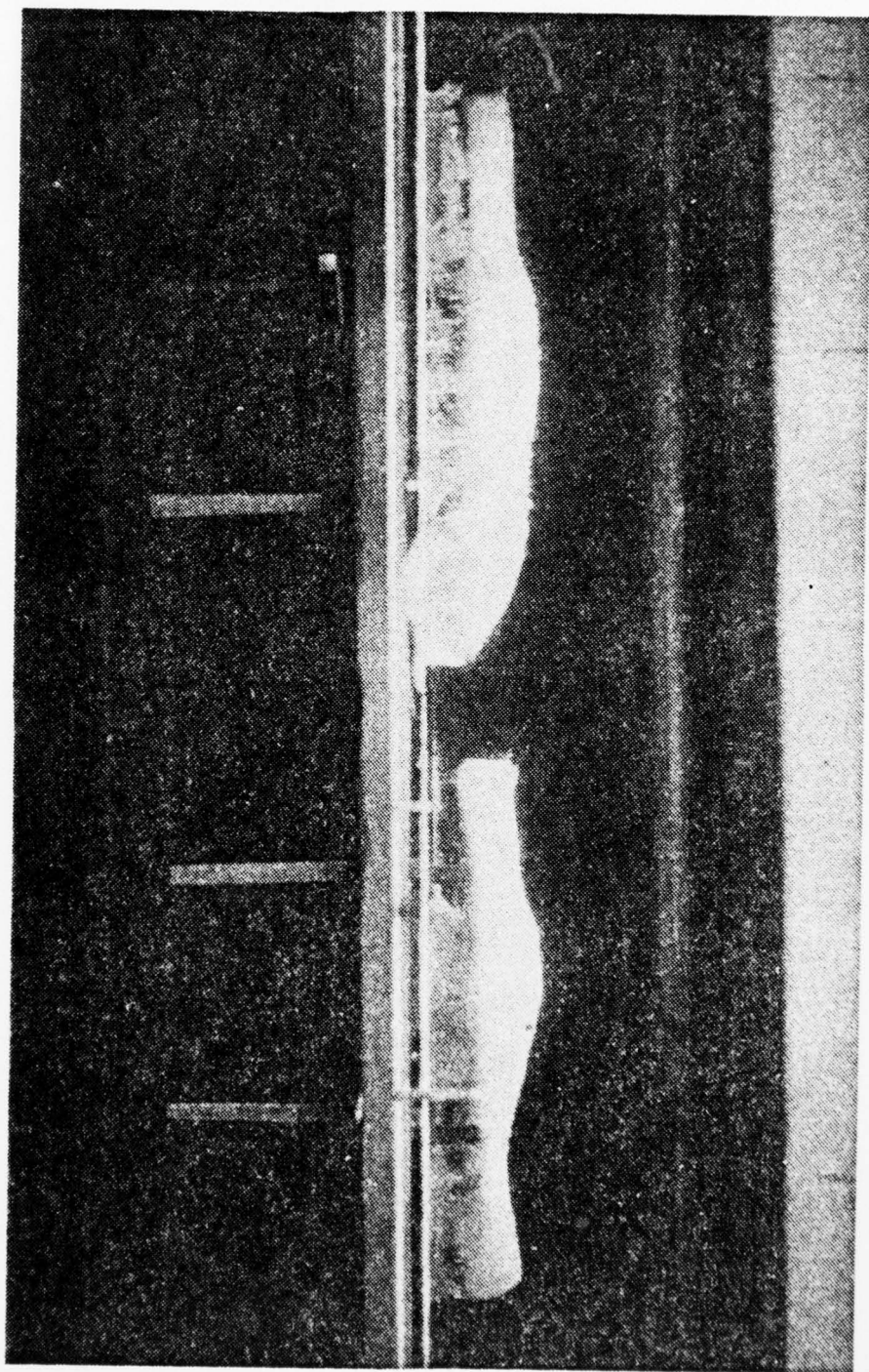
72. Ice model immediately after insertion in water channel.



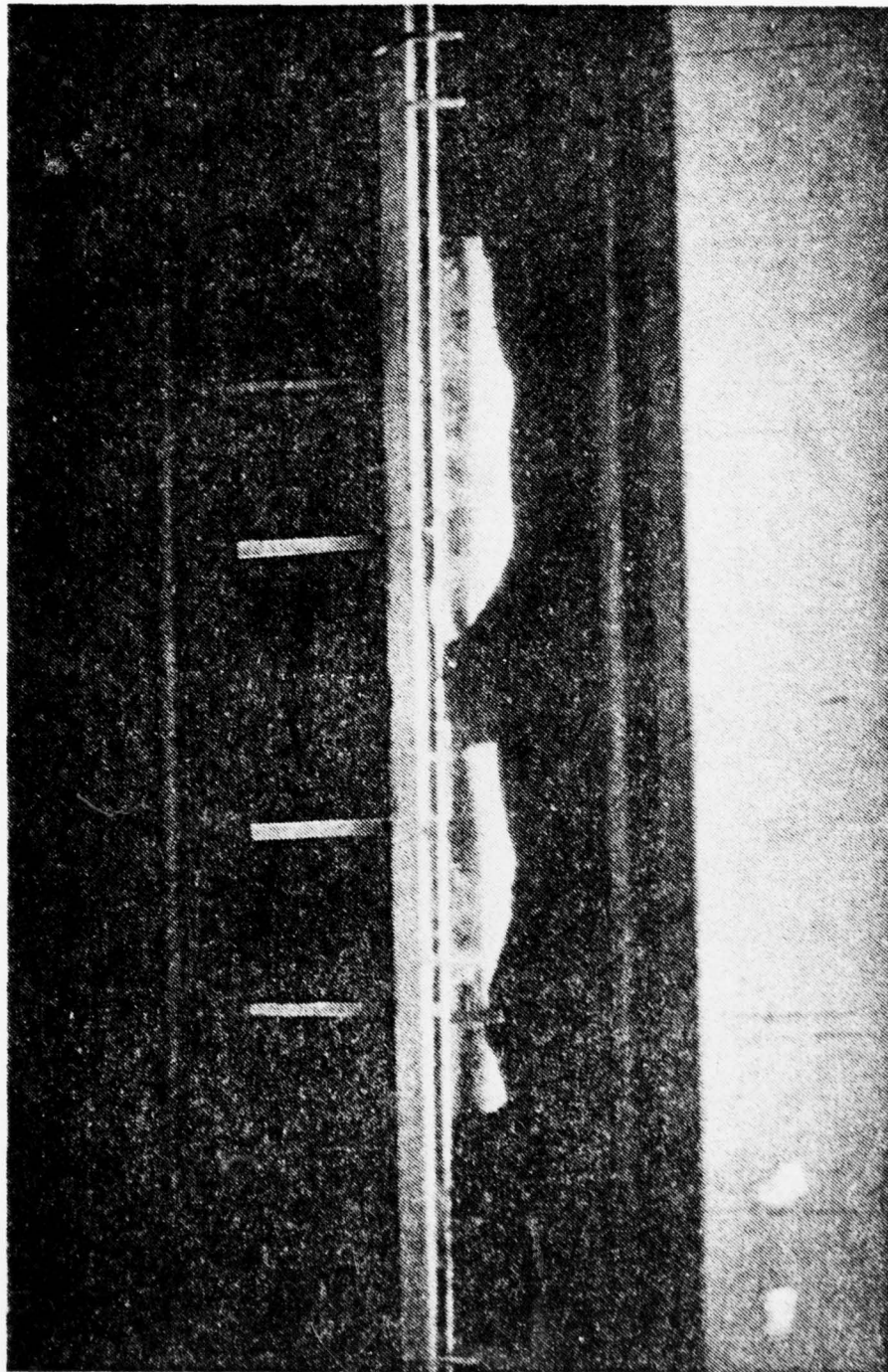
73. Ice model after two minutes in water channel showing dye injection.



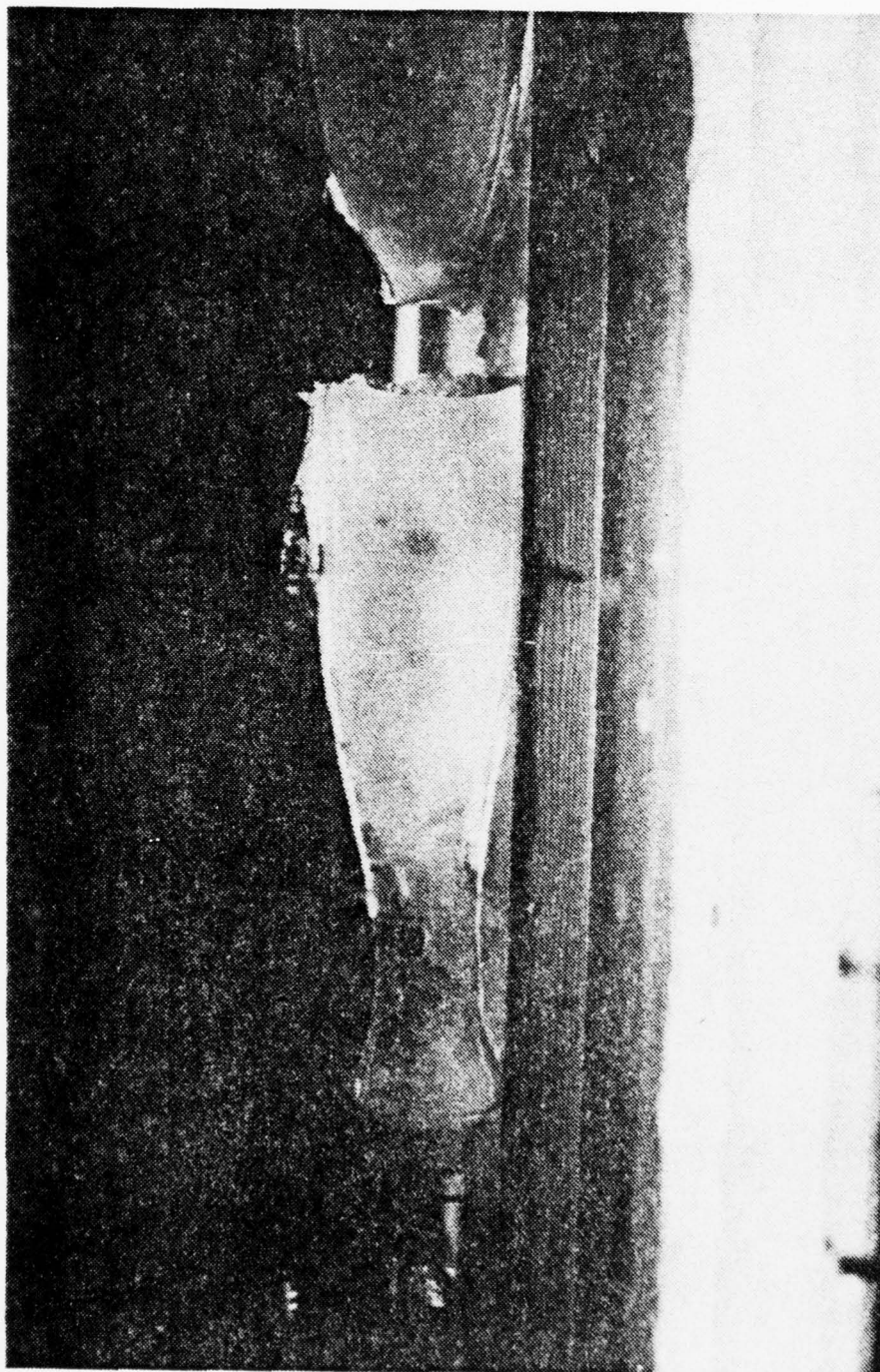
74. Tandem models in water channel immediately after insertion - separation distance = $W/3$.



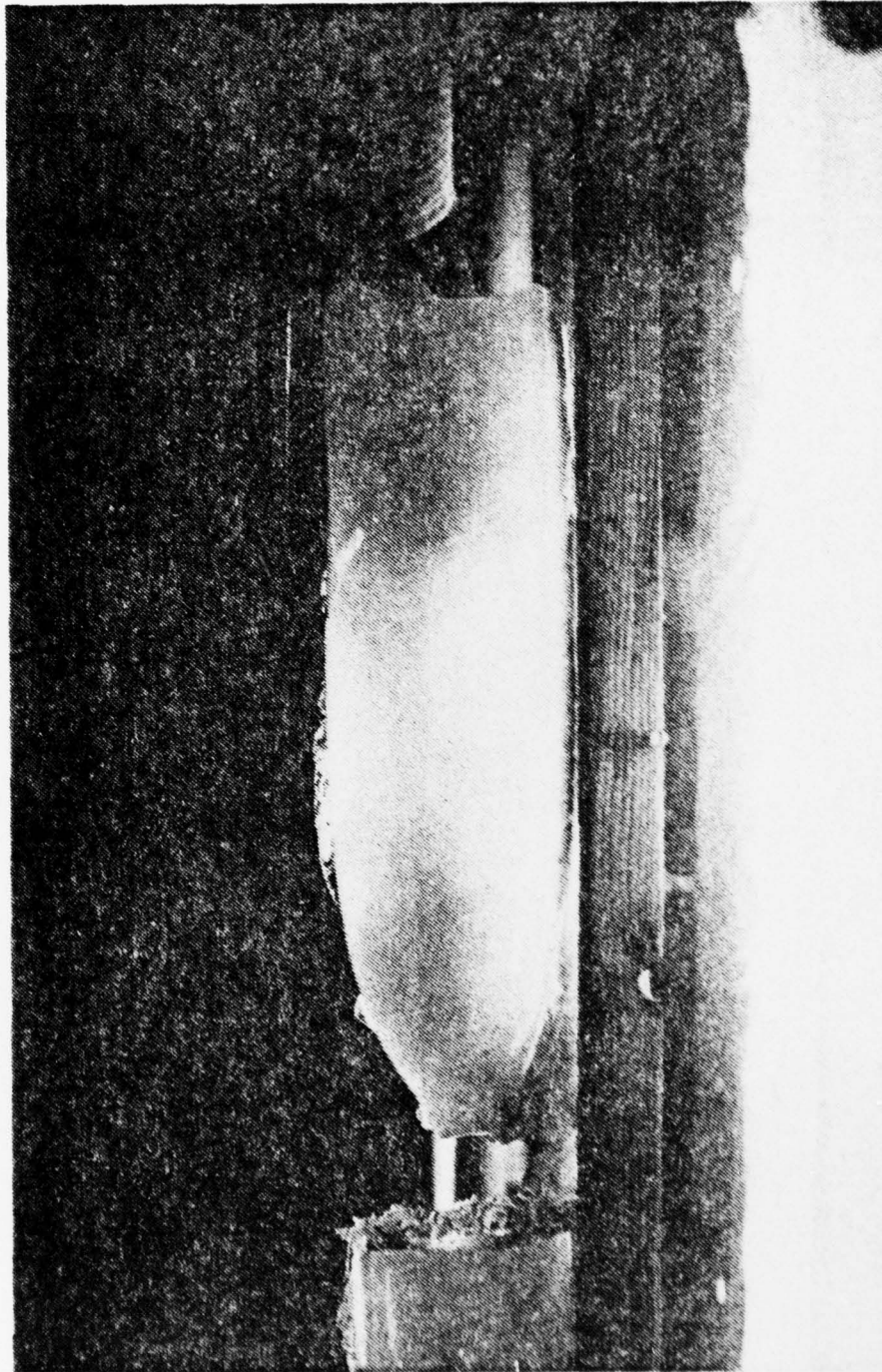
75. Tandem models after one minute in channel at $w/3$ separation distance.



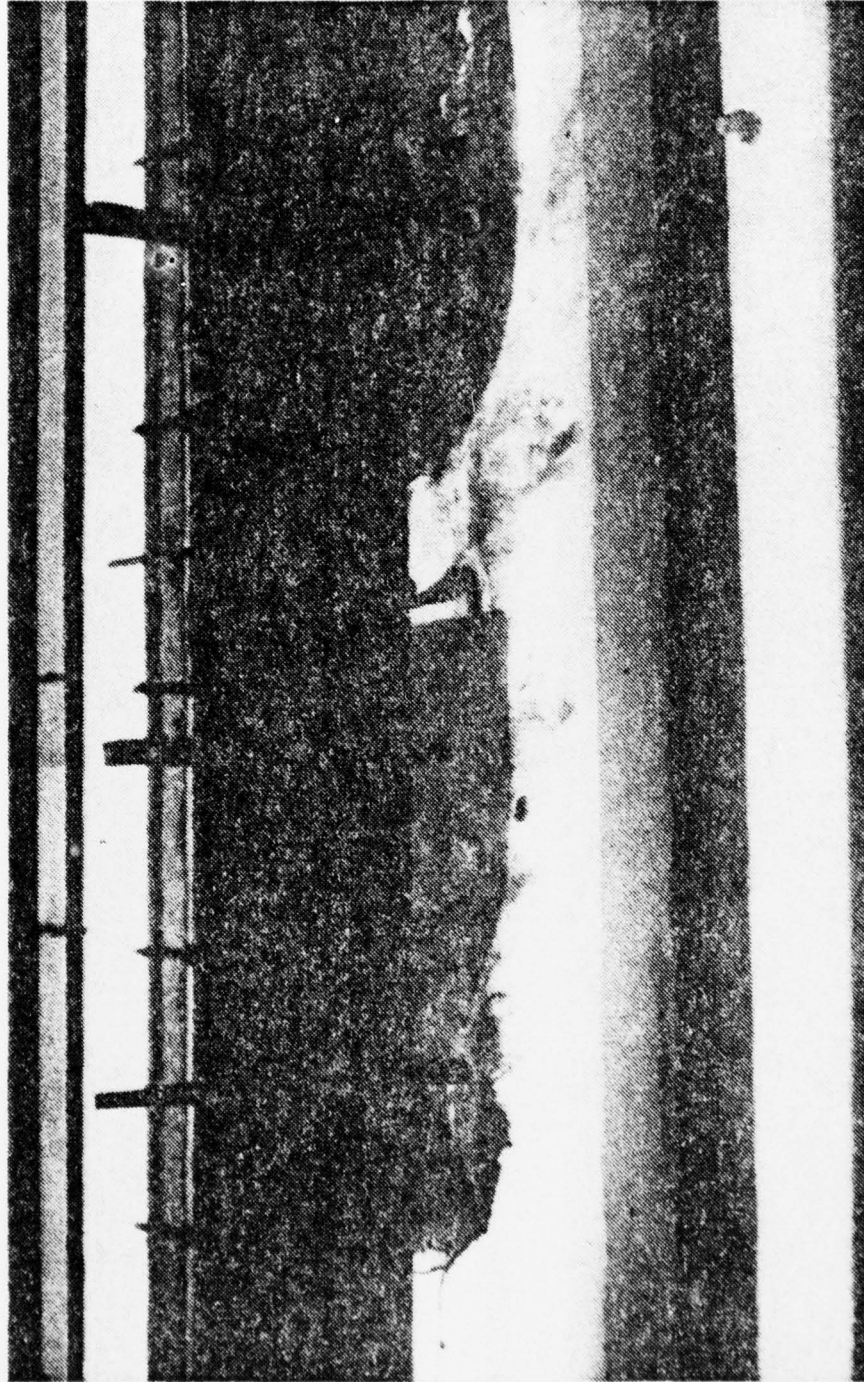
76. Tandem models after two minutes in channel at $W/3$ separation distance.



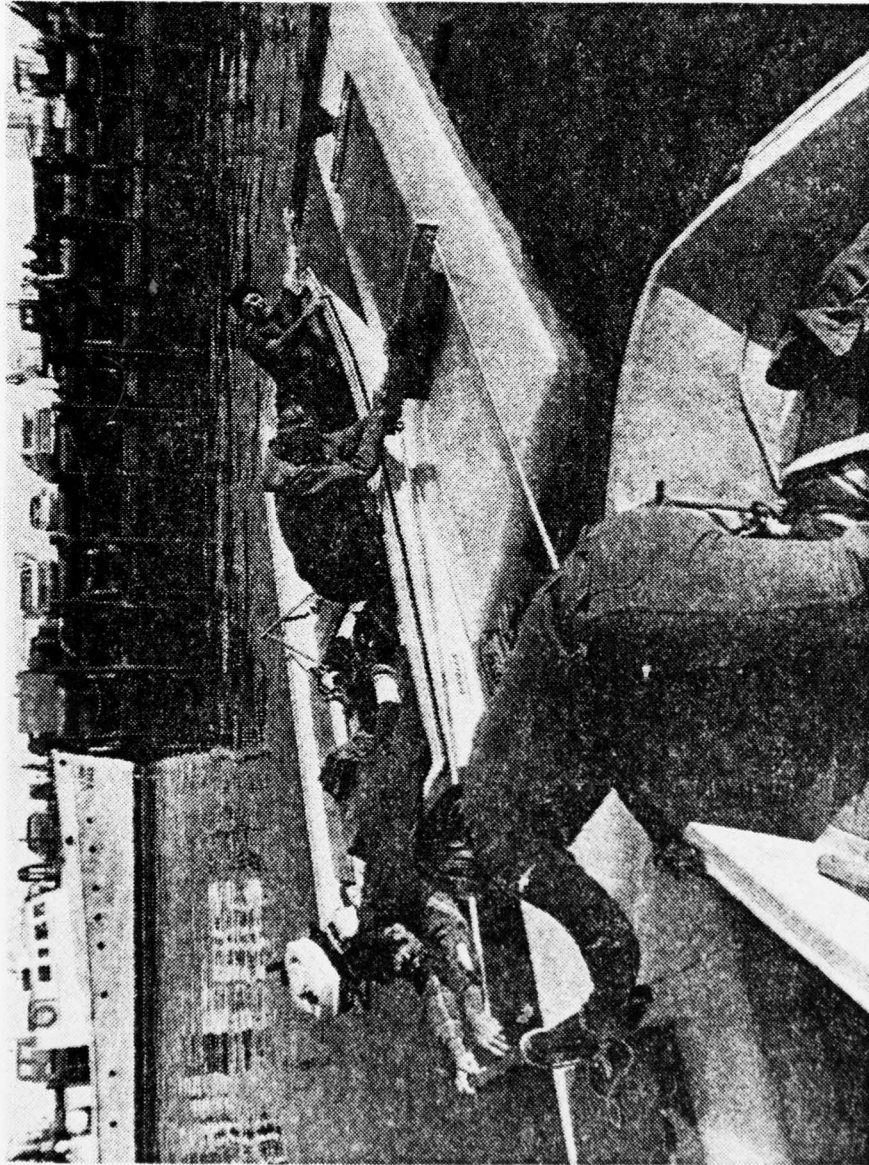
77. Forward ice model bottom view.



78. Rear ice model bottom view.



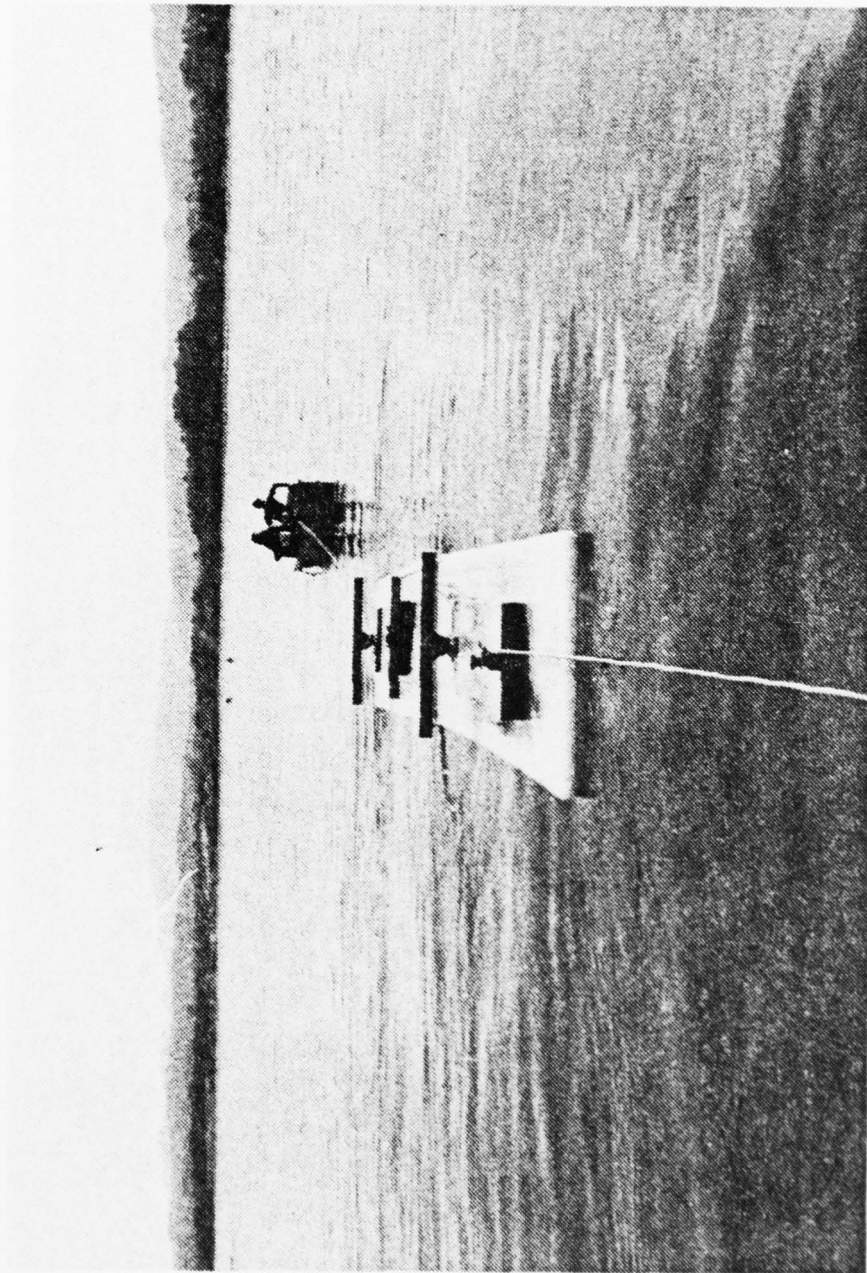
79. Dye accentuated flow visualization around tandem models at $1/3W$ separation distance after two minutes in channels.



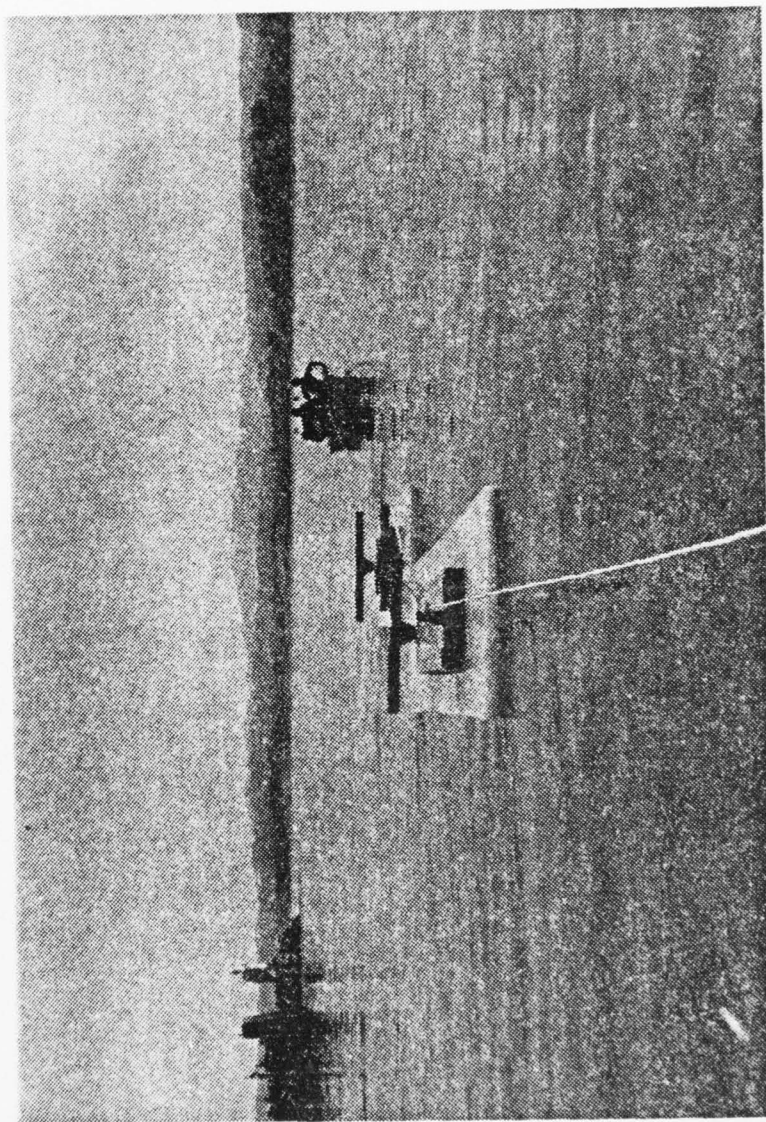
80. Hookup of tandem ice models in Monterey Bay.



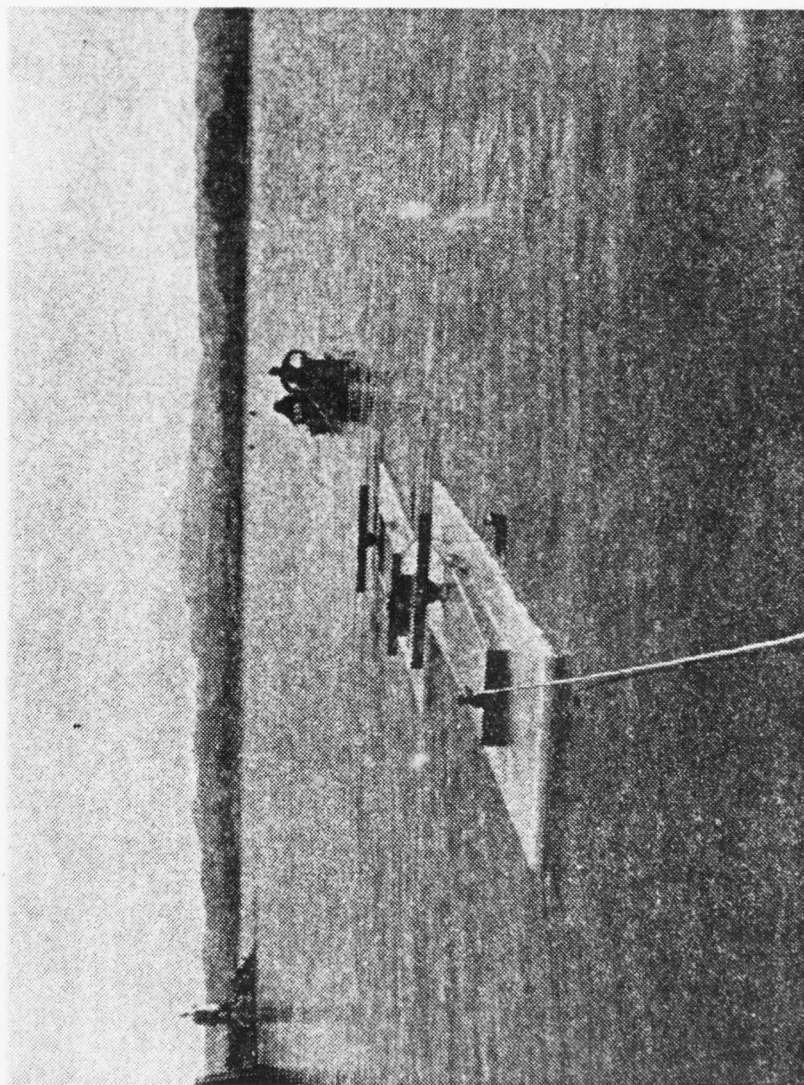
81. Side view of tandem ice models underway.



82. End view of tandem models underway.



83. End view of tandem models underway oscillation left.



84. End view of tandem models underway oscillation right (Note drag rope from rear model).

AD-A070 367

NAVAL POSTGRADUATE SCHOOL MONTEREY CA
EXPERIMENTAL DETERMINATION OF MELTING RATES OF ICE MOVING IN SE--ETC(U)
MAR 79 W F CLIFFORD, R J ERMAN

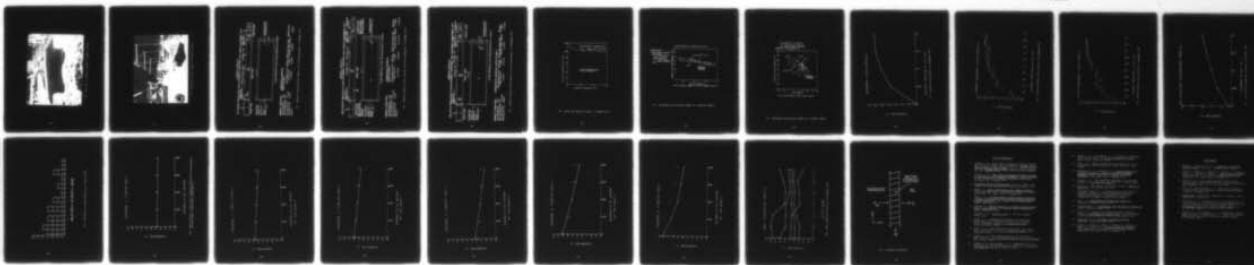
F/6 20/13

UNCLASSIFIED

NL

3 of 3

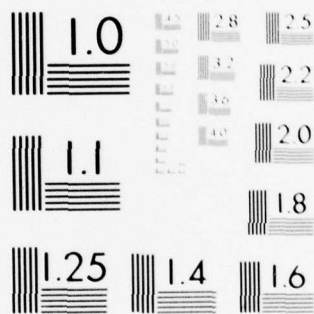
AD
A070 367



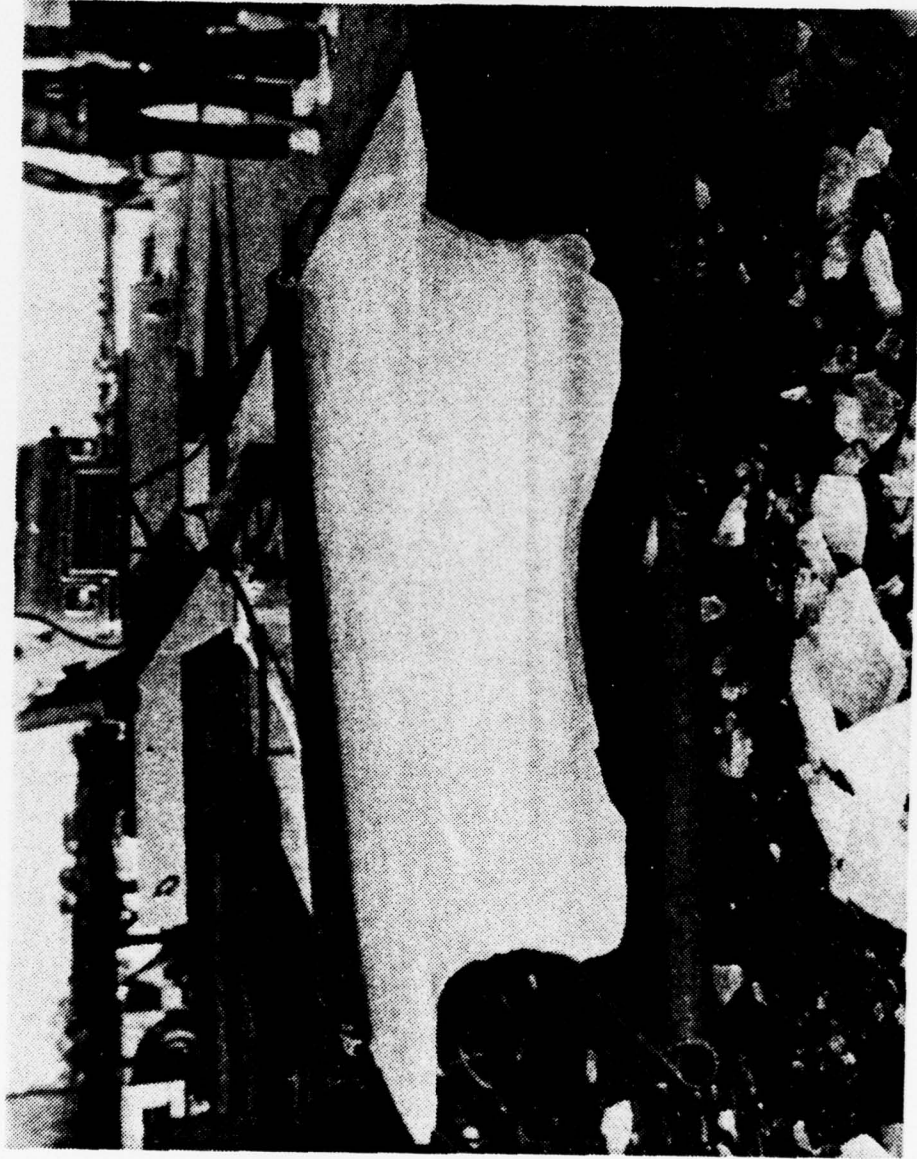
END
DATE
FILMED

7-79

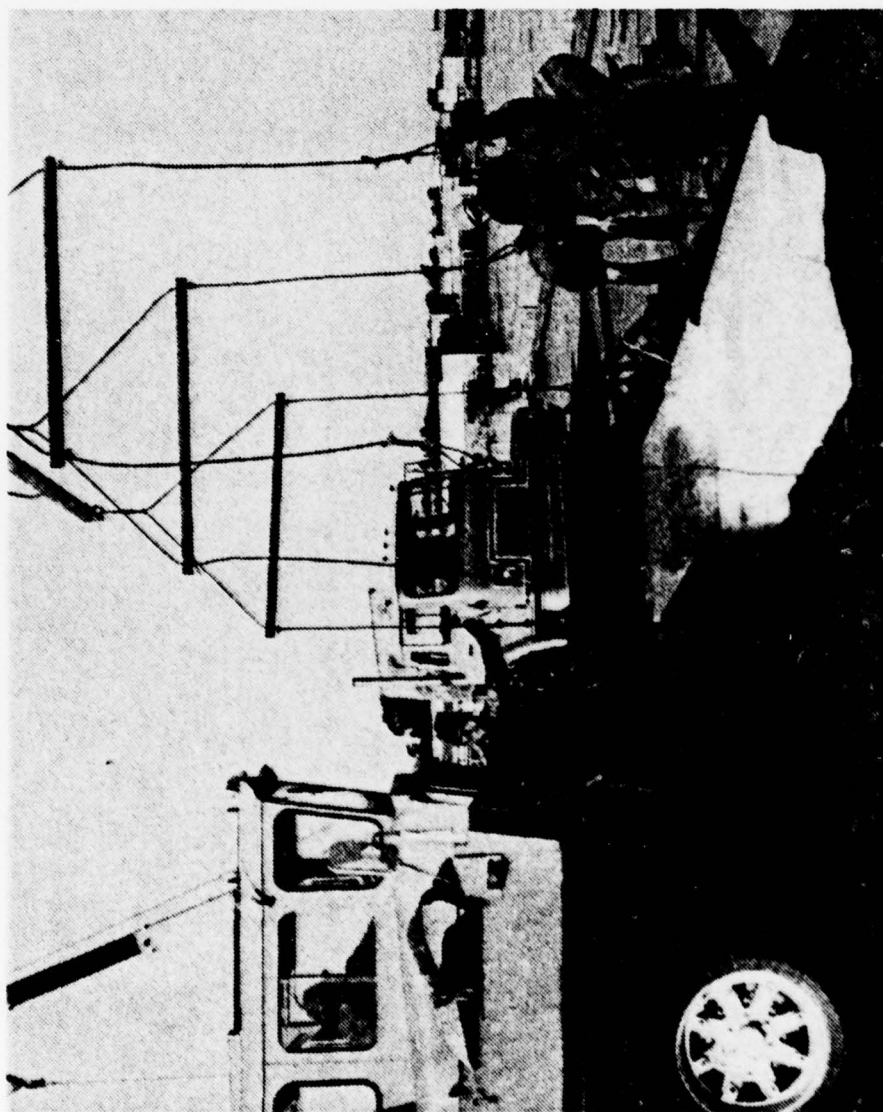
DDC



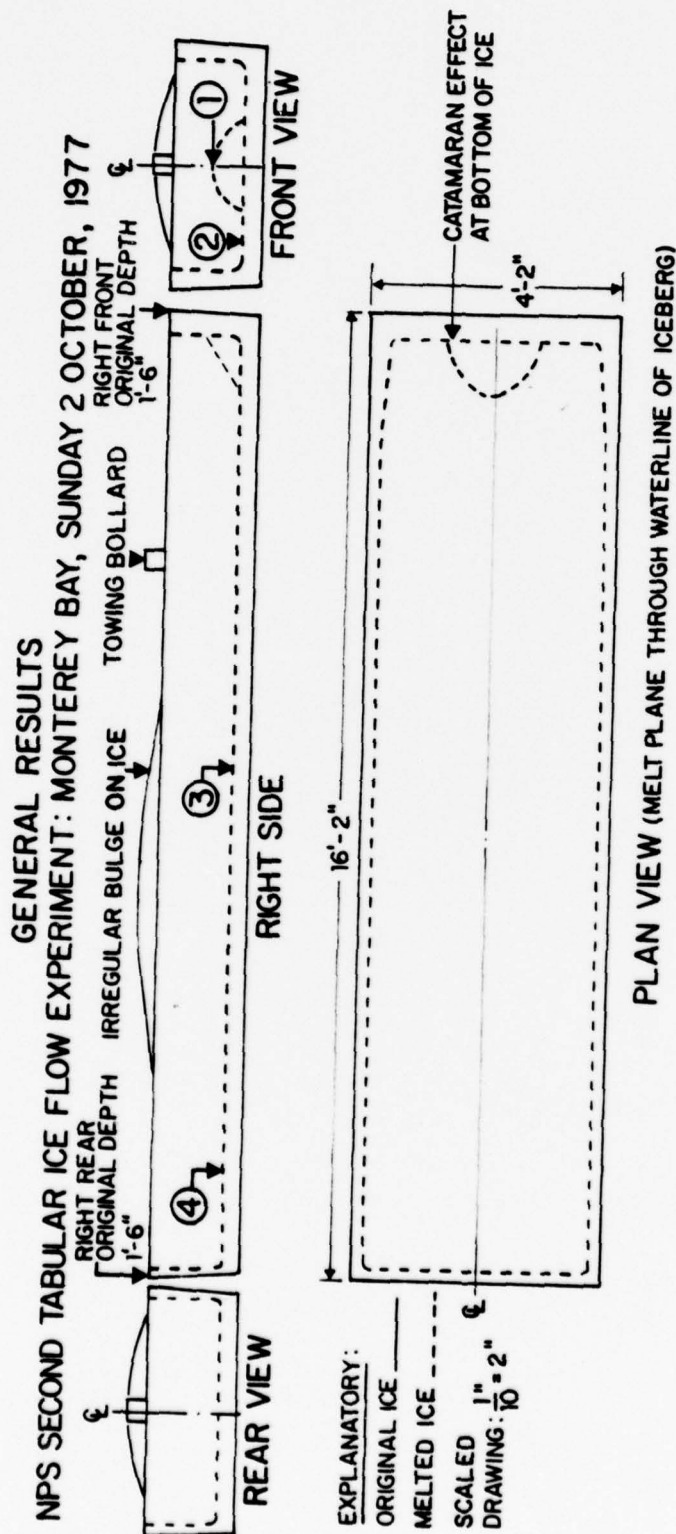
MICROCOPY RESOLUTION TEST CHART
NATIONAL BUREAU OF STANDARDS-1963-A



85. Bow view of forward tandem ice model on pier.

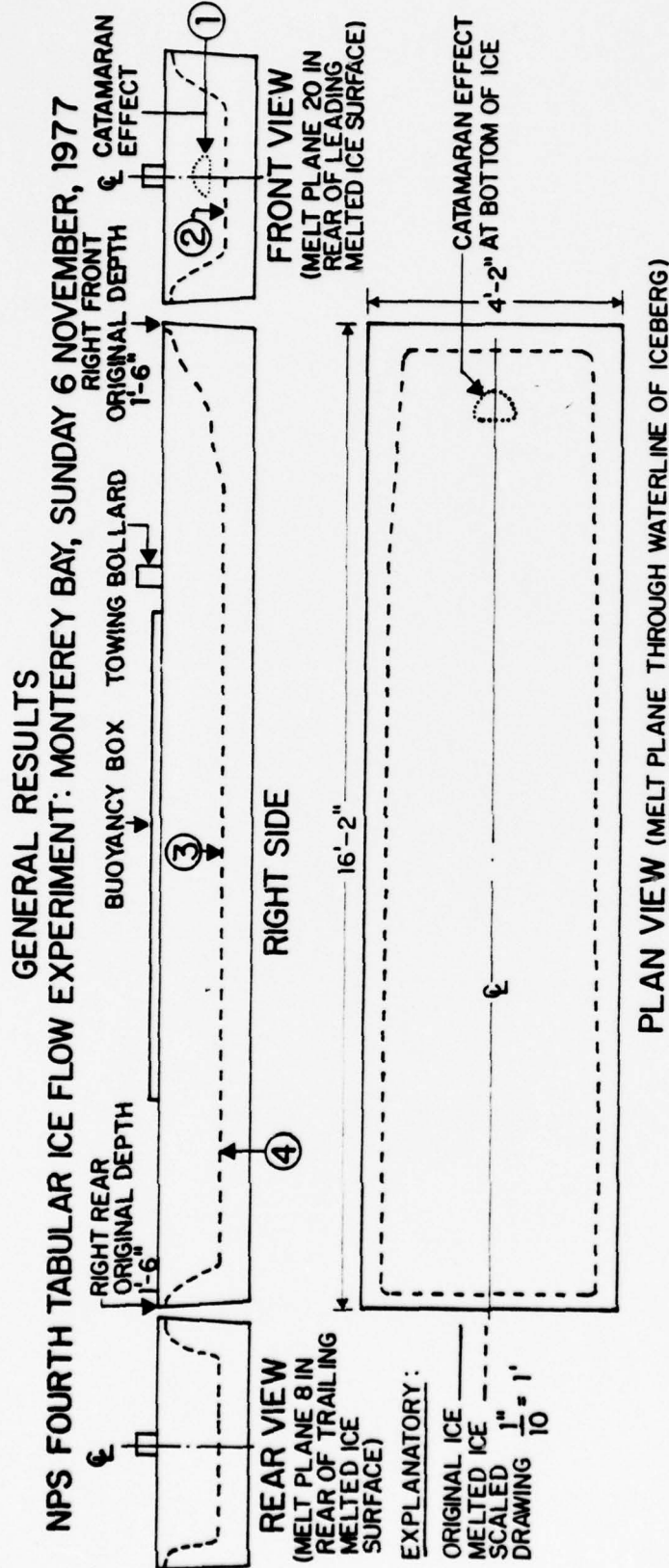


86. Bow view of rear tandem ice model on pier.



AMBIENT CONDITIONS:		SUMMARIZED EMPIRICAL RATES OF MELT:	
AIR TEMPERATURE	58°F	① MAXIMUM (AT FRONT LOWER CENTER)	27.5 IN/HR
WATER TEMPERATURE	61°F	② FRONT LOWER	15.0 IN/HR
AVG TOW VELOCITY	1.5 FT/SEC	③ BOTTOM 8' BACK FROM ORIGINAL FRONT SURFACE	8.1 IN/HR
DURATION OF TOW	24 MIN	④ REAR LOWER	8.1 IN/HR
SALINITY			

87. General results second tabular ice flow experiment, 2 October 1977.



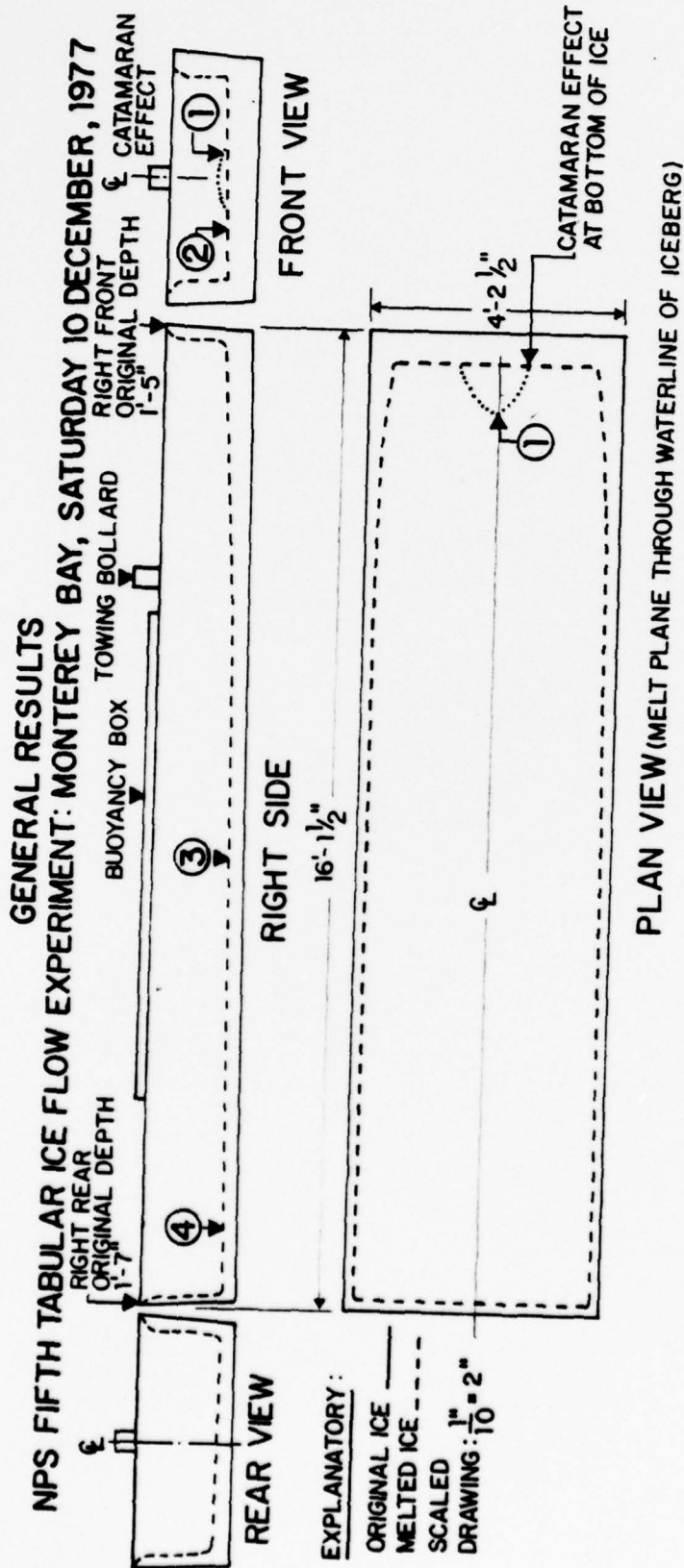
AMBIENT CONDITIONS:

AIR TEMPERATURE 53°F
WATER TEMPERATURE 56°F
AVG TOW VELOCITY 2.4 FT/SEC
DURATION OF TOW 40 MIN
SALINITY

SUMMARIZED EMPIRICAL RATES OF MELT:

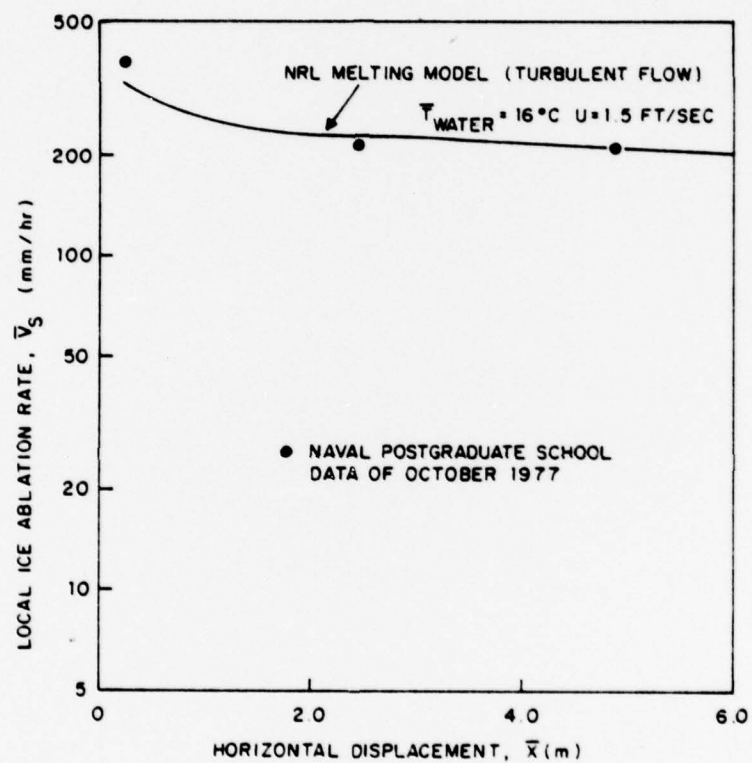
① MAXIMUM (AT FRONT LOWER CENTER)	22.5 IN/HR	② FRONT LOWER	19.5 IN/HR	③ BOTTOM 8' BACK FROM ORIGINAL FRONT SURFACE	8.3 IN/HR	④ REAR LOWER	8.3 IN/HR
-----------------------------------	------------	---------------	------------	--	-----------	--------------	-----------

88. General results fourth tabular ice flow experiment, 6 November 1977.



AMBIENT CONDITIONS:		SUMMARIZED EMPIRICAL RATES OF MELT:	
AIR TEMPERATURE	58°F	① MAXIMUM (AT FRONT LOWER CENTER)	11.5 IN/HR
WATER TEMPERATURE	54°F	② FRONT LOWER	8.7 IN/HR
AVG TOW VELOCITY	1.3 FT/SEC	③ BOTTOM 8' BACK FROM ORIGINAL FRONT SURFACE	5.9 IN/HR
DURATION OF TOW	38 MIN	④ REAR LOWER	4.7 IN/HR

89. General results fifth tabular ice flow experiment, 10 December 1977.

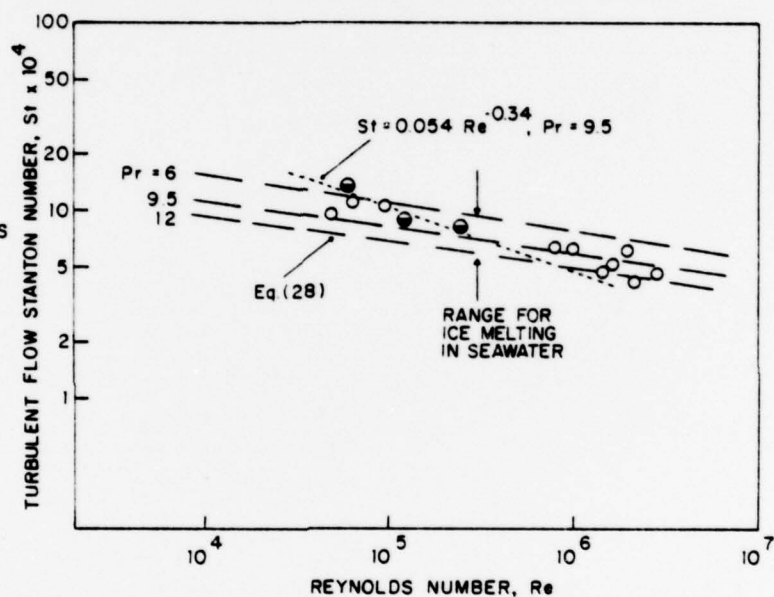


90. Local ice ablation rate: 2 October 1977.

CURVE PREPARED BY O. M. GRIFFIN, NRL (1/27/78)

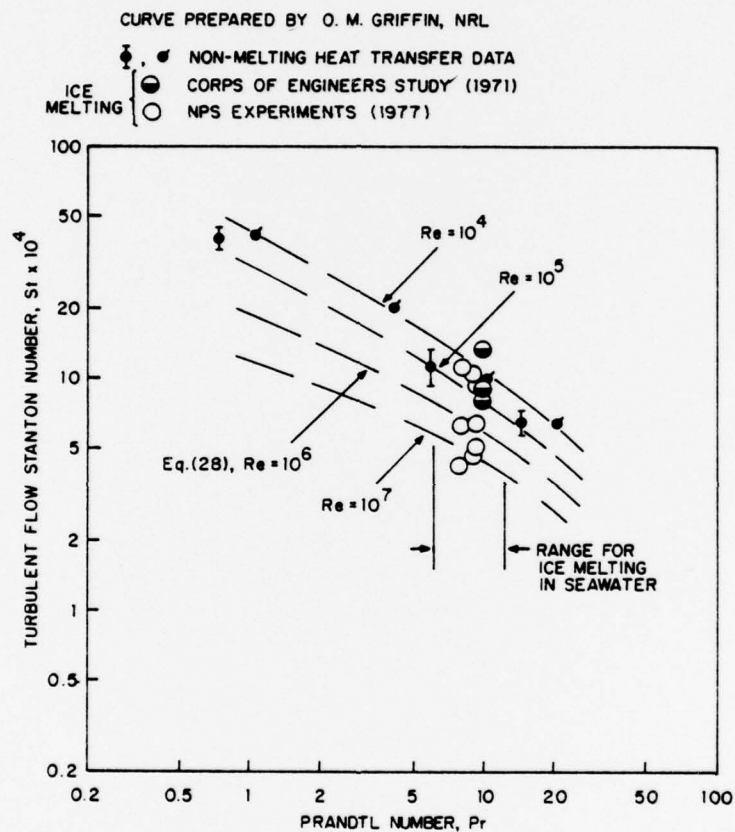
LEGEND FOR DATA:

- ARMY CORPS OF ENGINEERS STUDY (1971)
- NPS EXPERIMENTS (1977),
- , STANTON NUMBER PREDICTION
- , LEAST-SQUARES FIT TO CORPS OF ENGINEERS DATA



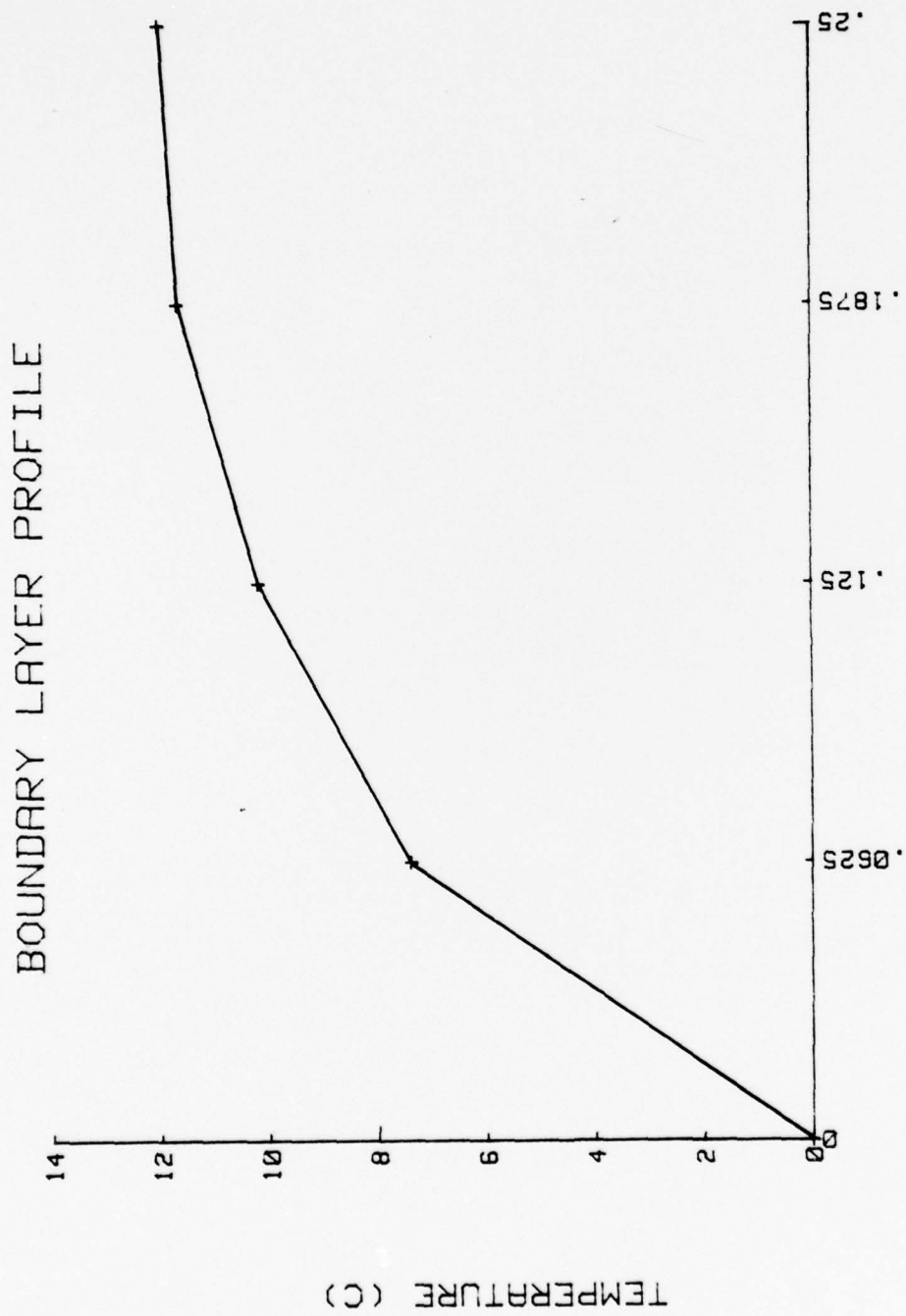
PLOT OF STANTON NUMBER VS. REYNOLDS NUMBER ICE MELTING

91. Turbulent flow Stanton number vs. Reynolds number.

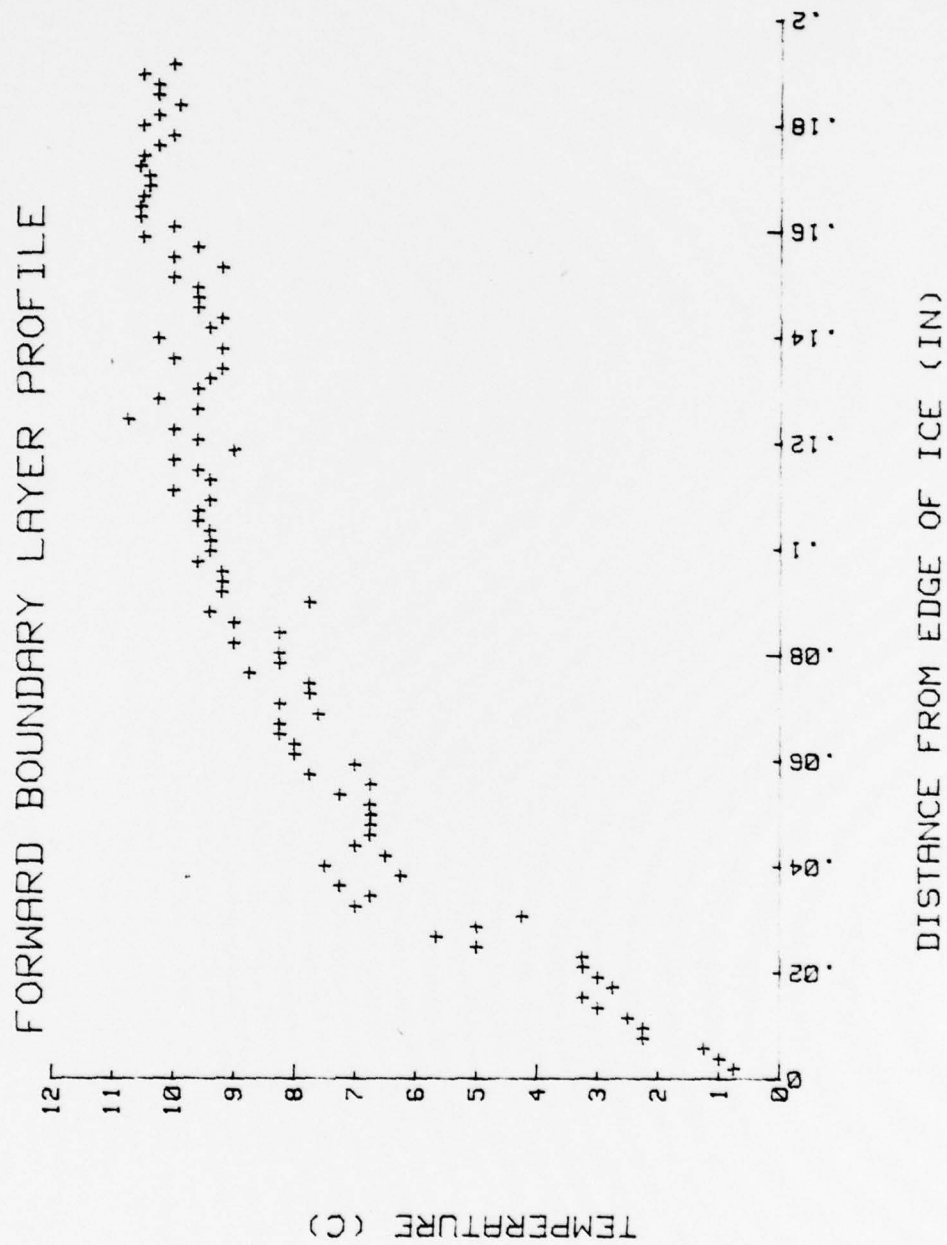


PLOT OF STANTON NUMBER VS. PRANDTL NUMBER ICE MELTING

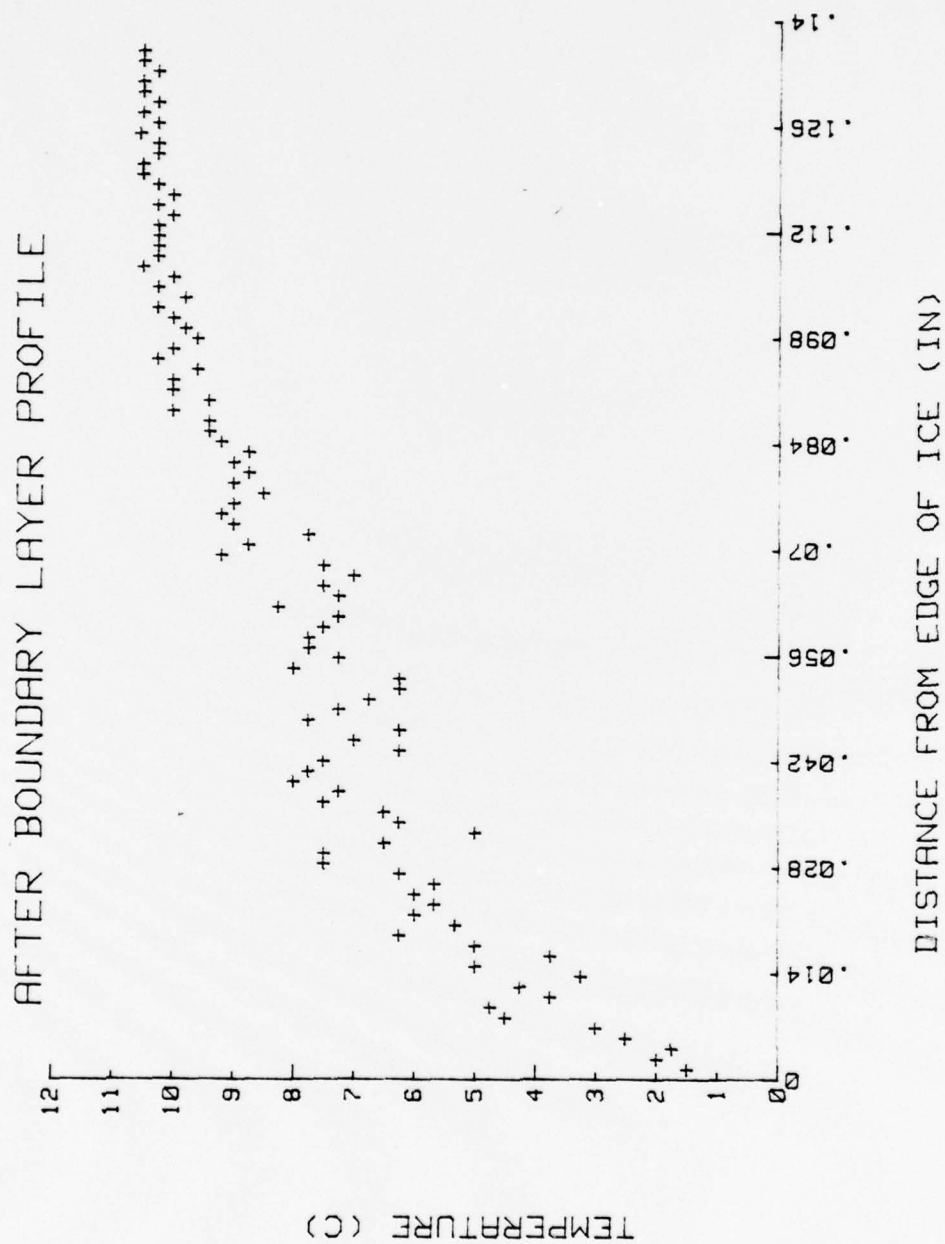
92. Turbulent flow Stanton number vs. Prandtl number.



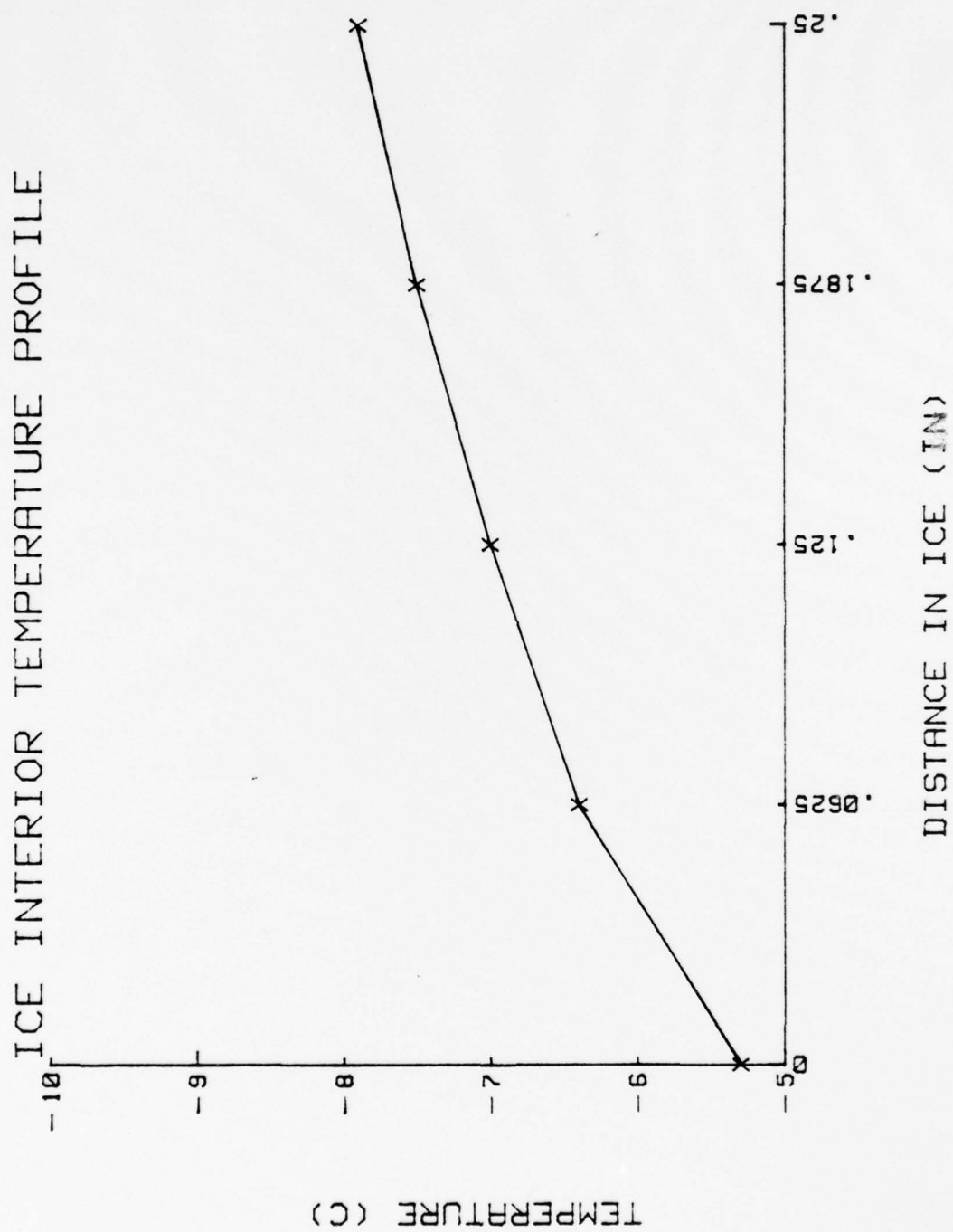
93. Boundary layer profile, 6 November 1977.



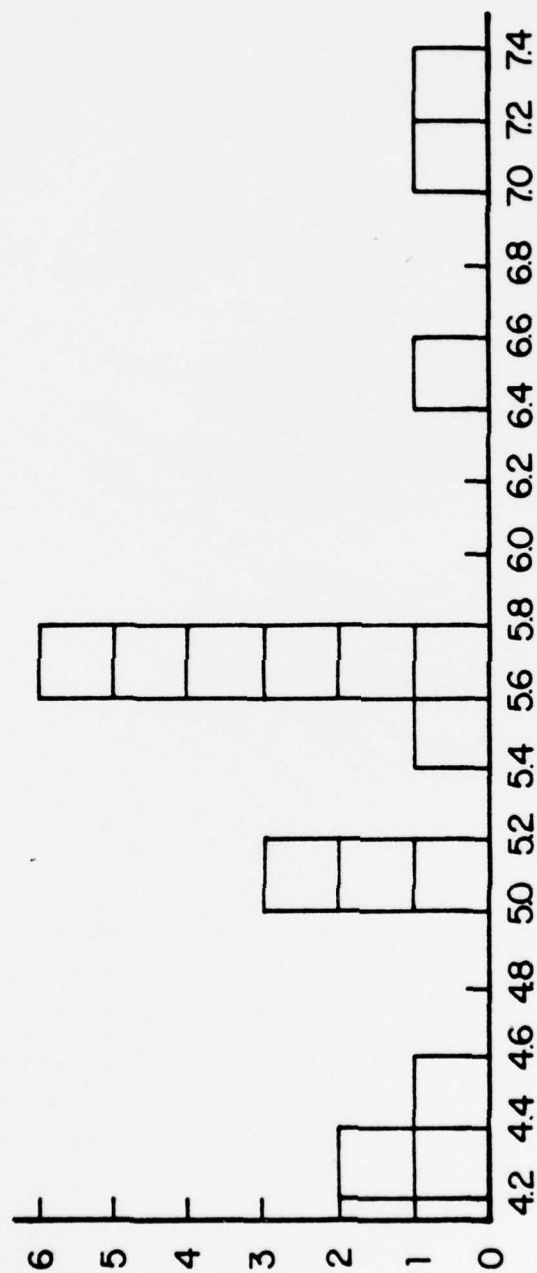
94. Forward boundary layer profile, 10 December 1977.



95. After boundary layer profile, 10 December 1977.

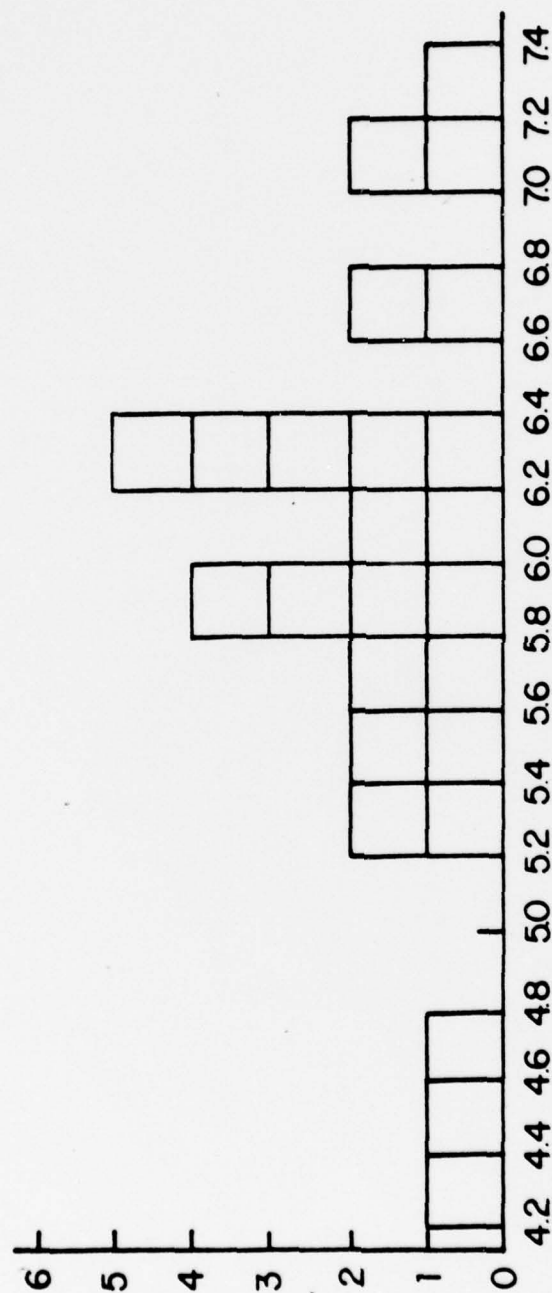


96. Ice interior temperature profile, 6 November 1977.



WAVELENGTH OF RIPPLES, INCHES

97. Histogram of ripples along ice, 3 October 1977.



WAVELENGTH OF RIPPLES, INCHES

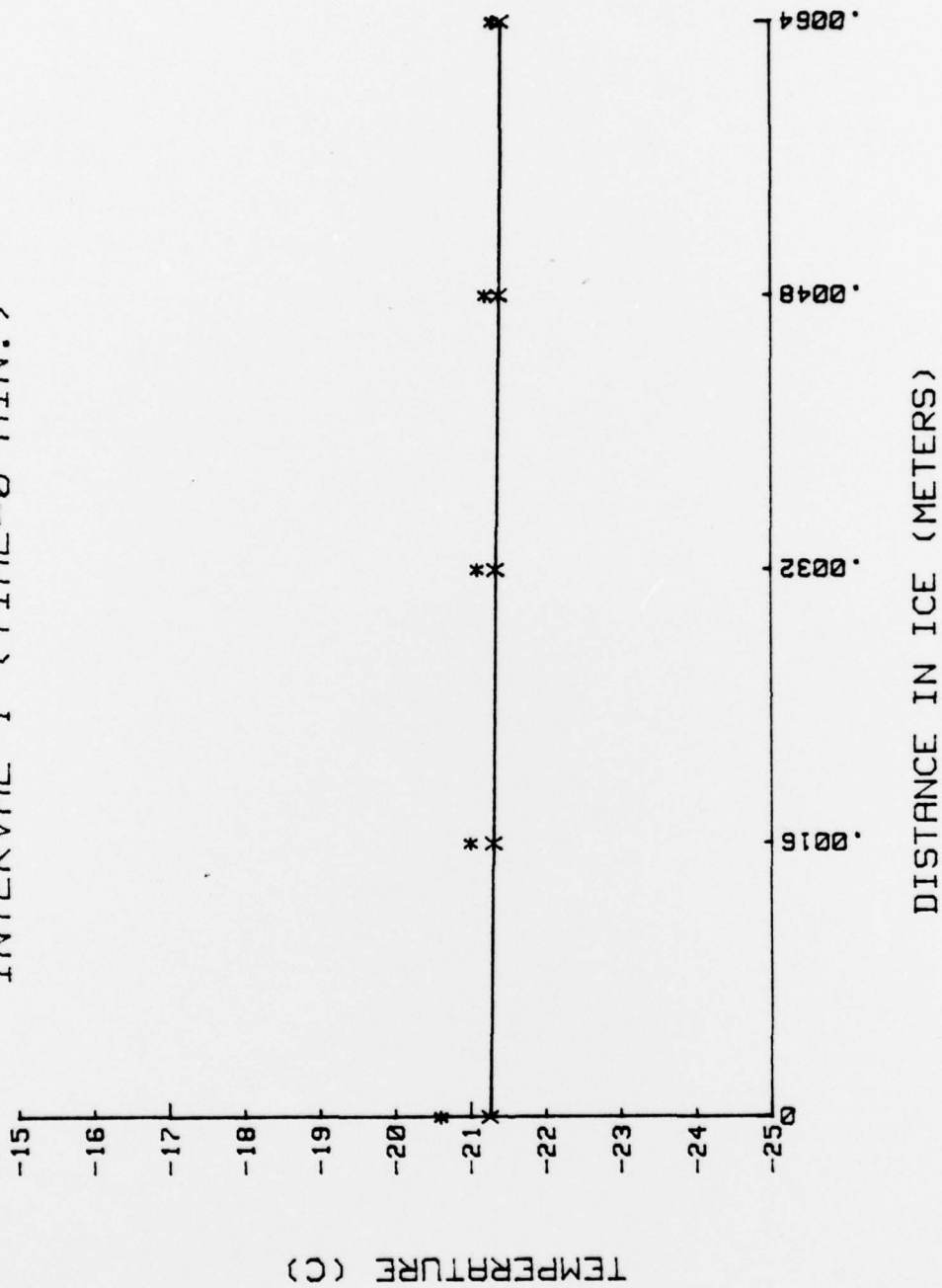
98. Histogram of ripples along ice, 10 December 1977.



WAVELENGTH OF RIPPLES, INCHES

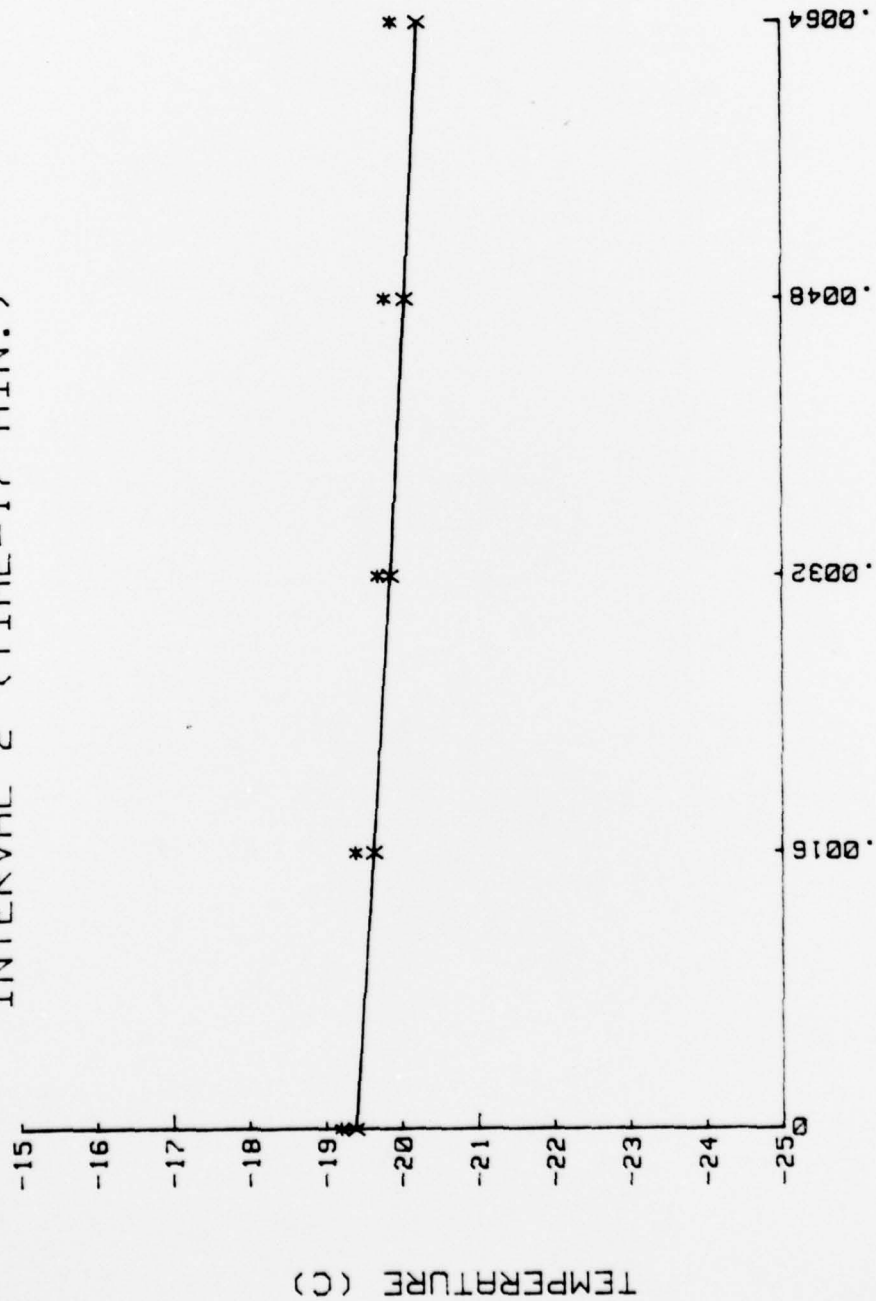
99. Histogram of ripples along ice, 27 April 1978.

INTERVAL 1 (TIME=0 MIN.)



100. Time interval 1; solid line represents theoretical calculations and data points (asterisks), experimental.

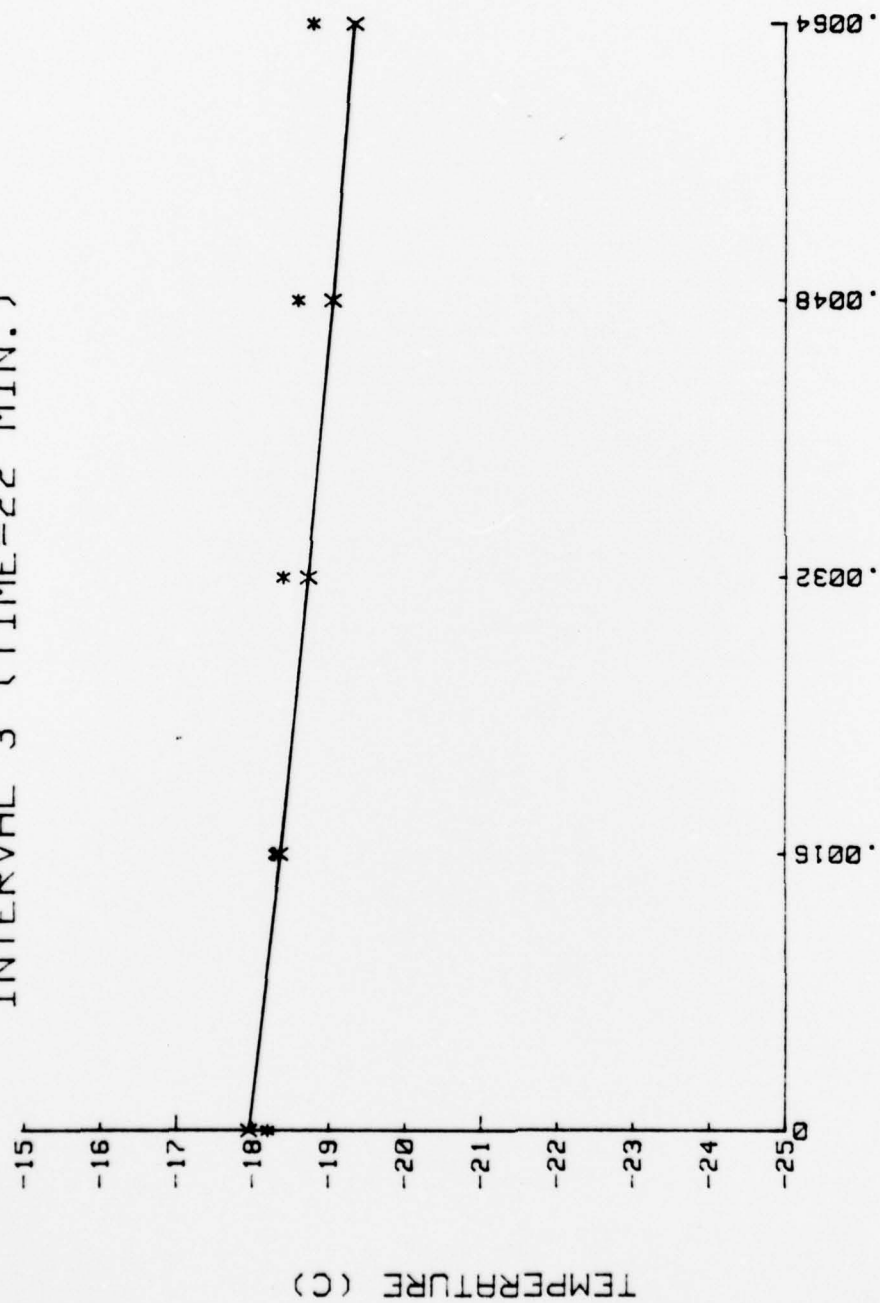
INTERVAL 2 (TIME=17 MIN.)



DISTANCE IN ICE (METERS)

101. Time interval 2.

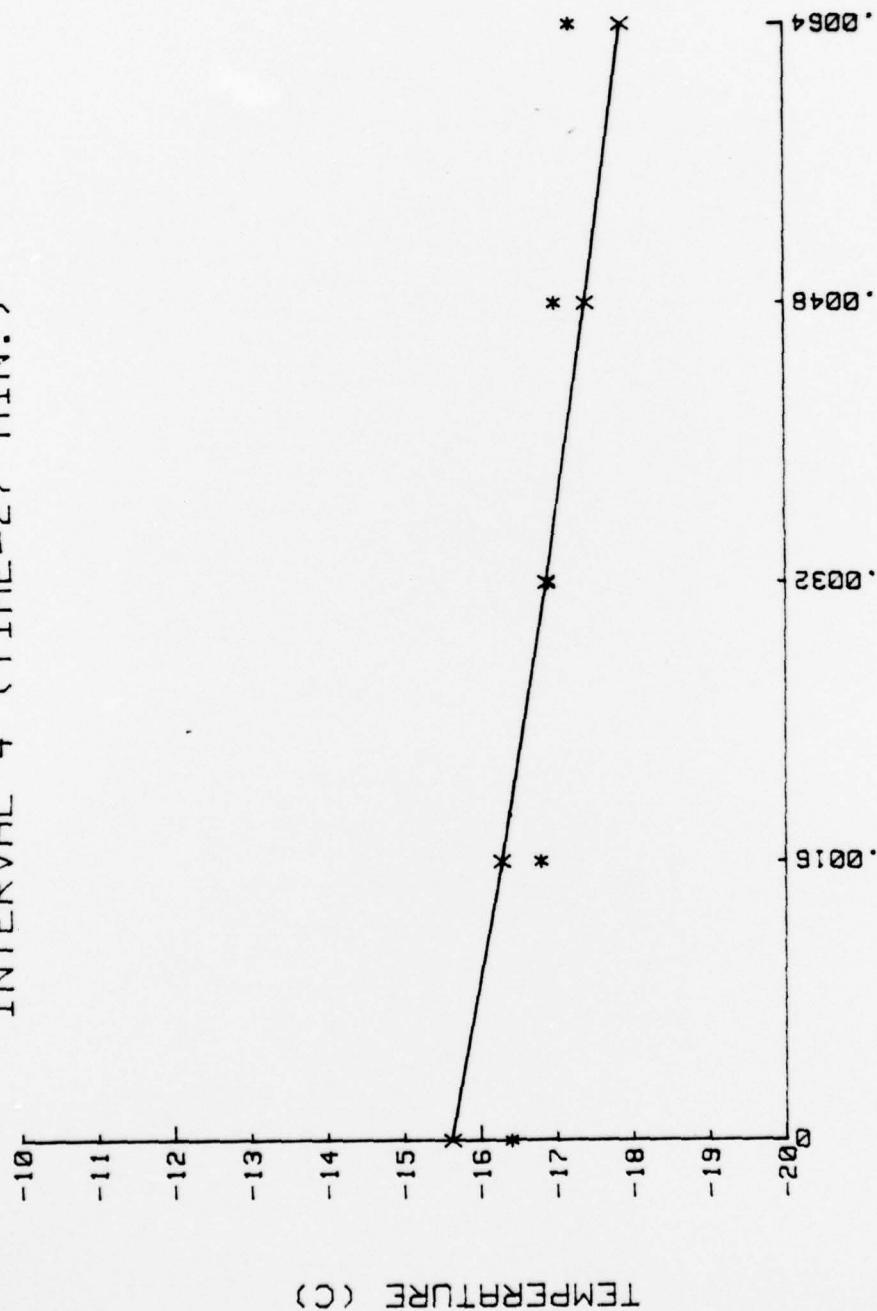
INTERVAL 3 (TIME=22 MIN.)



DISTANCE IN ICE (METERS)

102. Time interval 3.

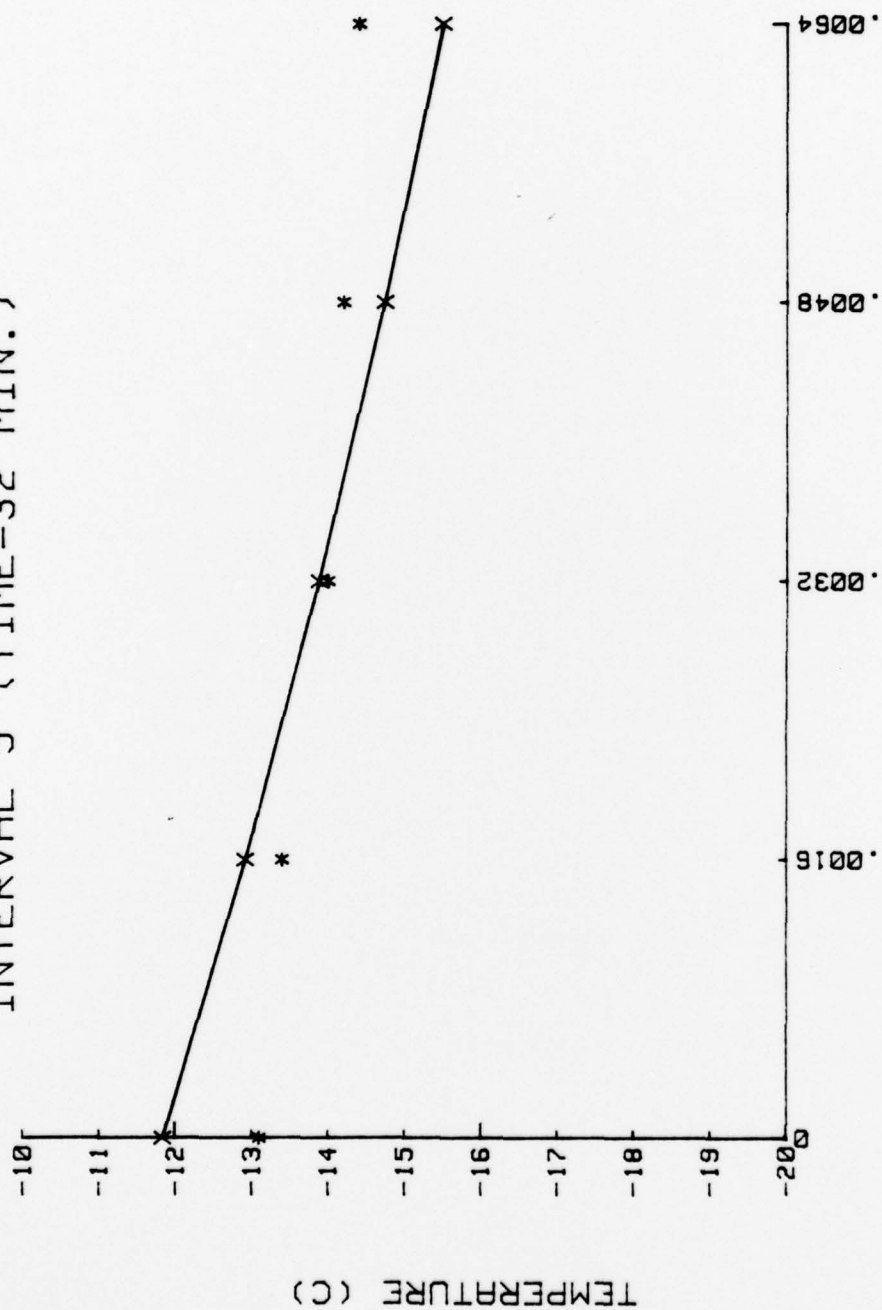
INTERVAL 4 (TIME=27 MIN.)



DISTANCE IN ICE (METERS)

103. Time interval 4.

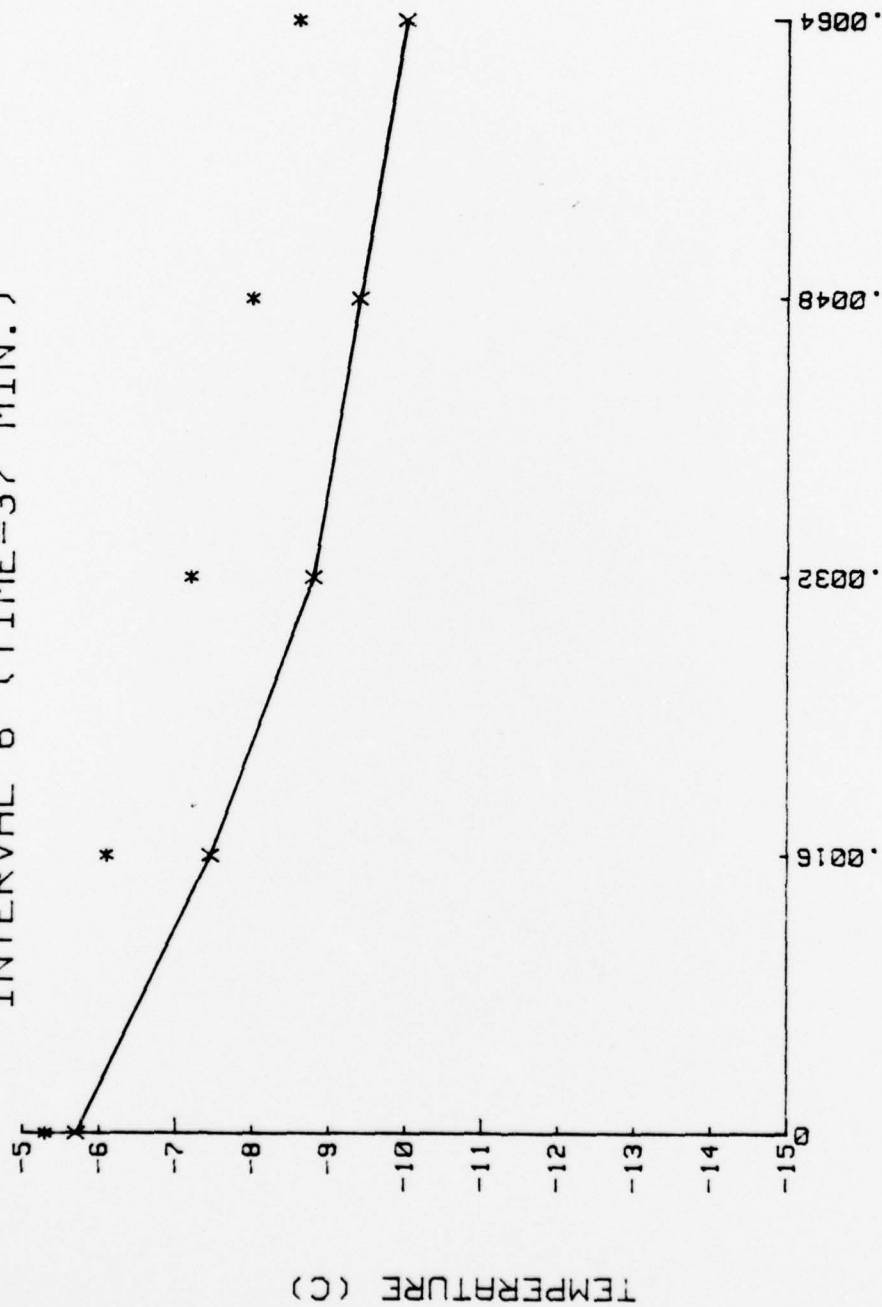
INTERVAL 5 (TIME=32 MIN.)



DISTANCE IN ICE (METERS)

104. Time interval 5.

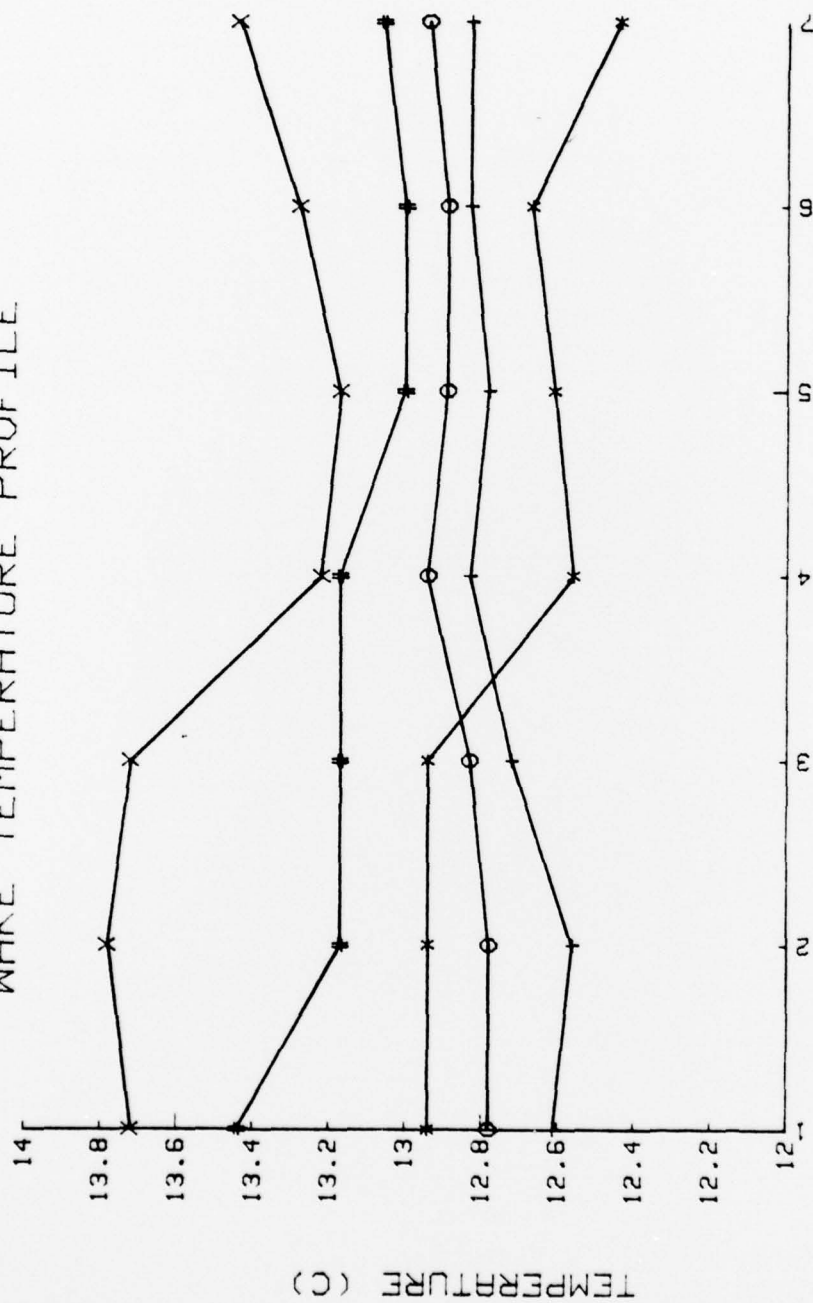
INTERVAL 6 (TIME=37 MIN.)



DISTANCE IN ICE (METERS)

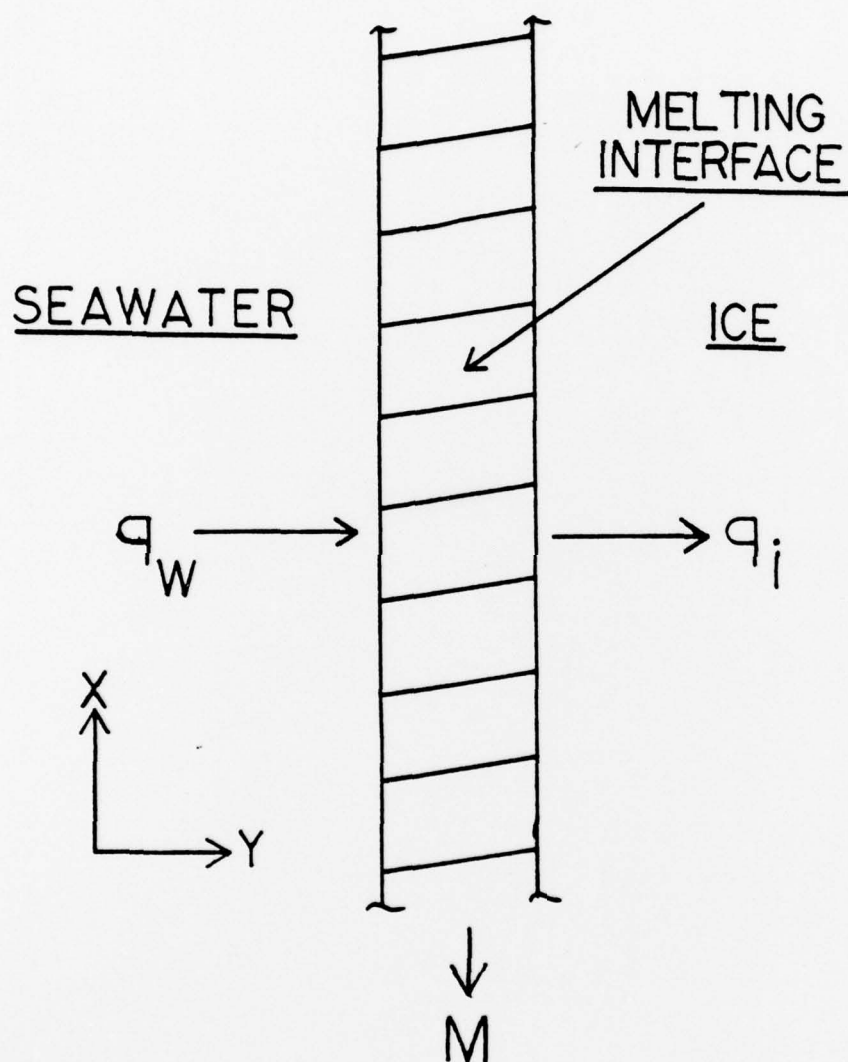
105. Time interval 6.

WAKE TEMPERATURE PROFILE



STATION NUMBER

106. Wake temperature profile, 10 December 1977.



107. Ice-water interface.

LIST OF REFERENCES

1. Griffin, O. M., "Heat, Mass and Momentum Transfer During the Melting of Glacial Ice in Seawater," Transactions of ASME, Journal of Heat Transfer, Vol. 95, 317-323 (1973); see also Transactions of ASME, Journal of Heat Transfer, Vol. 97, 624-626 (1975).
2. Griffin, O. M., Heat, Mass and Momentum Transfer Effects on the Ablation of Icebergs in Seawater, paper presented at the International Iceberg Utilization Conference, 1st Ames, Iow, 3 October 1977.
3. Principles of Naval Architecture, 3rd ed., Chapter VII, Society of Naval Architects and Marine Engineers, 1967.
4. Murphy, G., Small Scale Modeling of Iceberg Transport, paper presented at the International Iceberg Utilization Conference, 1st, Ames, Iowa, 3 October 1977.
5. Meyer, J. F., An Experimental Investigation of the Heat Transfer Characteristics of a Heated Cylinder Placed in a Cross Flow of Air, M.S. Thesis, Naval Postgraduate School, Monterey, 1973.
6. Kösemen, E., Thermal Studies of a Heated Cylinder Placed Near a Plane Surface, M.S. Thesis, Naval Postgraduate School, Monterey, 1975.
7. Pounder, E. R., Physics of Ice, p. 86-129, Pergamon Press, 1965.
8. Carey, K. L., "Observed Configuration and Computed Roughness of the Underside of River Ice," St. Croix River, Wisconsin, U. S. G. S. Professional Paper, 550-B, B192-B198 (1966).
9. Carey, K. L., "The Underside of River Ice," St. Croix River, Wisconsin, U. S. G. S. Profesional Paper, 575-C, C195-C199 (1967).
10. Larsen, P. A., "Head Losses Caused by an Ice Cover on Open Channels," J. of the Boston Society of Civil Engineers, 56-1, 45-67 (1969).
11. Ashton, G. D., and Kennedy, J. F., "Temperature and Flow Conditions during the Formation of River Ice," I. A. H. R. Ice Symposium, Reykjavik, Iceland (1970).

12. Ashton, G. D., and Kennedy, J. F., "Ripples on Underside of River Ice Covers," J. of the Hydraulics Division, ASCE, 98-HY9, 1603-1624 (1972).
13. Hsu, K. S., "Spectral Evolution of Ice Ripples," Ph. D. Dissertation, The University of Iowa, Iowa City, Iowa (1973).
14. Tatinclaux, J. C., Kennedy, J. F., Ripple Formation at Ice-Flow Interfaces: Potential Effect on Iceberg Transport, paper presented at Iceberg Utilization Conference, 1st, Ames, Iowa, 3 October 1977.
15. Uzuner, M. S., "The Composite Roughness of Ice-Covered Streams," J. of Hydraulic Research, 13-1, 79-102 (1975).
16. Mellor, M., "Engineering Properties of Snow," Journal of Glaciology, Vol. 19, No. 81, 1977.
17. Josperger, Edward G., "A Laboratory and Field Study of the Role of Natural Convective Boundary Layers in Iceberg Deterioration," Proceedings of the First Conference on Iceberg Utilization (in Press).
18. Lin, C. C., The Theory of Hydrodynamic Stability, Cambridge University Press, 1955.
19. Chandrasekhar, S., Hydrodynamic and Hdromagnetic Stability, Oxford University Press, 1962.
20. Shen, S. F., "Stability of Laminar Flows," Section G, Volume IV, The Theory of Laminar Flows, Princeton Series on High Speed Aerodynamics and Jet Propulsion, 1964.
21. Greenspan, H. P., The Theory of Rotating Fluids, Cambridge University Press, 1968.
22. Stolfi, R., Fuhs, A., Wang, P., Bourke, R., Denner, W., Erman, R., Clifford, W., Ice Moving Through Seawater, paper presented at International Iceberg Utilization Conference, 1st, Ames, Iowa, 3 October 1977.

BIBLIOGRAPHY

1. Cebeci, T. and Smith, A. M. O., Analysis of Turbulent Boundary Layers, New York: Academic Press (1974).
2. Fuhs, A., Denner, W., Kelleher, M., Erman, R., Clifford, W., Stolfi, R., Bourke, R., Wang, P., Self Propelled Iceberg, paper presented at International Iceberg Utilization Conference, 1st, Ames, Iowa, 3 October 1977.
3. Griffin, O. M., "An Integral Method of Solution for Heat and Mass Transfer Problems with Phase Transformation," Heat Transfer, 1974, Vol. I, 211-215 (1974).
4. Hult, J.L. and Ostrander, H. C., "Antarctic Icebergs as a Global Fresh Water Resource," RAND Corporation Report R-1255-NSF (October 1973).
5. Proceedings, International Symposium on Icebergs, Paris, France (24-26 June 1977).
6. Pozvonkiv, F. M., Shurgalskii, E. F. and Axseldrod, L. S., "Heat Transfer at a Melting Flat Surface Under Conditions of Forced Convection and Laminar Boundary Layer," International Journal of Heat and Mass Transfer, Vol. 13, 957-962 (1970).
7. Weeks, W. F., and Campbell, W. J., "Icebergs As a Fresh Water Resource: An Appraisal," U. S. Army, Gold Regions Research and Engineering Laboratory Research Report 200 (January 1973).

INITIAL DISTRIBUTION LIST

	No. Copies
1. Defense Documentation Center Cameron Station Alexandria, Virginia 22314	2
2. Library, Code 0142 Naval Postgraduate School Monterey, California 93940	2
3. Department Chairman, Code 69 Department of Mechanical Engineering Naval Postgraduate School Monterey, California 93940	1
4. Professor A. E. Fuhs, Code 69Fu Department of Mechanical Engineering Naval Postgraduate School Monterey, California 93940	5
5. Professor Russel Stolfi, Code 56SK Department of National Security Affairs Naval Postgraduate School Monterey, California 93940	1
6. Professor Peter Wang, Code 53WG Department of Mathematics Naval Postgraduate School Monterey, California 93940	1
7. Professor Warren Denner, Code 68DW Department of Oceanography Naval Postgraduate School Monterey, California 93940	1
8. Professor Robert Bourke, Code 68BF Department of Oceanography Naval Postgraduate School Monterey, California 93940	1
9. Professor Wilford Weeks, Code 68We Department of Oceanography Naval Postgraduate School Monterey, California 93940	1
10. Mr. Thomas Christian, Code 69Ck Department of Mechanical Engineering Naval Postgraduate School Monterey, California 93940	1

- | | | |
|-----|--|---|
| 11. | LCDR William Clifford, USN
68 Yankee Peddler Path
Madison, CT. 06443 | 5 |
| 12. | LT Reginald Erman, USN
Code 331
Charleston Naval Shipyard
Charleston, S.C. 29408 | 5 |
| 13. | Dr. Owen M. Griffin, Code 8841
Ocean Technology Division
Naval Research Laboratory
Washington, D.C. 20375 | 1 |